EUROPEAN COMMISSION
5th EURATOM FRAMEWORK PROGRAMME 1998-2002
KEY ACTION : NUCLEAR FISSION

HTR-E

High-Temperature Reactor Components and Systems

CONTRACT N°
FIKI-CT-2001-00177

HTR-E WP1 Turbine
HHV data and turbine inlet thermal insulation
- State-of-the-Art Report on HTR Thermal Insulations -

Rodica Exner, Peter Broekerhoff, Werner von Lensa

FZJ

Germany

Dissemination level : RE
Document N°: HTR-E-03/05-D-1-1-3-1
Status : Final
Deliverable n° 4
FZJ identification number : HE0306HGL

Contents

1. Introduction
2. Problems / Requirements
3. State of the Art prior to Project Start
4. Types of Reactor Insulation
5. Development Steps and Qualification Programme for Insulating Materials within the Framework of the PNP Project
6. Qualification of Mechanical and Thermal Material Properties of the Insulation MVP III 1600 S
7. General Remarks and Fundamentals for Determining the Heat Transport in HTR Insulations
8. General Remarks and Fundamentals for Calculating the Depressurization Accident
9. Computer Programs for Shaped Fibre Structures
10. Historical Description of Test Programmes, Test Objects, Test Facilities
10.1 General Remarks on Thermal Behaviour
10.2 Selections of Insulation
10.3 Complete Insulating Systems
10.3.1 Metallic Insulation
10.3.A Foil Insulation
10.3.B Wire Mesh Insulation
10.3.C Special Geometries
10.4 Fibre Insulation
10.4.1 Shaped Fibre Structure
10.5 Rigid Ceramic Insulation
10.6 Combinations
11. Depressurization
12. Selections of Insulation
13. Complete Insulating Systems
14. PNP Development Programme for Shaped Fibre Structures at the Balcke-Dürr Manufacturer and Testing in the KVK Test Facility
14.1 Construction of Test Bodies and PNP Materials Concept
14.2 Manufacturer Experience in Mounting a Fibre Insulation System
14.3 Manufacturing Quality Assurance for Fibre Structure Insulation Systems, Construction Supervision and Acceptance
15. Experimental Data, Description of Experiments and Results with PNP Hot Gas Insulations

16. Proposal for the 'Data Sheet' of a Hot Gas Insulation
17. Résumé
18. Recommendations for the HTR-E Programme
19. References
20. Nomenclature

1. Introduction

This report summarises activities on insulations for hot gas ducts and vessels for helium cooled high temperature reactors (HTR). Theoretical as well as experimental work was carried out approximately in the time between 1972 and 1987 in the frame work of some project HHT, PNP and NFE.

In the project HHT it was provided to run the helium in the reactor heated up to a temperature of about 850 °C at a pressure of 50 bars directly into a gas turbine. Partners of this Project were Kernforschungsanlage Jülich (KFA), Brown Boverie & Cie AG (BBC), Hochtemperatur-Reaktorbau GmbH (HRB) and Swiss companies.

In the late 60s or early 70s KFA and Rheinische Braunkohlenwerke AG (Rheinbraun) dealt with the application of nuclear process heat plant concepts (NPGH). In the PNP project Prototype Plant for Nuclear Process Heat the partnership was extended to include the Bergbauforschung GmbH, HRB and the Gesellschaft für Hochtemperaturreaktortechnik mbH (GHT), later INTERATOM, see Mausbeck and Baust [MAU84] as well as significant component manufacturers as Balcke-Dürr, Steinmüller (Germany) or Sulzer (CH). The goal was to develop processes for the conversion of solid, fossil fuels using the heat from high temperature nuclear reactors. The HTR seemed to be specially qualified to deliver the heat needed. The temperatures were defined to be in the range between 800 °C and 950 °C, the pressure about 50 bars. The project Long-Distance Nuclear Energy Transport (NFE) was applied in 1975 by KFA and Rheinische Braunkohlenwerke AG [HAR84]. One aim of this project was to elaborate the data necessary for the design and construction of a heat transport system using the thermo-chemical cycle steam reforming/methanation [NFE85].

Within the framework of the project Prototype Plant for Nuclear Process Heat (PNP), high-temperature insulation systems were developed in 1980 to 1986 for the helium/helium intermediate heat exchangers, steam reformer and hot gas insulations.

The aim was to develop systems based on known forms of high-temperature insulation technology, which satisfy the high technical and safety-related requirements of the PNP plant. On the materials side, optimizations and new developments led to an insulating material allocated to the group of fibre ceramics. This MVP III material family was subjected to a metallurgical qualification programme. On the design side, detailed solutions extending up to a flexibly applicable overall concept were derived, which finally led to a joint concept of the project partners (DIDIER WERKE AG, INTERATOM, BALCKE-DÜRR AG). This was implemented as a component and subsequently tested in the KVK test loop of Interatom.

The experimental results obtained suggested a positive completion of the component test and the qualification of the overall system.

In order to attain the aims extensive theoretical and experimental work was needed. Handling the coolant medium helium improvement of existing test facilities were required. In addition new and large facilities must be designed and erected, in which full-scale components at reactor conditions could be tested. These are e.g. pebble beds, heat exchangers, steam reformers, armatures, blowers and connecting tubes or vessels. Due to the high temperatures concurrent with the high pressures and nuclear safety aspects, a new epoch of material developement started. This development work included metallic materials as well as insulations.

2. Problems / Requirements

All heat-exchanging and heat-carrying components of a HTR plant must be insulated in order to

- protect their metallic structures against high temperatures and steep temperature transients and

- keep the thermal efficiency of individual components and of the whole plant as high as possible.

Thermal insulations are of great significance for HTR plants. Work on the insulation systems primarily aimed at solutions for the PNP He/He intermediate heat exchangers (HELIX, URKO), but should also be directly transferable to hot gas ducts and the steam reformer.

For the conventional technology, insulations were known which reliably controlled temperatures of up to 1,700 °C under inert gas and up to far above 2,000°C in vacuum.

The question therefore arises of why these solutions cannot be referred to for the HTR plants and, instead, development work was considered necessary and was carried out.

The reason is to be seen in the fact that, compared to the requirements of a nuclear facility, those of conventional technology are less stringent. Safety thinking is less necessary here; although a failure of insulation systems *) is never desirable, it can be tolerated in conventional applications, especially since defective insulations can be replaced rather easily in most cases.

The insulation systems of the PNP/HTR plant must fulfil the following essential requirements:

- chemical, physical (mechanical) and mineralogical stability during at least 140,000 hours of operation
- low bulk density (<< 1,000 kg/m³) along with the highest possible mechanical stress capacity
- high insulating effect in helium at approx. 1,000°C/40 bars
- resistance to depressurization accidents
- high thermal shock resistance
- high resistance to abrasion and erosion

*) Insulation systems are understood to be combinations of insulating materials and their structural integration (concept).

These requirements primarily and selectively concern the insulating material.
The structural integration of the material into the overall system (sealing elements, mounts, load applications) should not adversely influence the material properties.

The above reasons and the requirements just listed show that direct transferability between conventional and nuclear technology is not given.

The aim of work was therefore, based on known solutions, to find ways of optimization and, if necessary, also embark on new developments in order to meet the requirements of the PNP plant.

3. State of the art prior to project start

High-temperature insulation systems are executed in conventional technology using numerous materials and various shaping and mounting techniques.

Those most commonly used will be briefly described in the following.

Insulating and lightweight firebricks are processed as standardized formats, occasionally also as shaped bricks. They are thermally pretreated. Normally, the bricks are bonded with temperature-resistant cements and mortars and form the backing for a wear-resistant, but poorly insulating inner layer.
Applications are also known, e.g. in furnace construction, in which the bricks are directly exposed to the furnace atmosphere.

The use of insulating bricks is restricted to temperatures below 1,000°C, lightweight firebricks are used for higher temperatures. Depending on composition, their application limit ranges from 1,000 to over 1,700°C. Appropriate bonding cements and mortars are used.

In terms of strength, insulating and lightweight firebricks are at the lower limit of the conventional refractory product range.

Their thermal shock resistance is poor to satisfactory. In geometrically complicated wall structures or if no bricks can be used for other reasons, unshaped products (lightweight refractory compounds) are applied, which then form the insulation. These materials are wet-processed on site and harden by chemical bonding (at room temperature) or ceramic bonding (during the first operating cycle). In view of the monolithic and, in most cases, large components, no good thermal shock resistance may be expected. Of disadvantage is also the tendency to releasing volatile constituents, e.g. water vapour.

For about forty years now, inorganic fibres (especially so-called ceramic fibres) and their products have been increasingly used for high-temperature thermal insulation. This includes, in particular, fibre blankets, fibre blanket modules, fibre mats and vacuum-moulded fibre products. The insulation concepts based on these materials may be counted among the conventional solutions from the present point of view, since they are successfully applied along a wide front. The product diversity of ceramic fibre components is great. Fixing is achieved by (inorganic, fireproof) cementing. Of disadvantage is the post-shrinkage of the ceramic fibre products in long-term application and their low mechanical stress capacity. Very positive features are the favourable insulation properties, low storage capacity and very forgiving behaviour towards thermal shock. They are therefore steadily gaining in popularity despite in part relatively high investment costs.

In comparing the properties (advantages and drawbacks) of conventional high-temperature insulating materials, however, it has been found that only part of the requirements for the PNP/HTR plant are fulfilled, so that conventional materials cannot be used for resolving this task.

This applies analogously to the other elements of the insulation systems, such as the holding elements, load applications, sealings and, where required, coatings.

4. Types of reactor insulation

The simplest possibility for a classification is regarding to the materials used, see Table 1 where only the main items are given.

1	metallic insulation
a	*foil insulation*
b	*wire mesh insulation*
c	*special designs*
2	fibre insulation
a	stuffed insulation
b	*fibre blanket insulation*
3	rigid ceramic insulation
4	combinations from 1a and 2
5	combinations from 2 and 3

Table 1: Insulation (corresponding to the applied materials)

Foil and wire mesh insulation belong to the metallic design. There were also other proposals, e.g. designs with rhombic cells, which were not realised. The category of fibre insulation is the most important one. Insulation made of rigid ceramic were mainly provided for regions of very high temperatures. In contrast to fibre insulation in which there exist a large cohering free space filled with the cooling medium rigid ceramic insulation has open as well as closed pores. In general the portion of the solid is higher than that containing gaseous substances. Rigid ceramic materials are e. g. pumice concrete, kohlestein, graphite and silica. The last two groups of the table stand for combinations of the other groups.
A further classification may be done corresponding to the materials used. As mentioned before from the thermal behaviour point of view the insulating systems should have a high flow resistance. From the depressurisation point of view, however, the gas might escape easily. This ability is called permeability. Because of their homogeneous structure fibre insulation without metallic internals belong to the category with a homogeneous or isotropic permeability, see Table 2.

1	isotropic structures
2	anisotropic structures
a	*high axial permeability*
b	*high radial permeability*

Table 2: Insulation (corresponding to the structures)

Regarding the problem two dimensional as usual in the fist case axial as well radial permeabilities are equal. Foil insulation are belonging to the second group. Their permeabiltity in the radial direction, also perpendicular to the foils and in the direction of the temperature gradient, is rather low, but in the direction of the foils high. Wire mesh insulation without any internal structures are counted among the first classification. But in case of mounting only one single foil their permeability becomes anisotropic.

5. Development of the insulation within the PNP-project

Development steps and qualification programme

Even before the start of project work, it had been ascertained that the conventional high-temperature insulating materials so far known could not satisfy the requirements of the HTR/PNP plant. At the same time, however, it was also perceivable that the working target could be reached by optimizing these materials. It was therefore attempted to build on known materials and their manufacturing processes.

This procedure will be explained in the following with the aid of a few considerations.

From the operating conditions of the HTR/PNP plant, the following requirements result for the high-temperature insulating material:
thermal stability up to 1,100 °C

- stability in helium, 40 bars, mechanical and corrosive
- easily reducing (primary loop) easily oxidizing (secondary loop)
- thermal shock resistance
- resistance to depressurization accidents
- high resistance to abrasion and erosion
- mechanical strength

Furthermore, the following normal operation requirements are to be met by the material:

- high insulating effect
- low bulk density (< 1,000 kg/m³)
- chemical, physical, mechanical and mineralogical resistance during at least 140,000 hours of operation

From the PNP and other HTR material programmes it had already been known prior to the start of work that only materials from the alumina/silica system were candidate materials.

From conventional high-temperature insulation technology, materials are known which satisfy this requirement, but do not simultaneously fulfil the other conditions. Lightweight firebricks, insulating bricks and unshaped products are rejected due to their moderate to poor temperature cycling resistance, conventional fibre products due to insufficient mechanical stability. Considerations therefore aimed at further developing the inorganic fibrous materials of interest due to their thermal behaviour in such a way that an improvement of their mechanical properties was achieved without simultaneously cutting back their favourable thermal behaviour and thermomechanical properties. At the same time, work was to ensure that the issues of shaping and machining were adequately taken into consideration, since the components to be made from the fibrous materials must be sufficiently accurate to size.

Since the known fibrous materials exhibit a very low bulk density (< 350 kg/m³, status approx. 1980), but higher density necessarily leads to an increase in mechanical strength, the first experiments aimed at producing materials with higher densities.

5.1 Different process-engineering approaches were pursued here:

5.1.1 Dry pressing

A shaping process known in conventional technology is pressing (dry pressing). This involves the compaction of crumby raw material batches under pressure into brick-like bodies in moulding boxes using a press.

Normal formats (square specimens of brick size), occasionally also shaped bricks are preferentially produced in this way. The size of the formats to be pressed is greatly limited upwards.

As a rule, the compacts are subjected to a thermal post-treatment.

In connection with work for the PNP plant, this process was also tested with fibre batches. It was found that it is basically possible to apply this shaping process, but with the above restrictions. Bulk densities around 1,000 kg/m3 were achieved. The material properties correspond well to the requirements of the PNP plant in a first approximation.

The relatively high bulk density and the format limitation resulting from this shaping technique seemed to be of disadvantage.

5.1.2 Stamping

Another commonly used technique is stamping, especially for shaped bodies. This involves the stamping, pressing, of the raw compound into a multipart mould using a stamping tool. This process is carried out manually with a few exceptions.

This technique was also tested, for example, for tubular geometries. Basic feasibility was demonstrated. The disadvantages were also seen here in an also fairly high bulk density. Another characteristic of this process was regarded as a disadvantage: it is

poorly reproducible as long as it is carried out manually. The solid rings produced tended to cracking during thermal post-treatment.
The tests were deferred for this reason. Stamping as a shaping process would only have been suitable for very limited applications within the PNP plant.

5.1.3 Injection moulding

As a prelude to the supported project, Didier-Werke AG tested injection moulding. In conventional refractory technology, this process is used if large wall surfaces without formwork are to be lined with refractory material. It is basically related to machine-applied plastering known from construction engineering.

The task set for the development work was to modify the process so that material can be injected into a mould. This mould had to be permeable for air because air was the delivery fluid. It was also attempted to produce blocks in a freehand manner, so that they could serve as a basis for later reworking.
The experience acquired with these tests made it appear advisable to refrain from further experiments.

Although lower bulk densities than with the stamping and pressing processes were achieved here for the first time, an insufficient homogeneity of the material was also found here.

5.1.4 Centrifugal moulding

Centrifugal moulding is used on a large technical scale, for example, to produce concrete shapes such as masts and tubes. This approach also initially appeared promising and was tested for the fabrication of tubes on the basis of ceramic fibres.

Difficulties were already encountered at the beginning of the tests: the raw batch is hardly flowable since, in contrast to concretes, only small amounts of binder or additives (fillers, auxiliary materials, e.g. flow improvers) can be added to the candidate fibrous materials due to the low density desired. This poor flowability is further enhanced by the fibres. It therefore cannot be expected that such fibrous compounds can be poured or adequately introduced into a moulding drum by pouring. Instead, atomizing was tried. The results were not satisfactory; work in this direction was abandoned at an early stage.

5.1.5 Extrusion pressing

Another well-known shaping method is extrusion pressing, where ceramic raw compounds are plasticized by auxiliary materials. A known and commonly used plasticizer is clay. It makes the raw compounds suitable for being processed and extruded. Shaped bodies can be continuously produced within wide limits by selecting suitable mouthpieces. A number of tests revealed that extrusion pressing is a very suitable technique for shaping ceramic fibre compounds. For this reason, further experiments were performed for these techniques and the processability of more than 50 formulations was investigated on a laboratory extrusion press. Several batches proved to be very well processable.

The limits of this process became apparent in large-scale testing. It was also demonstrated here that this shaping technique is suited for the production of large-size parts. Due to pronounced difficulties in drying the shaped parts, this on the whole far advanced technique was not further pursued.

5.1.6 Vacuum moulding

Vacuum moulding plays a significant role especially for conventional ceramic fibre materials. It also enables the production of rather complicated shapes. The process can be basically described as follows: ceramic fibres, binders and auxiliary materials are homogeneously distributed by stirring in aqueous suspension. In order to obtain the desired shape, a corresponding suction mould has to be produced. This normally consists of a supporting frame covered by a fine-meshed sieve fabric, which represents the contour of the later shaped body. After the suspension has been prepared, the mould is dipped in and evacuated. The mould thus sucks in aqueous fibre suspension so that filtration takes place on the sieve fabric and the later shaped body deposits as filter cake on the sieve. After completion of the suction process, the mould is taken out of the bath and the filter cake (= shaped body) is lifted off by a compressed-air blast. The shaped bodies are dried, occasionally also baked. They can be impregnated. Reworking is often possible.

5.1.7 Densification of fibrous materials

The basic idea described here led to the later MVP III material in the course of development work. It was considered and tried to impregnate fibre blankets with binders, press them and dry them in the densified state applying a load. These tests were initially not very satisfactory, so that the shaping processes mentioned further above were tested first.

Only in the further course of work was this idea taken up again, although in a slightly modified form.

Experiments showed that a subsequent densification of fibrous materials, such as blankets and boards, adversely affected the material properties and, in part, even led to their destruction during shaping.

The following theoretical approach remained as a solution: the fibre must be densified in the wet to sufficiently moist state. Densification provides a considerable potential concerning the increase in strength to be expected.

The vacuum moulding technique described above had been known by then, but it could only provide materials with comparatively low density and low mechanical strength. An increase in density and strength could only be achieved by excessive crushing of the fibres and adding an undesirably high fraction of fillers.

An increase in density was therefore to be achieved by redensifying the filter cake in the wet or semi-wet state. For this purpose, a lab unit was planned and constructed at Didier-Werke AG, which enabled the moulding of shapes (solid cylinders) with 280 mm diameter and about the same maximum thickness. This material was designated MVP I for project purposes. The lab unit essentially consisted of a hydraulically driven lower punch for densifying the filter cake, a fixable upper punch, and a round moulding shell. The filter cake was completely enclosed during the densification process. The water flowing out during densification was **sucked off** through sieve fabric provided on the upper and lower punch. The tests were very promising. A component test set up at DW for testing the wall structure for the "Central Riser" was in part built up with such materials and successfully tested. Still insufficient at this point in time was the small blank format with which shapes of the geometry later likely to be needed could not be achieved.

During the development of the fibre ceramics, DW had procured a large-area press working at relatively low pressures for producing a totally different product. It was attempted to reproduce the process run on the laboratory press. The material obtained was designated MVP II for project purposes. The disadvantage of the larger press: it was not equipped with a moulding box, so that flow processes occurred during the densification in filter cakes (base area: 0.5 x 1.0 m). This led to a very pronounced texture and thus caused the large-format fibre plates thus produced to crack along the texture planes.

This proved to be of great disadvantage in the manufacture of the insulation components for the axial valve subcomponent (Figure 1). Nevertheless, it was possible to execute the order. The axial valve subcomponent was tested in the component test loop at Interatom.

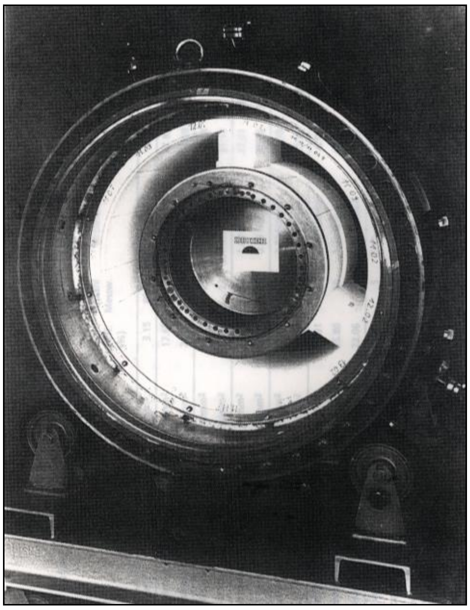

Figure 1: Axial valve

MVP II was to be seen as an interim solution. The tests for MVP 1 had already shown that the use of a moulding box was of decisive significance in densification and for the material.

Following this finding, a larger press was designed and ordered at an early stage.
The tests with this unit were immediately started after delivery. It was found that the right decision had been taken. In the course of optimization work, the MVP III material was produced in densities from 200 kg/m^3 up to 800 kg/m^3. The tests, and

simultaneous material investigations, showed that the globally most favourable material properties were to be expected in the range from 250 kg/m^3 to 650 kg/m^3.
For this MVP III material group, a qualification programme was drawn up and the material investigations carried out accordingly. Work for material qualification was performed both at DW and at Interatom. The test specimens were provided by DW.

6. Material qualification of MVP III 1600 S

6.1 Introduction and summary

In connection with the R&D activities for the PNP plant, the Interatom and DW project partners performed a multitude of investigations on the MVP III 1600 S material group. The material data found were statistically validated and the goal of work was thus achieved. The MVP III 1600 S material group meets the requirements of the PNP plant and thus, in general, of the HTR plant.
Work for the optimization and further development of materials, which led to the MPV fibre ceramic, has provided an appropriate material for the insulation of components of the PNP and HTR plant. Even if investigations showed that this material group meets the requirements of the PNP or HTR plant, only its suitability has thus been proved. The insulation system consists (as already stated further above) of the material and its structural integration into the overall system. This means that structural solutions which must also satisfy the requirements have to be evolved with this material. Thus, for example, components must be manufactured, configured and mechanically fastened. Under the conditions of the PNP or of the HTR plant, the durability of an insulation component (shaped body) depends decisively on the resistance to temperature change. As is well known, the mechanical loads on a shaped body increase with its volume during temperature change. In the most unfavourable case, a poorly designed shaped body can be destroyed by temperature transients. This is not allowed to happen in the PNP plant. Moreover, due to the mechanical integration of insulation components, it is important to know their mechanical stress capacity. Furthermore, the reliability of the data available must be known.

The aim of work for material qualification was therefore to obtain statistically validated material data so as to provide a basis for the computability of this fibre ceramic group.

6.2 Procedure

Concerning the nomenclature of the MVP fibre ceramic

The requirements of the PNP or the HTR plant made it necessary to have MVP fibre ceramics with different bulk densities. For this reason, the qualification programme was carried out for different material densities. Since the material properties uniquely depend on the bulk density (steady performance), it was furthermore possible to determine with sufficient accuracy by interpolation the properties of MPV fibre ceramics not investigated.
Anisotropic materials performance was taken into consideration in the investigations.

In assessing the material properties, however, it must be taken into account that, except for the bending strength, no values under temperature have been determined concerning the mechanical properties.
Materials for thermal insulation are generally characterized by the grade name and a combination of numbers. The first number relates to the bulk density in kg/m^3, the second as the classification temperature provides information about the level of possible temperature loads. But the classification temperature is not a characteristic for determining the maximum possible application temperature (= application limiting temperature).

6.3 Manufacturing the blanks

There were produced MVP-III blanks for material qualification as follows:

MVP III 610/1600 S 12 blanks 850 x 350 x 150 mm
MVP III 550/1600 S 13 blanks 850 x 350 x 150 mm
MVP III 510/1600 S 10 blanks 850 x 350 x 150 mm
MVP III 250/1600 S 14 blanks 850 x 350 x 160 mm

These blanks were used by DIDIER to manufacture the required test specimens (Figures 2,3). For each bulk density level only those blanks were used whose average density came closest to the bulk density aimed at. A total of 30 blanks were thus available for the investigations (Figure 4).

PNP-Project	AP300	Material qualification				
LN 640x			Status as of: 08.07.1986			
Material tests and tested geometries						
Test Number	Form	Dimensions/ mm [Tolerances]	Sketch	Test	by	Remarks
LN 640x/y.25	Cylinder	∅ 36 x 130 [-0, +0.1 x +1]	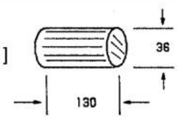	Shearing resistence	Interatom GmbH	
LN 640x/y.26	"	"		"	"	
LN 640x/y.27	"	"	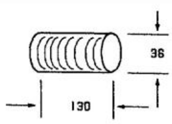	"	"	
LN 640x/y.65	"	"		"	"	
LN 640x/y.28	Bolt	40 x 40 x 72 [± 0.5 each]	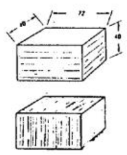	Transverse contraction	Interatom GmbH	Surfaces 40 x 40 parallel < 0.1
LN 640x/y.29	"	"		"	"	"
LN 640x/y.30	Cuboid	115 x 15 x 60 [± 1 each]	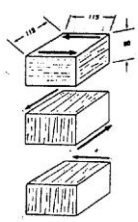	Shear modules	"	Surfaces 115 x 115 parallel < 0.5
LN 640x/y.31	"	"		"	"	"
LN 640x/y.32	"	"		"	"	"

Figure 2

PNP-Project	AP300	Material qualification				
LN 640x			Status as of: 08.07.1986			
Material tests and tested geometries						
Test Number	Form	Dimensions/ mm [Tolerances]	Sketch	Test	by	Remarks
LN 640x/y.41	Disc	∅ 100 x 25	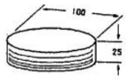	Heat conductivity Dr. Klasse	Didier-Werke AG	
LN 640x/y.42	"	"	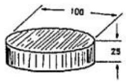	"	"	
LN 640x/y.43	Cylinder	∅ 12.5 x 50	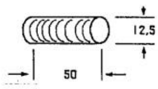	Heat expansion	"	
LN 640x/y.44	"	"	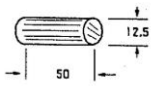	"	"	
LN 640x/y.45	Bolt	64 x 64 x 120 [± 2 each]	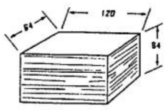	Resistence for temperature transients	"	
LN 640x/y.46	"	"		"	"	
LN 640x/y.47	"	"	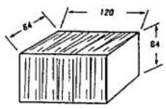	"	"	
LN 640x/y.48	"	"		"	"	

Figure 3

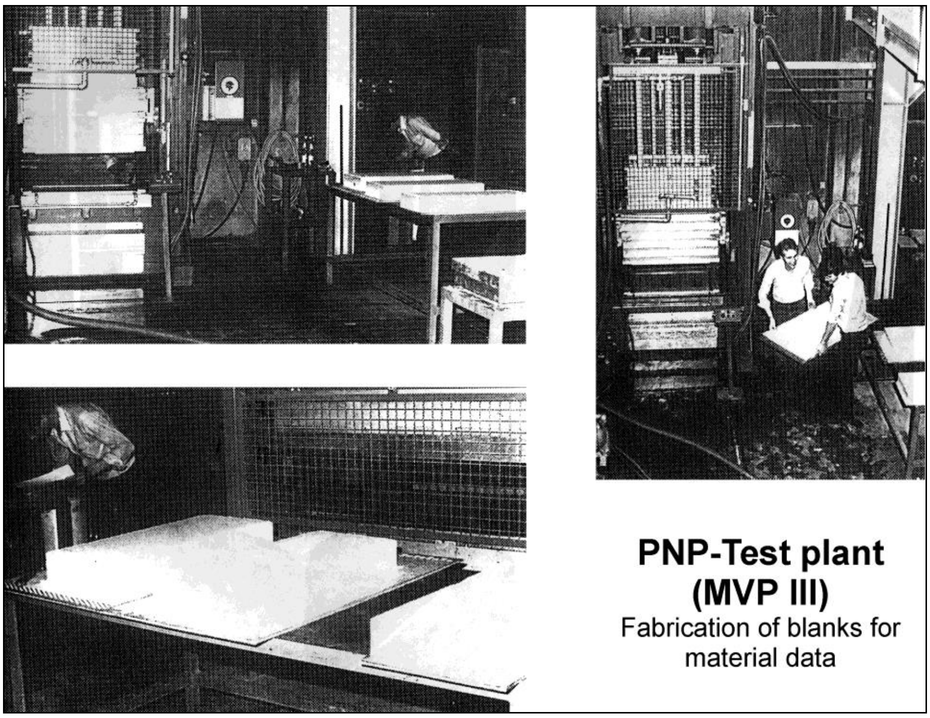

PNP-Test plant (MVP III)

Fabrication of blanks for material data

Figure 4

Blanks with 510 kg/m^3 were taken out of the investigation in favour of those with 250 kg/m^3

In the following, a survey will be given concerning the investigations performed and responsibilities.

6.4 Qualification programme (Mechanical and thermal properties):

Chemical composition and microstructure
bulk density
porosity
chemical and mineralogical composition

Mechanical properties

- cold crushing strength
- bending strength as f(T)
- tensile strength
- dynamic modulus of elasticity
- static modulus of elasticity
- shear strength
- lateral contraction
- modulus of shear
- erosion, air
- abrasion on metal
- abrasion on itself

Thermal properties

- thermal expansion
- thermal conductivity according to Dr. Klasse in air
- thermal conductivity according to the hot-wire methods in nitrogen and helium at P = 1 and 40 bars
- temperature cycling resistance, testing according to DIN performance under temperature transients

6.5 Boundary conditions for testing

Here a few remarks which are to draw attention to special aspects of the investigations.

Microstructure MVP III 1600 S is an anisotropic material with a layered texture (Figures 5,6). For this reason, different material performances were codetermined in the tests, depending on the direction of layering and stressing. A system of coordinates was defined to better understand the fibre orientations considered.

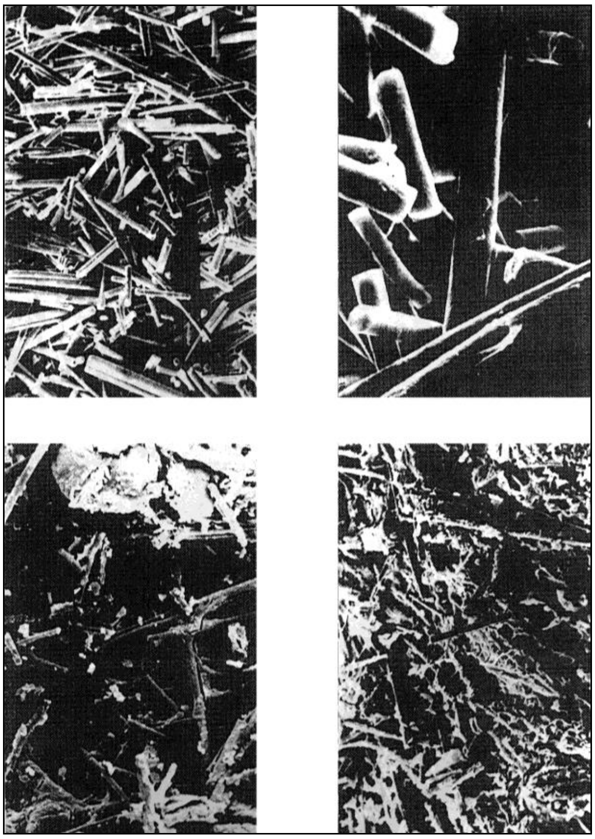

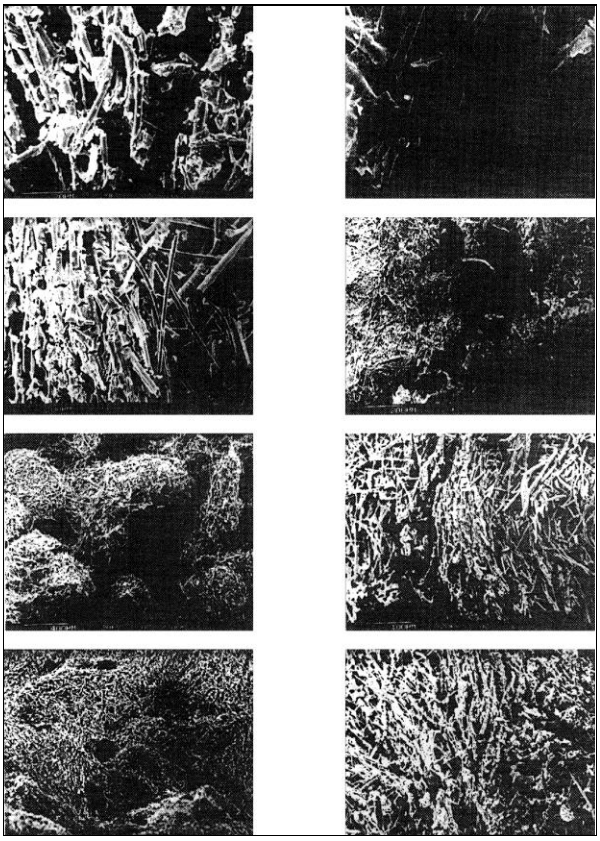

Exposure of the photos from scanning electron microscope microstructure of compact fiber material

Figure 5 Figure 6

Boundary conditions and explanations concerning the measurements performed

- **Bulk density**

The bulk density was determined by dimensionally measuring (slide callipers) and weighing (1/100 gram) all test bodies available. In this way, it is possible to make rather precise statements on the reproducibility of the bulk density.

- Porosity

No investigations were made concerning the porosity. It can be easily calculated by knowing the material's absolute density. The MVP III material group is known to be predominantly open-pore. The bulk density is clearly above 75 vol.% in the cases to be considered.

- Chemical and mineralogical composition

The chemical and mineralogical composition corresponds to the requirements of the PNP plant.

- Bending strength as f(T) (Figures 7-11)

In this subinvestigation, the values of cold bending strength and hot bending strength are combined at the temperature levels of 600 °C and 1,000 °C. As expected, the bending strength is found to increase with the bulk density.

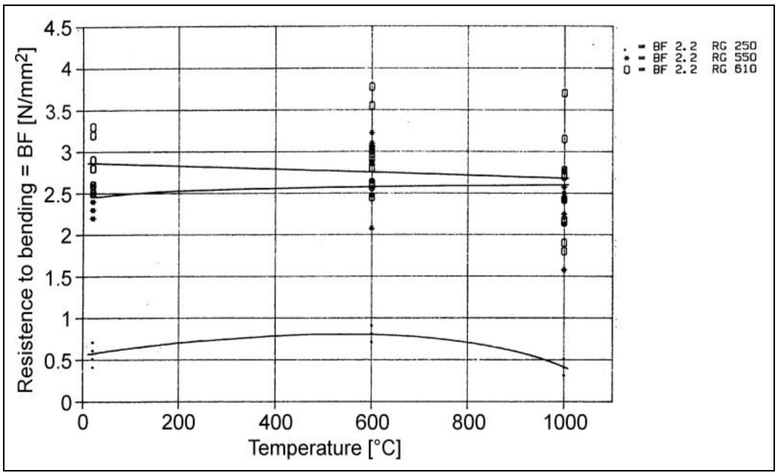

Figure 7: Resistence to bending 2.2 = F (T)
MVP III 1600 S

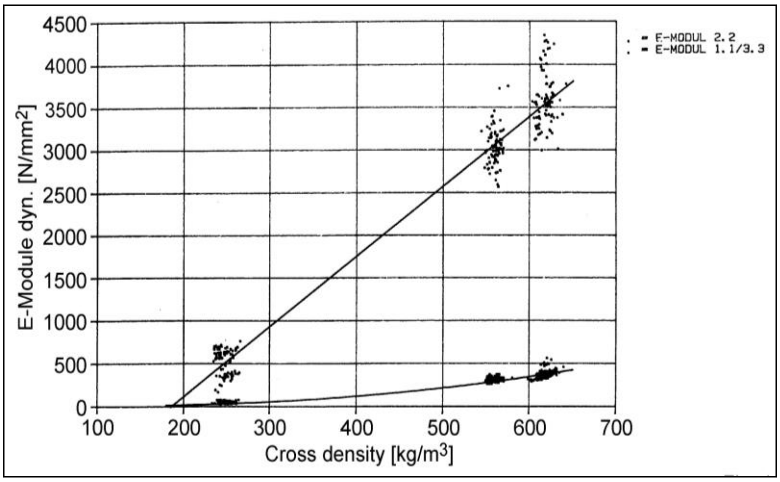

Figure 8: E-Module dyn.
MVP III 1600 S

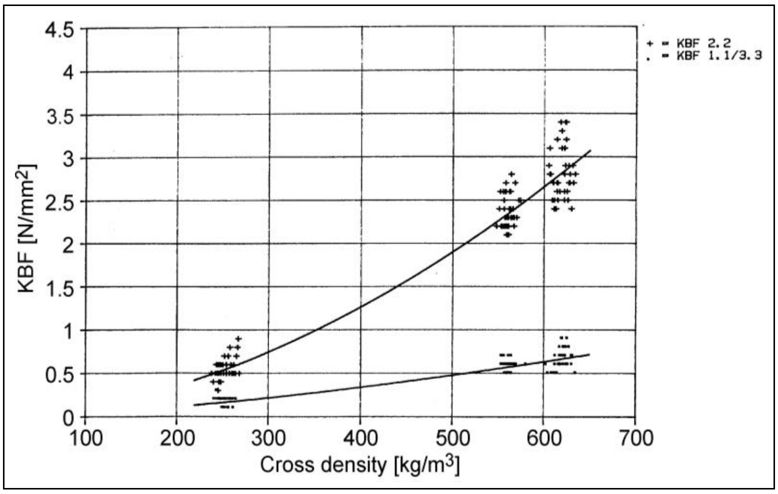

Figure 9: KBF
MVP III 1600 S

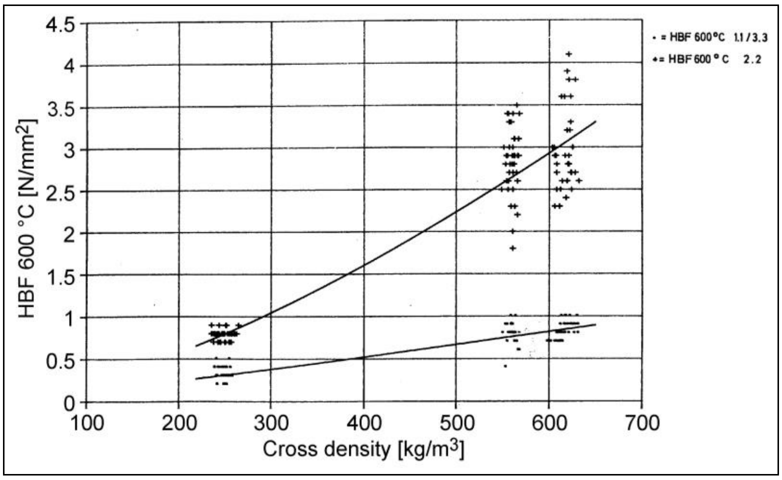

Figure 10: HBF 600 °C
MVP III 1600 S

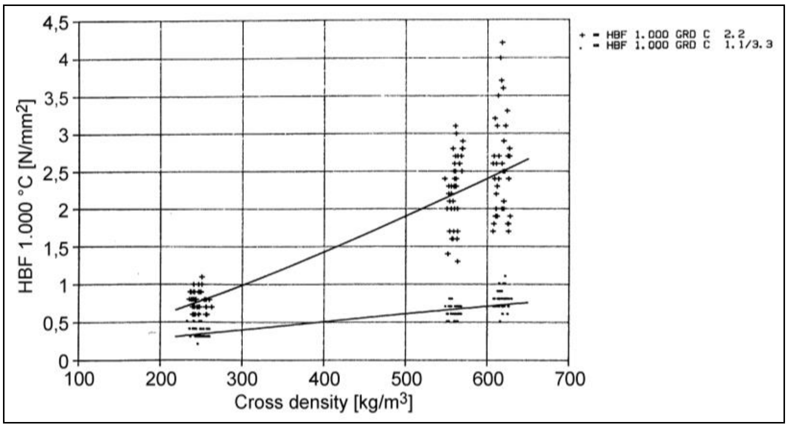

Figure 11: HBF 1000 °C
MVP III 1600 S

It is interesting to note that the bending strength slightly increases up to a stressing level of approx. 600 °C and only decreases slightly in the further course up to 1,000 °C to values similar to the cold test.

- **Modulus of elasticity**
  dynamic modulus of elasticity (Figure 8)

This test was carried out on all test bodies according to the ultrasonic travel time procedure. Difficulties are encountered with fibre ceramics in that the application pressure of the ultrasonic transmitters must not be too high, since otherwise the test body surface is damaged. On the other hand, good coupling must be ensured in order to obtain reproducible results. The determinations on MVP III 250/1600 S were hampered by the material's sound insulation effect.

The application limiting temperature of insulating materials is dependent on the raw materials used, on the type of thermal post-treatment and on the operating conditions. For the MVP materials, the thermal post-treatment was performed so that after shrinkage of the materials is completely ruled out at a maximum operating temperature of the PNP plant of 1,000 °C.

Temperature cycling resistance, testing according to DIN. The testing of the temperature cycling resistance according to DIN was included in the qualification programme as an orientation procedure especially since this is a testing method rich in tradition. The MVP materials showed satisfactory to very good performance depending on the direction of stressing.

- **Performance under temperature transients**
  Since the testing of the temperature cycling resistance only permits trend statements to be made, it was attempted to obtain quantitatively usable data through tests on MVP III in a transient furnace (Figure 12). Square specimens and rings were tested.

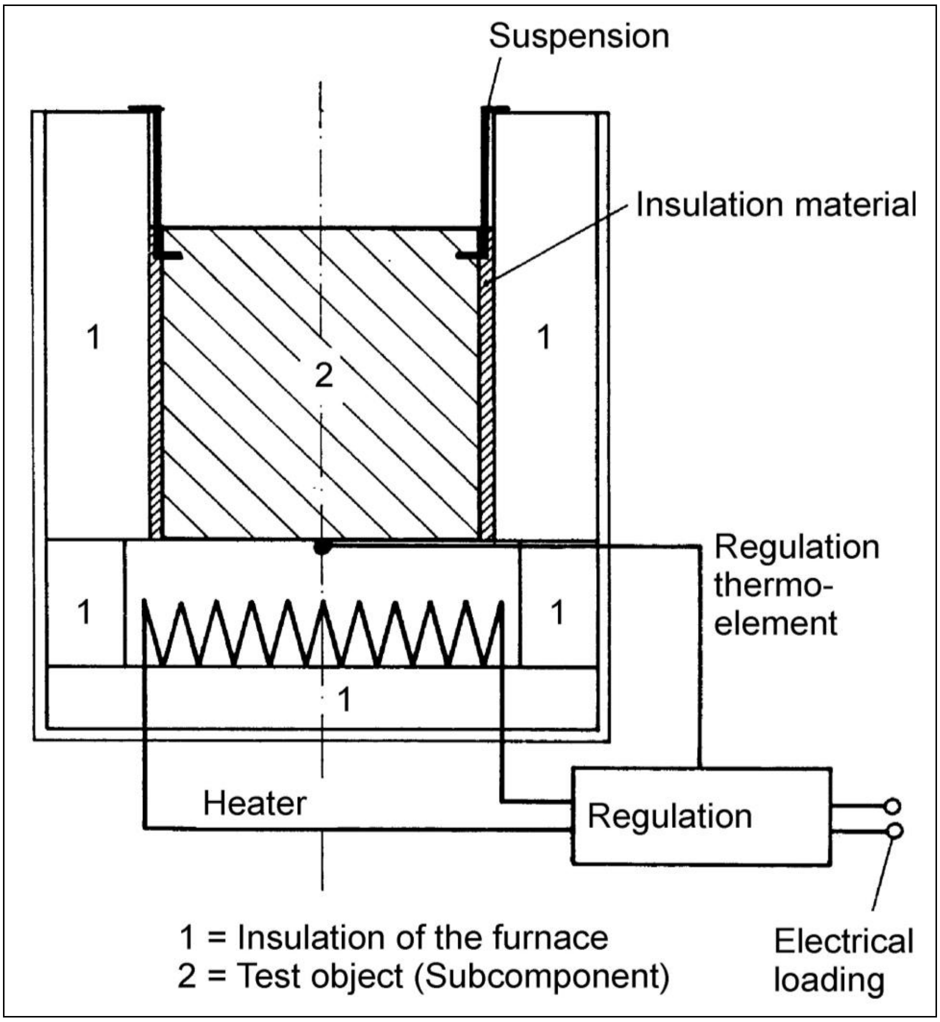

Figure 12: Schematic: Furnace for testing the transients on test objects (Subcomponents)

The square specimens were rapidly heated unilaterally. The test bodies (Figure 13) were subject to a thermomechanical stress produced by unilaterally leading thermal expansion. If the stresses become so high that they exceed the strength of the test body, cracking occurs. In addition to the material properties, the specimen geometry and the heating rate (peaking of the temperature transient) play the decisive role in this test.

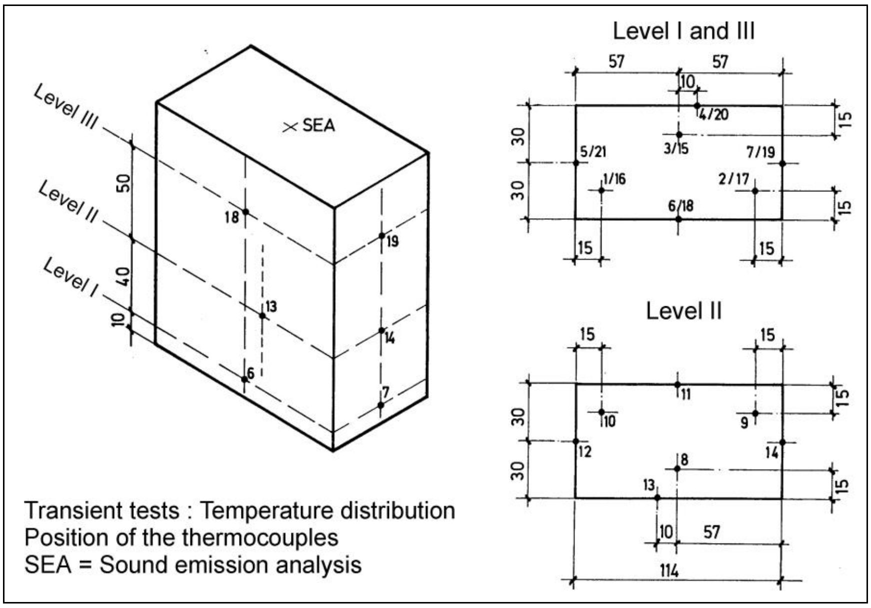

Figure 13

Cracking can be precisely localized in terms of time in these investigations via the acoustic emissions of the crack event, the crack location is macroscopically perceivable in most cases after removal of the test body from the furnace and can then be dimensionally measured.

It was now first investigated from which heating rate upwards cracking actually occurred. When the times and locations of cracking were known, an attempt could be made to obtain information about the precise position of this threshold region

The tests with/on square specimens revealed the following: no cracking occurs on the test bodies in grades MVP III 250/1600 S and MVP III 550/1600 S at transients up to 5,000 K/h, if the front of the isotherms is perpendicular to the course of the material layering planes. Higher transients could not be examined, since it would not have been possible even with more apparatus expenditure to increase the power density of the test furnace. Cracking only occurred on MVP III 550/1600 S as soon as the course of the material layering planes was parallel to the isotherms.

Cracking must be expected here above about 1,000 K/h for the test body format selected.

Another possibility of examining the stresses caused by temperature transients was given by the so-called ring test, where ring-shaped test bodies are rapidly heated from inside and the crack behaviour is observed. Ring inside and outside temperatures are recorded in each case. As soon as a crack occurs which propagates through the whole ring wall thickness (acoustic emissions), the difference between inside and outside temperature is defined as the critical temperature difference. These tests also enable the critical heating rate to be delimited. The detailed results can be seen from the MVP III materials manual.

Thermal expansion (Figure 14)

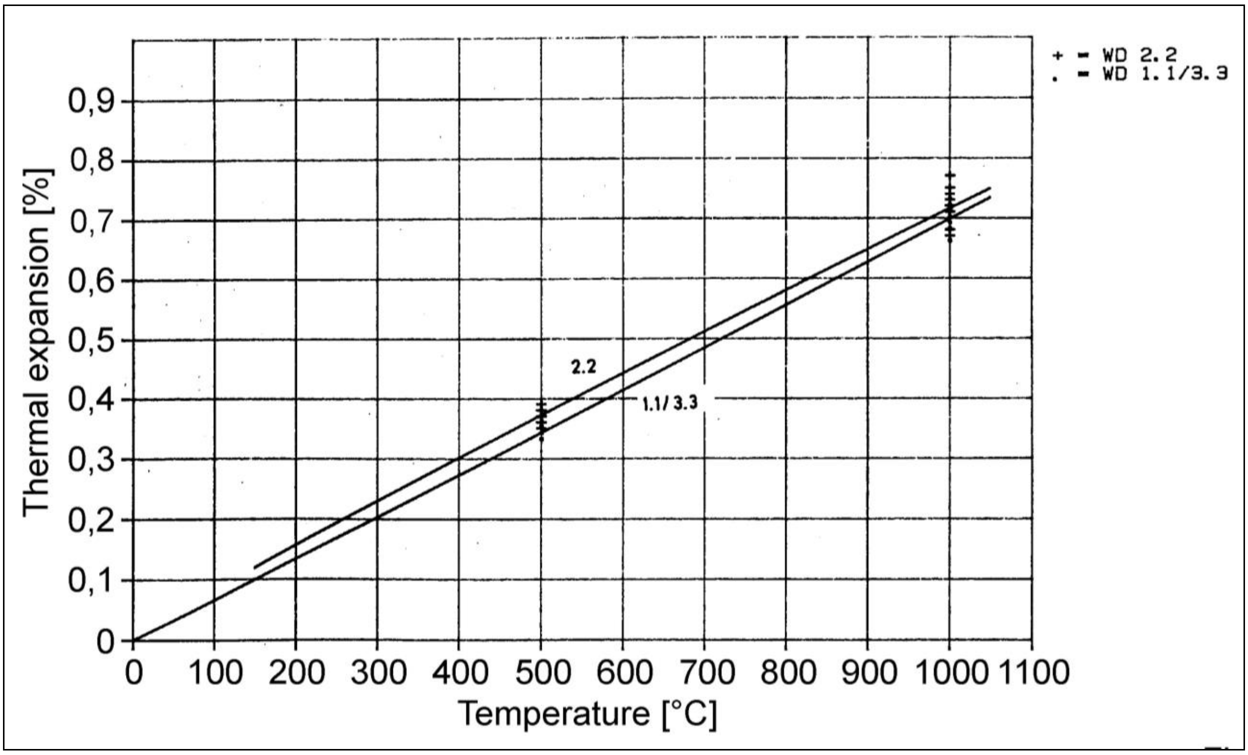

Figure 14: Thermal expansion
MVP III 250…610 / 1600 S

Heat conduction (Figure 15)

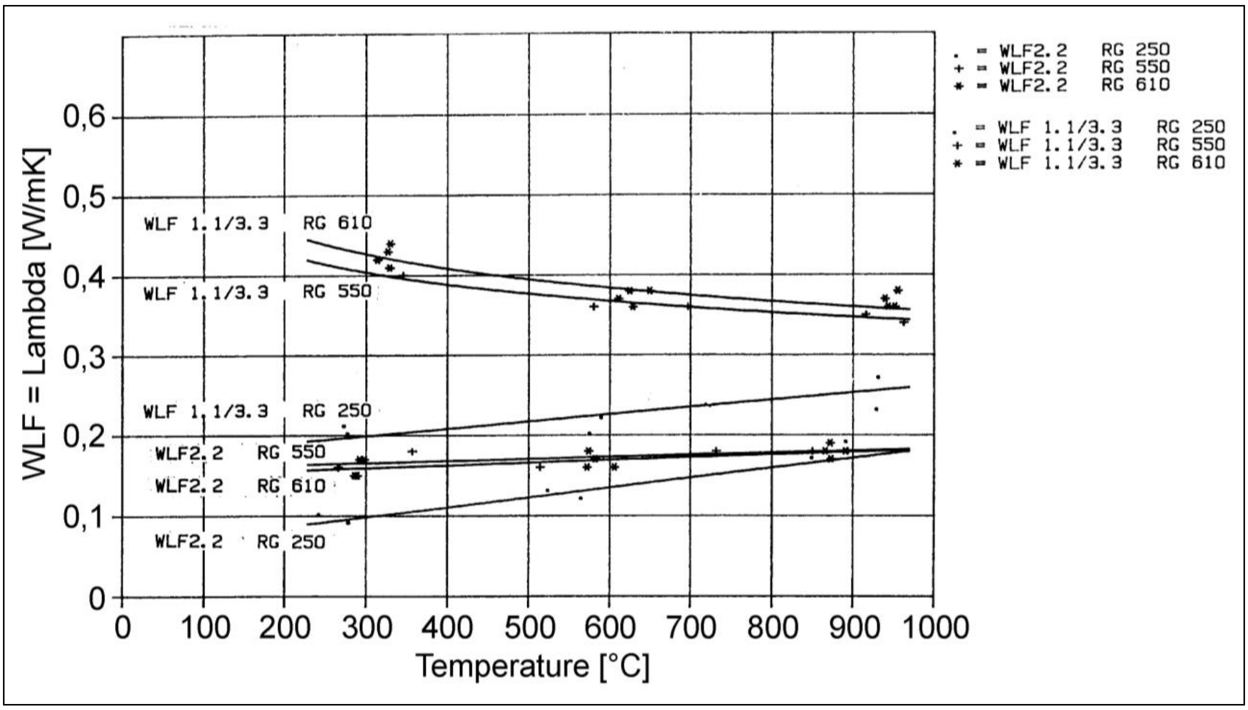

Figure 15: WLF
MVP III 1600 S

Statistical evaluation of the measured data Table 2 / Figure 16

PNP-Project **AP 300** **Material qualification** **MVP III 1600 S** **Hersteller: Didier-Werke AG**

Statistical evaluation of the measurements
DIN 1319 / 2

Date: 22.05.1987 **File MVPSTAT.FW : n = Number of measurements**
: (1) = Average cross density / kg/m³
: (2),(4) = Coefficients of variation / %
: (3) = Average of measurements / N/mm²

Test	Orientierung	MVP III 250/1600 S					MVP III 550/1600 S					MVP III 610/1600 S				
		n	(1)	(2)	(3)	(4)	n	(1)	(2)	(3)	(4)	n	(1)	(2)	(3)	(4)
KBF	2,2	39	252	3,39	,56	20,81	40	561	1,02	2,38	7,49	39	619	1,29	2,80	10,65
E-Module, dyn.	1,1	40	252		496		40	561		3044		40	619		3568	
KBF	1,1	40	251	2,23	,18	28,20	39	561	,95	,59	10,86	40	619	1,12	,67	17,55
E-Module, dyn.	2,2	40	251	2,23	39	38,21	40	561	,97	305	7,21	40	619	1,12	366	16,15
HBF 600	2,2	40	248	3,24	,78	7,93	40	560	,85	2,85	13,84	40	618	1,16	2,93	16,05
E-Module, dyn.	1,1	40	248	3,24	557	23,44	40	560	,85	3024	5,76	40	618	1,16	3589	9,24
HBF 600	1,1	40	250	2,05	,32	23,7	39	561	,78	,79	14,62	40	617	1,40	,84	11,69
E-Module, dyn.	2,2	40	250	2,05	38	32,67	40	561	,78	310	7,85	40	617	1,40	368	14,81
HBF 1000	2,2	40	247	2,90	,79	16,20	40	560	,94	2,28	19,76	40	617	1,09	2,55	25,57
E-Module, dyn.	1,1	40	247	2,90	456	37,34	40	560	,94	2995	6,25	40	617	1,09	3554	8,40
HBF 1000	1,1	40	249	2,75	,36	23,83	40	560	,96	,63	13,55	40	618	,84	,80	15,16
E-Module, dyn.	2,2	40	249	2,75	35	32,88	40	560	,96	292	7,73	40	618	,84	361	13,22
Heat expansion E-Module, dyn.	1,1	7	252	4,11	571	23,82	10	559		3159		10	628	1,51	3659	12,53
E-Module, dyn.	2,2	7	250	2,64	62	32,76	10	559	,97	294	9,21	8	619	1,48	360	13,44
WLF E-Module, dyn.	1,1	10	245		505											
TWB E-Module, dyn.	1,1	20	254		443		10	559	1,70	3159	11,85	20	623		3709	
							20	562		3095						
E-Module, dyn.	2,2	20	250		34		20	564		318		20	622		372	

Figure 16: Statistical evaluation of the measurements

7. General remarks on heat transmission

The total heat rate $\dot{Q}_t$ transported through an insulation is composed of several portions. The fist portion is heat conduction through the solid material $\dot{Q}_s$. It is only depending on the thermal conductivity of the material. The second portion results from the transport through the gas within the pores or spaces of the insulation $\dot{Q}_g$. Thermal radiation $\dot{Q}_r$ between the surfaces of the cells is the third portion. The thermal conductivity through the gas may be enhanced due to natural and free convection. These part are

The influence of the gas within the insulation on the heat conduction caused by temperature changes is rather low. Major changes could arise in case of chemical reactions between the gas and the solid. Thus the materials used must be adapted to the media. In order to reduce the heat losses of the ducts materials with low thermal conductivities may be utilised or insulating systems with a low portion of metal may be designed.

The gas conductivity is fixed with the choice of the medium. In the British and French gas cooled reactors carbon dioxide was used as the coolant. In contrast to helium provided for the High Temperature Gas Cooled Reactors the gas conductivity of the CO_2 is lower by o factor of 5 to 6. The advantage of noble gas helium, however, is the independency on pressure. Applying air or carbon dioxide the insulating systems are more sensitive against pressure gradient. Furthermore natural convection will cause higher thermal fluxes at elevated pressures as will be shown later. By means of suitable constructive measures, e. g. avoiding gaps, the permeability and thus the through flow causing high thermal fluxes and temperature peaks on the pressure bearing walls may be reduced.

Thermal radiation is particularly important for insulation at high temperatures. Contrary to carbon dioxide helium as noble is not radiant itself. This portion, however, will be low in any case.

Corresponding to the explanations made before the total heat rate $\dot{Q}_t$ is roughly the sum of the different portions as follows

$$\dot{Q}_t = \dot{Q}_s + \dot{Q}_g + \dot{Q}_{c1} + \dot{Q}_{c2} + \dot{Q}_r \,. \qquad (1)$$

Summing up the portions of convection to $\dot{Q}_c$ leads to

$$\dot{Q}_t = \dot{Q}_s + \dot{Q}_G + \dot{Q}_c + \dot{Q}_r \,. \qquad (2)$$

The complicated heat transfer behaviour is resumed in an over-all heat conduction coefficient λ_{eff}, which is defined in form of the Fourier equation

$$\dot{Q}_t = \frac{\lambda_{eff}}{d} \cdot \Delta T \cdot A \,, \tag{3}$$

where ΔT is the temperature difference between two solid surfaces to be overcome in the direction of the thermal flux, A is the corresponding area, d the difference between both surfaces and λ_{eff} the effective thermal conductivity. Equation 3 strongly stands for flat surfaces. It can easily be shown that the deviation is less than 1 % using flat instead of curved surfaces in case of duct or vessels. Division by the area A leads to the heat flux

$$\dot{q}_t = \frac{\lambda_{eff}}{d} \cdot \Delta T \,. \tag{4}$$

It was the aim of numerous investigation to determine the effective thermal conductivity by means of theoretical considerations or experimental investigations. It offers the possibility to compare the quality of different insulation. A comparison of the thermal fluxes would lead to a wrong assessment. Still better than a comparison of the conductivities is a comparison of nondimensional numbers, e. g. the Nusselt-number. In literature two numbers are defined. The first one is the ratio of the effective thermal conductivity to the conductivity without any convection within the insulation, see equation 5

$$Nu = \frac{\lambda_{eff}}{\lambda'_{eff}} \,. \tag{5}$$

Is Nu corresponding to this equation greater than 1, yields the difference Nu – 1 as the natural convection. This ralation is by v. der Weyden [WEY71], Kinkead and Pitchfort [KIN69], Lakin [LAK71] and Furber and Davidson [FUR69]. Because it is very difficult or nearly impossible to suppress any gas movement within insulating systems even at ambient pressure other authors prefer another definition, which is indeed not in accordance with the theory. It is, however, easier to handle. After this relation Nu is the ratio of the effective thermal conductivity to the gas conductivity λ_g as follows

$$Nu = \frac{\lambda_{eff}}{\lambda_g} \,. \tag{6}$$

Particularly in Saclay/France this equation was used. Also in the following this equation will be utilised.

The governing characteristic number for free convective flow in gaps is the R, defined as a Rayleigh-number Ra defines as a product of Grahof-number Gr and Prandtl-number Pr. It is defined as

$$Ra = Gr \cdot Pr = \frac{g \cdot \beta \cdot \Delta T \cdot x^3 \cdot \rho^2 \cdot c_p}{\eta \cdot \lambda} \,. \tag{7}$$

The terms are

g gravity,
fluid density,
coefficient of thermal expansion for ideal gases,
ΔT temperature difference,
x gap width,
dynamic fluid viscosity,
thermal conductivity and
c_p specific heat capacity.

The orientation as well as the direction of heat flow is the gaps or cells are of importance for the natural convection. Only for horizontal gaps heated from below there exist a critical Ra-number up to which heat is transported only by conduction. The boundary layer value is in the range between 1700 – 2000. In this case the Nu-number which denotes the increase of heat transfer by convective motion is equal to unity. Also for vertically orientated gaps such a boundary value seems to exist.

A relation of Kraußold [KRA34] fits published results of Mull and Reiher [MUL39], Beckmann [BEC31] and Schmidt [SCH27] for vertical and horizontal, cylindrical and flat gaps may be represented very well. The critical Ra-number seems to be 1700, too. The gaps investigated were larger than 9 mm. Narinski and Sheinin [NAR69] realised an enhancement of the thermal conductivity for vertical gaps lower than 9 mm due to convection. The thickness of the boundary layers could not be neglected compared with the gap dimensions. The maximally admissible gap width can be calculated from formula 7. It is advantageous to start the computation at the cold side of the insulation, in order to catch the most unfavourable case.

Under the assumption of the same pressures p, temperature differences ΔT and gap widths x the free convection is mainly depending on the molecular weights M of the gases used. A comparison between helium and carbon dioxide yields

$$\frac{Ra_{He}}{Ra_{CO_2}} = \left(\frac{M_{He}}{M_{CO_2}}\right)^2 \cdot \left(\frac{\eta_{CO_2}}{\eta_{He}}\right)^2 \cdot \frac{Pr_{He}}{Pr_{CO_2}} . \qquad (8)$$

As the ratio of molecular weight of helium and carbon dioxide is 1:11, one obtains for the case of helium as the coolant much smaller Ra-numbers. Assuming the same maximal Ra-number and the same conditions for both gases to be compared, for instance ΔT = 200 K and p = 40 bars, the gap width for helium is calculated to be four times greater than for carbon dioxide as described by Knirsch and Schmiedel [KNI67]. Thus the disadvantageous influence of the high thermal conductivity of helium is almost, but not fully compensated.

Another regard of the Ra-number after equation 7 yields an important result. Keeping the properties with the exception of the pressure independent on the pressure as helium is a noble gas and takes the dependency on the temperature according to the kinetic gas theory as

$\eta \sim T^{1/2}$, $\lambda \sim T^{1/2}$, c_p = constant and $\beta = \frac{1}{T}$, the Ra-number may be given as

$$Ra \sim \Delta T \cdot x^3 \cdot \frac{p^2 \cdot M^2}{T^4}, \qquad (9)$$

see e. g. Gröber, Erk and Grigull [GRÖ63]. This relation shows, that an insulation with no gas movement inside due to convection is quite safe against convection in case of higher temperatures. Also in case of elevated temperature differences ΔT mostly the power T^4 of the denominator will overbalance. That means that the natural convection will increase with the square of the pressure an decrease with increasing absolute temperature. If an insulation is very sensitive against natural convection experiments at high temperatures should be excluded. For this case investigations at high pressures are recommended. Doing so the influence of thermal radiation, however, cannot be realised.

As will be shown in this report fibrous materials play an important role for insulating purposes. There exist a lot of relations to calculate the heat transport in such materials which, indeed are basing on simplifications and certain assumption. >In the simplest case the effective thermal conductivity may be written after equation 2 as sum. It is

$$\lambda_{eff} = \lambda_s + \lambda_g + \lambda_c + \lambda_r \qquad (10)$$

The single parts are explained before. This notation is often found, e. g. at Th. E. Schmidt [SCH61] and Larkin and Churchill [LAR59]. Sometimes as e. g. at Koglin [KOG67], who the heat transport in foam investigated or at Hager and Steere [HAG67] the portion due to heat conduction are concentrated. Such a separation as given by formula 10 is not allowed in a strict physical sense, because the single portions are interacting. Depending on the model used describing the configuration of the fibres relation 10 will change considerably. The single portions do not appear any longer as terms of a sum. An often used is the plate model. Likely Nusselt [NUS13] has applied first such a model. It is based upon the assumption that the structure exist of rigid plates, which are arranged with regular distances. The space between the plates is filled with gas. In the case of fibrous materials the configuration is random or regular. The thermal flux is perpendicular to the plates. Furthermore a constant fibre diameter δ is assumed. Each plate formed by the fibres is of the same diameter as that of the fibres. The insulation must not contain any loose particles, because they may influence the transmittance. Nusselt assumes, that the heat will be transported in parallel due to conduction through the rigid material λ_s and thermal radiation λ_r and in series due to conduction through the gas λ_g. Together with the densities of the solid ρ_s and gas ρ_g these assumptions lead to

$$\lambda_{eff} = \frac{1}{\left(1-\frac{\rho}{\rho_s}\right)\cdot\left(\frac{1}{\lambda_g+\lambda_r}\right)+\frac{\rho}{\rho_s}\cdot\frac{1}{\lambda_s}}. \qquad (11)$$

Eucken [EUC32] applied a relation for thermal conductivity calculations of refractory materials given already by Maxwell which had been deduced in order to determine the electric resistance of mixtures consisting of two compounds. The gas containing pores of the material is assumed to be of spherical shape and uniformly distributed within the solid. If in contrast to Eucken the portion of radiation is also regarded as done by Thipgen and Short [THI59] one gets

$$\lambda_{eff} = \frac{\frac{\rho}{\rho_s} + \frac{3}{2 \cdot \lambda_s + \lambda_g + \lambda_r} \cdot \left(1 - \frac{\rho}{\rho_s}\right) \cdot \left(\lambda_g + \lambda_r\right)}{\frac{\rho}{\lambda_s \cdot \rho_s} + \frac{3}{2 \cdot \lambda_s + \lambda_g + \lambda_r} \cdot \left(1 - \frac{\rho}{\rho_s}\right)} . \qquad (12)$$

Verschoor, Greebler and Manville [VER51] applied the plate model with irregularly distributed fibres within each layer. If each fibre is surrounded by gas the heat transmission that one of the gas. Because the fibre content is low and the thermal conductivity of the fibres λ_s compared to the conductivity of the gas high the effective thermal conductivity may be calculated after the following relation

$$\lambda_{eff} = \frac{\lambda_g + \lambda_r + \lambda_c}{1 - \frac{\rho}{\rho_s}} + \lambda_s' . \qquad (13)$$

The term λ'_s takes into account the low heat conduction due to the irregular contact of the fibres.

Thipgen and Short [THI59] refer to a model which is similar to a crossed heat exchanger.The fibres of each layer are randomly orientated. They are parallel each other. Their distance is constant. The adjacent layers are staggered 90 °. A similar layout is used by Strong, Bundy and Bovenkerk [STR60].

The widely spread meaning that thermal radiation would solely occur at high temperatures is not true at least for fibrous materials. Published results show that already at low temperatures, e. g. ambient temperature, a measurable portion accounts for heat conduction. After Poltz [POL62] it is very important always regard the thermal radiation during conductivity measurements. At high radiation fractions the measured total thermal conductivity is in particular dependent upon the thickness of the sample. Furthermore it is a function of the surface emission and the shape of the sample.

With the emission coefficients of the plates ε_1 and ε_2 which enclose the sample to be tested and the Stefan-Boltzmann constant σ the heat transmitted by thermal radiation can be evaluated by means of

$$\dot{q}_r = \frac{\sigma \cdot \left(T_1^4 - T_2^4\right)}{\frac{1}{\varepsilon_1} + \frac{1}{\varepsilon_2} - 1} . \qquad (14)$$

It was assumed that the sample is flat and thus the areas of both sides are of the same site. In addition the material may not absorb. In the case of equal emission coefficients for both sides equation 14 leads to

$$\dot{q}_r = \frac{\sigma \cdot \left(T_1^4 - T_2^4\right)}{\frac{2}{\varepsilon} - 1}. \tag{15}$$

If the temperature difference $\Delta T = T_1 - T_2$ is small the term $T_1^4 - T_2^4$ may be written as

$$T_1^4 - T_2^4 \cong 4 \cdot T^3 \cdot \Delta T.$$

Here T is the mean temperature formed by both temperatures T_1 and T_2. Thus equation 15 may be expressed by

$$\dot{q}_r = \frac{4 \cdot \sigma \cdot T^3 \cdot \Delta T}{\frac{2}{\varepsilon} - 1}. \tag{16}$$

Using equation 4 the thermal radiation conductivity may be written as

$$\lambda_r = \frac{4 \cdot \sigma \cdot T^3}{\frac{2}{\varepsilon} - 1} \cdot d. \tag{17}$$

In case of black boundary surfaces $\varepsilon = 1$ and thus the denominator 1.

In the following some relations found in the literature are presented without any further comments. Only the authors are mentioned.

Nusselt [NUS31]:

$$\lambda_r = 4 \cdot \sigma \cdot T^3 \cdot \delta \cdot \left(\frac{\rho_f}{\rho} - 1\right). \tag{18}$$

Hager and Steere [HAG67]:

$$\lambda_r = 4 \cdot \sigma \cdot T^3 \cdot \delta \cdot \frac{\rho_f}{\rho}. \tag{19}$$

Strong, Bundy and Bovenkerk [STR60]:

$$\lambda_r = \sigma \cdot T^3 \cdot \delta \cdot \frac{\rho_f}{\rho} \cdot \frac{H \cdot \pi}{\varepsilon'}. \tag{20}$$

and

$$\lambda_r = 4 \cdot \sigma \cdot T^3 \cdot \frac{4}{3} \cdot L. \tag{21}$$

Van der Held [HEL53]:

$$\lambda_r = 4 \cdot \sigma \cdot T^3 \cdot \frac{4}{3} \cdot \frac{n^2}{k}. \tag{22}$$

Cznerny and Genzel {[CZE52]:

$$\lambda_r = 4 \cdot \sigma \cdot T^3 \cdot \frac{4}{3} \cdot \frac{n^2}{m^2}. \tag{23}$$

Verschoor, Greebler and Manville [VER51]:

$$\lambda_r = \pi \cdot \frac{1}{\varepsilon'^2} \cdot \sigma \cdot T^3 \cdot \frac{\delta}{\rho/\rho_f}. \tag{24}$$

Thipgen and Short [THI59]:

$$\lambda_r = 4 \cdot \sigma \cdot F_a \cdot F_\varepsilon \cdot d \cdot T^3. \tag{25}$$

A more detailed summary is given by Bröckerhoff [BRÖ73].

8. General remarks on depressurisation

As far as known at first E. Schmidt [SCH65] dealt with the problem of rapid depressurisation. He had to estimate the force acting on a vessel of a water cooled nuclear reactor in case of a crack of the wall and the sudden outpouring of the coolant. Further investigations were done by Aranovitch et. al [ARA71a] and [ARA71b] and Aranovitch [ARA72] in Ispra/Italy on a foil insulation for a helium cooled reactor.

After Schmidt [65] sound velocity is given by

$$a_s = \sqrt{\frac{2}{\kappa + 1}} \cdot \sqrt{\kappa \cdot R \cdot T_0}. \tag{26}$$

R is the gas constant, κ the adiabatic exponent ant T_0 the temperature at beginning. Up to the critical pressure ratio

$$\frac{p_{sa}}{p_{0a}} = \left(\frac{2}{\kappa + 1}\right)^{\frac{\kappa}{\kappa - 1}} \tag{27}$$

there exist sound velocity. The pressures are absolute ones. p_s is the pressure in the narrowest cross section, p_0 the pressure at the beginning, when the time is 0. p_{aa} is the ambient pressure. When psa $>$ p_{aa} the velocity in narrowest gap is equal sound speed if

$$p_{0a} > \left(\frac{\kappa+1}{2}\right)^{\frac{\kappa}{\kappa-1}} \cdot p_{aa} . \tag{28}$$

When the cross section of the crack is no longer fully filled with the coolant the pressure will decrease from the initial pressure to the transient pressure $p_a(t)$ and at least to the ambient pressure. Taking into account the decreasing mass within the vessel one obtains the pressure ratio $\pi(t)$

$$\pi(t) = \frac{p_a(t)}{p_{0a}} = \left(\frac{1}{1+a\cdot t}\right)^{\frac{2\kappa}{\kappa-1}} \tag{29}$$

with

$$a = \frac{\kappa-1}{\kappa}\cdot\left(\frac{2}{1+\kappa}\right)^{\frac{1}{\kappa-1}}\cdot\left(\frac{2\kappa}{1+\kappa}\right)^{\frac{1}{2}}\cdot\frac{A_v\cdot f_v}{V}\cdot(R\cdot T_0)^{\frac{1}{2}} . \tag{30}$$

A_v defines the open cross section of the crack. f_v means a factor which regards the contraction of the stream, V is the volume of the vessel. The differential quotient dp(t)/dt yields with equation 31 for t = 0 the maximal value

$$\left.\frac{dp_a(t)}{dt}\right|_{t=o} = -p_{0a}\cdot\frac{A_v\cdot f_v}{V}\cdot\left(\frac{2}{1+\kappa}\right)^{\frac{1}{\kappa-1}}\cdot\left(\frac{2}{1+\kappa}\right)^{\frac{1}{2}}\cdot(R\cdot T_0)^{\frac{1}{2}} . \tag{31}$$

It is called the depressurisation transient. As shown by equations 30 and 31 it may mainly be influenced by the initial pressure, the free cross section and the factor f_v if the experimental conditions, e. g. medium initial temperature and volume are not changed.

Comparing two depressurisation rates of different gases, e. g. helium (he), air (a) and nitrogen (N_2) at the same initial conditions one obtains the following values:

$$\frac{\left(\frac{dp}{dt}\right)_{He}}{\left(\frac{dp}{dt}\right)_{L}} = 3{,}38 \qquad\qquad \frac{\left(\frac{dp}{dt}\right)_{He}}{\left(\frac{dp}{dt}\right)_{N_2}} = 3{,}33$$

The main reason for the approximately 3.3 higher rates in case of helium is the gas constant which is about 7 times higher, that is 2078 J/(kgK) to 287 J7(kgK). The adiabatic exponents are nearly identical. Their influence on the result is rather small.

The above mentioned permeability is according to Darcy

$$B = v \cdot \frac{1}{dp/dy} \cdot \eta \,. \tag{32}$$

In this relation v is the velocity within the pores of the insulating material of the fluid, η the dynamic viscosity and dp/dy the pressure gradient over the thickness dy of the insulation. Their unit corresponds to that of an area. If the pressure difference is known the permeability can be determined.

Figure 17 shows a device as used in France or great Britain for investigations on insulation, see [WEY71]. The gap to be insulated is filled with fibrous material. In general it proves a homogeneous permeability. In addition for further explanations a

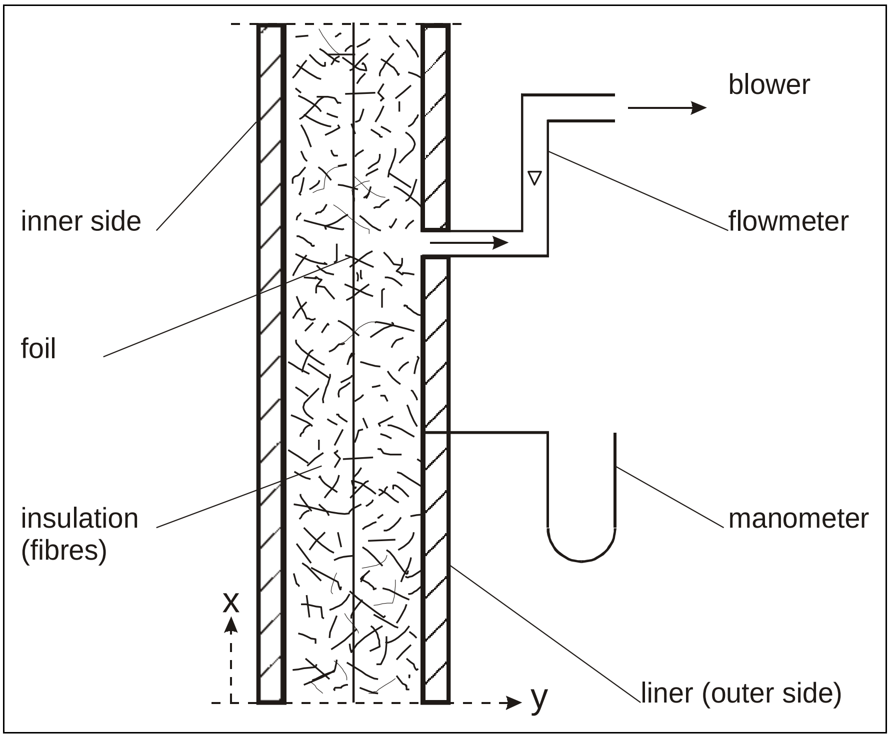

Figure 17: Assembly for permeability measurements

foil is also drawn. If the pressure gradient dp/dy and the absolute pressure are measured by means of pressure transducers or flow meters and the temperature to determine the viscosity η is known B may be calculated. After Davidson [DAV67] mostly two permeabilities are defined, one perpendicular to the foil, the other one in parallel to it. The directions x and y are specified in the figure. If one splits the pressure difference in a term dependent on the viscosity and a dynamic portion it can be written as

$$\frac{dp}{dy} = \eta \cdot \frac{v_y}{B_y} + C_y \cdot \rho \cdot v_y^{\,2}. \qquad (33)$$

C_y is a pressure drop coefficient. From a permeability change before and after depressurisation conclusion may be drawn on the mechanical behaviour of the insulation and possible damages. In case of foil insulation it is advisable only to consider the permeability perpendicular to the foil.

9. Computer programs for shaped fibre structures

The whole package of tasks for the computational investigation of shaped fibre structures comprises two major subtasks:

- In a first step, states of stress and strain were to be determined by existing approaches on simple block geometries under thermal load and compared with the corresponding test results.

- Secondly, the shaped fibre structure was to be optimized for later use in the test section of the central riser of the URKO heat exchanger.

The test results were compared with the calculation results obtained using the IAGUAR-FiniE program (Figures 18,19).

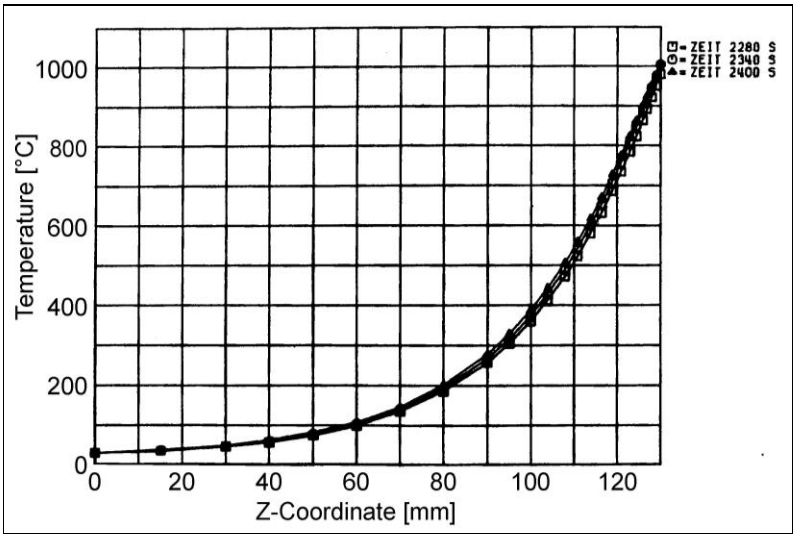

Figure 18: Temperature distribution
MVP-550-Cross section

The stress analysis is adapted on a block geometry according to the Manufacturer test arrangement and boundary conditions. This means that the block is loaded on one side in the longitudinal direction with a temperature transient and the opposite side is left at room temperature. All the other sides were regarded as ideally insulated free end areas. The analyses for temperature and stress determination were performed with the following experimental data:

transient T = 1477 K/h

cracking time t_R = 40.8 min

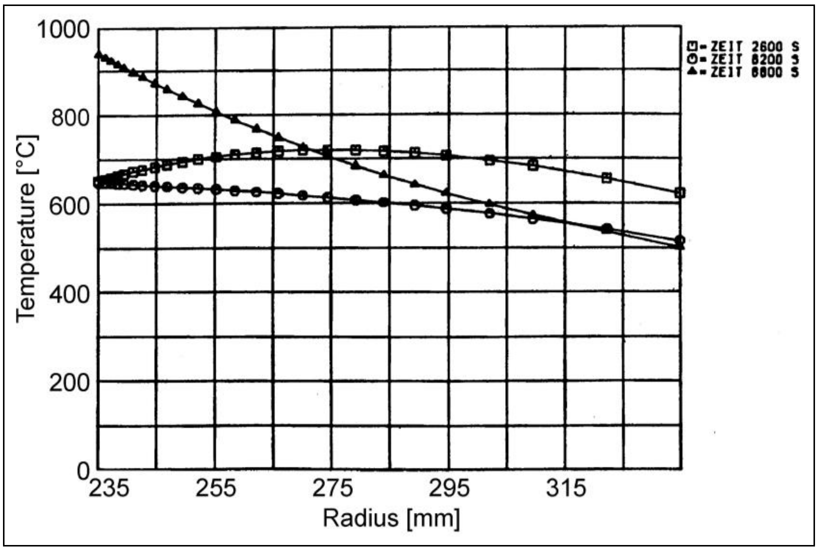

Figure 19: Stress distribution over the insulation
Temperature vs. radius

In the comparison, the failure of the MVP III 550/1600 S material due to exceeding one of the ultimate strengths in the fibre or transversally to the fibre was assumed. For the theoretically determined stress values, the ultimate tensile stress was found to be exceeded by 27.5 % at the time t_R = 40.8 min transversally to the fibre, which may be interpreted as a conservative fracture statement compared to the test results. It can furthermore be concluded that the direction of cracking was computationally confirmed and that in comparison to the measured cracking time there is good agreement between the largest calculated normal stress and the ultimate strength.

For the purpose of optimizing the shaped MVP III 1600 S fibre structures, stress analyses were performed and transient temperature distributions determined taking the raw block sizes for several geometrical variations into account.
The materials data from corresponding tests were included here.

Due to the temperature distribution and the stress analyses performed for optimizing the shaped fibre structures, the following variants proved (at that time) feasible:

a) pitch T = 6 = a = 60°
height h = 283.33 mm

b) T = 7 = a = 51.4°
h = 283.33 mm

c) T = 6
h = 212.5 mm

d) T = 7
h = 310 mm

e) T = 9 = a = 40°
h = 500, 600 and 700 mm

10. History of different test concepts
Test facilities, samples and results

In the following investigations and results regarding the thermal and depressurisation behaviour will described. In addition also experiments with respect to materials, e. g. fibres and ceramics will be presented. Because of the big number of publications the following presentation may not be complete. Only the most important test facilities and results will be selected. Detailed descriptions may be found in the literature.

10.1 Thermal behaviour

The thermotechnical investigations dealt with the thermal conductivity measurement of small samples and the test of nearly full-scale components. In this case thermal losses, thermal conductivities, temperature distributions and so on were measured.

10.2 Sections of insulation

The knowledge of the thermal conductivity or their single portions is of importance for designing complete insulation systems, because their test is very time consuming and expensive. It proved best to gain these single portions on small samples. Therefore two test facilities were built in which the investigations could be done faster and cheaper than in big facilities.

In order to determine thermal conductivities two procedures are used in practise. In a way whether the temperature distribution within the specimen is constant or not they are called steady-state or transient. Because the transient methods are nor suitable to study the effect of thermal radiation the steady-state procedure was applied. The most known is the so-called Poensgen method after Poensgen [POE12] basing on guarded hot plates. Set-up and handling are according the standard [DIN79]. The corresponding American standard is defined in [AST78]. Differing from this method also the steady-state cylinder and sphere measurement procedures exist. They are basing on a simple solution of Fouriers´ heat conduction equation.

The test facility is schematically shown in Figure 20. The measurement set-up was arranged in a vessel with an inner diameter of 1000 mm and a height of 600 mm. Two test facilities were available. The older one was designed for experiments at ambient pressure, the second one for pressures up to 60 bars. The heating unit consists of the main or central heater and the auxiliary heaters, see Bröckerhoff [BRÖ75a] and Tebroke [TEB92]. In general the samples to be tested were positioned between the central heater and the top counter heater, since primarily the influence of natural convection should be investigated. In this case the temperatures of the main heater and bottom counter heater were kept at the same level. The vacuum pump enabled a vacuum of a few torrs which was sufficient for investigations of the radiation conductivity. By means of the valve the teat gases mainly helium were fed into the vessel. The gas pressure was controlled by a manometer.

In the guarded hot plate apparatus either round or square plates are needed after DIN, see Büttner et al. [BÜT84]. In the Institute of Wärmeschutz square plates were used according to Zehender [ZEH64]. Thus a more constant thermal flux was attained. The influence of the temperature distribution of the plates due to the radial heat losses was deliberately accepted.

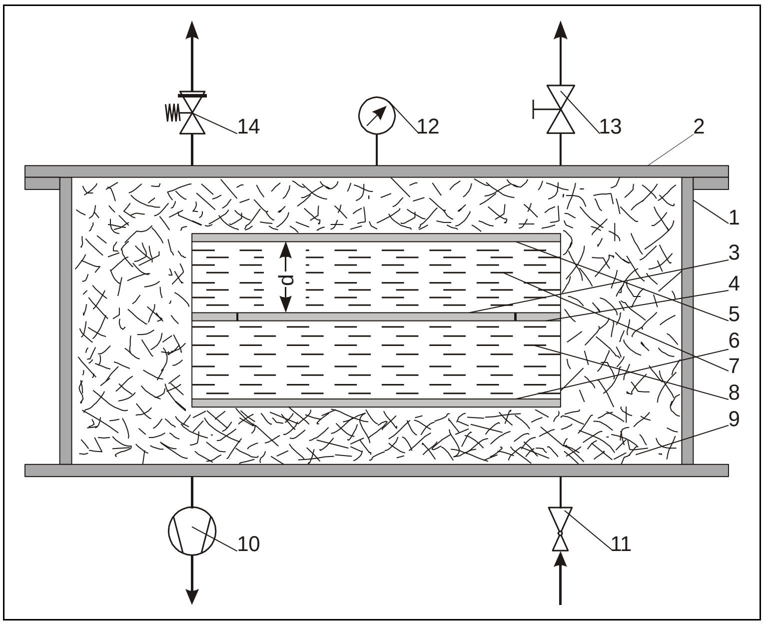

(1: vessel, 2: lid, 3: main heater, 4: guard heater, 5: top guard heater, 6: bottom guard heater, 7: sample 1, 8: sample 2, 9: insulation, 10: vacuum pump, 11: valve, 12: pressure transducer, 13: outlet valve, 14: safety valve)

Figure 20: Apparatus for thermal conductivity measurements of small samples

Often the heaters consist of copper and insulated heating elements put into milled nuts and cemented by a good heat ducting material. Because of the high temperatures up to 900 °C on the hot side plates made of stainless steel were used. In order to avoid blasting of the heating elements each heating unit consisted of two plates with the heating wire in between. The elements were made of uninsulated wires which diameter was 2 mm. They were coiled like a meander.

The following four figures show the heating units in more detail. Figure 21 presents the set-up schematically. each system consists of not insulated wires, two electrical insulators and two metallic plates. The length of the wires and the size of the plates had to be adapted to the requirements.

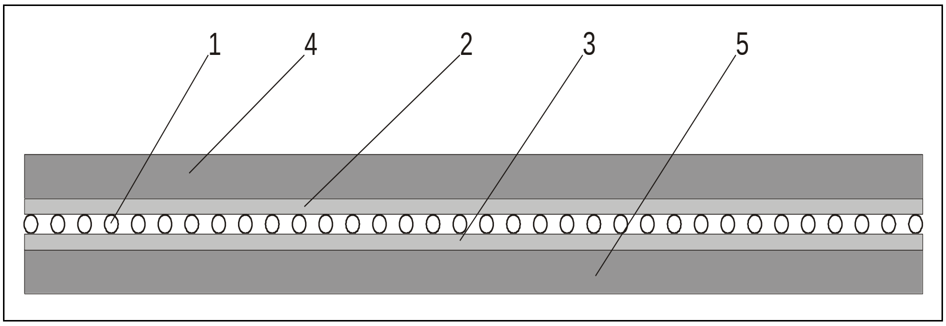

(1: heating element, 2: top electrical insulator, 3: bottom electrical insulator, 4: top plate, 5: bottom plate)

Figure 21: Set-up of a heating unit

A view onto the central heater ,the surrounding guard heaters and the thermocouple positions is given in Figure 22. The main heater is of a square shape with an edge length of 250 mm. The dimensions of each guard heater is 100 mm x 250 mm. The thickness of the heating units consisting of stainless steel was 3 mm. In order to determine temperatures in the centre of the central heater and near the edges of the five heaters Ni-NiCr thermocouples were used. Their positions and distances from the edges are given in the figure.

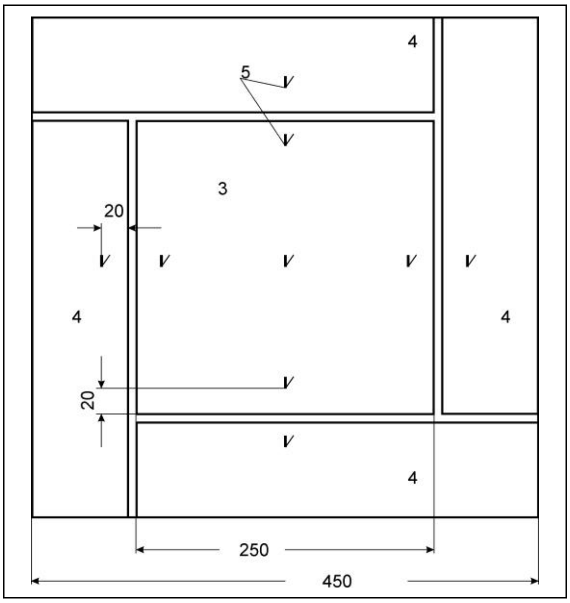

Figure 22

As the four thermocouples at the edges were not sufficient for adjusting the power a series of thermocouples was used near the edges, see Figure 23,. in consisted of brazed thermocouple wires. Thus at the soldering joints a new thermocouple was formed with in total 16 couples. By these means the electric power of the guard

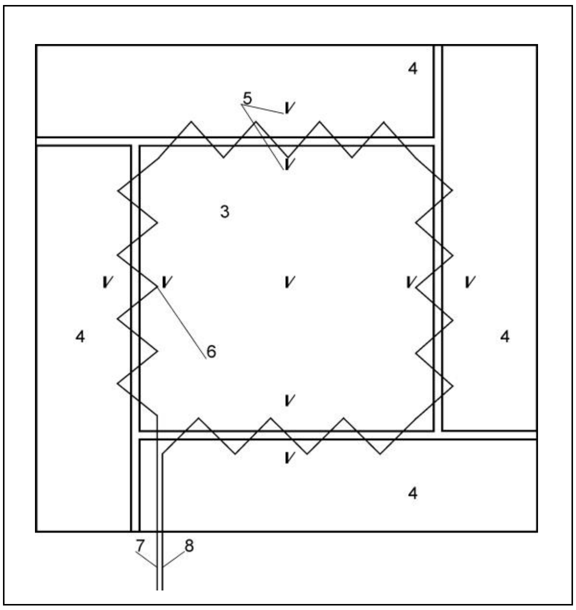

Figure 23

heaters could be controlled by a stabiliser. Furthermore the power was manually adjustable. A 1 mm thick Kaowool layer served as electric insulator between the plates and the series of thermocouples.

The heating wires consisted of Kanthal. The diameter was 2 mm. It is a high temperature alloy made of 72 % iron, 22 % chromium, 5.5 % aluminium and 0.5 % cobalt. Its operating temperature is 1400 °C. The specific resistance is only weakly dependent on temperature.

Figure 24 illustrates the heating wires of the central and guard heaters. Their lengths were 7.5 m for the main and 2.2 m for each guard heater. For each of the top and bottom heaters the lengths were 24.75 m. After mounting of the assembly into the vessel at first the organic binder within the stuffed fibre insulation or the test sample was removed under air. For this purpose the heating units must be heated up to a temperature of approximately 400 °C. Otherwise the binder would have been deposit e. g. in the specimen causing the material to become electroconductive.

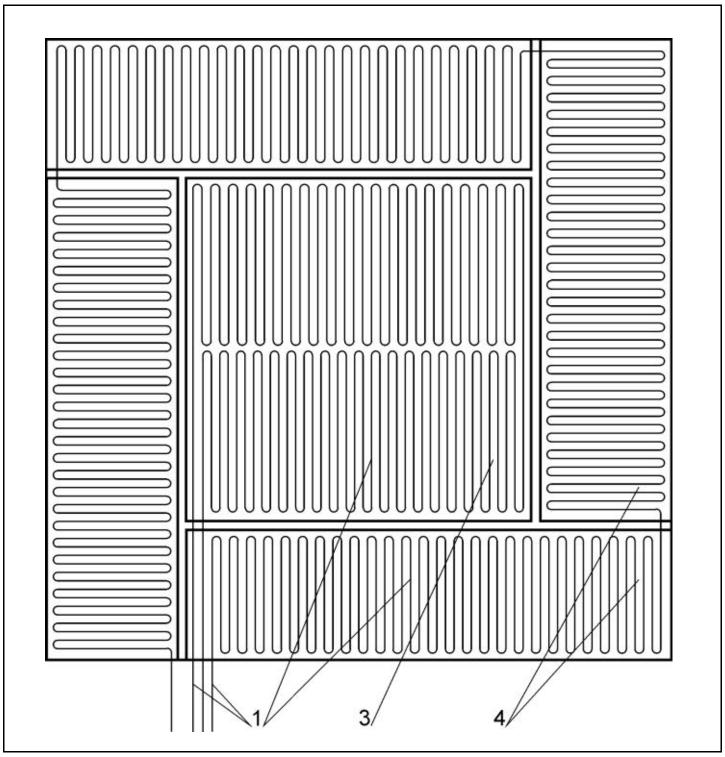

Figure 24

Each test series was started with experiments under vacuum followed by investigations with air. At last measurements in helium atmosphere were conducted. Besides the pressure the mean sample temperature averaged with the temperatures of the main and bottom heaters represents another parameter. The power supply of the three guard systems was done by alternating current. A stabilised power supply unit provided the main heater with direct current.

The temperatures of the central heater were increased in steps of about 100 K. Its power and also the power of the top guard heater was kept constant. The surrounding guard heaters were kept at the same temperature as that of the central heater. In this case there were no heat losses from the main heater to the surroundings. The thermal conductivity of the sample to be determined was calculated according to equations 3 or 4. Contrary to investigations of complete insulation systems described later on the heat passed the specimen was removed by means of free convection to the ambient air. Consequently it took at least two days to get steady-state conditions. The time could be estimated from the design dimensions and the Fourier-number (Fo) after Gröber et al. [GRÖ63]. Because of the low thermal conductivity the corresponding time for the vacuum experiments took about two weeks. The temperatures were digitally recorded. When their change was zero or about zero over a period of about eight hours the condition counted stationary.

Table 3 contains some data of fibrous materials which have been widely investigated.

Item	Main components	Fibre diameter / μm
Refrasil B1	99 % SiO_2	5 - 10
Kerlane	46 % Al_2O_3, 48 % SiO_2	2,8
Kaowool	45 Al_2O_3, 52 % SiO_2	2,8
Quartz et Silice	about poor SiO_2	?
Dynaflex	?	?
Fiberchrome	Chromium/aluminium silicate	?

Table 3: Fibres of various manufacturers

More detailed information about the products Dynaflex and Fiberchrome of Johns-Manville is not available. It may be assumed that also the main components are also Al_2O_3 or SiO_2. The composition of Kerlane and Kaowool is nearly identical. Also their fibre diameters are of the same order. Refrasil consists of approximately poor SiO_2. The density ρ_f of the substances used for manufacturing is unknown. For a rough estimation it is regarded to be 2200 kg/m^3.

Refrasil has been tested first in the vessel suitable for ambient pressure. The blanket has been delivered from the British company Darchem Engineering. The sample thickness was 50 mm. Thus the corresponding fibre density resulted 84 kg/m^3.

Figure 25 shows the measured thermal conductivities as sum of radiation and material conductivities in dependence on the average sample temperatures. The given results are valid for two different temperature differences. Detailed information is given by Bröckerhoff [BRÖ75a]. The portion of solid conduction is rather small. For comparison radiation conductivity calculated after equation 18 are plotted. The fibre diameter mentioned by the manufacturer yields too low conductivities. A nearly doubled diameter lead to an agreement between measured and calculated results.

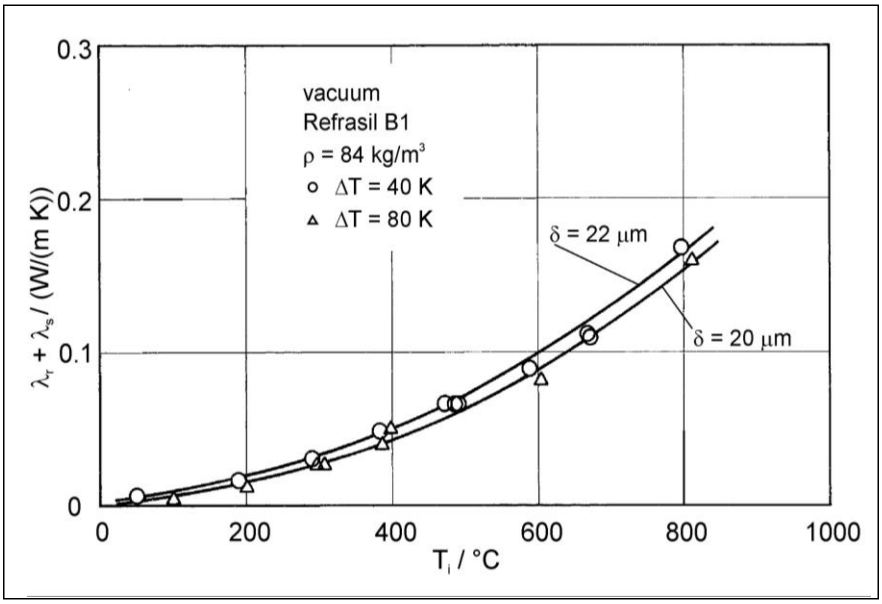

Figure 25

In Figure 26 results versus the mean specimen temperature are given for air and helium at ambient pressure. They are compared with conductivity values after Thipgen and Short [THI59]. The portions due to radiation and solid conductance are regarded. The gas conductivity was calculated after Hammeke et al. [HAM66] and Harth and may be observed using air as coolant. In the case of helium, however, both measured and calculated results agree rather well. This may be due to the smaller influence of free convection caused by the lower density.

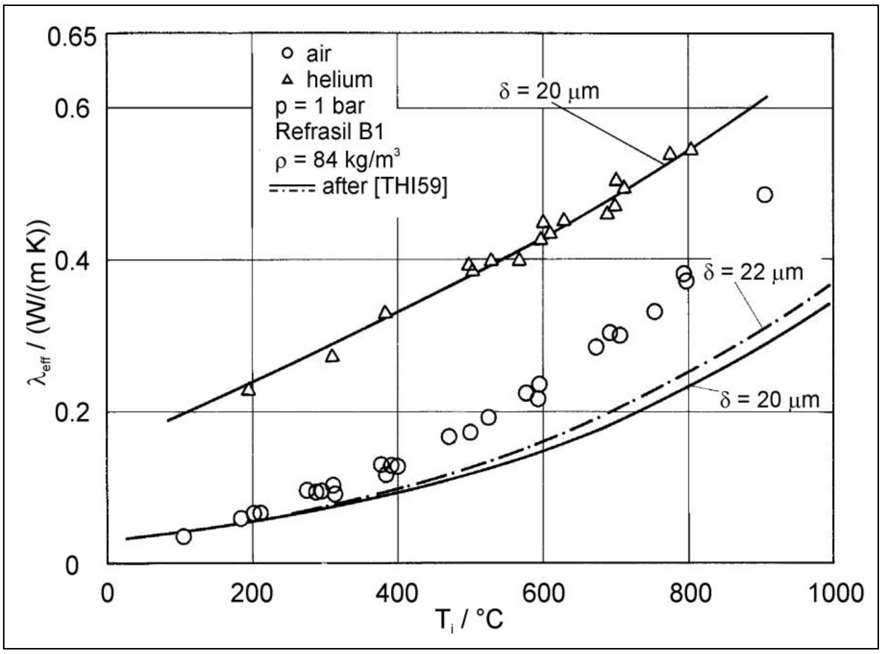

Figure 26

In Figure 27 measured conductivities are presented versus the average sample temperature for Kaowool. The results are valid for experiments as well in vacuum as in air and helium. The fibre densities were 95 kg/m^3 and 165 kg/m^3. Higher densities could not be achieved by means of the plate system chosen. Because of the low temperature differences of approximately 50 K the mean temperature within the specimen could be increased to about 900 K. In all cases the thermal conductivities are increasing with the sample temperature as already was observed before. For comparison results of the Ministry of International Trade and Industry (MITI) and Engineering Research Association of Nuclear Steelmaking (ERANS) in Japan [MIT79] are plotted. In the mentioned report the results obtained at the same conditions are presented within a band which regards the scattering. The density, however, was 192 kg/m^3. The fibres were arranged within a tube causing higher densities. The own results agree well with the other ones. The differences may be caused by different fibre densities. About the influence on thermophysical properties of insulation see Tye and Desjarlais [TYE83]

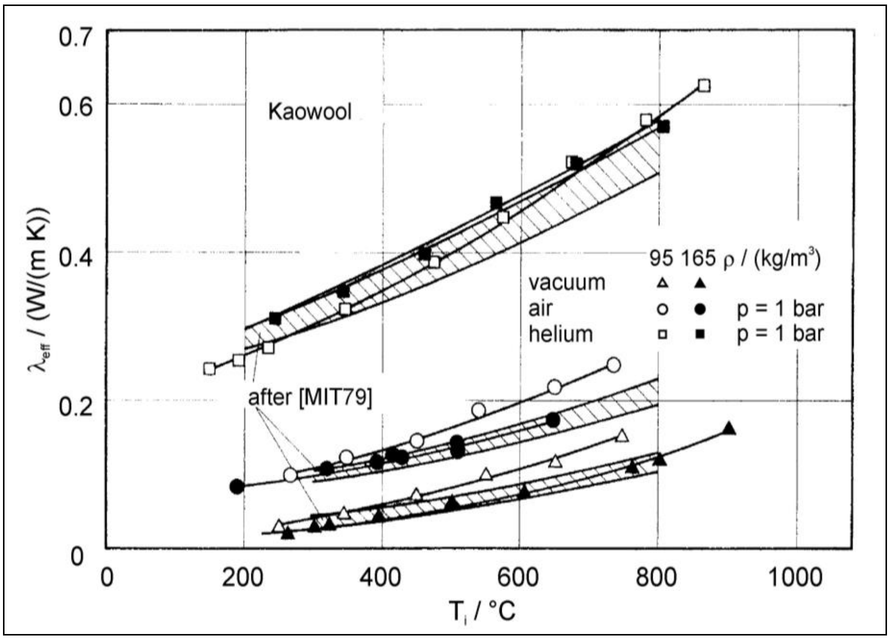

Figure 27

Following rigid ceramic materials were tested. In contrast to the fibrous materials they were mainly provided for the inner ducting shrouds. Because of their high temperature resistance they seemed to be more suitable than metals. In order to design insulation systems their thermal conductivities was needed. Plates, heating units and guard systems were not changed. The samples consisted either of only one piece, which covered main and guard heaters, or of five pieces, see Bröckerhoff [BRÖ81a] or Bröckerhoff [BRÖ83a].

Figure 28 contains effective thermal conductivities versus average sample temperatures. The results stand for helium as a coolant. The pressure was 1 bar. Comparing these results with the former ones at fist one notes the well higher conductivities and the different run of the curves. The results are decreasing with temperature while they increase with the main temperature in case of the fibrous materials due to the high content of gas causing increased thermal radiation. Because of the high thermal conductivities only low average sample temperatures could be achieved.

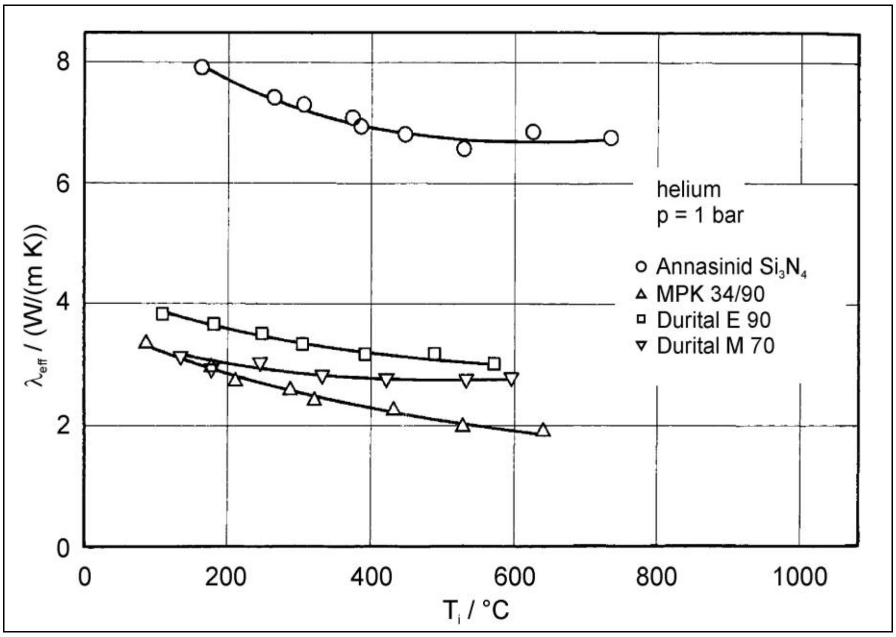

Figure 28

Silicon nitrite (Si_3N_4) with the trade name Annasinid showed the highest conductivities between 8 W/(mK) and 6.6 W/(mk). For this reason and because of the very difficult machining of this material it was eliminated very soon as a candidate. Also the remaining materials seemed to be improper, although their conductivities were much lower. The samples were not stable enough. Some of them decomposed during the experiments due to temperature load.

10.3 Complete insulating systems

In the following at first the various insulation will be described corresponding to the order of table 1. Their application will be mentioned, e. g. for vessels or pipes. In parallel a description of the test facilities used will be given.

10.3.1 Metallic insulation

10.3.A Foil insulation

The relatively wide space attended to the foil insulation seems to be justified in view of the development work primarily Great Britain. All prestressed concrete reactor pressure vessels operated till to approximately 1975 and cooled with carbon dioxide and some steel vessels were insulated with foil insulation. Also the steel pressure vessels of the power stations Latina in Italy and Tokai mura in Japan bear such insulation systems. The insulation of the last named plant has been damaged caused by aerodynamic loads. Hence parts of the insulation fall down from the ceiling and blocked a steam generator. The prototype of the Advanced Gas Cooled Reactor (AGR) in Windscale was insulated with a fibre insulation, also the Peach Bottom Reactor the first HTR in the United States. Manufacturer of this “Solami” called design was the Solar Division of Harvester Corporation. The insulation for the AGR in Windscale was made by the company Darchem Engineering. Another manufacturer was the Sud Aviation in France.

Figure 29 shows a sketch of a liner insulation for a prestressed reactor pressure vessel. The main components are the liner, a gas-tight skin, which is fixed to the concrete wall, thin foils consisting of stainless steel, wire mesh as spacer elements and cover plates at the hot side. Prior designs showed sinusoidal shaped foils as spacers. Lining the pressure vessels of the Magnox reactors in Great Britain alternately foils and spacer elements have been stacked, then covered with the cover plates and braced by screws. In general the edge width of the foils shown at the left side of the figure was 600 mm. Due to overlapping gas movement from one room into the other should be avoided. The wire meshs together with the foils should form small cells in which the gas was enclosed.

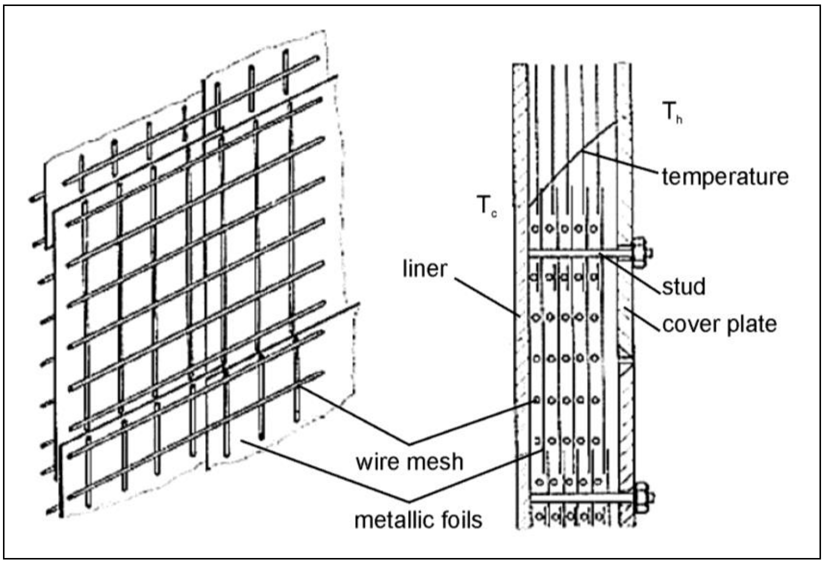

Figure 29

The insulation of the Oldbury reactor is presented in Figure 30 according to Furber, Hopkins and Stuart [FUR75]. The spacers of following designs consisted of so-called dimpled foils. In addition to the already spacers further plates were used in order to fix them. Contrary to the thin foils the cover plates contacted each other at the edges without overlapping. Initially only one central stud was used. Because of difficulties occurring during operation the design had to be modified. At the edges small plates and an additional stud were added. By these measures it was ensured that in case of a loose screw e. g. due to vibrations each cover plate was held by at least three studs. Nevertheless, this solution was not yet sufficient. later on four studs per each plate were used. The reactor in Hartlepool showed as could be seen and as was explained during an inspection cover plates with an edge width of 300 mm near the blower. The cover plates smaller by a factor of four were fixed by eight studs. In this region such high mechanical loads were expected that this expensive solution had to be taken. In addition the foils were protected by an acoustic skin which was positioned directly beneath the cover plates. This costly design was required from the Darchem point of view. The foils arranged in parallel largely suppressed the transmission of heat due to thermal radiation. Moreover, the metallic conduction was small because of the low portion of solid and the metallic conduction due to the high thermal resistance at the contact areas. Garrard and Salmons [GAR75] describe design and construction of insulation for the reactors in Hartlepool and Heysham. Indications of the insulation for the Wylfa power station is given by Williams [WIL71]

When designing an insulation in general the items thickness and number of foils may freely be disposed. Kinkead and Pitchfort [KIN69] tried to calculate the effective thermal conductivity λ_{eff} in dependence upon the foil number. In doing so the single conductivities must not just be added. In order to determine the part of natural convection a Ra number of 2000 was assumed, see equation 7. Thus gas movement should be excluded.

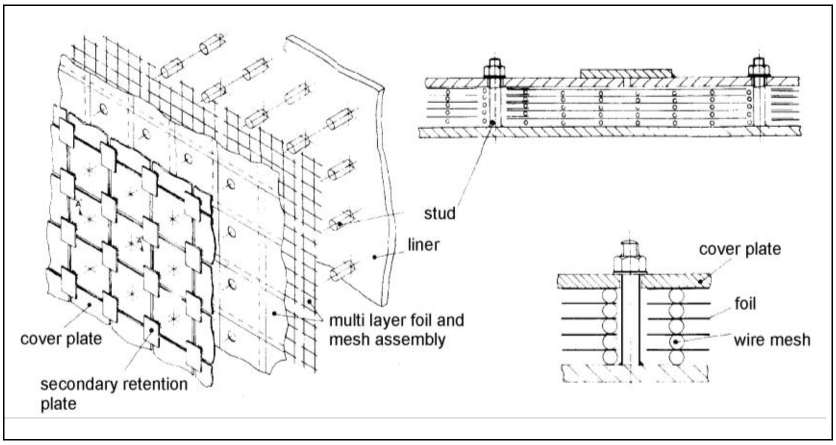

Figure 30

Figure 31 illustrates the effective conductivity of an insulation as function of foils for helium and carbon dioxide. The thickness of the insulation was 84.5 mm, the temperatures at the hot and cold sides were 380 °C and 60 °C, respectively. The mean pressure was 39.3 bars. Using high numbers of foils only an unimportant improvement of the heat damping coefficient can be reached. Furthermore, the percentage of free convection at the effective thermal conductivity is shown. Taking 20 foils this ratio is already zero in case of helium. That means that heat is only transported by radiation and conduction. Concerning carbon dioxide as a coolant even for a high number of foils the percentage of natural convection is considerable. The conductivity of the spacer elements were not taken into account. The presented results were not validated by measurements.

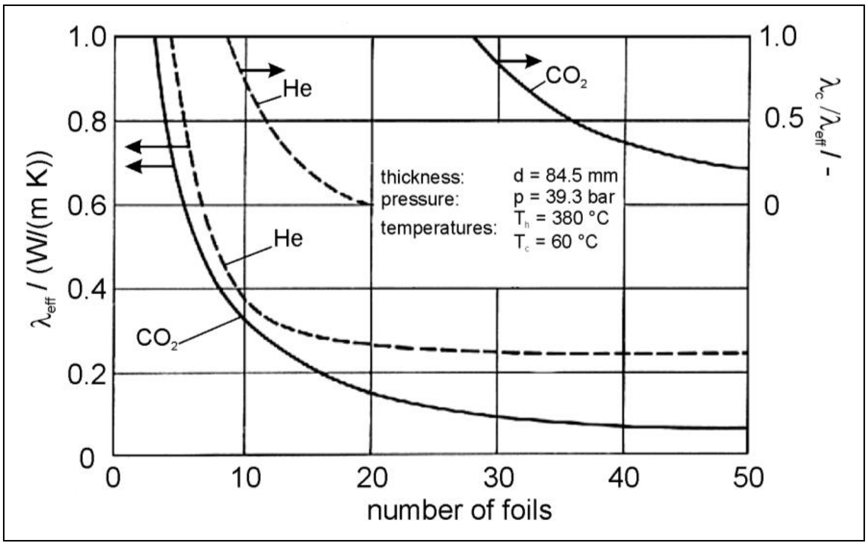

Figure 31

In Figure 32 left hand side the total heat flux of a foil insulation is presented as a function of the total thickness for helium. The parameter is foil number. Using seven foils an increase of the insulation thickness beyond 80 mm is of no use, as the heat flux cannot be reduced. At the right hand side the dependency of the heat flux on the pressure of helium is demonstrated again with the number of foils as parameter. The rise of heat losses with increasing pressure is due to the influence of natural convection. The Ra numbers of the layers at the cold outer side were within 10,000 and 80,000.

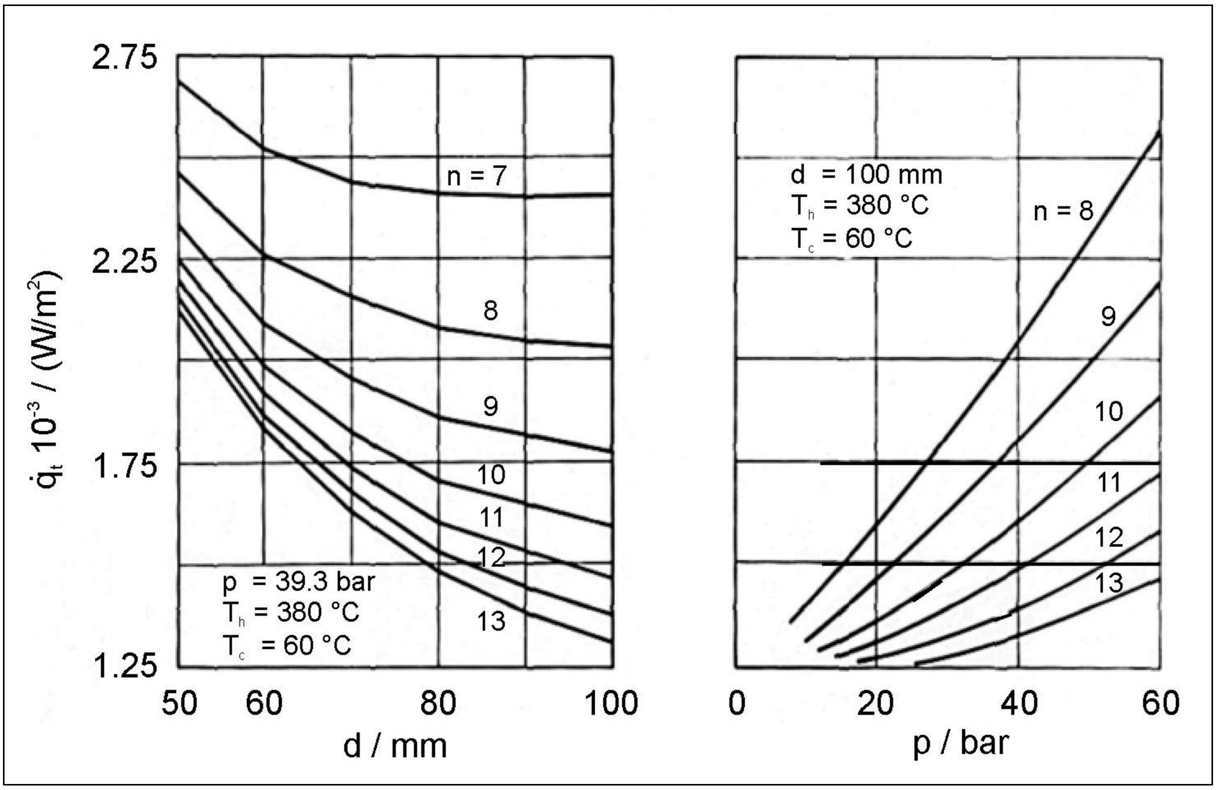

Figure 32

The occurrence of free convection within gaps of a foil insulation is demonstrated on the basis of experimental results as published by Cowap and Furber [COW67]. The manufacturer of this type of insulation, the Darlington-Chemical company, predicted the conductivity basing on experiments with carbon dioxide. The insulation was specially made for testing purposes. It did not correspond to that of the Oldbury reactor. The thickness of the sample consisting of 31 foils was 52.4 mm. The length was 2 m, the thickness of a foil 0,1 mm and the distance between two foils was 1.575 mm. During the experiments with carbon dioxide and helium the test section was in a horizontal position. In Figure 33 the temperatures along the hot and cold sides are given over the nondimensional height of the specimen x/L. The pressure was 37.2 bars. In vase of helium the temperatures are nearly identical. For carbon dioxide, however, there is an increase from 45 °C to 150 °C. At the hot side a strong temperature gradient may be observed in the region $0.1 \leq x/L \leq 0.4$. How far these results were influenced by the flanges and the lid could not be determined. For carbon dioxide the gaps were too wide. in the upper part of the figure the effective thermal conductivities are given versus the height. The efficiency is clearly affected near the flanges in case of carbon dioxide.

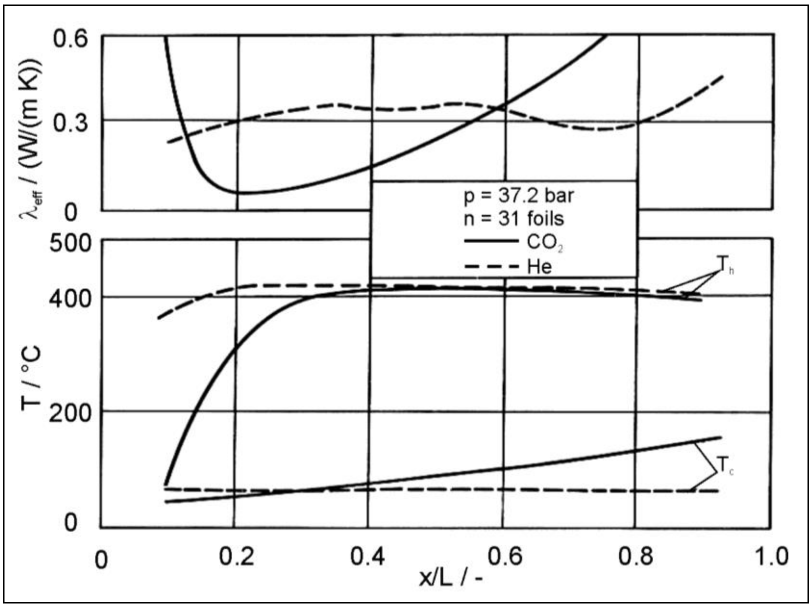

Figure 33

Figure 34 gives a comparison of calculated and measured values for the conductivity of a foil insulation as a function of temperature. The Darchem people predicted the conductivity for helium basing on experiments with carbon dioxide. Indeed Darchem used a different method in order to calculate natural convection. Basis of the results discussed were measurements of the permeability of the complete design. The full line represents the conductivity for a pressure of 40 bars. The experimental results given by Cowap and Furber are plotted for comparison. The agreement of calculated and experimental results is good. The unimportant dependency of the conductivity on pressure points to a small influence of natural convection. For comparison also the conductivity helium is shown which makes a contribution of about 75 %. The remaining 20 % are due to radiation, free convection and conduction through the metallic structure in equal parts.

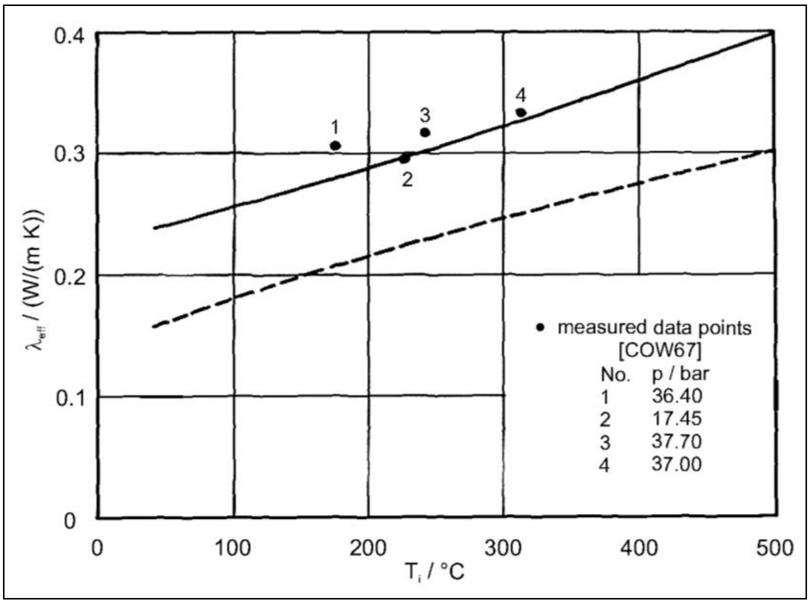

Figure 34

Further experiments were carried out by the Bertin company in France for the pressure vessel of the THTR in Hamm Uentrop in order of the previous BBK company, later on HRB. The experiments were conducted on reactor conditions. The temperature of the hot face was 200 °C, the pressure was 40 bars. The test facility is presented in Figure 35. It consisted of a cylindrical part and two hemispheric end sections. The heated helium was recirculated by means of a blower. The flow direction is indicated. Two samples of the Darchem company were tested simultaneously in the vertical position and at the top of insert. In the top a breakthrough of a stand pipe through the ceiling should be simulated. The facility enabled the test of both specimens attached to the walls of the hexagonal insert. The foil thickness of each insulation was .1 mm, the diameter if the wire mesh was 1.22 mm. Sample 2 showed a mesh widths of 100 mm in lengthwise and 50 mm in cross direction. Both test samples differed from the number of foils namely 40 opposite 15 and from the thickness, 70 mm opposite 84 mm as published by Bobleter, Chiron, Grossin and Naudin [BOB70].

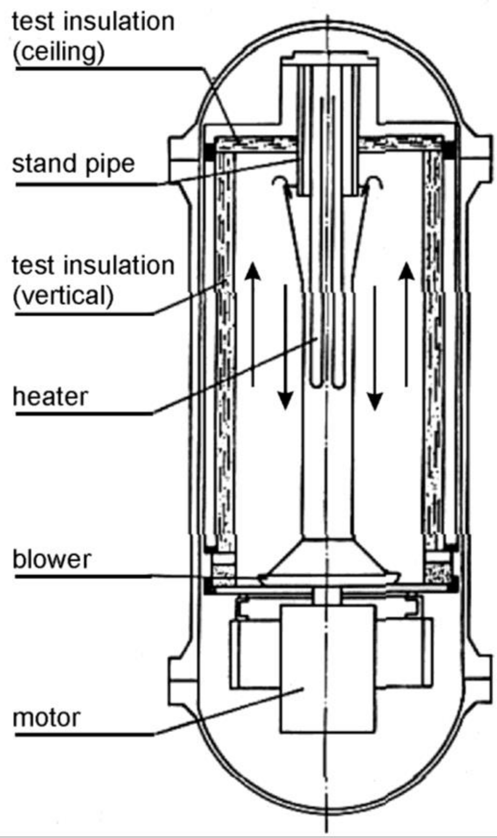

insulation	dimensions 1	2
number of foils	40	16
thickness of foil	0.1 mm	0.1 mm
thicknesss of wire	1.22 mm	1.22 mm
wire mesh	50 x 50 mm	50 x 100 mm
thickness	70 mm	84 mm
length	600 mm	760 mm

Figure 35

In Figure 36 mean thermal losses in dependence of the cover plate temperature of both designs are shown for the vertical position of the test section according to von der Weyden [WEY71]. Design 2 with the lower number of foils causes heat losses to be almost 15 % smaller than insulation 1 with 40 foils. This fact may be explained by the lower number of spacers and the larger thickness of insulation 2. However, the effective thermal conductivity of both insulations is almost identical. The helium velocity was always 3.3 m/s. Increasing pressure induced higher heat losses due to natural convection.

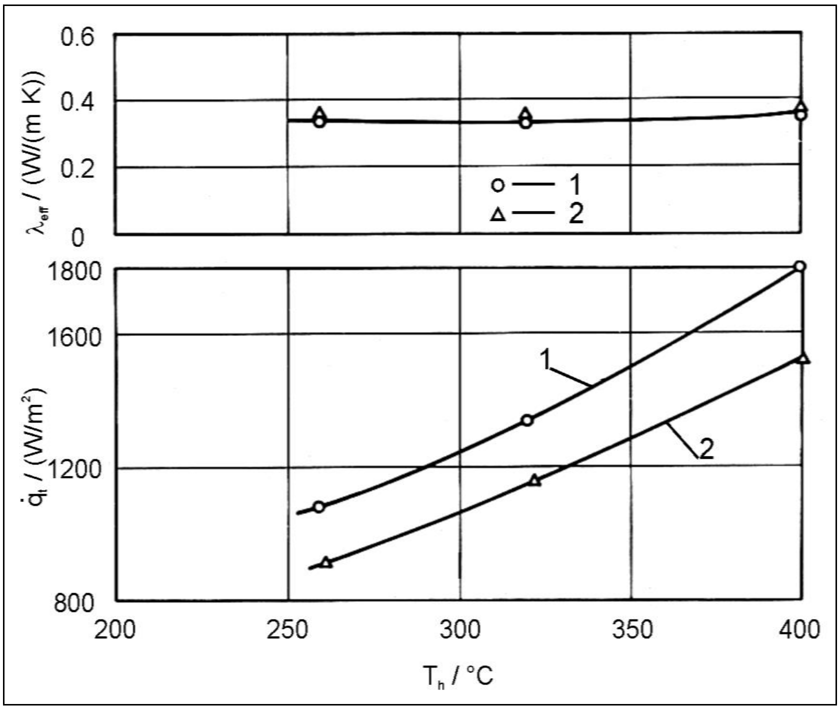

Figure 36

The influence of the helium velocity on the thermal conductivity of the open designs was also investigated as given in Figure 37. For this purpose two test runs were performed. At a pressure of 1 bar the pressure difference caused by the flow in the direction of flow was varied between the limits 0.029 mbar $\Delta p \leq 0.59$ bar, at a pressure of 40 bars between the limits 2.94 mbar $\leq \Delta p \leq 10.58$ mbar. The Nu-numbers of the different sections of the insulations varied at the lower pressure from

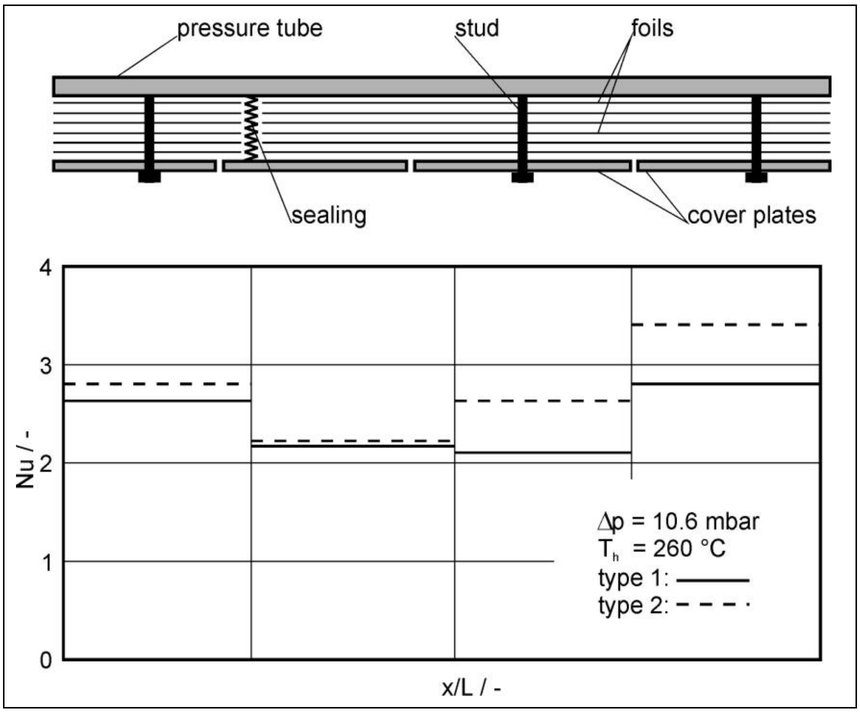

Figure 37

1.1 to 1.6. That means a low pressure influence. The Figure shows Nu-numbers versus the length x/L of the insulation for the higher pressure, the highest pressure difference and a temperature of 260 °C. In upper the part of the Figure the insulation consisting of foils, cover plates, studs and sealing elements is presented. There are considerable differences of the Nu-number for the different sections. They decrease from approximately 3 to 2.2. After that they increase to a maximum of 3.5. The very low results are caused by the axial sealing elements, which avoid an axial permeation. In all sectors insulation 2 showed the highest thermal losses due to the low foil number and thickness. When the hot face temperature was increased from 320 °C to 400 °C the Nu-numbers decreased considerably. This may be explained by the Ra-number, which increases with increasing pressure and decreases with increasing temperature.

Theoretical calculations of the thermal conductivity of such complex insulation proved to be very difficult or nearly impossible. Davidson [DAV67] attempted such calculation by applying the main equations, which describe the flow and the heat transport in anisotropic media, and by coupling them with the relation describing the temperature distribution. The equations could only solved under certain simplifications. Because Davidson only presented calculated results and not measured data his theory cannot be proved.

Another type of a foil insulation is the so-called bobbin design. Whereas the insulation described before – type open design – could be mounted on location and was designed for small local axial pressure gradients, the bobbin insulation was completely manufactured in a factory and pushed in a tube to be insulated. It was mainly suited for straight tubes. Consequently its application range is limited. Problems, e. g. the ovality of the pressure tubes, had particularly to be regarded. Furber and Sheppard [FUR82] described such an insulation designed for the Dungeness B reactor. In Figure 38 this insulation is shown. It consisted of foils and wire mesh as spacers. Following designs had dimpled or corrugated foils as spacer elements. Contrary to insulating systems which will be described later the bobbin design is closed besides the gaps near the sliding connections. In case of rapid depressurization the gas between the elements can escape through the z- shaped end pieces positioned downstream and then through the gap between adjacent end pieces near the overlapping into the hot outer space. This represents an older option

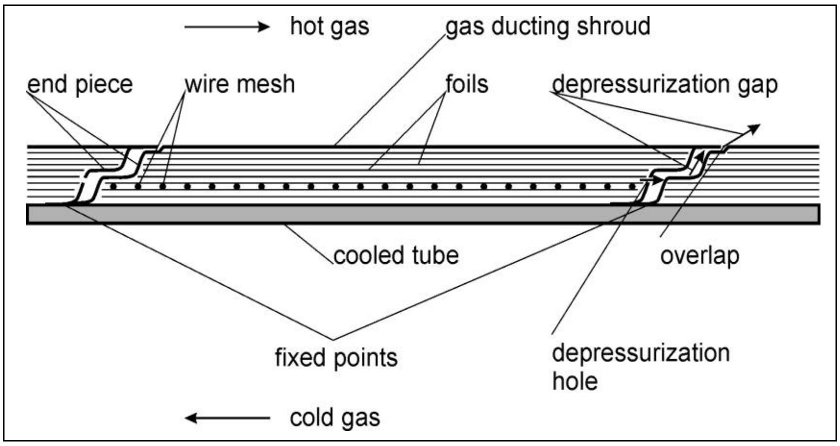

Figure 38

end pieces positioned downstream and then through the gap between adjacent end pieces near the overlapping into the hot outer space. This represents an older option which had been modified after experiments in Ispra/Italy. In following designs the gap was missing. In place of this gap depressurization or breather holes near the overlapping were used. The insulation showed a fixed point at one end. The other one could freely move.

As far as known in Germany the bobbin insulation has been investigated only in two laboratories. Such a design was mounted into the coaxial test section of the helium test facility HVK. The main data of this facility were: pressure 20 bars, temperature 800 °C, mass flow 1 kg/s. It had been erected on the KFA campus for preliminary tests [GHH70]. Later on experiments for the Geesthacht II reactor should be carried out. The withdrawal of the GHH company stopped the preparing activities. The test facility was sould to the Instituto de Energia Atômica in São Paulo/Brazil. There it was reconstructed with the assistance of the institute of reactor components (IRB). The experiments planned by the Brazilian people should start in June 1975. Indeed the hot and cold sides of the bobbin insulation were equipped with only seven thermocouples. Consequently the expected results seemed not to be very significant. The experiments would only be reasonable, when the mass flow of the cold helium should have been reduced by a factor of 10. Then the thermal losses through the insulation would have been calculated due to the temperature increase of the cold helium. With the aid of the IRB another insulation was ordered, delivered and mounted. The experiments will be described later on.

Long term experiments of a bobbin insulation were conducted since the midyear of 1973 in the Dragon reactor in Winfrith/GB. The investigations were part of a collaboration contract between the Dragon project and KFA. The insulation manufactured by the Darchem company consisted of five bobbins each 600 mm long. It instrumentation with thermocouples did not allow reliable statements regarding the thermal behaviour. Besides the thermal losses and temperature distribution also the materials of the components, the thickness of the foils, the end pieces and inner and outer shrouds played an important role. In addition different types of spacers were used.. The insulation was mounted inside one of the six tubes, in which hot helium was conveyed from the reactor plenum to the heat exchanger. The insulation was arranged in vertical position. The flow direction was upwards. The cold helium from the blower picked up the heat flowing through the insulation. Outer and inner diameters of the tube, which bore the insulation, were 235 mm and 222 mm, respectively. Its length was 4.3 m.

Figure 39 shows according to a report of Mc. Iver, Sage, Simon and Harper [IVE74] measured temperatures along the outer side for a certain pairing of materials. The experiments have been carried out in 1975. On the abscissa the five bobbins B are marked. The temperatures were measured in the middle of each bobbin. The thermocouple positions are also indicated. Along the hot side there are only a few thermocouples. Consequently the temperatures along the cold side scatter to a lesser extent. Although the temperatures were measured in an axial section the maximum difference is 30 K. Probably hot streaks were generated due to a bad mixing. It seems to be sure that the temperature differences are not attributed to a worse insulation capability in the respective sections.

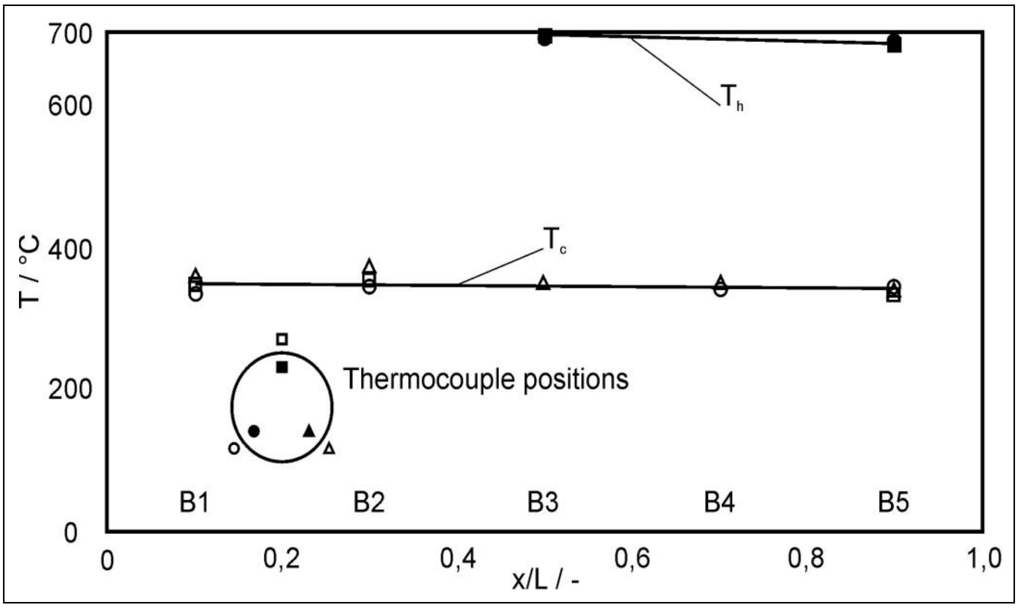

Figure 39

Additional investigations of a bobbin insulation have been carried out in the Institut für Theoretische Physik (ITP), the subsequent Institut für Grenzflächenforschung und Vakuumtechnik (IGV). The insulation consisted also of five bobbins each of them 600 mm long. The thickness was 150 mm. The inner diameter of the pressure tube was 884 mm and thus clearly higher than those described before. Dimpled foils were used as spacers. The 23 foils were .7 mm thick. All parts used consisted of Incoloy 800. In contrast to the insulating systems described before the bobbins showed depressurization holes in the inner ducting shroud at the downstream end. Consequently in a failure the helium could quicker escape from the insulation into the inner free cross section. The thermocouples had been installed during mounting of the insulation in the factory. The installation of the bobbins into the pressure tube took about one week. They were welded on a ring which was fixed to the wll of the tube.

The experiments were carried out by Henßen et al. [HEN76] in the depressurization test faclity and in the ARGAS (ARGONGAS) loop. The test assembly was either in the horizontal or vertical position. The ARGAS loop was a closed channel. In former times it was utilised for magneto hydrodynamic experiments (MHD). The loop will be described later on. The insulation was tested in the depressurization facility on quasi static condition and in the vertical arrangement. The pressure and the temperature were 40 bars and 950 °C, respectively. Also vacuum experiments were possible. The electric heater was freely pendant in the tube apart from the slide bearing.

The thermal fluxes presented in Figure 40 in dependence on the pressure are mean values of the lower three bobbins. The experiments had been conducted in the depressurization facility. Only over these bobbins the hot face temperatures were about constant. In the upper part of the assembly a temperature decrease of 100 K was measured. Because this effect was not observed under vacuum natural convection was assumed to be the reason for this behaviour. The given values stand for a hot side temperature of 500 °C. The average temperature within the insulation was 270 °C. The increase of the thermal fluxes with the pressure is linear.

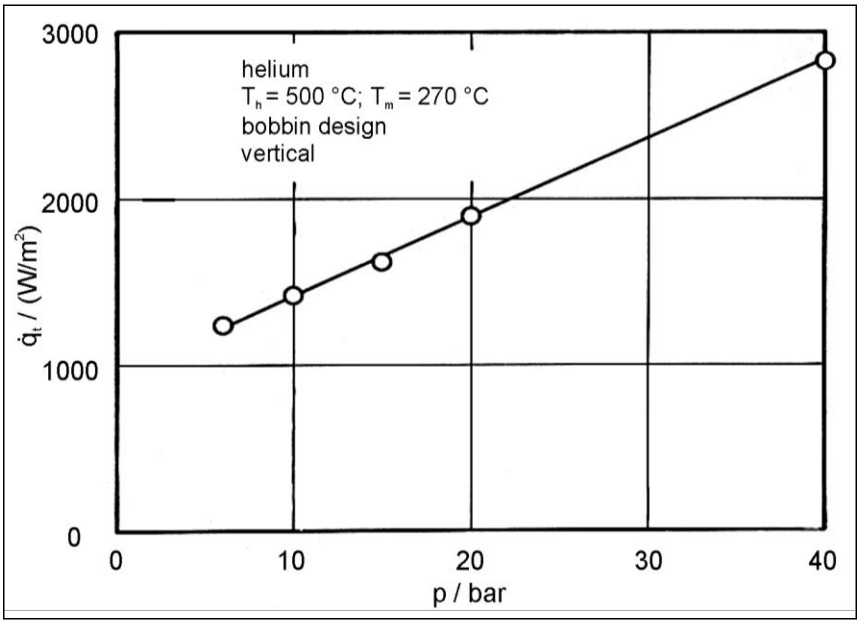

Figure 40

In Figure 41 shows thermal fluxes measured around the circumference for experiments under vacuum and for a pressure of 10 bars versus the hot face temperature. The vacuum results are much higher than expected. According to a definition given before the Nu number for temperatures above 800 °C is larger than 1. In spite of the high number of foils there seemed to be a considerable heat transport due to thermal radiation. Still steeper is the increase of the thermal fluxes in case of the pressure of 10 bars. This is caused by free convection. The transport of heat should have been take place within the 8 mm wide gap between the tube wall and the insulation. The ring was needed for welding the bobbins.

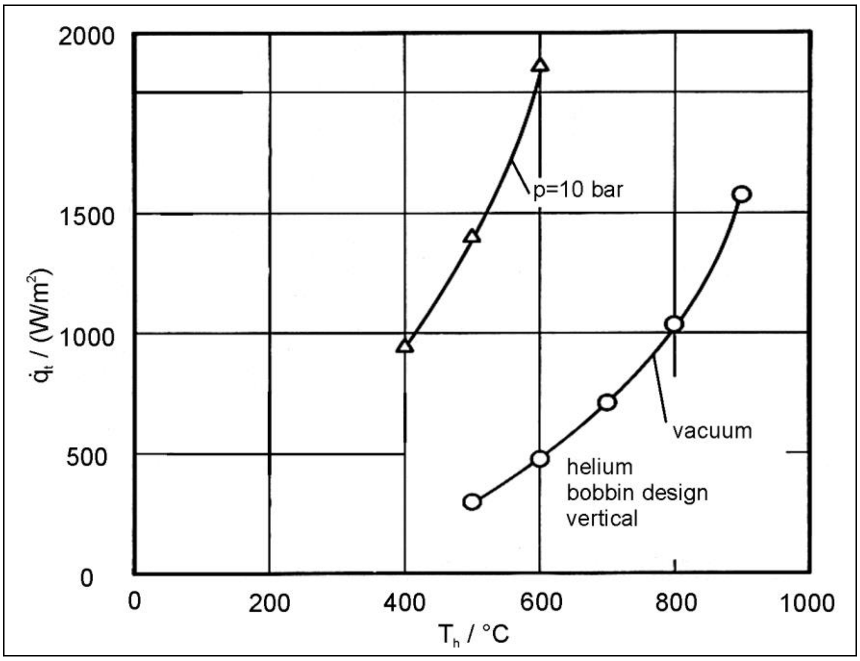

Figure 41

From these results and the investigations in the ARGAS loop it was concluded, that the bobbin design was not qualified for HRT application with respect to the thermal behaviour. This was not attributed to mechanical changes or deletions, as could be proved after decomposition of some bobbins. Thus this insulation concept, which provided only a limited field of application, was not followed up longer
.
Extensive experiments on complete insulation systems were carried out in a closed high pressure circuit (HD channel) of the Institut für Reaktorbauelemente (IRB) since 1973. This test facility was originally designed for heat exchanger tests under air, carbon dioxide and nitrogen. It was modified at the beginning of the 70s, when the HTR activities were started. After that it was also suitable for helium as a coolant. The facility is shown in Figure 42. The electric power of the heater and the blower was 2,000 kW and 300 kW, respectively. The other main data were: volume flow 7 m^3/s, pressure 40 bars, temperature 400 °C. The 2,000 mm tube of the wind tunnel was used for testing the heat exchangers. There models, single tubes and also pebbles were investigated with respect to heat transfer and pressure drop. Tubes and heat exchangers were also subjected mechanical loads caused by vibrations. More detailed information is given by Grosse and Scholz [GRO65]. For the insulation tests the smaller tube of 800 mm diameter was more suitable than the larger one. In the course of investigations also the bend behind the blower was used as test section.

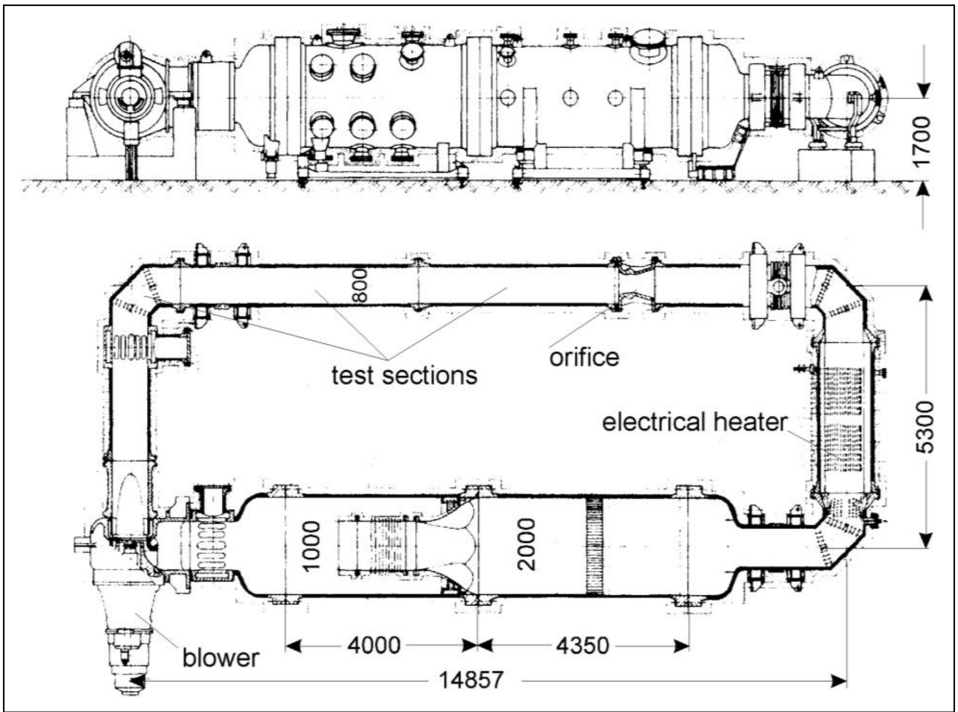

Figure 42

The inner diameter of the 4,800 mm long pressure tube was 927 mm. The wall thickness of 19 mm was able to resist the maximum temperature of 400 °C in case of the failure of the outer cooling. In order to remove the heat losses halved tubes were welded on the outer wall, through which water flowed. The inner diameter of these tubes was 12 mm, the wall thickness 2 mm.

Figure 43 shows the outer surface of the pressure tube and the welded cooling tubes. This section was manufactured by the ARG company in Ratingen, later on Reisholz near Düsseldorf. In addition thermocouples leads can be seen. Altogether approximately 150 thermocouples were needed for each test run.

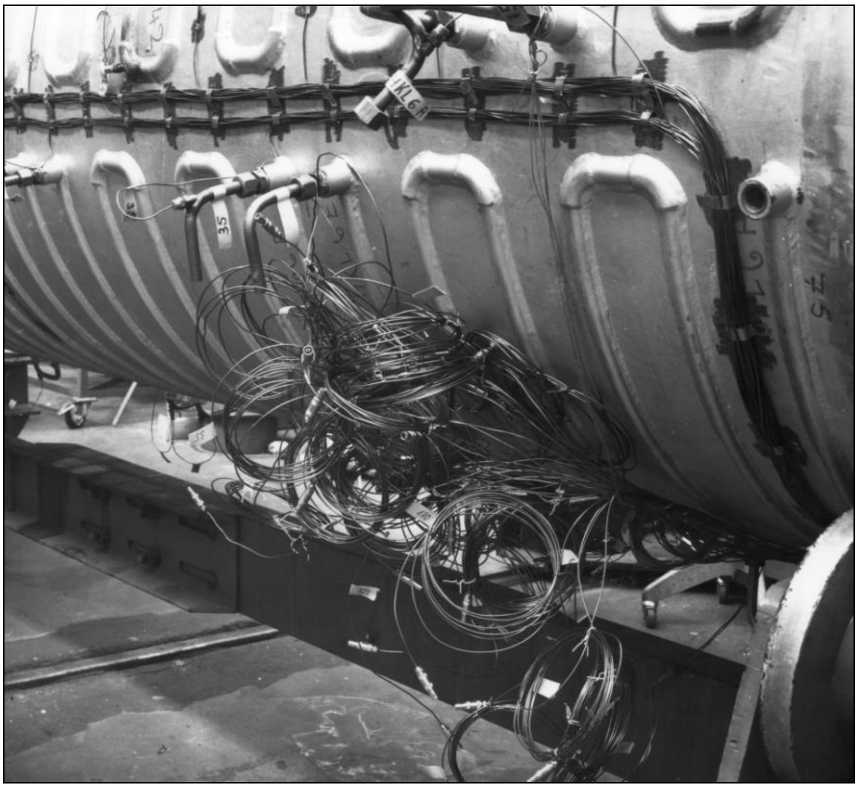

Figure 43

In order to size the pitch of the cooling systems the temperature distribution of the pressure tube was determined depending on the insulation thickness and the heat transfer conditions of the hot and cold surfaces. A pitch limitation of 100 mm proved to be practical. The calculations resulted in a maximum over-temperature of 10 K between neighboured cooling tubes. An outer mounted foam insulation with a thickness of 15 mm should reduce the heat losses to the surroundings. The initially provided helical cooling system must be modified very quickly because of the uneven thermal fluxes around the circumference. In order to analyze these thermal fluxes the cooling system was subdivided around the circumference fourfold according to Figure 43 and Figure 44. To avoid too high pressure drop due to the numerous bends the cooling systems were also subdivided in the axial direction. Thus in total eight cooling systems for picking-up the heat in the middle part of the tube and additional near the flanges as guard cooling systems were available. The arrows indicate the flow directions. This assembly consisting of pressure tube, cooling systems and instrumentation was used for all insulation tested in the wind tunnel. In the measuring sections, see the numbers 2, 3, 4, and 5, which stand for the foil insulation the cooling water left in the middle of the of the test section. The mass flows of the cooling water was adjusted to the same outlet temperatures of each sector. In this way heat conduction within the tube wall should be avoided or kept low. The end sections 1 and 6 were positioned under the shorter guard systems, as can be seen. Further explanation is given from Bröckerhoff and Scholz [BRÖ74a].

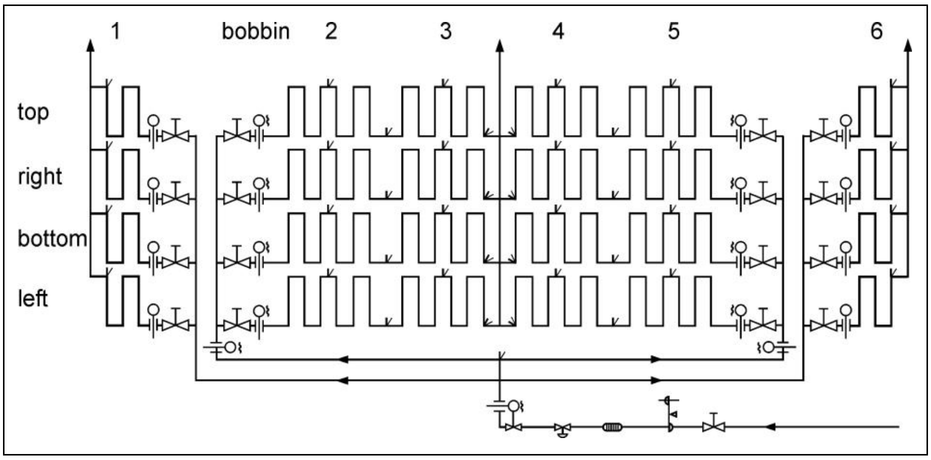

Figure 44

At the beginning it was rather difficult to exact registration of the cooling water mass flows. It was shown, that they must be low. The main condition for determining them was a constant water pressure. Because the cooling water should be taken from the net of the research centre and the pressure fluctuated between 6 bars and 8 bars during the day a pressure reducer and an electronic control valve were installed. The mass flow of each cooling system was determined by means of a combination of an orifice and a differential pressure transmitter. This configuration for measuring small water flows was specially fabricated by a manufacturer. It must be calibrated at each case. Because of the risk of blockage of the small orifices due to mud or lime a micro-filter and a phosphate filter were installed in the upstream side. For controlling purposes also the sums of the four left and right cooling systems were measured. Because a precise determination of the water flows of the outer guard systems was not needed, the measurement was done by means of rotameters.

As can be seen also in the Figure the temperature of the cooling water was measured before subdividing into the single cooling systems. To increase the accuracy of measurement the temperatures, which were needed for determining the temperature increase of each line, were measured in difference to this inlet temperature. The assembly enabled the determination of the temperature differences as well over the full length as also over smaller segments. Thus statements on thermal fluxes of the corresponding sections were possible.

Mostly the experiments were conducted at first with air, after that with helium at temperatures of 100 °C, 200 °C, 300 °C and 400 °C. The pressures were 2.5 bars, 5 bars, 10 bars, 20 bars and 40 bars. the air test counted as preliminary experiments. They should enable conclusions for investigations at high densities and thus Ra-numbers. Deviations from the given parameters were permitted. Besides the temperatures within the insulation to be tested also the gas pressures were recorded. Because of the lack of the orifice in the tubing system of the HD-channel the gas mass flows were measured by means of a Prandtl-tube. In spite of the numerous measuring points only the conditions of one section of the insulation could be analysed in more detail. For the remaining sections, however, the heat flows $\dot{Q}$ could be determined by means of the water flows and the temperature differences. For each sector applied

$$\dot{Q} = \dot{m}_w \cdot \Delta T_w \cdot c_{pw} \,. \tag{34}$$

Here $\dot{m}_w$ stands for the mass flows of cooling water, ΔT_w for the temperature increase and c_{pw} the specific heat capacity. The corresponding mass flows were determined by means of polynomial coefficients, which could be defined after calibrating the orifices. The applied relations

$$\dot{m}_w = a_i \cdot x^i \tag{35}$$

were of fifth order with the polynomial coefficients i = 0 – 5, x stands for the pressure difference recorded by the pressure transducers. The specific heat capacities were assumed to be constant because of the rather low and nearly similar temperature increases of each line. By means of relation 3 the effective thermal conductivities were calculated as follows

$$\lambda_{eff} = \frac{\dot{Q} \cdot 2 \cdot \ln \frac{D_1}{D_2}}{\pi \cdot L \cdot \Delta T_i} \,. \tag{36}$$

D_1 and D_2 are the confining diameters thus the inner diameter of the pressure tube and the outer diameter of the inner shroud. L is the length of each segment and ΔT_i the temperature difference across the insulation. The mean wall temperature on the hot inner surface was a mean value of the thermocouples installed there. The mean temperatures on the cold outer surface were formed for the top and bottom quadrants from a mean value of the cooling water temperatures and the wall temperatures between the cooling tubes. For the lateral quadrants, an arithmetic mean of the temperatures at the top and bottom was taken as the value on the cold side. The temperature drop in the pressure tubes was so low – in most cases, it was less than 1 K – that it could be disregarded. The measured gas pressure was assumed to be constant throughout the insulation. The mean temperature was a mean value of the temperatures of the hot and cold sides. The physical properties were also taken from the literature [HAM66] and [HAR70]. Nu numbers specified in the further course of this report were determined according to relation 6.

In contrast to the bobbin design described before, the insulation shown in Figure 45 belonged to the group of open systems. It had been investigated in the HP channel. For this type, however, the Darchem manufacturer could not guarantee the high axial depressurization rates of 15 bars for HHT applications, i.e. plants with gas turbines. Since the bobbin designs described before could not be used, new solutions had to be found. The design finally realized was a mixture of already presented systems. For example, the studs were taken from the liner insulation, the z-shaped end pieces from the bobbin design. The mounting of this insulation into the pressure tube took place on site. It took about five days. It should be noted here that almost a whole day was needed for installing the thermocouples. The overall length of the insulation was 3600 mm; its inside diameter was 800 mm, i.e. the insulation thickness was 63.50 mm.

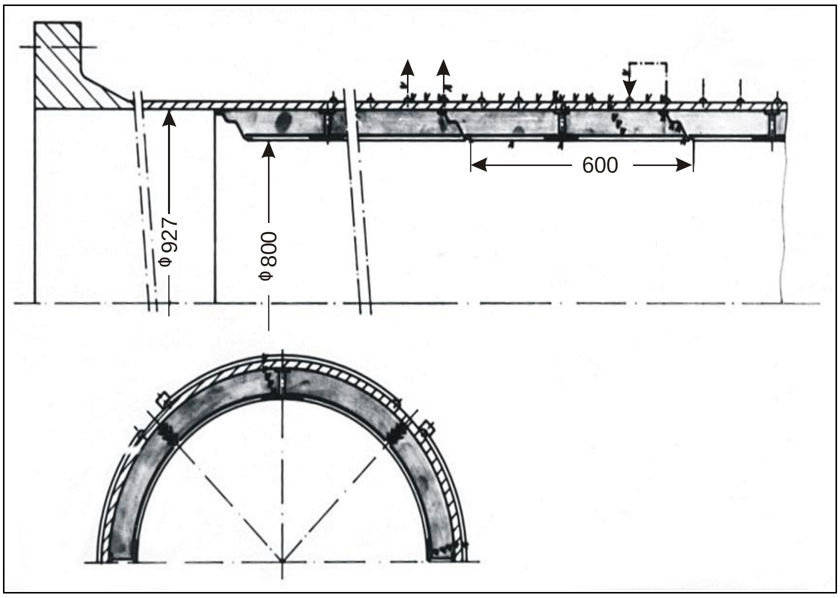

Figure 45: Foil insulation with pressure tube

The insulation consisted of six segments. The second to fifth segments were available for measuring purposes; the first and sixth segments served to reduce the tube wall temperatures in the non-insulated pressure tube wall to the values of the insulated wall. The foil elements were fixed to the pressure-bearing wall by studs and cover plates. Four studs each per segment were welded during mounting onto disks of 25 mm outer diameter and 6 mm thickness on the circumference.

The z-shaped transition pieces were externally connected gastight to rings and internally to the so-called ducting shroud, as shown in
Figure 26. They were intended to prevent a forced gas flow due to axial pressure gradients resulting in elevated thermal fluxes in the foil elements. On the non-welded edge, the shroud overlapped with the next z-piece, so that axial thermal expansions could be accommodated there by shifting.

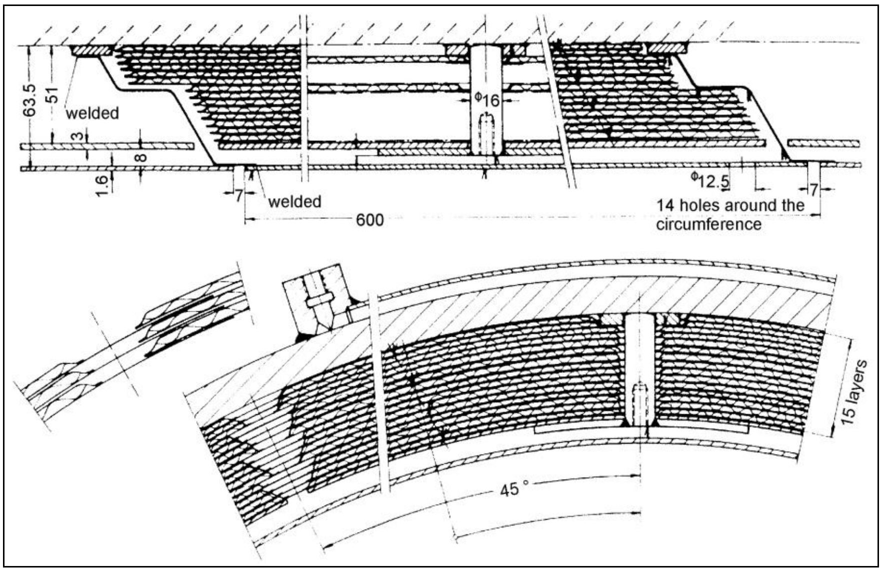

Figure 46: Foil insulation (element design)

The insulation consisted of different elements, hence it is named element design. The individual elements were held in place by the studs already mentioned. They consisted of two 0.1 mm thick smooth foils with dimensions of about 600 mm x 600 mm. They were separated by an equally thick third, but dimpled foil. The two outer cover foils were welded together on three sides of the circumference. On the fourth, downstream, side they were open for fast pressure compensation. Due to the fourfold subdivision across the circumference, where there was an overlapping due to the continuation of the bottom cover foils between neighbouring element layers, a convection movement across the circumference could be avoided. As can be seen from the latter two figures, the individual segments were positioned beneath the cooling systems arranged on the pressure tube outer wall. These systems were designed so that the thermal fluxes of all four quadrants could be separately recorded with the tube in the horizontal position. There was a circumferential annular gap between the cover plates of 3 mm thickness and the ducting shroud, 1.6 mm thick according to the drawing. The gap thickness was 8 mm in the cold state. It decreased to about 5.3 mm at a temperature of 400 °C. As will be shown later, this annular gap proved to be very disadvantageous.

There were further annular gaps on the z-pieces, whose axial extension was specified to be 6.5 mm on the left and 8.5 mm on the right. The gap on the right was required for pressure compensation processes, as already mentioned, because of the elements open to this side. Thermal expansions caused a reduction of the mentioned gap widths.

Mention must also be made of the fourteen 12.5 mm boreholes on the freely movable end of the shroud, see also
Figure 26. They had the task of preventing a major overpressure building up in the element layers and thus a buckling of the foils or ducting shroud in the case of rapid depressurization. They thus resembled the boreholes of the bobbin design.

A total of 15 foil elements were arranged on a thickness of 51 mm, i.e. there were 45 foils. These elements had a design thickness of 3 mm, so that a clearance of 6 mm resulted purely arithmetically. In reality, the elements could not be stacked on each other without a gap due to the manufacturing tolerances, so that the foil package was pressed against the vessel wall by studs with the aid of the cover plates. For recording the temperatures inside the insulation, in particular, segment 4 was equipped with thermocouples, as shown in Figure 45 and
Figure 26.

Although the experimental results for helium were much better than for air and an extrapolation to higher temperatures was likely to result in further improvements in agreement with theory, the results as a whole were regarded as unsatisfactory. Since the circumferential gaps were identified as the main cause for the behaviour subsequently discussed, a modification proposal was elaborated together with the manufacturer. Since the modifications were to be carried out quickly, they were only made on four segments. For this purpose, the first five segments had to be removed. The gas gap between cover plates and ducting shroud was reduced by two measures. On the one hand, the thickness of the cover plates was increased from 3 mm to 6 mm, on the other hand, a compressible foil element of 4 mm thickness

was placed into the remaining gap. This left a gas gap of arithmetically 1 mm , which was bridged due to thermal expansion at a temperature of 400 °C.
In order to reduce the gap on the z-pieces, the existing foil elements were extended at both ends by means of slipped-over caps consisting of two foils welded together at one rim. Complete closing of the gaps, especially at the downstream end, was not permitted because of the high pressure change rates to be expected under operating conditions, although this would have been technically feasible. For mounting reasons, the optimum could not be achieved at the rear end. The placed-on caps were provided with holes for pressure compensation.

Figure 47 shows a pressure-tight lead-through used in all experiments for the thermocouples installed inside the pressure tube. Other leads with similar diameters – the thermocouple diameters were 1.5 mm – could also be used in this way. The picture shows some leads routed in milled slots of two protruding rings. Sealing was effected by two Viton disks – one disk can be seen between the two rings – which were pressed together by a cap still to be externally attached and screwed onto the flange that can also be seen. This unit has proved efficient at many test stands and in many experiments at pressures of up to 80 bars and high temperatures. In some cases, the lead-throughs were water-cooled to protect especially the Viton seals against excessively high temperatures. However, these measures were not required in the HP channel, but later on for experiments in the HHV high-temperature helium test facility.

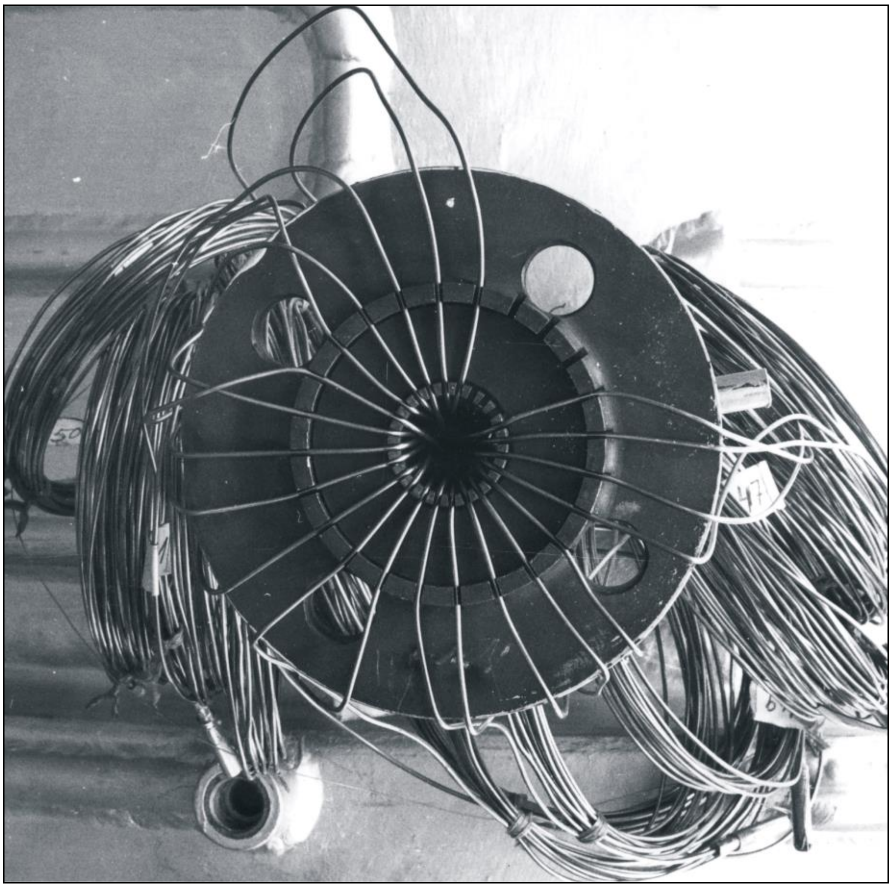

Figure 47: Thermocouple lead-through

In the following, the results from the two test runs – before and after reconstruction or modification – for air and helium will be compared. Unless specifically mentioned, the results apply to the highest hot gas flow rate of about 13 m/s.

Figure 48 shows the profile of the temperatures through the insulation for the air experiments prior to modifying the construction. The diagram on the left shows the results for a pressure of 9.3 bars, the diagram on the right those for the highest pressure of 38.6 bars. The symbols differentiate between the top, right, bottom and left sectors. These are valid in the following for all investigations concerning the insulations tested at the Centre. The insulation set-up is shown to scale underneath the diagrams.

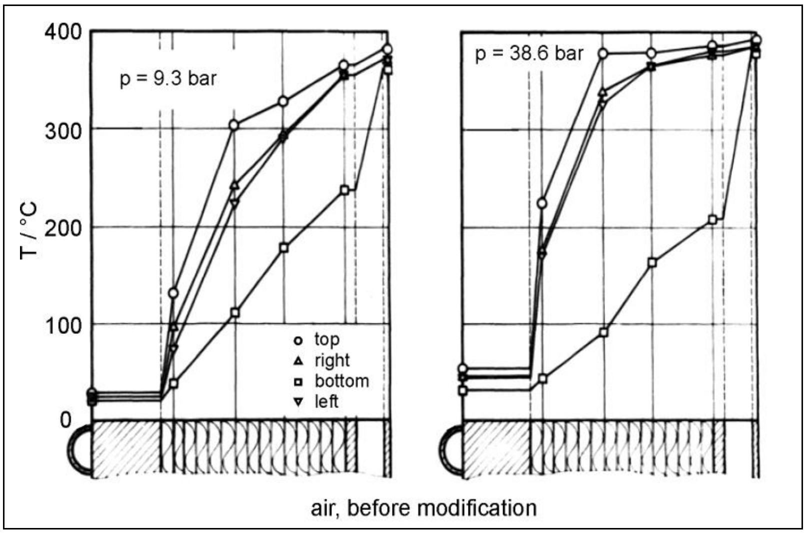

Figure 48: Temperatures within the insulation

In metal layers such as outer wall, cover plate and ducting shroud, the temperature profile was assumed to be constant. It can be seen, especially at the highest pressure, that the temperature reduction in the circumferential gap and the subsequent nine element layers at the top and the sides was very small. In the gap at the bottom, in contrast, the temperature dropped steeply. It varied nearly linearly through the insulation layer. This led to great differences between top and bottom within the insulation. The temperature difference was already 170 K on the cover plates. Since these differences clearly decreased with pressure, see diagram on the left, and thermal radiation could be ruled out as the cause, free convection was considered to be the reason. From the very small temperature reduction in the first layers at the top and sides it had to be concluded that a considerable portion of the heat had not flown through the foil elements, but convectively elsewhere, e.g. through the gap near the z-pieces, directly to the cooled wall. This convection flow was so high that the calculation of the effective conductivity of the top sector – not shown here nor later on – led to a value of about 160 W/(mK). It thus corresponded to the thermal conductivity of a good metallic conductor.

Figure 49 shows the conditions for helium. Figure 48 and these diagrams convincingly confirm the influence of density. However, there was agreement at a pressure ratio of 4 and not, as expected at 7.3, at which the densities are equal. Thus, for example, the data in Figure 49 at a pressure of about 39 bars almost correspond to those of air at a pressure of 10 bars, see Figure 48. The temperature differences across the gap between cover plates and conducting shroud could be clearly reduced in comparison to the tests with air, above all at lower pressure. But clear improvements can also be observed at the upper pressure of almost 40 bars.

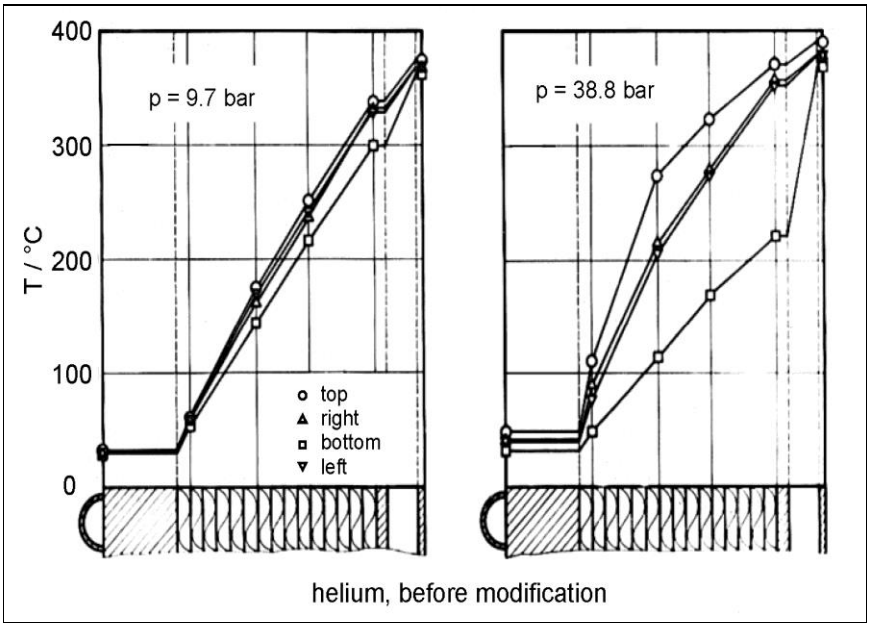

Figure 49: Temperatures within the insulation

The correctness of the assumption that the heat losses did not flow through the elements but directly to the wall is proved by Figure 50, which shows water and wall temperatures for the same gas data as in Figure 49 as well as the highest gas temperature. For simplification, the right end of segment 3, the whole segment 4 and the left end of segment 5 are drawn as the abscissa. The cooling tubes and the position of the thermocouples are indicated, and also the elements, end pieces and studs. At low pressure, the effect is not yet apparent, but in the right diagram a

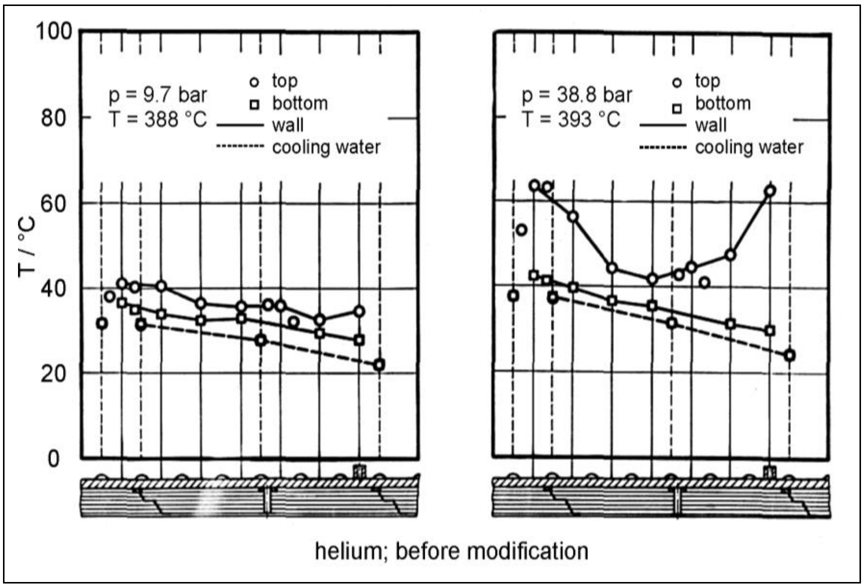

Figure 50: Wall and water temperatures

strong increase of the wall temperatures near the z-pieces is recognized for the top quadrant. In the bottom sector, the slope of the wall and water temperatures is approximately the same. The maximum wall temperature increases in the top sector near the z-pieces up to 63 °C at the highest pressure. It then drops to a value of 42 °C at the centre, but is thus still 7 K above that in the bottom quadrant. The difference from the water temperature is three times higher at the top than at the bottom. Since this difference is a measure of the local heat fluxes, greatly different thermal fluxes and Nu numbers are to be expected in the individual sectors.

The influence of the gap on the temperature distribution in the studs and on the rear z-piece of segment 4 was even greater, see Figure 51, which shows the temperatures along this z-piece for two pressures. The temperature differences on the cover plates, in contrast, were about 100 K at the lower pressure, but already 300 K at the upper pressure. In the upper part, no decrease of the temperatures can be observed up to almost half of the elongated length of the z-piece. The temperature only drops from 360 °C to 60 °C on the last 30 mm, seen in the radial direction. In the bottom region, in contrast, the drop is very steep on the first few millimeters and then very small behind the cover plate. These large temperature differences probably led to great stresses. Since the temperature differences on the end pieces were even higher than in the region of the plane, in which the radial distribution was measured, the convection flow must have been significantly greater in the gaps.

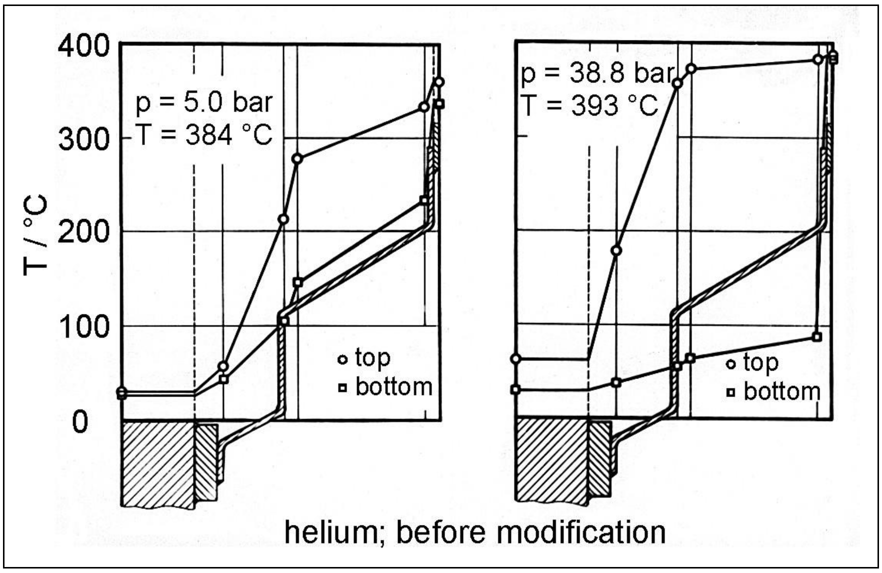

Figure 51: Temperatures on the rear end piece

In the following figures, Nu numbers are shown for the foil insulation described before. For lack of space, only a few selected results can be described.

These results also clearly show the influence of gas pressure, above all with air as the coolant, see Figure 52. The Nu numbers of the four sectors are shown here for air and the highest gas temperature of 400 °C as a function of pressure. Contrary to the definition given before, only the 15 element layers were chosen as the insulation layer in this figure. The gas gap between ducting shroud and cover plates was left out of consideration. In the sectors with unstable gas stratification, i.e. cold gas is superimposed on hot gas, heat transport is much higher than in the other quadrants, e.g. in that at the bottom, where the stratification is much more stable. A pressure influence should not be expected here at all. Nevertheless, an increase of the Nu numbers with pressure is also observed there. In the top sector, the effective thermal conductivity is almost 18.5 times greater at a pressure of 39 bars than the static air at the same mean temperature. At the bottom it is only 6.5 times higher.

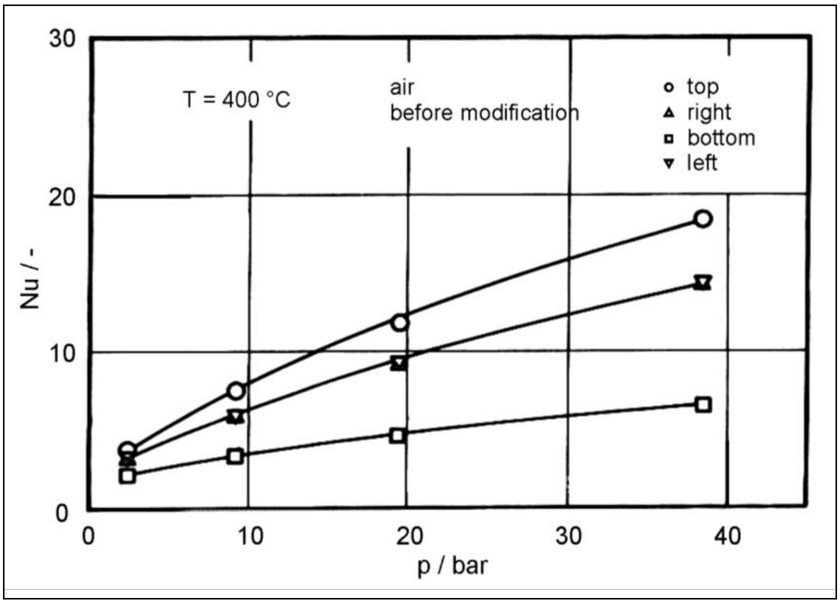

Figure 52: Nu numbers as a function of pressure

The conditions for helium at approximately the same temperature are shown in Figure 53, where at the highest gas pressure only the Nu numbers of 3.4 in the top sector and of 2.1 at the bottom were measured. This is not only attributable to the

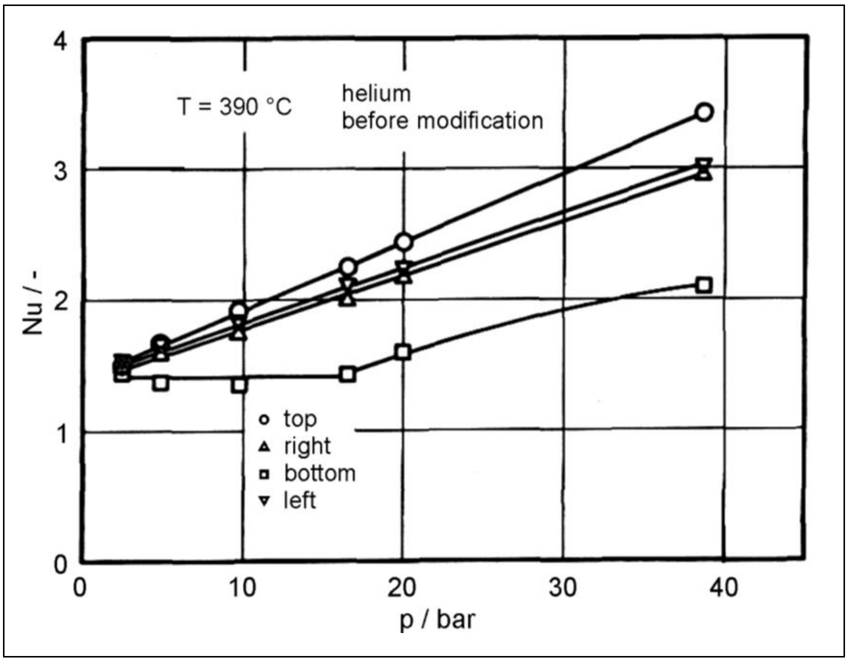

Figure 53: Nu numbers as a function of pressure

much lower density, but also to the much higher conductivity of helium. At pressures below 15 bars, free convection does not seem to provide any contribution in the bottom quadrant. It is to be assumed that a critical Ra number is only reached above this pressure at the bottom.

As expected, the increase of the gas velocity by the factor of four did not influence the Nu numbers, as can be seen from Figure 54. The values apply to the highest helium pressure. Two velocities are differentiated. It can be seen that there were different temperature dependences for the individual sectors, these being equal for the lateral walls. Although the two velocities at the same gas state resulted in different Nu numbers, the results for both velocities could be represented by one curve, since the mean temperatures also changed. The fact that, in particula, the measuring points for the bottom sector are shifted to the left may be explained by the lower mean temperature prevailing there in comparison to the other quadrants.

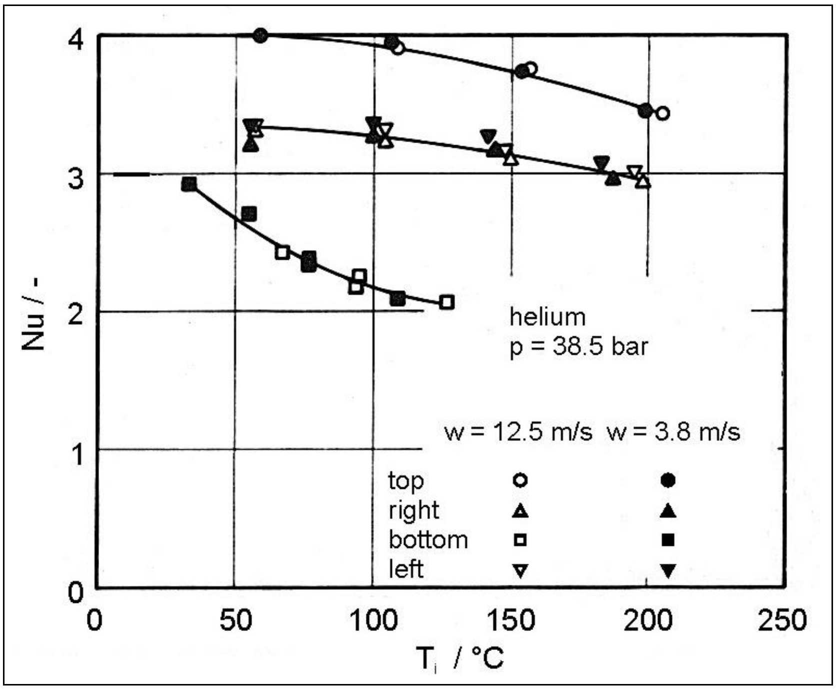

Figure 54: Nu numbers as a function of the mean temperature of the insulation

Although the results for helium were much better than for air and an extrapolation to higher temperatures was likely to result in further improvements according to theory, the results so far discussed had to be regarded as unsatisfactory. The cause was seen in circumferential gaps, as already mentioned when describing the insulation. Modifications were discussed and agreed upon with the manufacturer. The gaps near the z-pieces and between ducting shroud and cover plates were removed or made smaller, as already described. However, the gaps could not be completely removed for technical reasons, i.e. free spaces remained in which gas flows were still possible. These were also much more pronounced in air tests than with helium.

The modifications led to a quite essential improvement. Figure 55 shows temperature variations through the die insulation for air at a temperature of 390 °C and the two pressures of 9.7 bars and 39 bars. The temperatures on the cover plates were now almost equal. However, the temperature reduction at the top and bottom was so different that maximum differences of about 270 K must have occurred within the insulation.

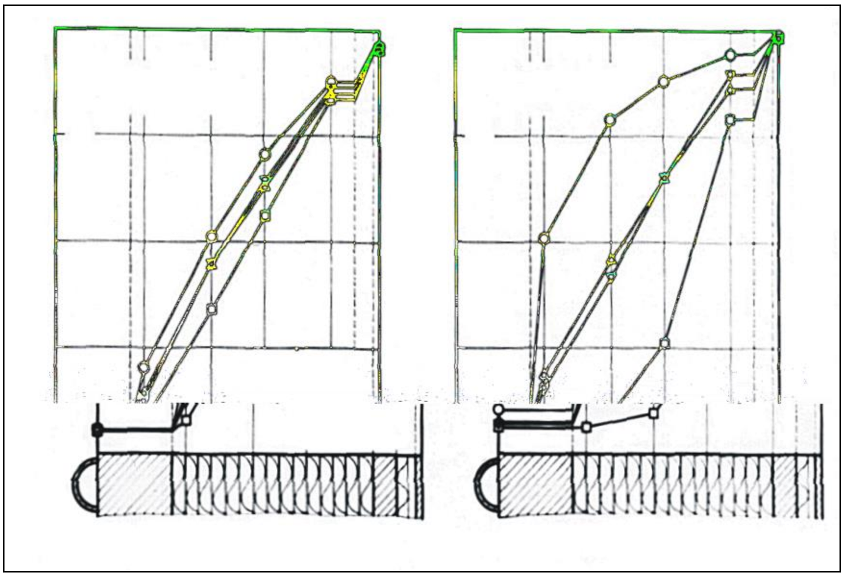

Figure 55: Temperatures within the insulation

Whereas the temperature curves at a pressure of 10 bars and for air in the tests of the first run corresponded to those at a pressure of 39 bars for helium, Figure 56 shows that the conditions for helium were now clearly more favourable. There were no remarkable differences between top and bottom any more, so that no significant further improvements seemed to be possible.

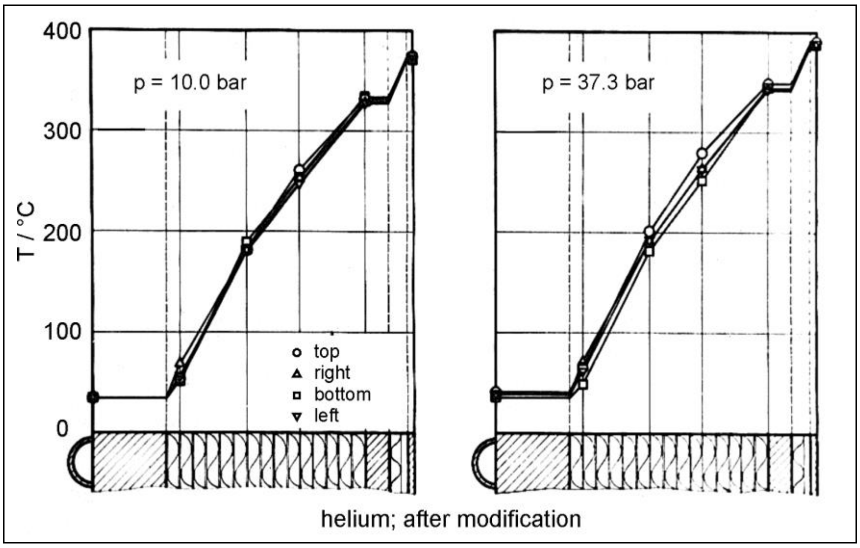

Figure 56: Temperatures within the insulation

From the curves of the water temperatures, see Figure 57, no essential improvements are to be observed for the test runs before and after modifying the insulation. The wall temperatures, in contrast, show a clearly different behaviour. Major deviations of up to 18 K can only be seen in the region of the right z-piece. This is attributable to convection in this region. At lower pressures, e.g. 10 bars, the temperatures in the top and bottom sector are approximately equal. The maximum temperature of the wall at the highest pressure was 18 K after modification and thus clearly below that of the first test run. Moreover, the differences from the water temperatures have become much smaller, so that lower thermal fluxes or Nu numbers could be expected.

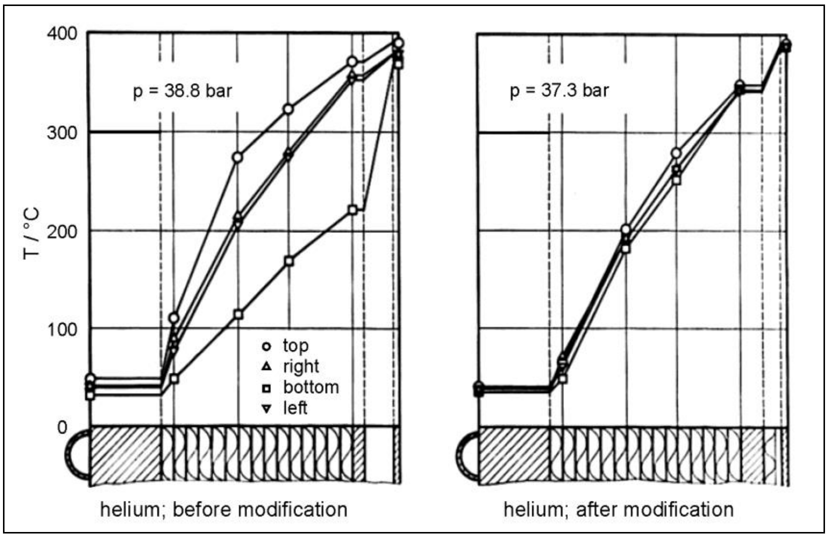

Figure 57: Wall and water temperatures

Before presenting the results, which in part will be discussed in connection with experiments with the test section in the vertical position, this experimental arrangement will be briefly described. The test section with insulation was flanged out of the duct system of the HP channel and positioned vertically. An electrical heating unit, see Figure 58, was mounted into the tube. It consisted of a cylinder, into which grooves were milled to accommodate the coiled heating rods, and six adjustable systems with two 2 kW heating rods each, so that the total electric power was 24 kW. Later experimental arrangements required higher heating powers. The heating coils were arranged so that the density of the rods was greater in the bottom region than in the top region, since hot gas was passed from the bottom to the top due to natural convection. The silver wires for connection to the heating elements were led out of the pressure vessel in the same way as the thermocouple leads. The tube was closed by a lid on both sides, whose inner surfaces had to be insulated. Due to the higher temperatures in the upper part, the lid there required a much thicker insulation than that at the bottom. In carrying out the experiments, particular attention was paid to maintaining constant temperatures at the ducting shroud. The cooling water flowed into the four cooling systems at the bottom and left them at the top, i.e. there was no division in the axial direction as in the tests in the HP channel. These experiments were aimed at investigating the influence of the orientation of the insulation on its performance. They were carried out with the gas virtually at rest. For control purposes, experiments in air were performed again, but only at the temperature levels of 300 °C and 400 °C. Due to the heating power available, temperatures of 570 °C were reached under helium at the hot gas side.

As expected, no great differences in temperature distribution were observed in the individual quadrants with this experimental arrangement of the test section. The difference still observed could be explained by differences in the fabrication, assembly or mounting of the thermocouples. The temperatures in the insulation, along the cooled outer wall or on the end pieces will therefore not be dealt with in the following.

Figure 58: Cylinder with heating coils

Figure 59 shows the Nu numbers as a function of gas pressure for the tests in the horizontal arrangement and under air as the coolant. The broken curves apply to the conditions in the original state of the insulation, the solid curves to the modified design. An extrapolation of all curves up to a pressure of 1 bar would yield about the same values for all sectors. With an unchanged insulation the Nu numbers markedly increase with pressure, above all at the top and at both sides. The values almost double even for the bottom quadrant. The reduction of the gaps caused a drastic decrease of the Nu numbers, but then also a weaker pressure dependence. At the highest pressure, on average, a decrease to almost one third of the originally measured values is to be observed. For the bottom sector, even a decrease with pressure is observed, i.e. heat flows from this region upwards.

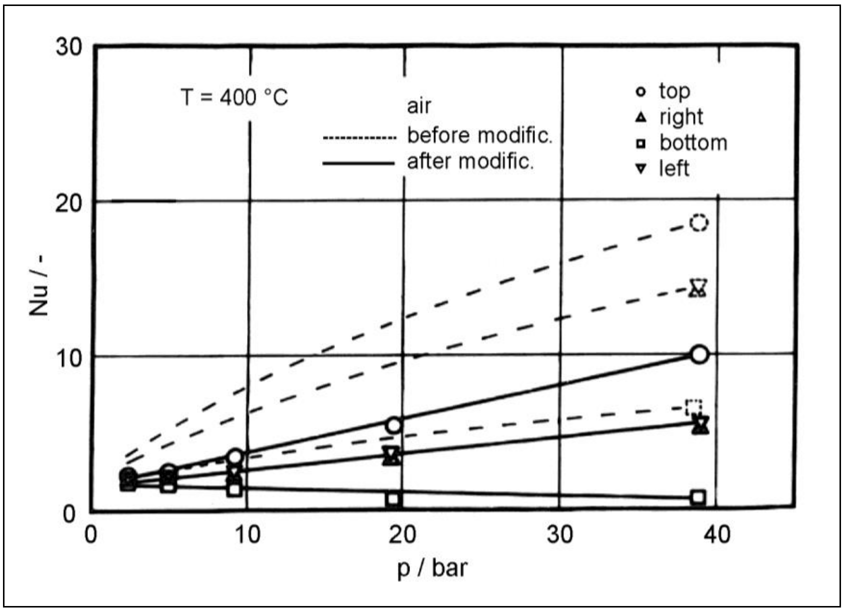

Figure 59: Nu numbers as a function of pressure

The Nu numbers shown in Figure 60 for helium are much more favourable than under air because of the lower density. Even in the case of the unchanged design, the highest values of about 3 are much lower. In the bottom sector there is almost no pressure dependence up to a pressure of 20 bars. The modification caused a homogenization of the Nu numbers at pressures up to 20 bars. The values only spread in the four sectors above this pressure. The mean value was about 1.5, which means that the heat losses of the insulation were 50 % higher than the gas conductivity. This seemed to be the attainable optimum. In view of the metallic structures and the still not completely closed gaps, the result achieved was satisfactory.

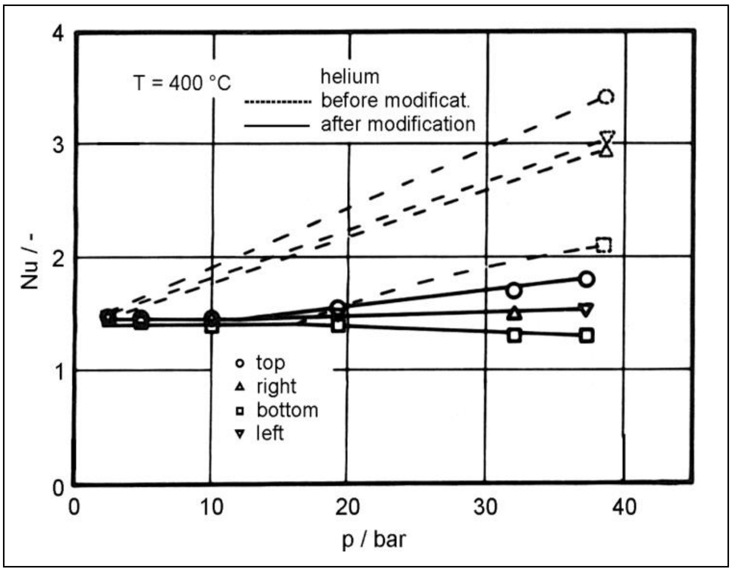

Figure 60: Nu numbers as a function of pressure

Figure 61 shows the Nu numbers for the tests after having modified the insulation with the test section in the horizontal and vertical positions as a function of pressure.

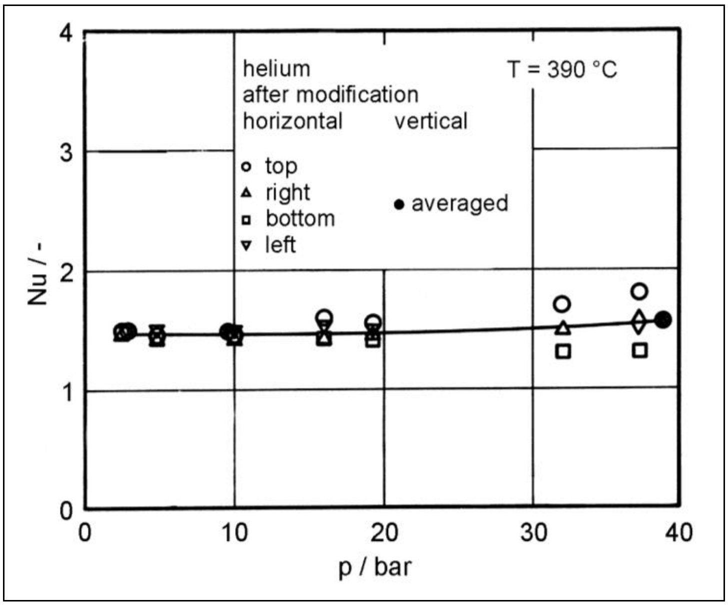

Figure 61: Nu numbers as a function of pressure

For the tests in virtually static atmosphere, a mean value was calculated and plotted for the four quadrants, since the differences in the losses and Nu numbers were small. These mean values are plotted as black points. The influence of pressure is only small, which suggests a small contribution by free convection. The diagram once again convincingly demonstrates the increasing differences between the four sectors with gas pressure for the tests in the HP channel.

Figure 62 shows the Nu numbers as a function of the hot gas temperature. The diagram contains the results from the tests after modification of the insulation and for both experimental arrangements. Good agreement with the averaged values can also be seen here. Moreover, in accordance with theory, a decrease of the

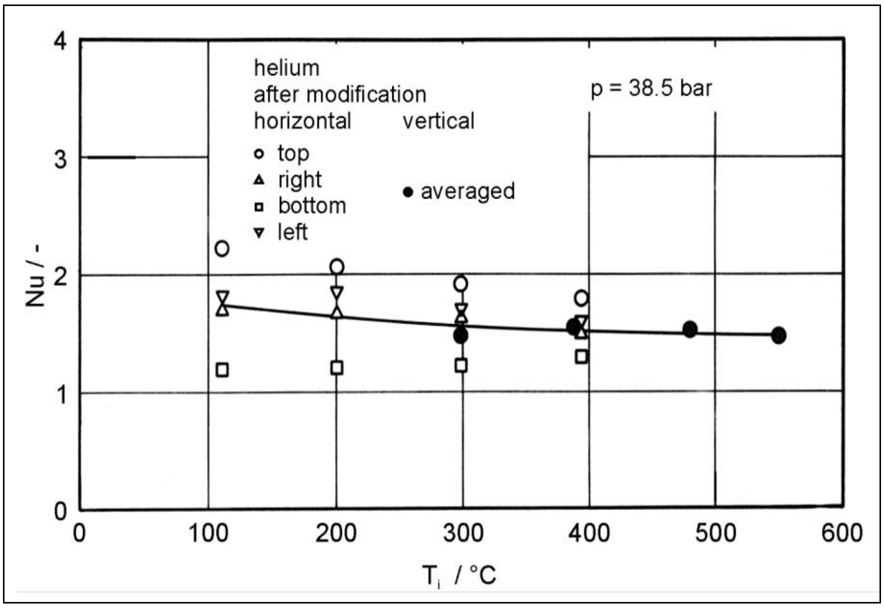

Figure 62: Nu numbers as a function of hot gas temperature

Nu numbers with rising gas temperature is observed. The limit value for temperatures around 800 °C could be a Nusselt number of about 1.4. Lower values are probably not attainable. In this case, too, an extrapolation of the Nu numbers to a gas pressure of 1 bar at one temperature level provides almost equally high values for both test runs. Theoretical calculations of the thermal conductivities and Nu numbers were not performed for this insulation. They seemed to be problematic and not very promising because of the gaps at the end pieces, whose dimensions were not defined and which could also change during the experiment due to thermal expansions.

For comparison, Nu numbers for two foil insulations are shown in Figure 63 as a function of pressure. The upper measurement series applies to the bobbin design, the lower one for the above-described design with foil elements. The mean gas temperature was about 500 °C in both cases. Both test sections were vertically arranged. Since no information was provided by the authors [HEN76] concerning the temperatures on the cold side, a constant temperature difference of 465 °C was assumed for the bobbin insulation. In the entire pressure range, the Nu numbers of the element insulation tested in the HP channel are below those of the closed design. This diagram alone demonstrates the superiority of the new insulation of element design manufactured by Darchem.

According to this company. there are restrictions for both designs concerning their outer diameters. In the case of the bobbin insulation, these are additionally dependent on the insulation thickness. Bobbins can be manufactured for tubes with inner diameter between 250 mm and 720 mm with insulation thicknesses of 50 mm. If the tube diameters are between 450 mm and 1100 mm, the insulation thickness can be increased to 150 mm. In the case of the element insulation, the limiting diameters for both insulation thicknesses are 600 mm and 1500 mm, respectively. The smaller

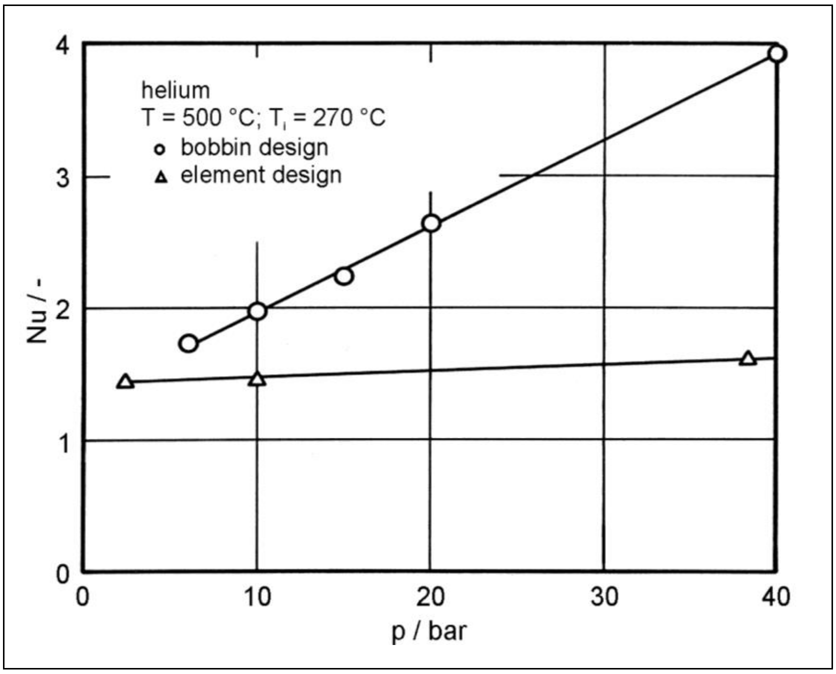

Figure 63: Nu numbers as a function of pressure

diameter is determined by the possibility of mounting, the greater by the possibility of manufacturing the z-pieces and the gap between ducting shroud and cover plates. In the case of the bobbin design, the limit of the tube diameter is 1100 mm because of the bobbin weight and the assopciated difficulty of handling. Smaller insulation thicknesses could be manufactured up to a diameter of 1300 mm. But in this case, the demands on the tolerances in manufacturing the end pieces and during installation are very high.

The above-described foil insulation based on single elements was further developed and tested, besides other components, in a large test facility constructed on the KFA premises. The high-temperature helium test facility (HHV) was part of the high-temperature reactor with high-power helium turbine programme (HHT), see [KRÄ73] and [NOA77]. The aim of this project was to demonstrate the technical and economical potential as well as the feasibility of such plants. Planning was performed by BBC in Mannheim. Construction on the campus started in April 1973. Commissioning took place in spring 1977.

The following test conditions were to be attainable with this facility:

- helium mass flow about 200 kg/s
- gas temperature 850 °C, increasable to 1000 °C

- gas pressure 50 bars
- helium purity corresponding to the reactor conditions
- test sections for different arrangements and operating conditions

Further data can be seen in the literature.

The hot gas duct with insulations was regarded as a particularly critical component. With a length of about 75 m, the duct system of the HHV facility enabled the installation of several samples. Positions 13 and 14 in Figure 64 served to investigate two insulations. Position 13 was lined with a fibre insulation to be described later, Position 14 with a foil insulation (element design).

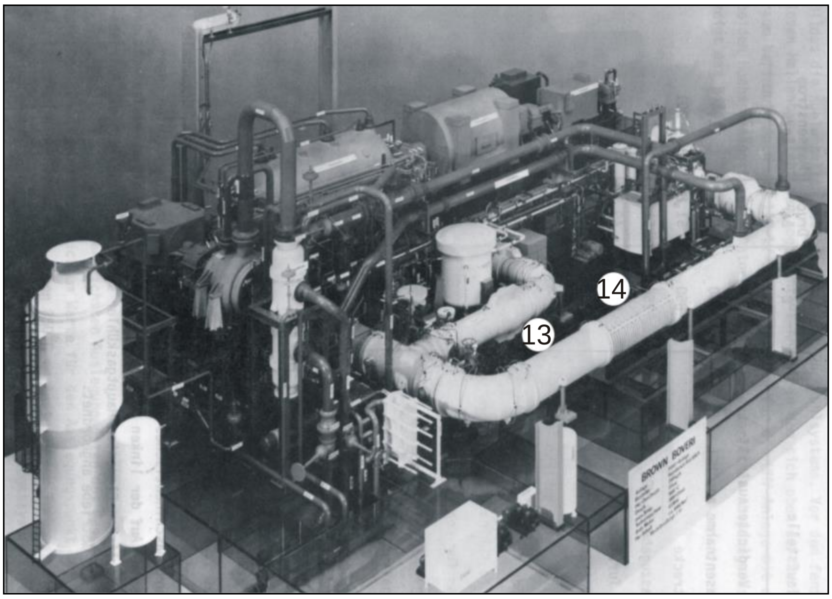

Figure 64: HHV facility (model)

The inner diameter of the pressure tubes of the facility was 1400 mm. The material for pressure tubes and flanges was fine-grained structural steel with a high yield point. The foil insulation is shown in Figure 65. The figure only shows a segment of the insulation with pressure tube. The weight was 5900 kg. Its length was 4800 mm. The insulation thickness of the entire duct system was 200 mm, so that the diameter of the free cross-section was 1000 mm. This allowed flow rates of up to 120 m/s. In view of the experience made in the HP channel, similar cooling systems were provided on the outer side for the two measurement segments of the duct. However, the pitch of the cooling tubes was 150 mm. Furthermore, the diameter of the halved tubes was increased from 12 mm to 19 mm. In the axial direction, the cooling systems were twofold divided as before. For each tube segment there were thus eight measurement zones. At the ends, eight guard cooling systems each were additionally provided to reduce disturbances in the flange region. Detailed descriptions, also with respect to mounting etc., can be seen from [BRÖ76].

The manufacturer and supplier of this insulation was also Darchem. In the direction of flow, the insulation consisted of nine sections. Parts of sections 6 and 7 can be seen in the figure. An insulation of element design was also used here. The individual elements consisting of a dimpled spacer foil and two straight sheets are shown. The

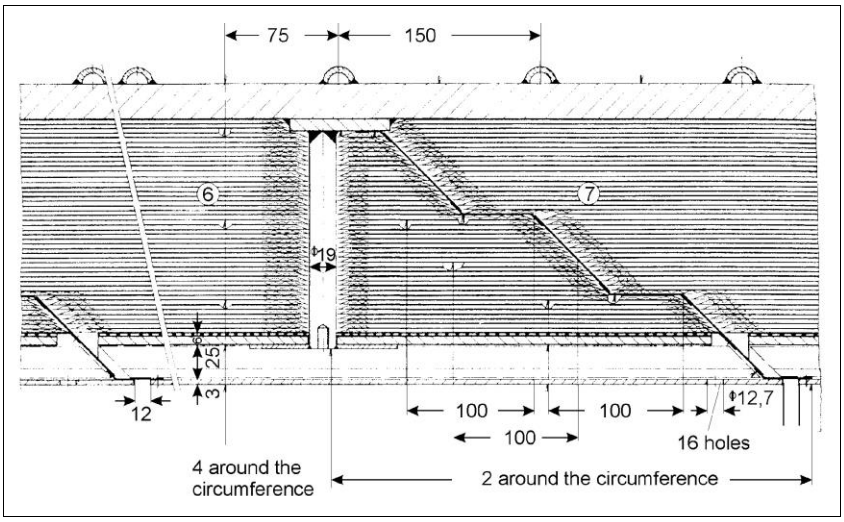

Figure 65: Foil insulation

two outer foils were welded together gastight on all four sides of the circumference. They had a hole of 2.5 mm diameter at the downstream side for pressure compensation. The individual elements were fixed to the pressure-bearing wall by studs of 19 mm diameter. Eight studs per segment were welded onto 75 mm wide rings of 15Mo3 on the circumference, which were connected to the pressure tube. This solution was chosen because the material of the pressure tubes could not be welded or only with great difficulty without being preheated. The variant used in this case differed from the first one in that the studs and end pieces, which were formed here as a double-z, were welded onto the same rings. In the earlier design. the studs had been placed on disks. Due to the larger insulation thickness – 200 mm compared to 63.5 mm – the axial extension of the end pieces was greater, so that the rings were sufficient. However, their width had to be increased from 22 mm auf 75 mm. Mounting of the insulation into the pressure tube was perfomed at the IRB of KFA. It took 30 days, including the internal instrumentation.

Ducting shrouds, end pieces, cover plates, further parts needed at the hot gas side, flow barriers, studs and the first eight element layers were made of Inconel 625, all the other parts of AISI 347. The thickness of the Inconel foils was 0.25 mm, that of the AISI foils 0.15 mm.

Figure 65 also shows the position of the thermocouples mounted into the two segments. Furthermore, this measuring segment was also provided with three sound measuring probes. In order to determine the positions of these measuring points, extensive preliminary theoretical work had been performed by the Institute for Gas and Steam Turbines of the RWTH Aachen University of Technology. The aim of this work was to determine the sound power radiated from the turbomachine. In view of the given tube dimensions and the frequencies to be expected, a complicated spatial and temporal sound field was expected to build up in the duct. The sound was conducted from the wall of the ducting shrouds through the insulation and pressure wall to the outside through tubes with an inner diameter of 3 mm. At the end of these tubes, condenser microphones were provided, which could be operated at temperatures of up to 50 °C. In addition, this tube segment, i.e. position 14, was provided with 19 strain gauges to ascertain whether the ducting shrouds were excited to vibrate due to turbulence-induced and turbine noise. The position of these strain gauges was determined according to calculations and preliminary experimental work by the Institute for Lightweight Construction of RWTH Aachen. The strain gauges were installed by BBC. The measuring line lead-throughs corresponded to those of the experiments in the HP channel, apart from the additional cooling, which seemed to be necessary in the HHV experiments due to the high gas temperature.

The outer walls of the pressure tubes were painted with a colour-changing paint (violet). This colour changed into blue above a wall temperature of about 150 °C, so that defects in the insulations could be detected.

Unfortunately, only 60 test hours were available after successful commissioning of the facility. However, this time could not even be used for testing the two positions 13 and 14, because the operating team was instructed to change the operational state of the facility approximately every thirty minutes, so that the required steady state of eight or ten hours was not reached. The temperatures recorded during these short intervals provided little information about the performance of the components to be tested. In the region of the end pieces, some blue spots were detected on the outer wall, i.e. the insulation did not meet the requirements. It was also concluded from the temperature profiles in the foil insulation that considerable convection movements had occurred in the region of the z-pieces. The end pieces were too instable, as had already been observed during mounting. They tended to becoming distorted due to temperature gradients.

Some results of these measurements can be found in Bröckerhoff [BRÖ82a] and [BRÖ84a]. In these publications, the measurement results from different measurement runs and test facilities, including the HHV facility, are compared with each other. The described investigations in the HHV facility provided Nu numbers of 4.67 and 1.43, respectively, for the sectors at the top and bottom. With a mean value of 2.96, the optimum limit value discussed before was greatly exceeded. For comparison, the above studies also specify results of Henßen et al. [HEN76] for measurements on the bobbin insulation at a pressure of 7 bars. In spite of the low pressure, the Nu numbers were far above the insulation tested at the IRB.

Surprisingly, it was decided to decommission the HHV facility. Attempts to resume the experiments at this facility and to execute the experimental programmes of those involved and interested failed. The working programme was thus terminated at a time when preliminary work was completed and the individual components could have been tested. However, according to the preliminary results, the foil insulation would have had to be modified for HHT applications. This would then have led to a prolonged standstill of the facility, since a different pressure tube provided with an inner insulation would have to be flanged in at position 14.

10.3.B Wire mesh insulation

As listed in Table 1, the metallic insulations also include the wire mesh insulation, see Figure 66, known under the tradename of METALISOL. This was and still is a French product manufactured by Creusot Loire (CL), as described by Hosegood and Jones [HOS74].

Development work had started as early as 1961. The EDF energy utility chose this type of insulation as a liner insulation for the Bugey I CO_2-cooled reactor. With a height of 40 m and a diameter of 17 m the cylindrical area to be insulated was 2000 m^2 alone.

The insulation consisted of a multitude of fine wire meshes. Several such meshes were stacked on each other forming a package. The packages thus formed were covered by thin metallic foils. The edge lengths of the foils and cover plates were 500 mm. Figure 66 shows at the top the vessel wall to be insulated and the studs onto which the packages with the cover foils were placed. These foils overlapped at the edges. In this way, they contributed to enhanced tightness. Several packages were laterally held together by U-shaped irons. Sealing elements, so-called washers, served as sealings at the stud heads, since gaps had to be present between foils / wire mesh and studs. The closure at the hot gas side was formed by cover plates, as in the foil insulation described before. The plates were fixed to each other at the corners.

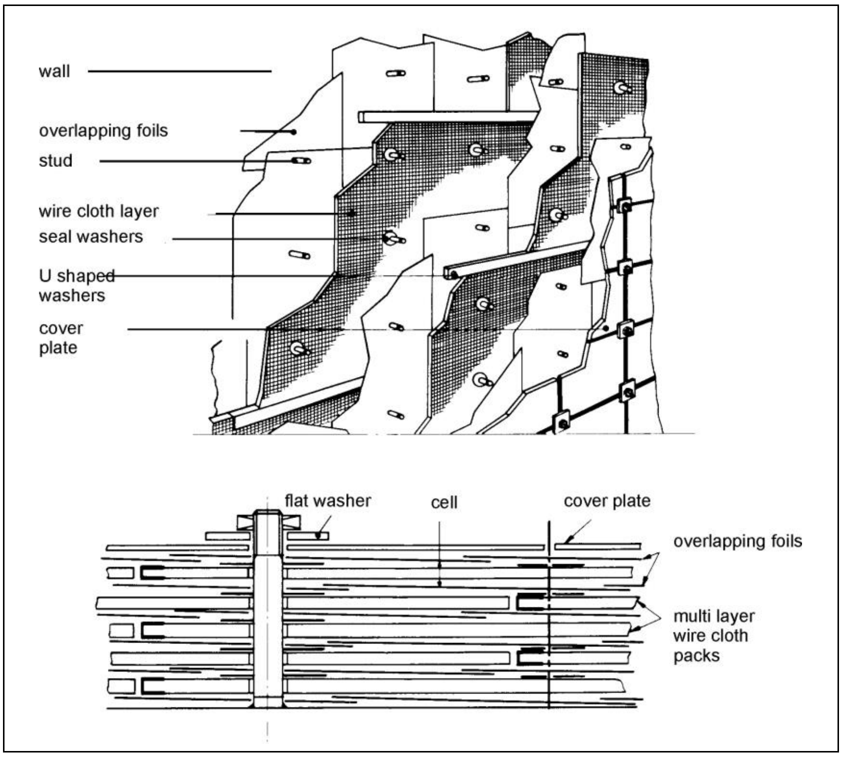

Figure 66 : METALISOL insulation

The aim of numerous investigations, primarily in France, was to develop an effective insulation. The structure of the insulation was modified, for example, by varying the number of meshes per unit area, the wire gauge and the number of layers. Furthermore, the experiments were conducted with gas virtually at rest and in forced motion in different atmospheres. Since carbon dioxide was to be used as the coolant in the French reactors, this work will only be briefly dealt with in the following.

In small test stands, experiments with gas at rest were carried out at temperatures of up to 800 °C and pressures up to 100 bars. Larger test facilities, such as Bidon 50 or Megabidon, were operated at EDF. The height and the diameter of the pressure vessels ranged between about 2.3 m and 7 m, and 1.9 m and 2.9 m, respectively. The maximum pressure and the highest temperature were 50 bars and 400 °C. Two large test stands, Chela and Carmen II, were available on the premises of CEA. In the Chela facility it was possible to reach temperatures and pressures of up to 850 °C and 80 bars, see [NAU72] and [GHT72]. The length of the test section was 3.5 m. Carmen II [CHA74] with a height of 15 m and a diameter of 1.25 m enabled gas data of 800 °C and 50 bars. In both facilities, the gas was in forced motion, i.e. by pressure gradients to be adjusted on the hot gas side it was possible to test their influence on the insulation performance.

Initial investigations primarily concentrated on the development of an insulation for the Bugey I reactor. The insulation thicknesses ranged between 5.5 mm and 55 mm, the number of meshes between 14 and 125. At a pressure of about 50 bars, Nu numbers between 2.7 at a mean temperature of 60 °C and 3.8 at a mean temperature of 300 °C were obtained. The increase with temperature was weak and probably attributable to the strong temperature dependence of the thermal conductivity of CO_2. Moreover, the increase of the Nu numbers with temperature suggested that transport processes other than free convection had to be decisive for this behaviour. With prevailing convection the values would have had to decrease. The causes could be the increase in thermal radiation or in metallic conduction. The heat losses specified were below 4000 W/m^2. According to Delort et al. [DEL69] the advantages of the insulation manufactured by CL were above all the resistance to shock and other loads, vibration resistance and simple mounting.

Since the hot gas ducts of the THTR in Schmehausen were to be lined with such an insulation produced in France – this decision was already taken in the late 60s – experiments with helium as the cooling gas were required.

Table 4 contains some data for the applications Bugey I and THTR for comparison. As already mentioned, the number of meshes per unit area or unit length is an essential parameter. The number of meshes relative to an edge length of 27.7 mm is specified in the first line. Thus, SC 50 means that 50 meshes or wires were present on a length of 27.7 mm. With the same wire gauge of 0.2 mm, the meshes envisaged for the Bugey reactor thus contained much more metal than the SC 20 insulation for the hot gas ducts of the THTR. Wire diameters and foil thicknesses were the same,

	Bugey *I* *liner*	THTR *hot gas duct*
Designation	SC 50	SC 20
number of wires per 27.7 mm	50	0.2
wire diameter / mm	0.2	0.2
thickness of foils / mm	0.2	0.2
thickness of a cell / mm	5	3; 4; 5; 10
number of layers per cell	13	10; 16; 32

material	AISI 304 L	T ≤ 500°C: AISI 304 L 550°C ≤ T ≤ 800°C AISI 347 T ≤ 800°C Incoloy 800
number of studs per m^2	4	4 - 16

Table 4: METALISOL insulations

but the cell thicknesses differed as did the number of layers per cell. This was attributable to the different temperature loads. In the lower temperature range, AISI 304 L was used in both cases. At temperatures around 800 °C, however, Incoloy 800 had to be used. In the THTR hot gas ducts, the number of studs had to be increased to $16/m^2$ due to the higher gas velocities.

Figure 67 shows experimentally determined values for the SC 20 insulation. The helium test gas was at rest. The gas pressure was 40 bars. In contrast to the foil insulation presented before, a weak increase of the Nu numbers with rising temperature is also observed here as under CO_2 atmosphere, namely from about 1.6 at a temperature of 0 °C to 1.67 at 450 °C. However, the foil insulation had only been tested at mean temperatures up to 220 °C. The effective thermal conductivity is also shown. It varied linearly in the entire temperature range.

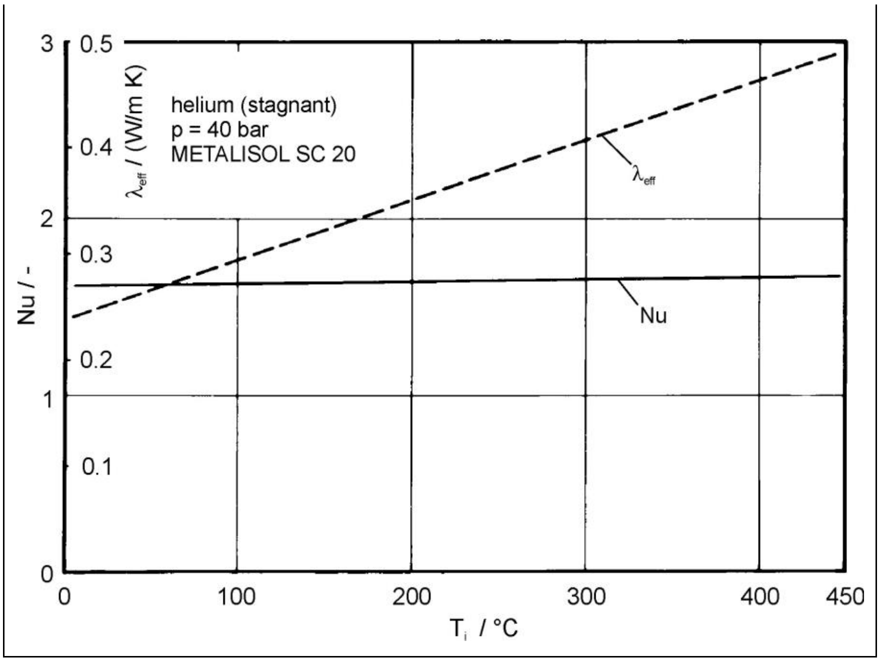

Figure 67: Effective thermal conductivities and Nu numbers
as a function of the mean temperature

Figure 68 shows Nu numbers according to Creusot Loire as a function of the mean temperature prevailing in the insulations for helium as the coolant medium.

Evidence for these investigations was not found. But it is certain that the gas was not in forced motion. The tests were performed for different wire meshes. The diagram contains both the designations of these meshes and the gas pressure adjusted. For

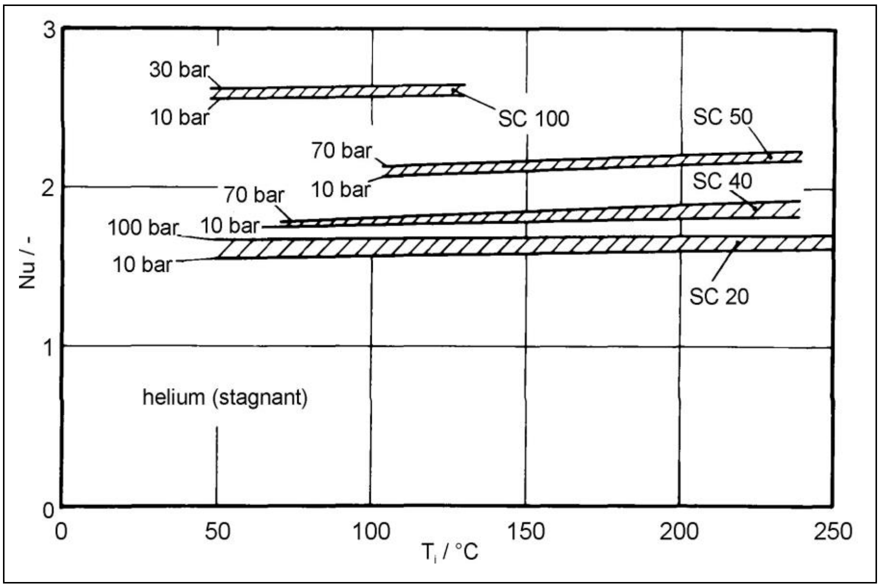

Figure 68: Nu numbers as a function of the mean temperature

each wire mesh, a band could be specified in which the Nu numbers were to be found. The influence of gas pressure is small. The high Nu numbers of the SC 100 mesh may be explained by the high solid content. With smaller numbers of meshes the Nu numbers also decrease. From the aspect of thermal behaviour, the SC 20 mesh probably represented the optimum. However, a further reduction of the number of meshes is not likely to lead to further improvements here, since the gas volume would then increase and thus the contribution of free convection would rise again. The influence of the gas temperature is negligible.

In cooperation between EDF and CL, experiments were carried out with the aim of investigating the performance of the METALISOL insulation under the influence of the outer pressure gradient with helium as the test gas. The test facility was the Chela loop in Saclay. Figure 69 shows some results of these investigations on the SC 20 and SA 20 meshes, see [GHT72] and [HOS74]. The wires of the latter mesh were also 0.2 mm thick. As compared with SC 20, flat wires with the dimensions of 1.4 mm x 1.8 mm were woven into the mesh with a spacing of 27.7 mm, that is the edge length of a unit area. To the right of the diagram, the insulation and flow channel are schematically shown. The pressure difference was generated by a flow barrier. In gas at rest, that is at $\Delta p = 0$, both meshes showed the same value of 1.7.

The maximum values were reached at a pressure difference of 0.15 bars. A further increase with rising pressure difference did not seem possible any more. The high Nu value of about 4.45 for SC 20 compared to 3.84 for SA 20 is surprising. In insulation SA 20 the flow resistance due to the additionally woven-in wires, which caused a better sealing, seems to have been higher. On the whole, however, the strong increase of the Nu numbers by a factor of 2.2 – 2.8 is not very satisfactory. In the direction of flow, additional or better sealings would be required, as realized e.g. by Darchem for the liner insulations or for the element design by the z-pieces. Axial pressure gradients of up to 0.002 bars should not have any measurable influence on the insulation effectiveness according to CEA.

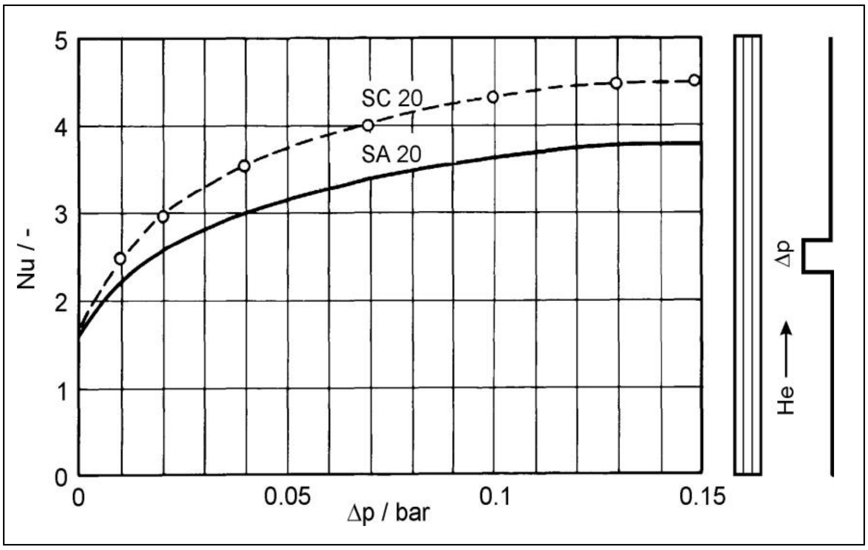

Figure 69: Nu numbers as a function of the
axial pressure difference

The time dependence of Nu numbers is shown Figure 70 for long-term experiments. The test gas was helium in all cases. The highest Nu numbers of about 2.5 were obtained in experiments in the Chela loop under the influence of axial pressure gradients. The values expected for long-term tests over a period of two years in the Dragon reactor were estimated to be about 2.15. They are plotted in broken line. This experiment corresponded to that performed on the Darchem insulation and already dealt with in the previous section. The temperature profiles indicate that the METALISOL insulation displayed slightly higher heat losses. Experiments in the Chela facility with gas at rest and over a period of 3000 h provided Nu numbers of 1.7. Over a period of 72 h the test was run without interruption at a temperature of 800 °C. The insulation was then subjected to 30 thermal cycles of 2.6 °C/min and – 5 °C/min. Although the insulation and the fixation system became loose in the course

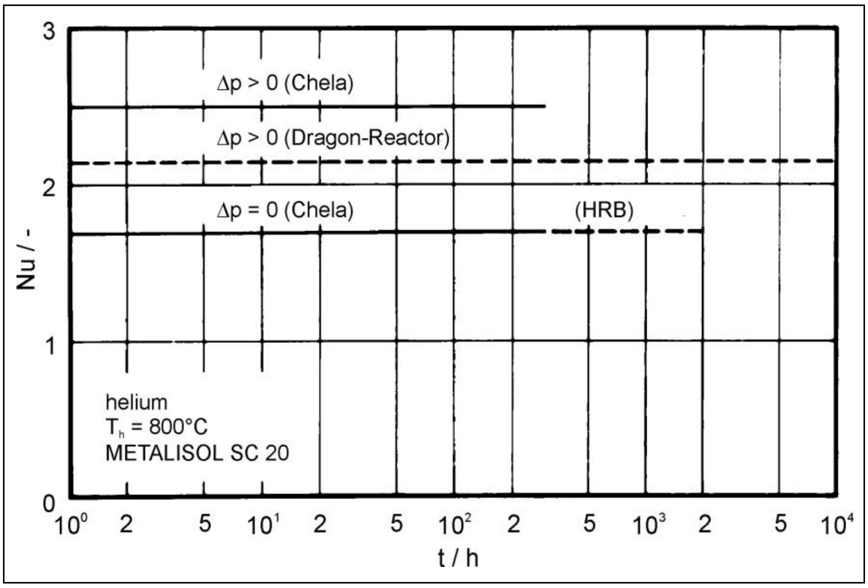

Figure 70: Nu numbers as a function of time

of time, the influence on the insulation performance was hardly or not measurable at all. Nu numbers of about 1.7 were also expected for the 2000-h test performed by HRB, also shown in broken line. The aim of this experiment was above all to test an insulation under thermal cycling.

The experimental facility used by HRB is shown Figure 71 after [HOS74]. Some data are contained. In addition to the investigations discussed in connection with Figure 52**,** friction wear between cover plates and insulation was also to be studied. Strictly speaking, this should be described elsewhere, but because of the thermal behaviour studies also performed by HRB the test stand and further experiments will be briefly dealt with here.

The cover plates were subjected to a frequency of 100 Hz and a load of 200 N. The temperature range from 600 °C to 800 °C was run through five times a day, constantly measuring the heat flux. The density of the insulation was 62 mm. The materials were AISI 304 L in the cold zones, AISI 347 in the hot zones and Incoloy 800 for the cover plates. This insulation corresponded in its structure to that envisaged for the THTR hot gas ducts. No problems were encountered for the slightly stressed meshes, whose friction coefficients were 0.8. At the fixing elements, however, corresponding values of about 3 were measured. They showed distinct traces of wear. The best results were obtained for the Hastelloy C combination for the sealing elements (washers) and Incoloy 800 for the cover plates. In the THTR insulation, the contact areas, e.g. on the cover plates or within the insulation, were coated with Cr_2C_3 and Ni/Ag to reduce friction in the case of thermal expansions and to avoid welding, see [BRÖ84b].

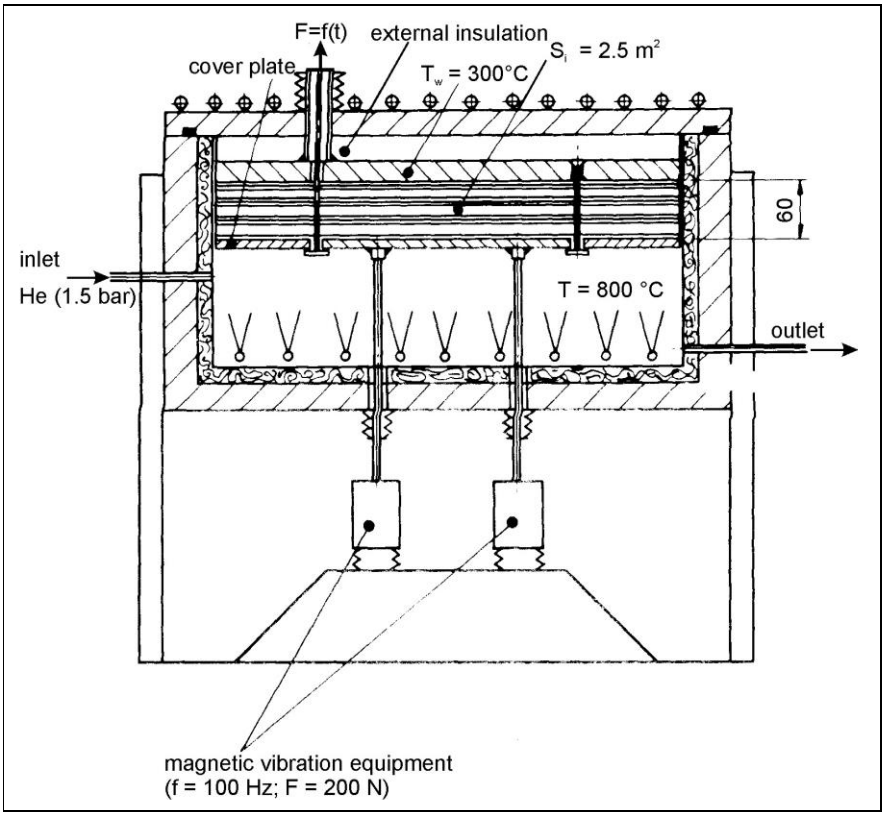

Figure 71: Facility for long-terms tests (HRB)

Figure 72 shows results from measurements concerning the resiliency of an insulation under load. The sample consisted of 20 meshes and 18 packages. It was pressed together by loads of up to 0.35 bars. The edge lengths of the sample to be tested were 380 mm. After the first loading, the sample lost 18 % of its original thickness. After load reduction it returned to 11 %. This value was also reached again

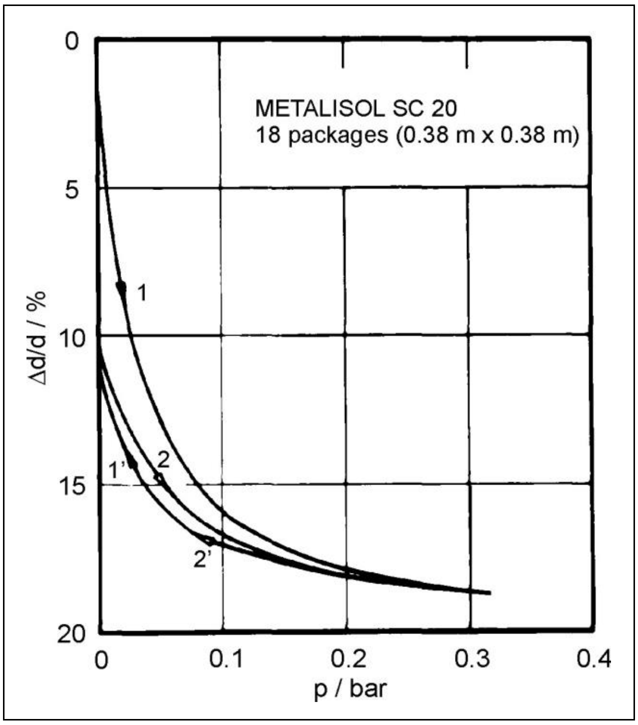

Figure 72: Compressibility as a function of load

after the second loading. The arrows indicate the direction of load. In the interesting range from about 0.05 bars to 0.2 bars, changes in thickness of up to 17.6 % were to be expected, which could no longer be neglected. In view of this loss, the occurrence of gaps was therefore expected, in which a flow due to free and forced convection with the consequence of an insulation reduction was possible.

For a large HTR with a power of 1160 MW three classes of insulation, as shown in Table 5, were proposed. The expected maximum temperatures in the different regions of the reactor plant and the proposed insulations are specified. For SC 15/5 mesh the wire diameters varied between 0.2 mm and 0.5 mm. The Masrock material will be dealt with in the further course of this report.

Class	Temperatures / °C	METALISOL
A	≤ 400	SC 20 SC 15/5
B	≤ 820	SC 15/5
hot gas ducts	local: 920	SC 20
C	≤ 820 hot streaks 1200	SC 15/5 or Masrock

Table 5: Wire mesh insulations for a large HTR

10.3.C Special geometries

Further metallic structures proposed earlier are found in Knirsch and Schmiedel [KNI67] as well as Narinski and Sheinin [NAR69], see Figure 55. On the right in the picture, marked by C, another form of spacers for a foil insulation is shown. Sheet metal strips were formed so that the cells produced looked like honeycombs. The individual layers were then covered by thin foils.

The insulations on the left in Figure 73 are stacks of sinusoidally corrugated foils of stainless steel, which were welded together along the contact lines. In this way, cells with rhombic cross-sections were obtained, which were closed at one end. The other open end was needed for pressure compensation processes. The insulations were installed so that the longitudinal axes of the cells were in parallel to the tube and vessel axes.

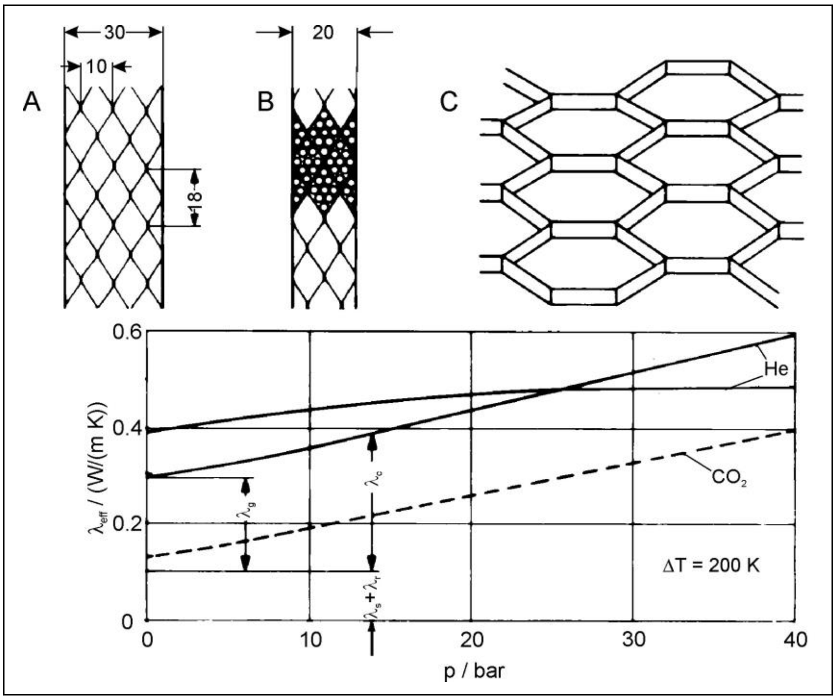

Figure 73: Cell insulations and effective thermal conductivities

Measurement results are only known for the systems shown on the left. The Alsthom company investigated two designs under contract to BBK, a subsidiary of BBC. Type A in the normal design with cells of 10 mm thickness and 18 mm length displayed a total thickness of 30 mm. Type B was 20 mm thick. Corresponding inserts also formed by foils permitted the basic structure of an elementary cell to be subdivided into smaller cells. The picture shows at the bottom effective thermal conductivities of the two insulations as a function of gas pressure. The maximum temperature difference across the insulation was 200 K. The results obtained in carbon dioxide atmosphere for type A are plotted for comparison. The pressure dependence under helium is greater than expected in view of the results measured in CO_2 before. Decomposing the total thermal conductivity into the individual fractions, the sum of solid conductance and thermal radiation, designated □□$_F$ and □$_S$, can be estimated as 0.1 W/(mK). The difference represents the contribution of the gas to the total thermal conductivity. At low pressures – free convection λ_K is thus not present – this fraction corresponds to that of the gas conductivity λ_G.

In Figure 74 the quotient of the thermal conductivities from free convection and gas conductivity is shown for both test gases. The Ra number was formed by the mean temperature difference across one cell and the cell thickness of 10 mm. The physical properties were related to mean pressure and mean temperature. A relation valid for both gases could not be derived from the measurement results due to a lack of intermediate values, e.g. in the range of Ra = 10^5. From the aspect of free convection, the cell thickness is too large for the use of CO_2. Smaller cells, however, would lead to increased material requirements again. For reasons of cost, this insulation was not used in any reactor.

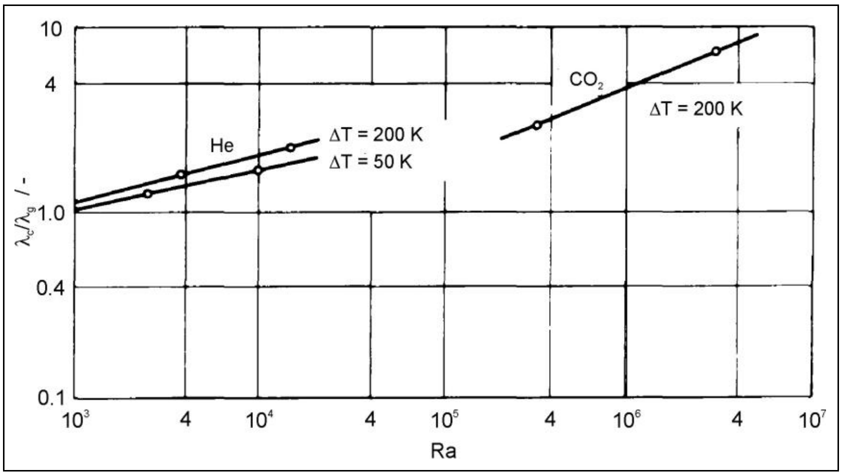

Figure 74: Dimensionless thermal conductivity as a function of the Ra number

10.4 Fibre insulation

Fibre insulations will be understood in the following as systems using fibrous materials for insulation, which fill in the cavities between the hot or warm ducting shrouds and the colder pressure walls and which contribute towards reducing the gas movements due to their smaller diameters. The starting materials are generally silica or alumina, whose material conductivities are low and which thus only contribute to thermal conductivity to a minor extent.

These insulations were primarily developed in Great Britain for large vessels and were hoped to eliminate the problems encountered with the metallic systems used for the Magnox reactors **–** outlet temperatures between 340 °C and 410 °C. These problems consisted in additional measures that became necessary for sealing off internal flows or leakages, e.g. near the not completely flat liners or in the case of breakthroughs, in spite of the good insulating properties. In the later CO_2-cooled AGRs, whose outlet temperatures were in the range of 650 °C, fibre blankets as described by Hosegood and Jones [HOS74] and Furber et al. [FUR75] were exclusively used. The pressure vessel of the Fort St. Vrain reactor built by General Atomic (GA) in the USA had also been lined with fibre blankets. It was initially planned to use a foil insulation similar to that in the American Peach Bottom reactor, where, however, irregularities were detected during the seven years of operation, which suggested changes of the foils, so that a new insulation was developed. But the main cause of the above problems was probably the gaps needed in metallic systems for reasons of mounting or expansion compensation, as discussed in detail in the preceding section. An alternative was therefore a fibre insulation, all the more since the Nuclear Power Group (NPG), which was charged with the construction of the Oldbury Reactor, was in delay precisely due to this insulation. Both companies were looking for a new insulation, which was not so sensitive to axial pressure gradients. Some of the fibre products initially selected were discarded after the first tests since they contained boron and corrosive salts. Kaowool largely fulfilled the requirements. According to Jones [JON69] it contains less than 100 ppm boron, 10 ppm chlorine, 50 ppm fluorine and 20 ppm sulphur. Its melting temperature is 1650 °C.

Figure 75 shows the insulation of the pressure vessel for Hinkley Point B after Colquhoun, Davidson and Bolton [COL75]. A similar insulation was also used for the vessel in Hunterston – also belonging to the Nuclear Power Group. The fibre blankets were pressed against the liner by means of cover plates and studs. A central stud and additional mounts can be recognized, which were to prevent a displacement of the cover plates. Metallic interlayers and z-shaped elements were to suppress or reduce free or forced convection in the insulation. On the hot gas side, a double layer of stainless-steel foils was to protect the fibres against the hot gas and, at the same time, prevent fibrous particles from being passed into the hot gas flow. The metallic foils were held by a system of first and second cover plates. The blankets of Kaowool fibres were compressed by about 20 % in most regions of the vessel. In this way, a connection between the fibres and any cavities, in which gas movements were possible, was to be prevented. An excessively high compression of the blankets had to be avoided in order to not destroy their fibres and prevent the internal pressure and, consequently, forces acting on studs and cover plates from becoming too high. For most regions a blanket pressure of 0.1 bars was considered to be sufficient. In the ceiling region, however, a pressure of 0.4 bars was allowed due to the high gas velocities.

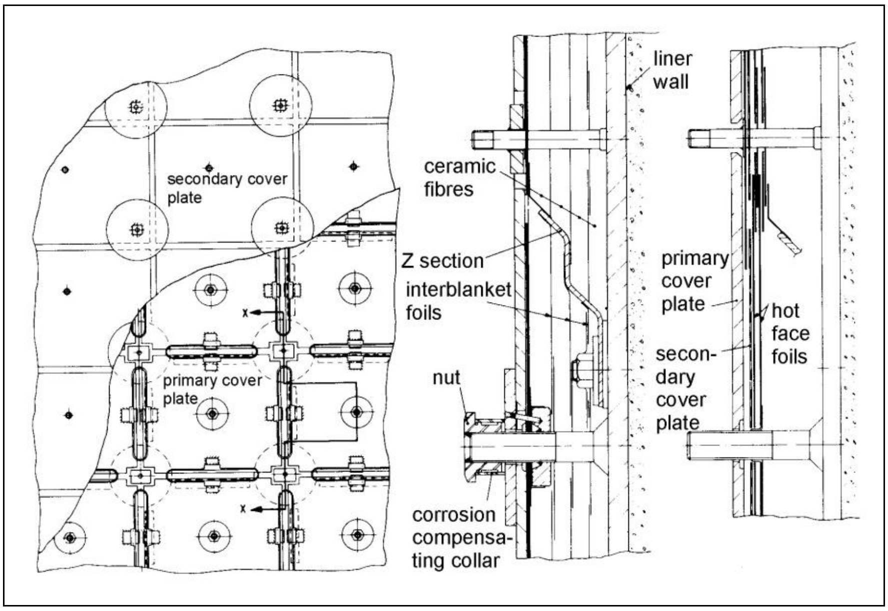

Figure 75: Liner insulation (Hinkley Point B)

Further data concerning insulation thicknesses, plate sizes, materials etc. can be found in the publications mentioned, where also information is given on the individual zones to be insulated, on experiments and design as well as on construction and licensing.

Figure 76 shows an exploded view after Furber, Hopkins and Stuart [FUR75] of the liner insulation of the Hinkley Point B reactor. Figure 77 shows a multi-stud design for a liner and highly stressed regions of this reactor from the same publication. It can be seen from both drawings that design and mounting is very sophisticated for both solutions. The authors particularly emphasize the resiliency, which is of significance above all for the long lifetime of the plants. A test facility for measuring this property is described. By means of a model it was attempted to extrapolate from short-term to long-term behaviour. In other test facilities, the resiliency of fibres under the influence of water, vibrations and radiation exposure was studied. Other questions concerned environmental problems, dust from the blankets and chemical resistance. Further summarizing information on liner insulations is found in Furber and Sheppard [FUR82]. Investigations had shown that Kaowool fibres only contained small

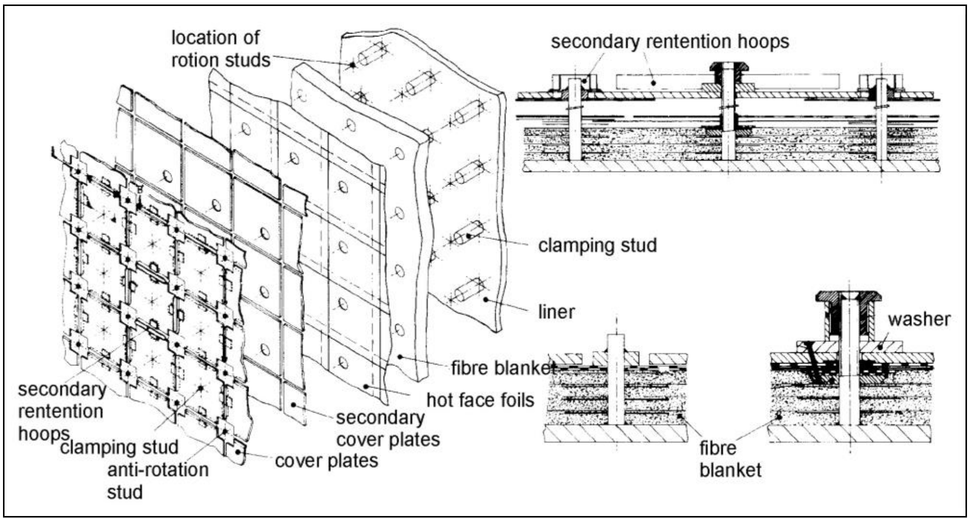

Figure 76: Liner insulation (Hinkley Point B)

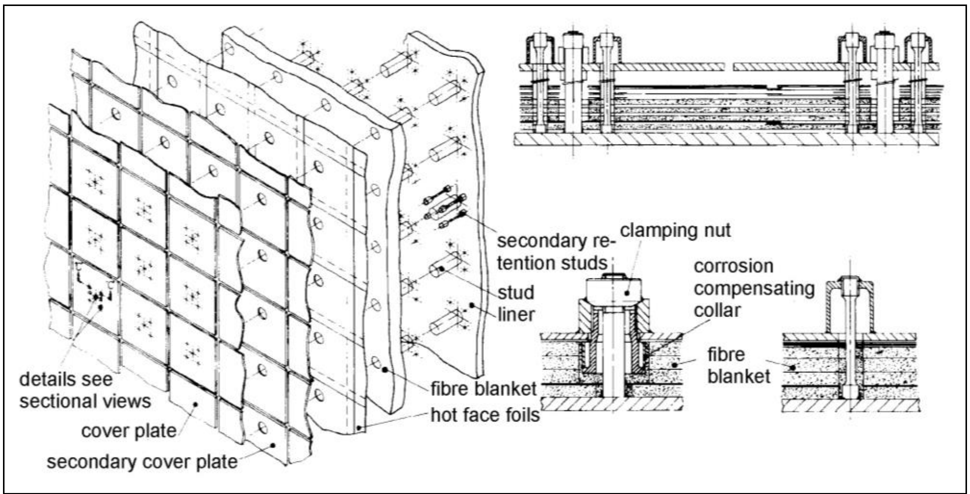

Figure 77: Liner insulation (multi-stud insulation, Hinkley Point B)

amounts of volatile and leachable impurities and were resistant to the coolant and to structural materials. Since a demonstration of the resistance over the entire lifetime of 30 years was not possible, the fibres were subjected to higher loads than under operating conditions. The results were then used to develop models with which predictions were possible concerning the operating time. The authors also discuss difficulties in mounting the liner insulation for Hinkley Point B. On account of welding problems, studs of two materials had to be replaced by studs of Incoloy 800, which could be directly welded onto the liner. Devitrification of the fibres had to be feared at temperatures above 650 °C at the end of or during the operating time. This was derived from experiments at temperatures up to 950 °C. Devitrification is to be attributed to a phase transition of the fibres due to recrystallization at elevated temperatures. According to [FUR82] the fibres can be destroyed directly or indirectly due to acoustically induced vibrations. The design was therefore such that so-called acoustic skins were used with which the fibres were to be protected against direct acoustic load. For the individual regions of the reactor, special designs were required, in which e.g. the necessary fibre densities representing a measure of the heat losses or thermal conductivities could not always be achieved or only under difficult conditions.

The Fort St. Vrain reactor was the first in den USA that was provided with a prestressed concrete pressure vessel. This required extensive development work for its internal insulation, see [HOS74] and Jones [JON75]. The gas pressure was about 48 bars, the helium mass flow 430 kg/s. The inlet and outlet temperatures were determined to be 400 °C and 777 °C, respectively. At full load, hot gas streaks of up to 1085 °C could occur at the outlet. For the design basis accident, loss of the coolant had been assumed. Consequently, the insulation in the bottom region had to be designed for temperatures of up to 1650 °C, since it was exposed to thermal radiation from the adjacent graphite structures.

The concrete temperature should not exceed a value of 59 °C in normal operation. Square cooling tubes – edge length 25 mm, wall thickness 3.2 mm – at the rear of the liner dissipated the heat losses. The cooling system had been designed for a mean temperature of 40 °C. The inlet and outlet temperatures were 35 °C and 46 °C, respectively. Thermocouples made it possible to determine the heat losses and detect defects in the insulation. The pitch of the cooling tubes was between 66 mm and 190 mm, depending on the level of expected heat losses. These should not exceed values between 2900 W/m^2 and 12600 W/m^2. The effective thermal conductivity was determined to be 0.43 W/(mK) with a safety margin of 2, with which the inaccuracies and a deterioration of the insulating properties during the lifetime should be taken into account.

The total insulation for the Fort St. Vrain reactor was divided into three classes, as was the METALISOL insulation. Class A was envisaged for the temperature range up to 427 °C, that is for the liner of the vessel in the core inlet region. At the core outlet, the higher-grade class B insulation was installed because of the higher temperatures of 777 °C. In the region below the core, i.e. at the reactor bottom, the insulation meeting the highest requirements, namely class C, was needed on account of the temperature streaks. The areas to be insulated were 1486 m^2, 140 m^2 and 55 m^2 according to Jones and Hedgecock [JON75] .

Figure 78 schematically shows the insulation for the low-temperature region of class A. The most important components are indicated. The fibres were available as blankets. The material was Kaowool. In the publications cited before, more detailed information can be found concerning the starting material, fabrication and properties.

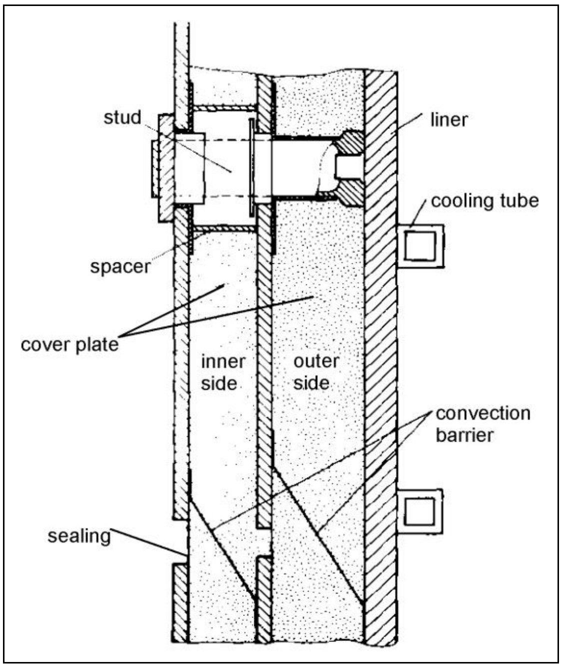

Figure 78: Insulation for the low-temperature region (class A)

The density as delivered was 128 kg/m^3. The blankets were pressed against the liner by cover plates via studs, until a fibre density of 192 kg/m^3 was achieved. This meant a reduction of the initial thickness by 33 %. The pressure of 0.2 bars needed for this purpose caused the fibres to adapt to the liner and avoided gaps. On the vertical walls, the blankets were held by fixing plates arranged at an angle of 45 °, so that slipping downwards was avoided. At the same time, however, they constituted an additional convection barrier in the axial direction. The closure to the gas plenum was formed by cover plates. At the sliding connections, 0.8 mm thick sealing foils were to prevent fibres from entering the gas plenum. The stud design was sophisticated. Thermal behaviour studies of this insulation had revealed low thermal conductivities on this insulation, which came close to those in helium at rest and suggested only a slight influence due to solid conductance. Under the influence of axial pressure gradients of up to 0.09 bars/m no increase was observed at the reactor inlet and even a reduction of the heat losses at the outlet.

The fibre blankets were examined with respect to

- chemical behaviour,
- tightening and associated fibre breakage,
- permeability as a function of tightening,
- resiliency as a function of temperature,
- behaviour upon dipping into water,
- drying rates and
- acoustic and mechanical vibrations.

The results were generally satisfactory with one exception. In testing the resiliency as a function of temperature, the material soon lost its capability of returning into the original state after having been stressed. This behaviour is shown in Figure 79 after [JON69]. One fibre packaged was pressed together in a helium atmosphere and heated over a defined time and then relieved again. The ratio of remeasured to original thickness is shown as a function of time for three temperatures. When extrapolating the measurement results to a time of 30 years, the lifetime of a reactor, a 50 % shrinkage of the insulation thickness had to be expected at a temperature of 537 °C. As furthermore reported, the loss in thickness was only 10 % at a temperature of 426 °C, if the fibres had been pressed together to 70 % of the initial thickness. This behaviour made it necessary to select and test further materials, which retained their resiliency even at temperatures up to 800 °C. General Atomic found a product at the French Quartz et Silice company, which met these requirements after thermal treatment of the fibres. The fibres consisted of almost pure silica. Concerning its appearance and properties, however, the material should correspond to Kaowool. It was selected for more highly stressed class B insulations because of its good resiliency. Hastelloy X was used for the metallic parts at the hot gas side and Inconel 600 for colder zones. The structure of this insulation corresponds to that in Figure 78. In contrast to the liner insulation, it was prefabricated at the factory and installed into the ducts at the building site. Thermal conductivity measurements had led to higher values than expected, although the investigations had been carried out without axial pressure gradients. This was due to gaps between liner and insulation, which, however, could be eliminated.

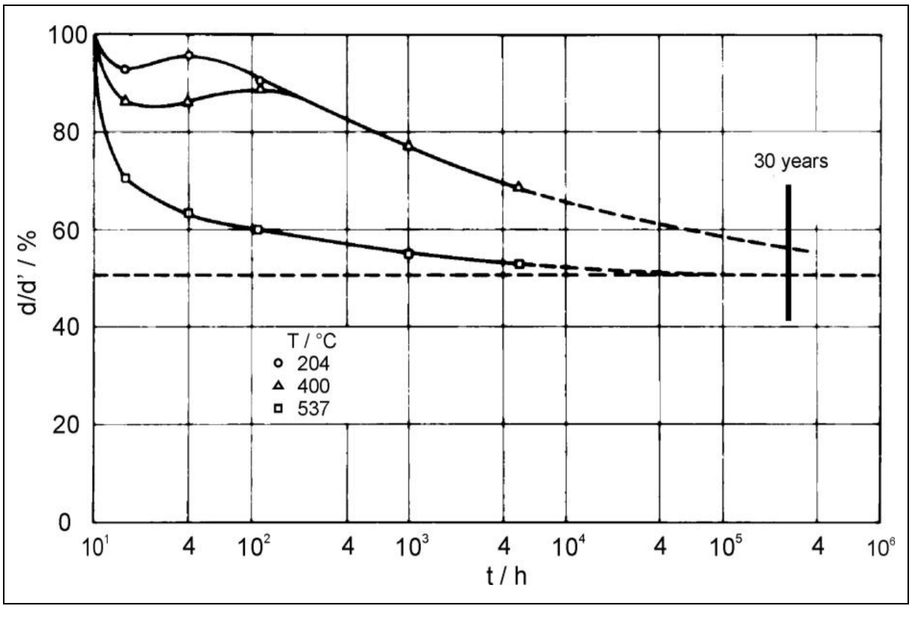

Figure 79: Resiliency of Kaowool as a function of time

Since numerous investigations had been performed on the insulation of the prestressed vessels, many measurement results were available and practical experience could be used, it was decided at the then KFA in agreement with the project partners to test fibre insulations for pipes after the metallic systems. Such an insulation was envisaged for the HHV facility as a test sample. Furthermore, the entire duct system except for the tube segment was to be lined with a fibre insulation. A pretest in a smaller test facility therefore seemed to be necessary.

Work was started at the IRB. The above-described HP channel was available for measurements, see Bröckerhoff and Scholz [BRÖ75b]. The pressure tube was the tube also already discussed, which had been procured for investigating the foil insulation. Since poor behaviour similar to the foil insulation had to be feared, two designs were envisaged. The experimental procedure and the evaluation of the measurement results largely corresponded to the work on the foil insulation. The pressure tube with cooling system and the position of the tube in the duct system of the HP channel also corresponded to those of the insulations discussed before.

The test insulation was supplied by Brown Boveri-Sulzer Turbomaschinen (BST) AG/Zürich, see Figure 80. The inner diameter of the insulation was 630 mm. This gave an insulation thickness of 148.5 mm, which corresponded to the thickness of the HHV insulation. Two versions were installed into the pressure tube, as mentioned before. The version with an intermediate tube can be seen at the bottom of the picture. The upper design had two intermediate tubes. The metallic ducting shrouds were welded onto V-shaped end pieces, which had the same function as the Z-pieces in the foil insulation. They were to prevent the effect of axial pressure gradients on the insulation behaviour. At the non-welded end, the ducting shrouds overlapped with short tube pieces connected to the adjacent V-piece. In this way, axial expansions due to shifting could be accommodated .The end pieces were externally connected gastight to 22 mm wide rings welded to the pressure tube. The dot-dashed perforated sheet had the task of separating the actual insulation space with the fibre stuffing from the hot gas plenum and of enabling the gas to escape from the insulation space in case of rapid pressure reductions. For this purpose, the ducting shrouds were provided with 16 holes, whose diameter was 20 mm. The perforated sheets were covered by a fine wire mesh to prevent loose fibre particles from entering the gas plenum. As can be seen, the perforated sheets were connected to the ducting shrouds. X10CrNiNb was used as the material for the metallic parts.

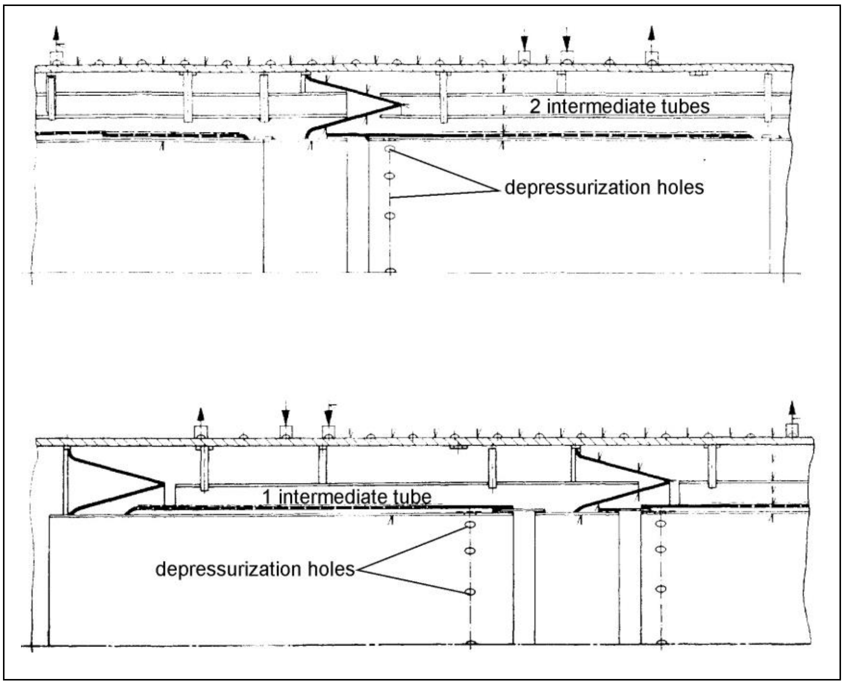

Figure 80: Fibre insulation (stuffed)

The insulation consisted of three segments of 1200 mm length each. Since the gap of 12 mm provided by the manufacturer between ducting shrouds and perforated sheets was considered to be too great according to experience made with the foil insulation, only one and a half segment lengths were now fabricated with this gap width, see bottom diagram. The remaining segments only had a gap of 4 mm. Furthermore, two intermediate tubes were provided here. They were to reduce or prevent a feared convection. The remaining two or three gaps were stuffed with refired Kaowool. Firing should expel the lubricants necessary for the spinning process. Since stuffing was carried out by hand, local irregularities in the packing density could not be ruled out. In total, mean densities of 400 kg/m^3, bottom diagram, and 280 kg/m^3, top diagram, were achieved. The differences could be explained, on the one hand, by the larger gap widths in the insulation with only one intermediate tube. Another reason was the better mounting possibilities. The pressure tube was positioned vertically when the insulation was installed. Mounting took place as follows:

- welding in of the bottom V-piece
- fixing the intermediate tube(s)
- stuffing the gap(s)
- mounting the ducting shrouds with perforated sheets
- stuffing the gap
- welding in of the next V-piece

Work inside the tube could only be carried out by one man. When stuffing the last segment, help was possible from an external platform around the pressure tube, so that temporarily two men could work. This also explained the higher packing density. A critical point in placing the fibrous material was the cavities near the V-pieces. Statements on the densities achieved there were not possible.

As in the case of the foil insulation, the temperatures within the insulation were also to be measured. Figure 80 shows the two measuring levels for the thermocouples. The positioning of the thermocouples on metallic parts, i.e. ducting shrouds, perforated sheets, intermediate tubes and pressure tube, did not present any difficulties. The thermocouples within the fibres were attached without mounts. Their precise radial fixation was of particular significance. It had to be ensured that the measuring points could not be shifted during further stuffing. Figure 81 shows a mounting state. The pressure tube can be seen on the outside and the ducting shroud on the inside. The two gaps are already stuffed up to the level of the intermediate tube. Some thermocouple leads can be recognized. In each of the two sections, see Figure 80, five thermocouples each were installed in the top, right. bottom and left sectors. Further measuring points were located on two V-pieces and on the cooled outer wall.

The measurement programme largely corresponded to that of the foil insulation. With a total of 180 signals from the pressure, temperature and flow rate meters, the data acquisition system was used to capacity. In comparison to the investigations on the foil insulation, much longer waiting times were needed until reaching the steady-state condition. As long as the water temperatures still changed within a period of about 30 minutes, it was assumed that no steady-state conditions were established. The measured values where only recorded when these changes were zero or almost zero for one hour. When the temperature level changed, adjustment times of up to eight hours were required. These times coincided with an estimate of the test time using the Fo number. The waiting times were shorter for a pressure change at constant temperature level. The data reduction was the same as for the foil insulation.

Figure 81: Mounting state (fibre insulation)

From the abundance of measurement results only a few are selected. Figure 82 shows the temperatures within the insulation for helium, the highest gas pressure and the highest gas temperature for both versions. At the bottom, the insulations with pressure tube, intermediate tubes and perforated sheets are indicated to scale as the abscissa. The fibrous material is symbolized by the dots. The packing densities were 400 kg/m^3 (left) and 280 kg/m^3 (right). In the metal layers of the insulation, the temperatures were assumed to be constant. The vertical straight lines indicate the position of the thermocouples in the fibrous material. On the whole, the distribution of the temperatures in the insulations was considered good compared to that of the foil

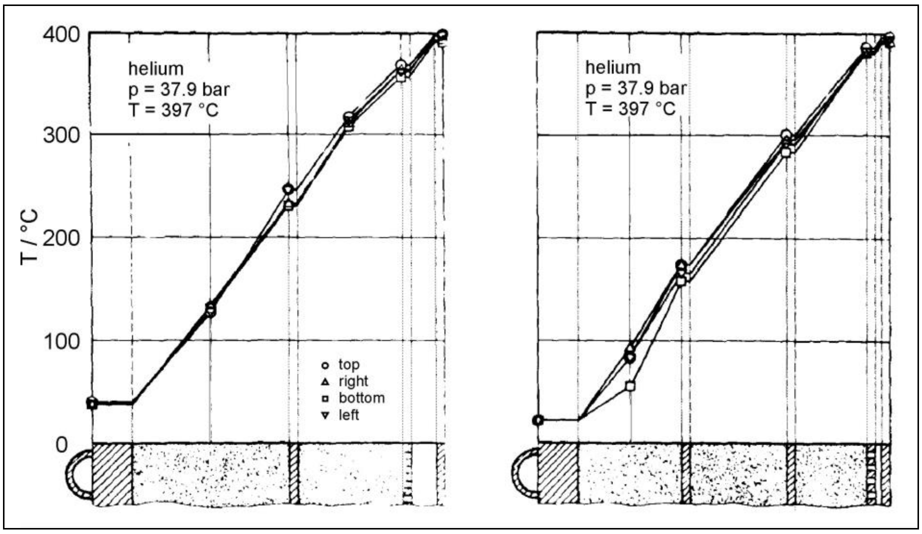

Figure 82: Temperatures within the insulation

insulation. However, the temperatures curved upwards are indicative of further effects, such as radiation and convection, in addition to pure heat conduction. Since the temperatures with air as the test gas were also much more homogeneous than in the foil insulation, a significant influence of convection can be ruled out. This had already become clear when considering the results at low pressures, see relation 9.

Figure 83 shows the temperatures along the cooled tube wall and in the cooling water. The gas data correspond to those of the last diagram. As before, the two test insulations are symbolically shown at the bottom. One end piece each was arranged in each measurement section. The cooling water temperatures vary nearly linearly. Due to the smaller stuffing density, the sector with two intermediate tubes exhibits small temperature differences between top and bottom, which are, however, insignificant. The wall temperatures differ more significantly, above all in the region of the V-pieces, whose stuffing was pointed out before. However, their difference from the water temperatures is small. Therefore, low heat losses or thermal conductivities were expected. Following the measurements in the HP channel, investigations were also performed in the vertical arrangement of the test section using the electric heating as before. Due to the lower heat losses, temperatures of up to about 770 °C were reached on the hot gas side.

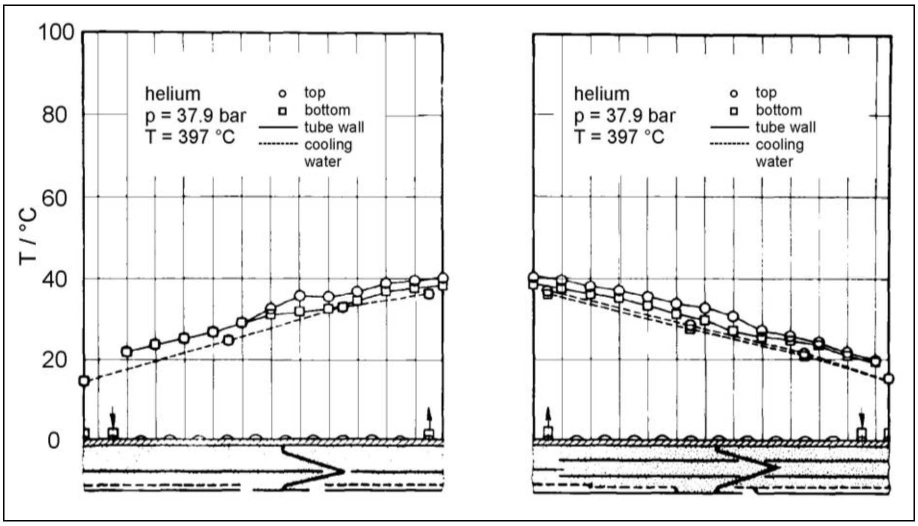

Figure 83: Wall and water temperatures

Investigations on a similar design were carried out by Bruners, Lang and Noack [BRU75] in the ARGAS facility at temperatures up to 1000 °C and pressures up to 10 bars. These measurements, as well as those in the HP channel, served to select a suitable design for the HHV facility. Figure 84 shows the fibre insulation of segment 13 of this facility after [BRÖ76]. The inner diameter of the pressure tube was 1400 mm, the length of the segment was 4400 mm.

As can be seen, the design with one intermediate tube was selected as the solution. The pressure tube and the insulation weighed 5700 kg and 4000 kg, respectively. All metallic parts of the insulation were made of Inconel 625. The gap between ducting shroud and perforated cylinder was 15 mm. The stuffing material was also Kaowool. Part of the insulation had already been installed at the Swiss manufacturer's factory, BST. The packing density of this part was 337 kg/m^3. The other part, which was to be equipped with thermocouples, was installed at IRB of KFA. The measurement section is shown in the figure. Its stuffing density was 290 kg/m^3. In contrast to the insulation tested in the HP channel, no thermocouples were provided in the fibrous material of the HHV fibre insulation, but only on metallic parts. The position of the thermocouples can be seen in the diagram. This measurement segment was additionally provided with 14 sound measuring probes.

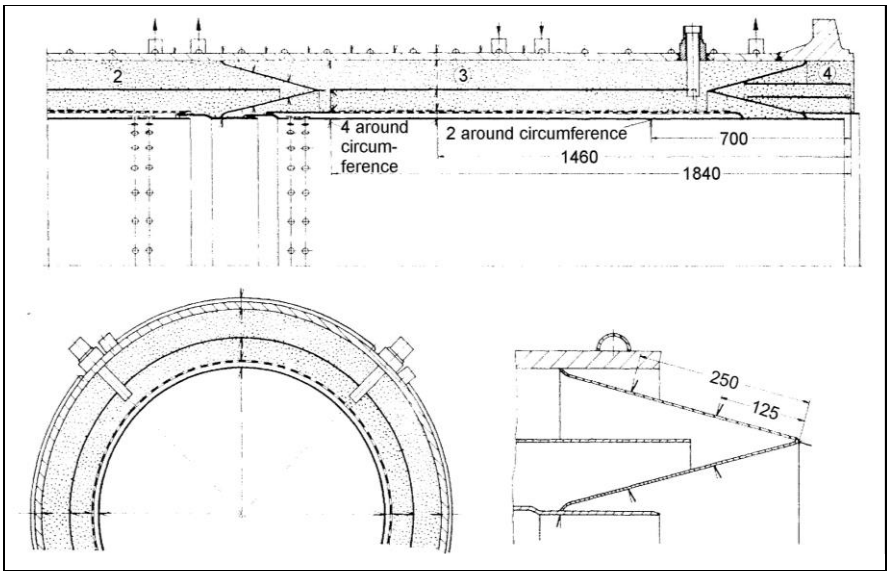

Figure 84: Fibre insulation

Figure 85 shows Nu numbers as a function of the mean temperature in the insulation for various insulations and experiments. The diagram shows the results from measurements in the HP channel, in the ARGAS facility and in the HHV facility. In contrast to the foil insulations investigated, the fibre insulation tested in the HP channel, whose density was 400 kg/m^3, only displayed Nu numbers of 1.95 for the top and 1.8 for the bottom sector, i.e. free convection was only small. The averaged

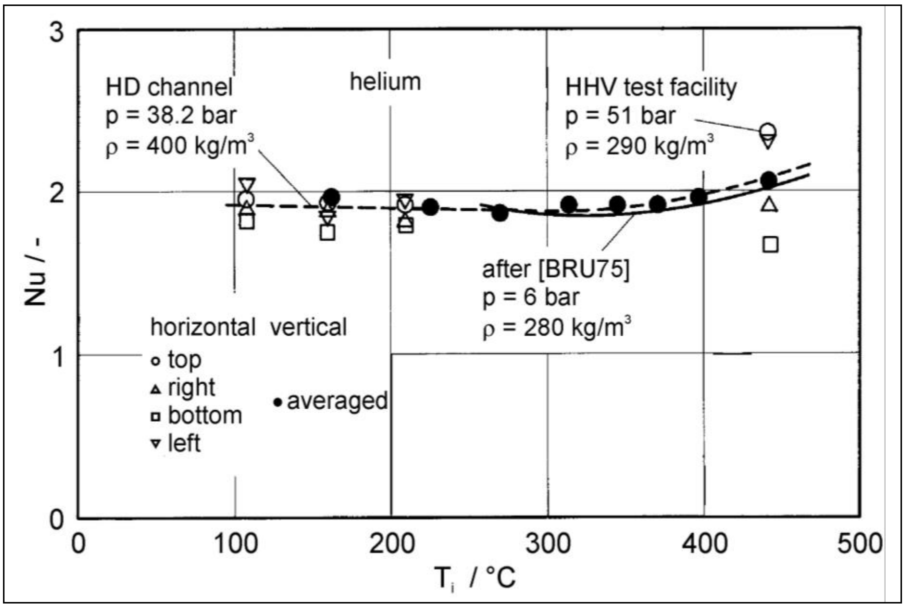

Figure 85: Nu numbers as a function of the mean temperature in the insulation

Nu number was only 1.9. The values measured with the test section in the vertical position are in good agreement with the other measuring points. At a mean temperature of 320 °C within the insulation, the Nu numbers seem to pass through a minimum of 1.85. They then rise continuously. In the region of low temperatures, the influence of free convection was greater than that of heat radiation, because the fibres become more permeable for heat radiation at higher temperatures. On the whole, the broken curve appropriately reflects the measured values. The results are also in good agreement with results of Bruners and coworkers [BRU75], although the fibre density was only 280 kg/m^3. Moreover, the pressure was only 6 bars. Because of the small influence of the gas pressure, the mean value of 2.07 from the HHV measurements also agreed well with all the other values. However, the differences of the Nu numbers between top and bottom quadrant were greater than expected. These differences could be attributable to inhomogeneous stuffing densities, above all near the end pieces. For this reason, fibre blankets were envisaged for further designs of the project partners, with which more homogeneous packing densities seemed to be attainable due to the cover plates used. These systems will be described later.

In summary, Figure 86 shows averaged Nu numbers as a function of the mean temperatures in the insulations. As in the diagram before, the values shown for the tube segment are only valid for the version with one intermediate tube, that is with the high stuffing density, and with helium. However, Figure 68 contains results for three pressure stages. The test section was in the horizontal and vertical position. The results of [BRU75] are also plotted. As was already seen when discussing Figure 67, the differences between the top and bottom sectors were small, so that the representation chosen in Figure 68 seems correct and suitable for designing similar systems. The error would only be small assuming a mean value of 2. Further details on this and on the investigations of the foil insulations are to be found in Bröckerhoff and Scholz [BRÖ77a] or Bröckerhoff [BRÖ78a].

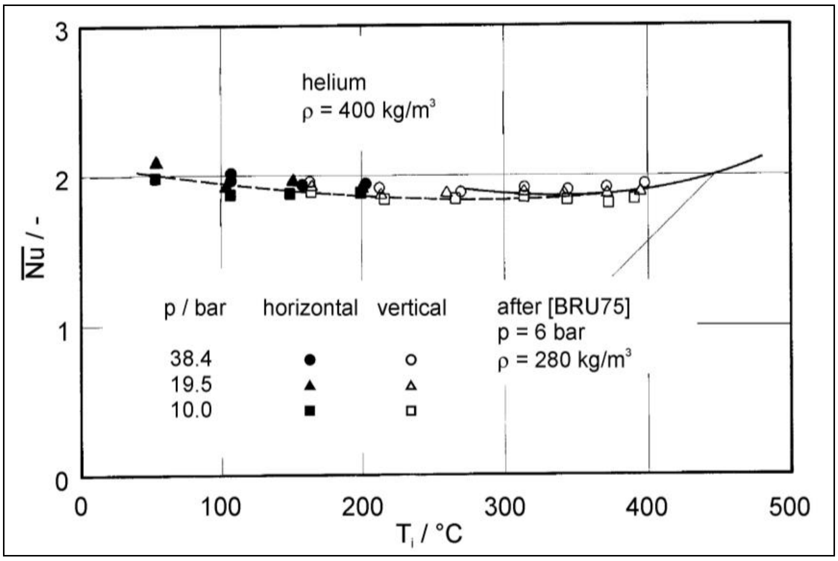

Figure 86: Nu numbers as a function of the mean temperature in the insulation

Tebroke and Achenbach [TEB92] computationally determined the temperature and flow fields of internally insulated hot gas ducts. They used the Boussinesq approximation and Darcy's law. The physical properties except for the density in the buoyancy term were first assumed to be constant. Following these calculations, variable properties were gradually introduced. With the discretized relations, the temperature and flow fields for different number products were then calculated up to a value of Ra·Da = 2000. The Darcy number Da is the ratio of permeability B to the square of a characterizing length, e.g. the tube diameter. The internal temperatures of 950 °C prevailing in a typical hot gas duct were taken as the basis. The pressure was 40 bars. The outside temperatures were chosen to be 100 °C and 300 °C. Calculations corresponding to the data observed in the HP channel were added. Helium was mostly assumed as the cooling gas. Alternatively, calculations with air were also performed. In the realistic case of application, however, the number product of Ra·Da = 2.65 obtained was so small that the change of the convection flow was not reflected in the result. A variation of the parameters of diameter, stuffing density, fibre diameter and gas pressure showed, however, that convection reliability was not given in all cases. The tendency of a fibre insulation to convection increases with rising diameter ratio, pressure and fibre diameter and decreasing packing density. If all these parameters are changed in an unfavourable direction, a number product higher by a factor of 37 is obtained resulting in an increase of the Nu number to 1.57. Achenbach [ACH88] and [ACH91] also used the Boussinesq approximation for calculating the heat transport due to free convection in the fibre insulations. His results in part coincided very well with the values measured in the HP channel.

A fibre insulation was also tested in the helium test facility of the IEA in São Paulo/Brazil. The channel was designed for a mass flow of 2 kg/s and a pressure of 20 bars. The blower speed was 12000 r.p.m. The pressure tube and the metallic parts had been manufactured by ARG-Mineralölbau GmbH. Mounting of the insulation into the tube and thermocouple instrumentation were carried out at IRB of KFA. The length of the vertically arranged tube was 3080 mm. The outer and inner diameters were 457 mm and 425 mm, respectively. The inner diameter of the flow channel was 220 mm, so that the thickness of the insulation was fixed as 112.5 mm. The fibre material was also Kaowool. The version with one intermediate tube was taken because of the small diameters. The stuffing density was approximately 250 kg/m^3. The externally welded-on cooling system was fourfold subdivided in the longitudinal direction (two measurement and guard zones each). No subdivision could be made in the circumferential direction, but such subdivision did not seem meaningful because of the vertical arrangement. The cooling coils with a pitch of 100 mm were helically arranged around the tube and welded. In contrast to the above-described pressure tubes, no halved but complete tubes with an outer diameter of 14 mm and a wall thickness of 2 mm had been installed. The cooling system was designed for a pressure of 10 bars and a temperature of 100 °C.

During two four-week visits to the institute, numerous modifications had to be made at the test facility, the test insulation had to be placed into the duct system of the channel and welded and the measurement cable connected. Only the institute head was able to put the test facility with the magnetic-bearing blower into operation and keep it running. The tests were run according to the programme defined by the German side. The experiments had to be manually evaluated, although there was a computer available for data acquisition.
At the highest hot gas temperature of about 840 °C, the maximum wall temperatures were only 60 °C. As expected, they varied approximately linearly in parallel to the

cooling water temperatures. The temperatures measured in the insulation were almost identical in all sectors. The dependence on the gas pressure was very small. More precise analyses were not immediately possible and were not carried out by the Brazilians later, so that only approximate statements were possible concerning heat losses and Nu numbers. At a hot gas temperature of 400 °C, the heat losses were about 2000 W/m^2, the Nu numbers slightly below 2.

The heat transport in the fibrous materials due to free, forced and mixed convection was described by Konuk [KON78a], IEA staff member at that time, who solved the energy equation

$$\frac{\partial}{\partial r}\left(r\,\rho\, c_p v_r T\right)+\frac{\partial}{\partial \Theta}\left(\rho\, c_p v_\Theta T\right)-\frac{\partial}{\partial r}\left(r\,\lambda\frac{\partial T}{\partial r}\right)-\frac{1}{r}\frac{\partial}{\partial \Theta}\left(\lambda\frac{\partial T}{\partial \Theta}\right)=0 \qquad (37)$$

and the continuity equation

$$\frac{\partial \Psi}{\partial \Theta}\frac{\partial}{\partial r}\left(c_p T\right)-\frac{\partial \Psi}{\partial r}\frac{\partial}{\partial \Theta}\left(c_p T\right)-\frac{\partial}{\partial r}\left(r\,\lambda\frac{\partial T}{\partial r}\right)-\frac{1}{r}\frac{\partial}{\partial \Theta}\left(\lambda\frac{\partial T}{\partial \Theta}\right)=0 \qquad (38)$$

under assumed boundary conditions for horizontal and vertical arrangements of cylinders or rectangular geometries and for steady-state conditions. In these equations, r denotes the radius of a cylinder, v the velocity in the porous materials, T the local temperature, Θ the cylindrical angle coordinate and Ψ the stream function. The other quantities have already been used before and explained. The equations were solved numerically. Good agreement between measured and calculated results was reached for vertical flat walls. Since the author did not have any experimental results on cylinders at his disposal when he generated the program, it was not yet possible to demonstrate the suitability of the prediction calculated. This demonstration was to be made with the test results in the helium test facility. In a further theoretical study, see Konuk and Rodriguez [KON78b], concepts for hot gas ducts with insulations were recalculated.

Similar calculations were performed by Kondo and colleagues [KON84] from the Japan Atomic Energy Research Institute (JAERI). This work was closely related to the testing of components, including hot gas insulations, in the large HENDEL test facility (Helium Engineering Demonstration Loop). This facility and the investigations performed there will be dealt with in the following. The program had been developed to analyse the flow behaviour within an insulation with intermediate tubes for high-temperature reactors. It was based on a stuffed fibre insulation with one intermediate tube, i.e. two spaces. Stuffing was assumed to be two-dimensional and homogeneous. Darcy's law was applied. The aim was above all to investigate the influences of a bypass flow through the breather holes on the insulating behaviour. The insulation was assumed to be horizontally arranged. In the above publication, flow fields based on the numerical calculations are presented and discussed in connection with the heat transfer properties for typical Rayleigh numbers.

Among others, Hishida et al. [HIS84] and Yasuno et al. [YAS82] have described the HENDEL facility and the investigations performed there. The facility consisted of three parts, the so-called mother loop, the adapter loop (M and A loops) and the test sections. The first two sections supplied the test sections with the helium coolant. In the first phase of the project, the M and A loops were built. Design work had been commenced in 1978; the facility was available for tests in March 1982. It served to investigate

- fuel assemblies and control rods,
- support structures of the core or the reactor bottom,
- reactor components and reactor structure as well as
- high-temperature components of the heat removal system (primary and secondary cooling system).

The flow sheet and important data concerning the facility can be found in the publications mentioned. No further details are given here. In the following, only work on the insulations will be described.

Two hot gas ducts were tested. Duct A was connected to a main heater and a main cooler, Duct B connected two other main heaters. Table 6 contains some data on the two test pieces.

Designation	Duct A	Duct B
maximum gas temperatures / °C	1000	700
gas pressures / bar	40	40
tube wall temperatures / °C	350	350
Dimensions		
pressure tube diameters (outside) / mm	660.4	558.8
pressure tube wall thicknesses / mm	22	18
ducting shroud diameters (outside) / mm	355.6	355.6
ducting shroud wall thicknesses / mm	6	6
lengths of ducts / m	14	23.6
Materials		
pressure tubes	SB 42	SB 42
ducting shrouds	Hastelloy X	Incoloy 800 H
V-shaped end pieces	Hastelloy X	Incoloy 800 H SUS 304 SUS 316
studs	Hastelloy X Incoloy 800 H	Incoloy 800 H
insulation materials	Kaowool	Kaowool

Table 6: Data of hot gas ducts in the HENDEL facility

Figure 87 schematically shows the insulation for Duct A. Due to the internal temperature of 1000 °C, Hastelloy X was selected as the material for the ducting shroud. In contrast to the fibre insulations so far presented, the actual insulation space consisted of three layers separated by two foils of stainless steel. Kaowool with a stuffing density of 200 kg/m^3 was used as the insulation material for the inner two layers. The fibre density in the outermost interlayer was 250 kg/m^3. The v-shaped end pieces were welded to the pressure tube and ducting shroud at distances from 0.7 m to 1.4 m. The concept for duct B corresponded to that of duct A. A difference from the test pieces presented so far was the lack of water cooling on the outer wall. The heat losses were passed to the environment by means of free convection.

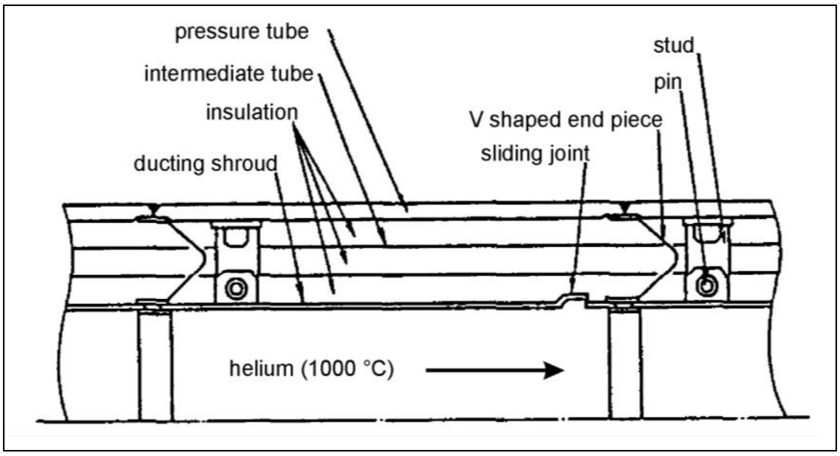

Figure 87: Fibre insulation (schematically)

The tests were carried out at temperatures between 400 °C and 950 °C, pressures between 10 bars and 40 bars as well as helium mass flows between 0.5 kg/s and 3.5 kg/s. The temperatures along the pressure tube walls and within the insulation were measured by thermocouples and the heat losses on the outer sides by heat flow meters. The flow conditions around the outer walls of the ducts were made visible by vaporized dry ice.

Figure 88 shows pressure tube temperatures measured in the circumferential direction. The diagram shows the distributions of the temperatures for the horizontal

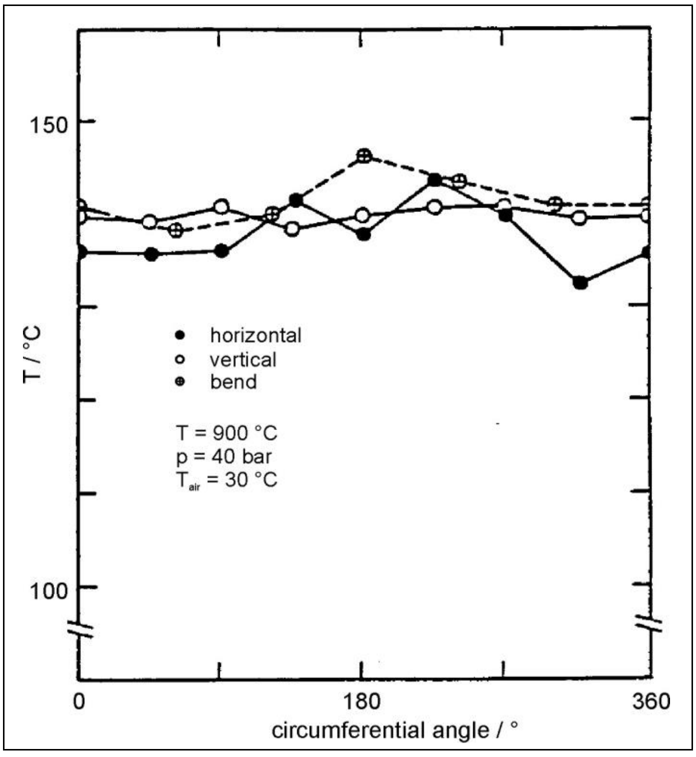

Figure 88: Temperatures of the pressure tubes

and vertical positions and for a bend. The maximum temperatures were 145 °C near the end pieces and studs. In total, they only differed by up to 15 K. In spite of maximum differences of about 30 K, the insulating behaviour of the test insulations was considered to be good. The temperatures measured in the radial direction within the insulations agreed fairly well with calculations performed with temperature-dependent thermal conductivities of the insulating material.

The heat losses taken from [HIS84] were less than or approximately 200 W/m^2. These values must be regarded as too low in comparison to the results discussed before. These low values are probably attributable to the measurement by heat flow meters. The effective thermal conductivities determined from these values are presented in the publications mentioned. They were compared with the results of numerous other authors. Differences of up to 50 % were discovered. These were explained by the composition of the stuffing material, by the stuffing methods and by the designs. Hishida and co-authors [HIS84] specify a relation each for the horizontal and vertical arrangement of the test insulations for calculating the effective thermal conductivities as a function of the mean temperature in the insulations. These are:

$$\lambda_{eff} /(W/(mK)) = 0{,}01963 + 4{,}702 \cdot T/(K) \cdot 10^{-4} \qquad (39)$$

for the horizontal and

$$\lambda_{eff} /(W/(mK)) = 0{,}02014 + 6{,}039 \cdot T/(K) \cdot 10^{-4} \qquad (40)$$

for the vertical position. The authors explain the about 25 % to 30 % higher thermal conductivities in the vertical position by free convection within the fibre layers.

As was seen during visits to Japanese companies, which took place in the course of numerous journeys to perform task manager activities within the framework of Japanese-German cooperation, tests on fibre insulations were also carried out at other places in Japan. However, the test facilities and thus also the dimensions of the test pieces were much smaller than the HENDEL facility. These measurements are therefore not described. All the tests required for HTR applications were carried out in the HENDEL facility of JAERI.

From the aspect of thermal behaviour, the fibre insulation was or is suited for application in gas-cooled reactors. This is also indicated by the fact that Barnert et al. [BAR85] had proposed fibre insulations for the planned, but not realized AVR modification as insulations for the hot and cold gas ducts. They were to serve as connections between hot-gas penetration at the AVR and steam reformer and between blower and cold-gas recycling. The hot and cold gas temperatures were defined as 950 °C and 200 °C, respectively, the helium mass flow as 6.5 kg/s. The pressure-bearing seamless tubes of 20MnMoNi55 were water-cooled and designed for an operating temperature of 100 °C. The insulating material was to be Saffil. The metallic parts of the insulation were to be made of Inconel 617.

The investigations so far discussed were confined to straight pipes. Measurements on bends were not available at that time. For this reason, a hot gas bend with a stuffed fibre insulation was ordered for investigations in the HP channel. This test component was flanged into the channel system behind the blower, see Figure 42. Stress calculations for the channel did not indicate the possibility of excessively high stresses in any location, although a completely different behaviour could be expected due to the omission of expansion bellows and due to the required external water cooling. The pressure jacket with feed section was manufactured by MAN. The inquiry for the insulation to BBC/Switzerland had led to the result that only a stuffed insulation was possible due to the small radius of curvature. Part of the feed section was also insulated to avoid axial heat conduction in the walls. A fibre blanket insulation to be described later served as wake section, see Bröckerhoff [BRÖ82b].

The bend and insulation are shown in Figure 89. With an inner diameter of 930 mm the pressure-bearing parts were adapted to the existing test tubes. Further dimensions can be seen from the diagram. The insulation corresponded to the already discussed fibre insulation with ducting shroud, perforated tube positioned behind with wire meshes for the retention of fine fibre particles, intermediate tube and fibres. After installation of the metallic parts for segment I, the annular gaps were stuffed with Kaowool. Following this, subsegments IIa and IIb were mounted. The ducting shrouds belonging to this segment were welded together at the centre. Stuffing densities of 230 kg/m^3, 214 kg/m^3 and 208 kg/m^3 were achieved for segments I, II and III. This gave a mean density of 218 kg/M^3. Irregularities and deviations could not be ruled out due to the geometry and the difficulties in stuffing, which were much greater than with straight tubes. Thermocouples were mounted in sections A-A, B-B and C-C in the four sectors at the top and bottom as well as outside and inside in the radial direction. The cooling systems were fourfold divided in

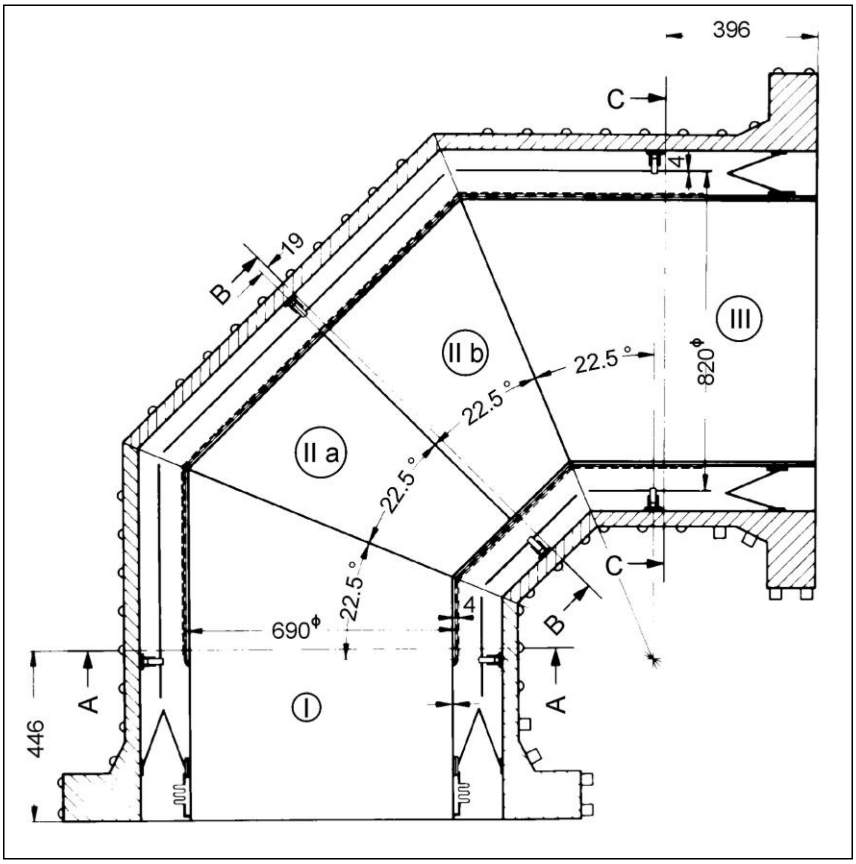

Figure 89: Fibre insulation (segmented bend)

the circumferential direction and twofold in the longitudinal direction. The cooling gas entered the bend at the bottom. Pressure compensation took place on the rear flange at the sliding connection between bend and wake section, i.e. the ducting shrouds had no breather holes.

Some results can be found in [BRÖ82a] and [BRÖ82b]. Figure 90 contains temperatures measured in section C-C in the insulation for tests with air (left) and helium (right) at the highest pressures, temperatures and velocities.

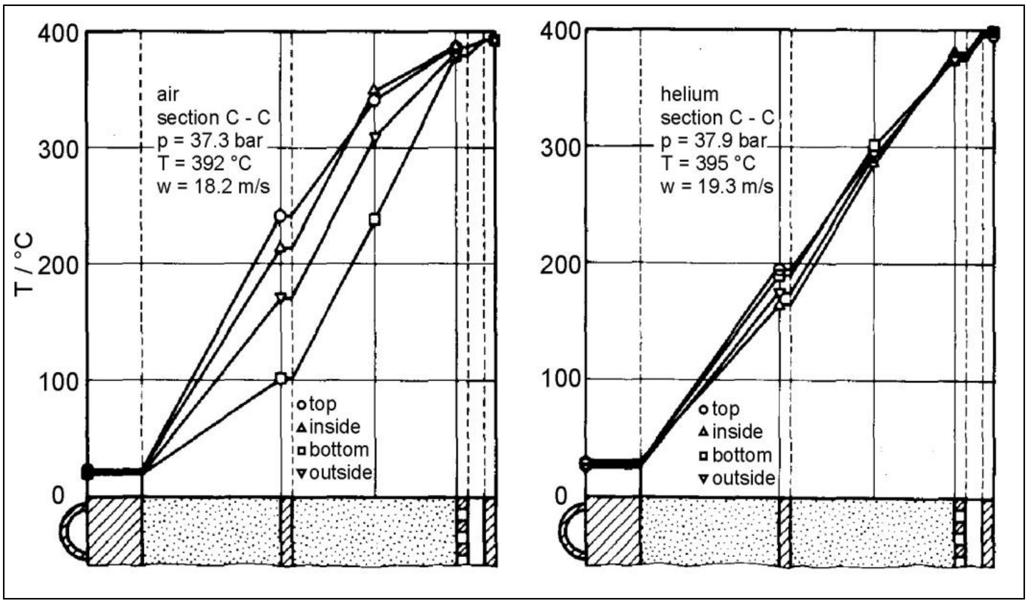

Figure 90: Temperatures within the insulation

The temperatures in the other sections approximately corresponded to those shown here. As expected and can be seen, temperature differences between inner and outer contours also occurred for the bend. This was not only explained by the low density, but above all by the geometry. On the intermediate tube, a difference of 140 K was measured between the top and bottom quadrants with air cooling. The differences were much smaller in the helium tests.

Figure 91 shows mean Nu numbers as a function of the circumference angle for the three segments. Compared to the results for tubes insulated with stuffed fibres, the Nu numbers are only valid for the spaces filled with Kaowool. Ducting shroud and gap were left out of consideration. In spite of the almost identical fibre densities for all segments, the Nu numbers differed considerably. Above all, the central section showed higher values than the other segments and the greatest differences across the circumference. In the top sector (circumference angle 0 °) the Nu number was 2.1, inside only 1.1 (90 °). The maximum was measured for the outside quadrant (270 °). The mean value of 1.84 approximately corresponded to that of Figure 67 and Figure 68. Lower and more homogeneous Nu numbers, on average, were found for segments I and II. Although the neighbouring feed and wake sections were insulated and the flanges cooled to avoid axial heat losses, an influence by these parts could not be ruled out. Temperature peaks on the cooled outer wall were not observed.

In the two tests described before, the ducting shrouds of the insulation were closed.

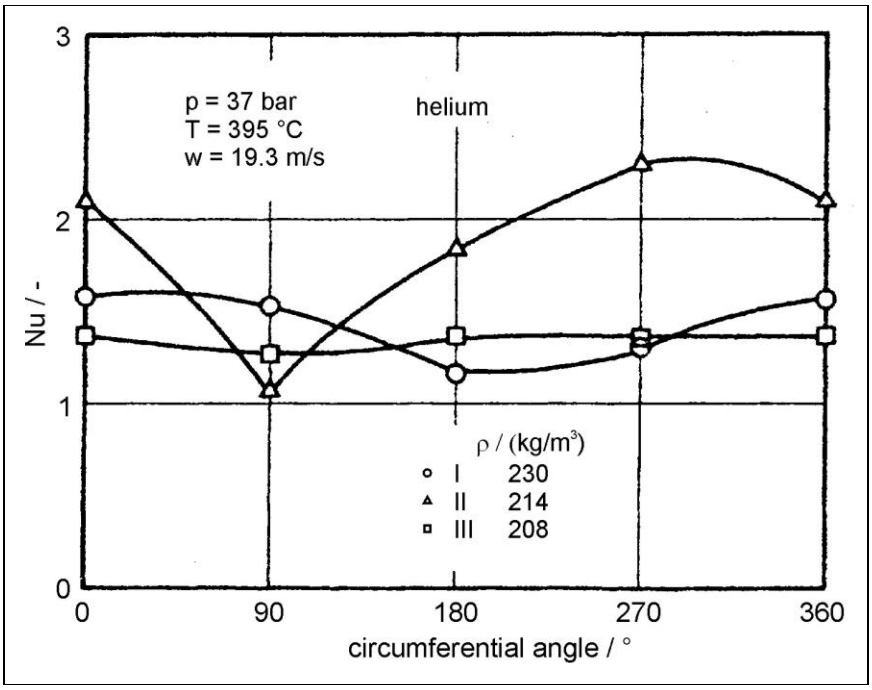

Figure 91: Nu numbers as a function of circumference angle

In three further test runs, holes of 10 mm diameter were then drilled into various sectors and planes for the simulation of damage. The pressure differences between opposite contours were measured by about 2 mm thick tube probes provided with lateral holes similar to Prandtl tubes. These probe tubes were arranged according to investigations by Achenbach [ACH73]. He had found out that the static wall pressure in the top and bottom sectors, relative to the bend presented before, was nearly constant along the bend wall. He therefore proposed to also provide breather holes there, if required. Furthermore, his results revealed the necessity of using a longitudinally separated insulation, which was to be pulled into the inlet and outlet sections. The greatest pressure differences according to [ACH73] were measured between outside and inside contours. If the breather holes of the ducting shroud were positioned at the top and bottom, as expected, no deviations of the insulation power of the bend were found. As soon as the maximum pressure differences between outside and inside contours became effective, the insulation space was flown through, as was shown by the temperature profiles. However, the effects on the heat losses and the thermal conductivities were less serious than expected. This insulation was and is therefore suited for HTR applications from the aspect of thermal behaviour.

Following the investigations on metal foil insulations and stuffed fibre insulations, designs of fibre ceramics and fibre blankets were also taken into consideration by the project partners. Since the hot gas side consisted of cover plates or tubes, which were not allowed to be completely closed, the fibre blankets were to suppress forced convection or keep it as low as possible. Moreover, it was hoped to achieve a more homogeneous fibre density with compressed blankets. In addition, less fibre breakage was expected in mounting. For this reason, tests on a fibre blanket insulation were needed. First of all, measurements were to be performed with closed and then with open hot gas side to study above all the influence of axial pressure gradients on the insulating behaviour in more detail, see [BRÖ80a].

Figure 92 schematically shows a segment from this insulation manufactured by the Swiss BBC company. Some dimensions, e.g. diameters, are indicated. The cooling systems can be recognized on the outside. The insulation is only indicated. Its length was 3600 mm. This design provided the advantage that the entire insulation could be prefabricated at the manufacturer's. The actual structure was an outer support tube with a sliding connection at the centre, studs, fibre blankets and cover plates. The support tube was in the vertical position during fabrication. After welding the studs, the fibre blankets were slipped over the studs and compressed.

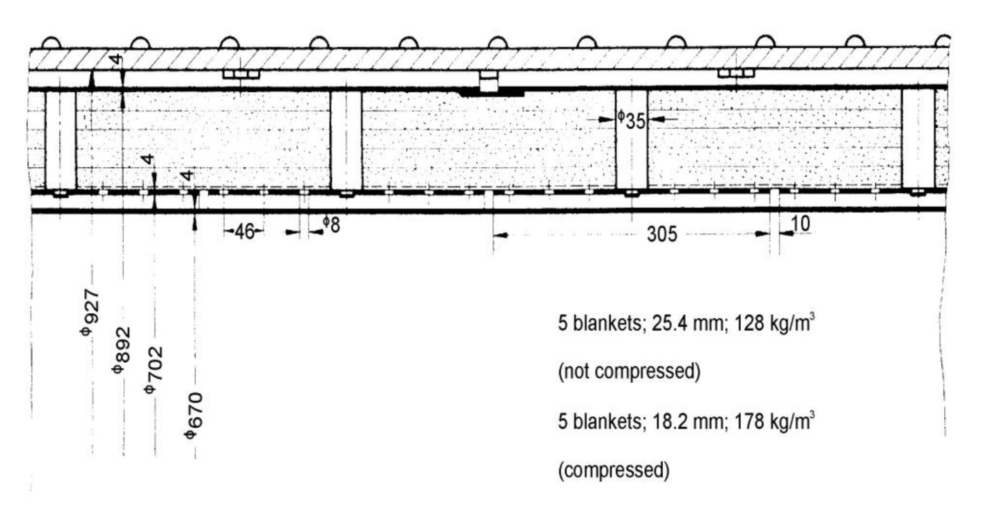

Figure 92: Fibre blanket insulation

As can be seen from the above study, six studs per plane were needed, i.e. a total of 60. Their pitch was 320 mm. At both ends, the support tube was welded gastight with v-shaped end pieces not shown in the drawing. During mounting, the thermocouples were installed in two axial sections across the thickness of the insulation in the top, right, bottom and left sectors. The instrumentation approximately corresponded to that of the other insulations. By means of the perforated cover plates, the five blankets of Kaowool were compressed to an insulation thickness of 91 mm and a density of 178 kg/m^3. The thickness and density of one blanket were 25.4 mm and 128 kg/m^3 , respectively, in the as-delivered state. They were internally covered by a wire mesh against escaping dust. On the inner side, the closed ducting shroud is shown, which was not needed in all experiments. Particular mention must be made of the gap between pressure and support tubes. Its width was 13.5 mm assuming a constant diameter. The rings of 5 mm width mentioned before and shown in the drawing, tolerances in the diameters of the two tubes and the mounting of the insert made this gap necessary. Without the rings, however, it could have been smaller.

Figure 93 shows the inside of this insulation with the cover plates arranged at a distance of 10 mm. The holes with a diameter of 8 mm were required for filling and above all in the case of rapid pressure reduction. A strand with thermocouple leads can be recognized in the direction of flow.

Initial measurements were performed without the inner ducting shroud, i.e. with open hot gas side. These were followed by investigations with closed gas duct. The flow rates of the air and helium cooling gases were between 13 m/s and 16.6 m/s. Finally, measurement series with flow displacers were carried out to achieve high axial and local pressure gradients. The aim was to investigate the influence of these gradients on the insulating behaviour with open hot gas side, as described by Bröckerhoff [BRÖ81b].

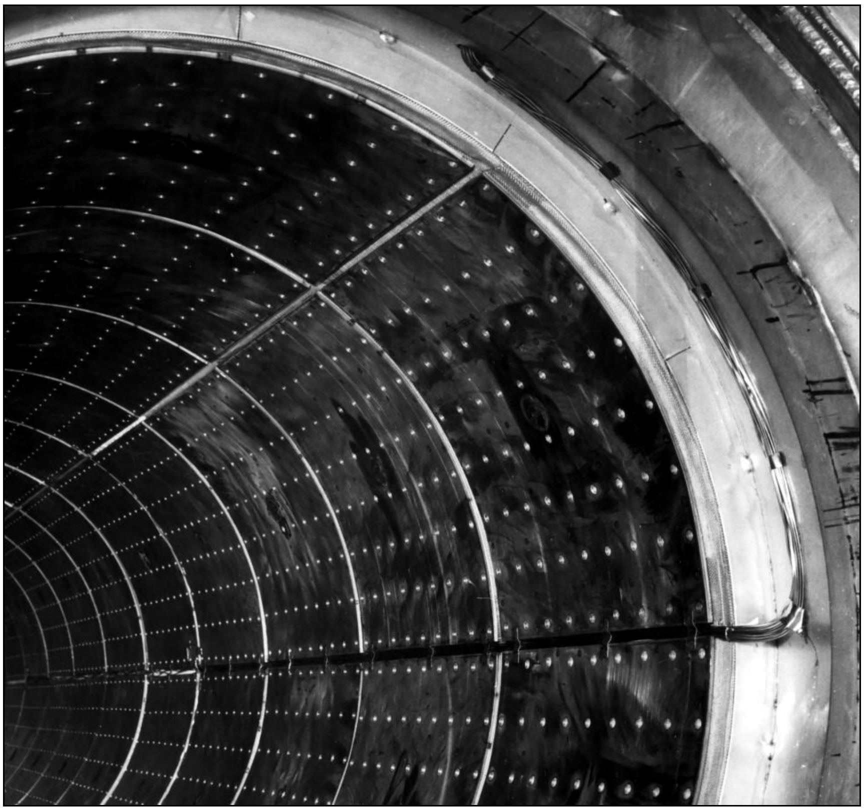

Figure 93: Cover plates of the fibre blanket insulation

Figure 94 shows a segment of the experimental arrangement not true to scale. The main components of this arrangement are explained in the legend. In order to achieve high axial pressure gradients, a flow displacer with an outer diameter of 510 mm was mounted. After completion of these test with displacer, designated V in the following, a displacer with a 20 mm thick straight disk was installed. This was to simulate the pressure conditions prevailing in a bend. The diameter of the disk was 530 mm, that of the displacer 273 mm and the inner diameter of the insulation 702 mm. With the disk in two different positions it was intended to find out whether hot gas was delivered through the sliding connection and breather holes on the support tube due to the disturbance. This possible heat transport is schematically represented in the diagram. Th arrows indicate the flow direction of the gas from the hot to the cold side. Accordingly, it could have flown through the holes and the gap of adjacent cover plates and the sliding connection and through the holes in the support tube. In the first measurement series, the disk was mounted 315 mm downstream of the sliding connection in a position marked with 1. The diagram shows position 2 of the disk at the level of the sliding connection. The pressure differences Δp caused by the disk were determined by two holes in front of and behind the disk. The pressure conditions on the support tube were determined by two probes placed into the fibre blankets at the level of the disk and installed upstream of the disk at a difference from the hole.

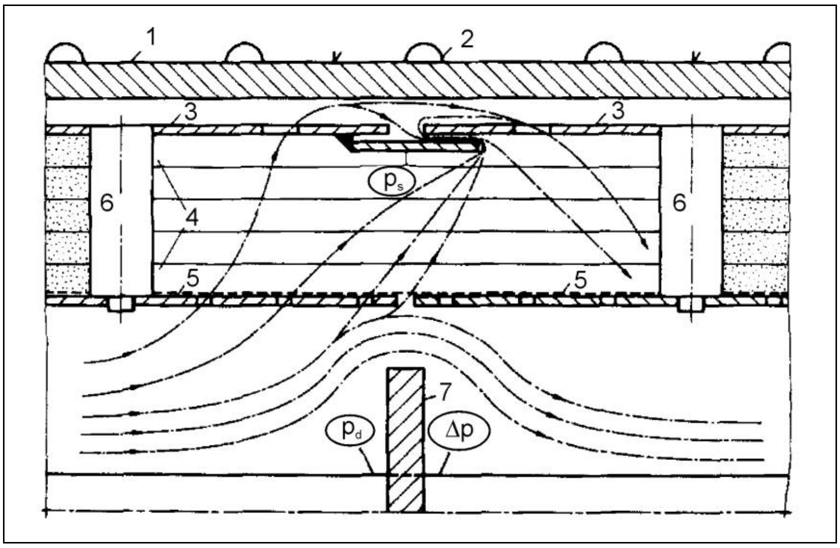

(1: pressure tube, 2: water cooling, 3: support tube, 4: fibre blankets, 5: cover plates, 6: studs, 7: disk)

Figure 94: Experimental arrangement and streamlines

Figure 95 shows wall temperatures measured in the top and bottom sectors for three test runs at the highest pressure and the highest temperature each for tests with air. The experiments carried out in the HP channel at pressures up to about 40 bars and temperatures up to 400 °C required long times until steady-state conditions were reached. Apart from the tests at the highest pressure, therefore, in most cases only

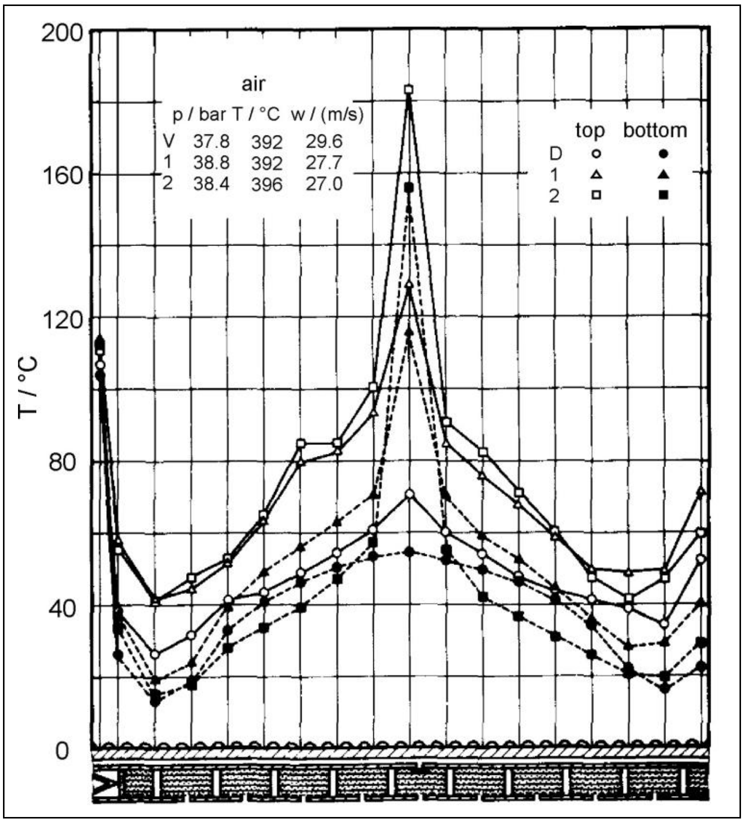

Figure 95: Wall temperatures

two speeds were run. The figure schematically shows the test configuration. The ducting shroud was missing in all cases. Pressures, temperatures and velocities are indicated.

The velocities in the tests with disk, denoted 1 and 2, apply to the gap between disk and cover plates. They corresponded to the pressure differences of 26198 N/m^2 and 25856 N/m^2 caused by the disk. For all three measurement series, high outlet temperatures of 105 °C to 115 °C were observed in the non-insulated region. Viewed in the flow direction of the cooling water, they then strongly decreased. Of particular interest in the further consideration were above all the maximum temperatures in the region of the cooling water outlet. The lowest values were measured here in tests with the displacer. They amounted to 70 °C in the top and 55 °C in the bottom sector. The disk mounted in positions 1 and 2 caused an increase of the corresponding values to 128 °C and 115 °C as well as 183 °C and 156 °C. As expected, the second test provided the higher values, since the disk was mounted in the immediate vicinity of the sliding connection indicated in the figure. The hot gas was pressed outside through this sliding connection and the holes of the front plane. Higher temperatures occurred in the top sector due to free convection in the gap between pressure and support tubes.

Figure 96 shows the heat losses measured across the circumference for air and two speeds as a function of the quotient $\Delta p/\rho$, which was formed from the measured pressure difference across the disk and the gas density. The gas temperature is a mean value. For comparison, the averaged values for four pressure stages with the displacer without disk are dotted on the left. In all cases, an increase of the losses with rising $\Delta p/\rho$ is to be observed. Moreover, the disk in the immediate vicinity of the sliding connection also caused higher losses, e.g. an increase from 4100 W/m^2 to 6900 W/m^2 at the highest pressure. The values only drop at abscissa values of about 250 m^2/s^2 or below, i.e. they are linearly extrapolated below the results with displacer. Since the helium losses approximately corresponded to those in Figure 96 both in terms of level and distribution, they are not specified.

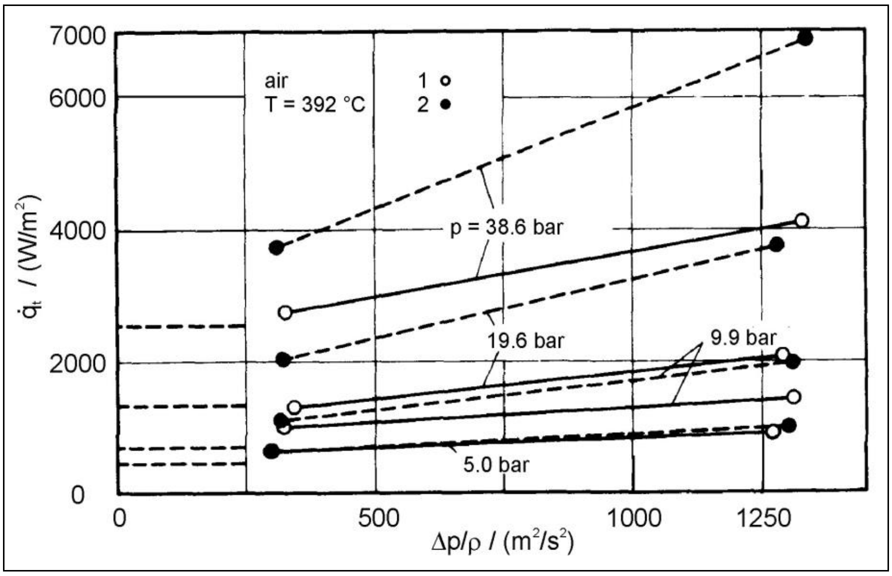

Figure 96: Heat losses as a function of the relative pressure difference

Until about 1981, only the HP channel was available for the testing of larger components, after the HHV and ARGAS facilities had been closed down. EVA-II was not suitable for the investigation of insulation systems. However, since test facilities for testing under original conditions were needed for work under the PNP project, above all at high temperatures, the companies HRB and INTERATOM had decided to construct new test stands. With support from the Federal and state governments, the facility for the long-term test of insulations (ADI) was built at HRB and the component test loop (KVK) at INTERATOM.

Corresponding to its name, the ADI facility was constructed for long-term investigations with the following main data:

- volume flow of helium 3.8 m^3/s,
- gas temperature 950 °C,
- gas pressure 60 bar,
- test period up to 10000 h and
- pressure transients 70 bars/s,

see Bröckerhoff et al. [BRÖ84b]. The length of the test facility, see Figure 97, was approximately 10 m. The inner diameter of the pressure vessel was 2 m. Whereas (external) water cooling was envisaged for cooling the pressure tube, the support tube was cooled with oil (inside) to achieve higher temperatures. An essential advantage of this test facility was the use of a hot-going blower, as described by Henßen [HEN84a] and Mauersberger [MAU84a]. This enabled clear energy savings with a view to the long-term tests. Furthermore, the helium-water heat exchanger integrated in the pressure vessel permitted a faster cooling of the test sections during temperature cycling. This solution was moreover of advantage for cooling the gas volumes required for continuous gas cleaning. The test vessel had been designed for a gas pressure of 80 bar. The power of the heater was 200 kW.

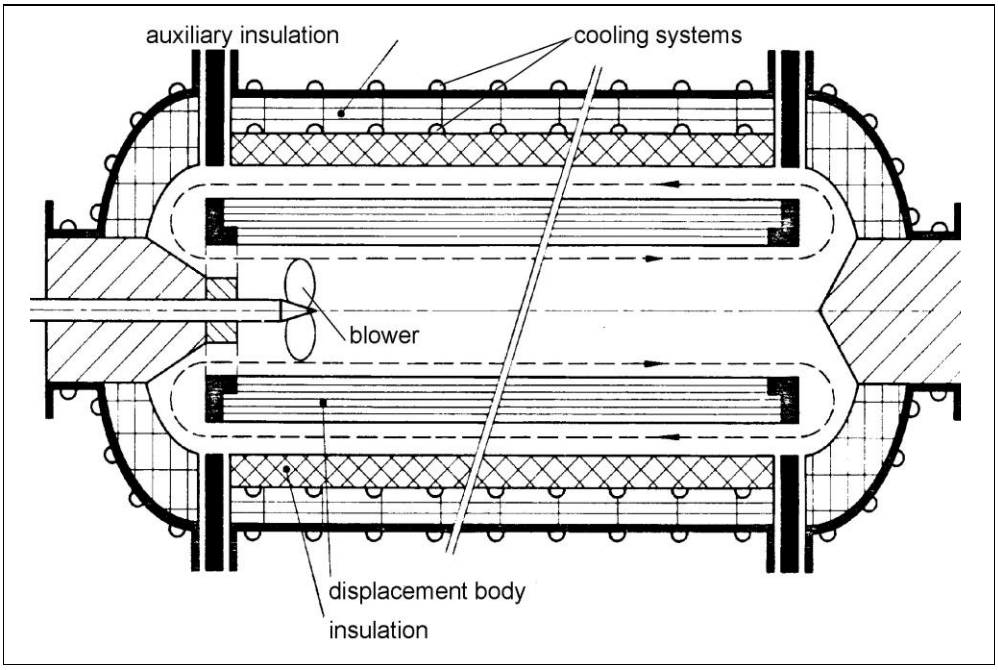

Figure 97: ADI test facility

The planning of the KVK facility had been preceded according to Mausbeck and Baust [MAU84] by the following basic requirements:

- completion of the investigations of components before starting to construct a PNP reactor,
- transparent extrapolation distance from the original component,
- construction of the facility with great flexibility concerning the components to be tested and
- investigation of further components according to the modular design in conformity with the project requirements.

The facility was originally envisaged for integral tests of PNP components. In the course of the further itemization of experimental work on components such as

- helium-helium heat exchangers,
- hot gas ducts and insulations,
- hot gas fittings,
- steam generators,
- process steam superheaters and
- heat exchangers for the afterheat removal system

a gap was discovered by Schumacher [SCH81] for the development stage of component and subcomponent investigations. At the request of the public sector, it was therefore examined whether a use of the test facility originally conceived for integral tests was also possible for investigations of components and subcomponents. This examination finally led to a modification of the facility, which involved a stepwise construction. In the first extension stage, KVK 1, component and subcomponent tests were to be performed. The essential feature of this stage was operation as a direct-cycle or a dual-cycle system with complete mass decoupling. Operation as a dual-cycle system, however, required an additional helium-helium heat exchanger with a power of 10 MW. The second stage, KVK 2, served to carry out integral tests on heat exchangers, hot gas ducts and hot gas fittings. In both construction phases, the same loop components could be used. During KVK 2 operation, KVK 1 was operated in parallel as a direct-cycle system. This permitted further tests to be carried out on components and subcomponents. Both construction phases were designed so as to enable an integration of further test objects such as steam generators, process steam superheaters and blowers without mayor additional expenditure. The main data of the two construction phases are shown in Table 7.

Designation	KVK 1	KVK 2
maximum hot gas temperature / °C	1000	1000
maximum pressure / bars	46	46
mass flow (design) / (kg/s)	3	20
mass flow (low load) / (kg/s)	0.6	6
temperature transients / (K/min)	5	5
pressure transients (normal operation) / (bar/s)	3	3
pressure transients (maximum) / (bar/s)	5	5

Table 7: Data of the KVK facility

As reported by Jansing [JAN84], the facility was put into operation in 1982. The dimensions of the building featuring a length of 50 m, a width of 20 m and a height of 25 m demonstrated the dimensions of the test facility. Helium was circulated by a centrifugal blower. The heat required for operating the facility was introduced into the loop by a natural-gas-fired and an electrically heated heater and removed by a steam generator. Part of the steam was used for preheating the helium in a recuperator. With a length of 145 m the operational hot gas duct was clearly longer than the HHV facility. Due to the good experience made, a fibre insulation with metallic shrouds had been chosen.

The two test facilities, ADI and KKV, are described here because of the description of further investigations on hot gas ducts, also with fibre blankets, but with ceramic and metallic ducting shrouds, which were to be carried out in the two facilities.

The pressure tube of 4600 mm length already used earlier was available for the investigations of the insulation described in the following. The insulation for a secondary loop duct had been developed by Kraftwerkunion (KWU) under contract to INTERATOM. Figure 98 schematically shows a cutout of the test object. The insulation consisted of closed graphite ducting shrouds on the hot gas side, wrapped-on fibre blankets and spacers. The figure shows test segment 3 in full length andparts of neighbouring sections 2 and 4. For the sake of clarity, inlet 1 and outlet 5 are not shown. The further description is taken from Bröckerhoff and Stausebach [BRÖ83b]. The outer and inner diameters of the ducting shrouds were 725 mm and 630 mm, respectively. The inner diameter thus corresponded to the carbon brick insulation to be described later. The length of 800 mm of the three central sections – 796 mm for the shrouds, 4 mm for the gap – had also been adapted to the carbon brick insulation. Axial thermal expansions of the shrouds were accommodated by so-called expansion gaps at the respective sliding connections. A smaller gap would have been sufficient for measurements in the HP channel, but since investigations were also envisaged in other channels at higher temperatures, a gap width of 4 mm was necessary. The ducting shrouds were of commercial-grade Diabon 0 graphite from Sigri in Meitingen.

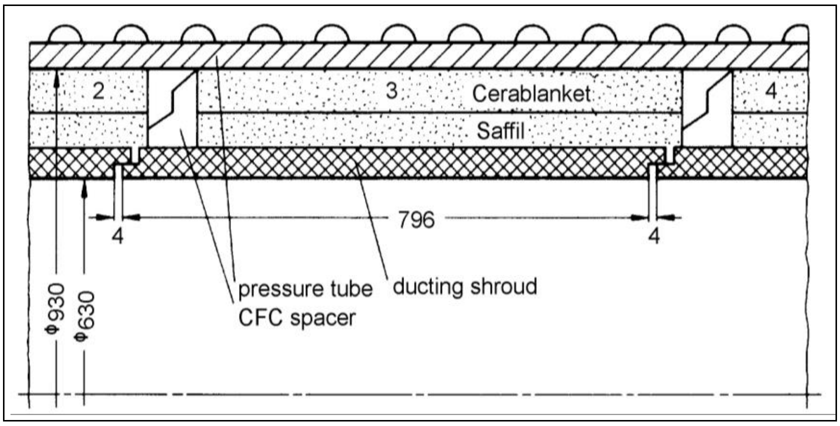

Figure 98: Ceramic fibre blanket insulation

The spacers for radially centring the ducting shrouds inside the pressure tube were of fibre-reinforced carbon (CFC). This material seemed suitable due to its very high strength. Grades from two manufacturers were selected because the material was still largely unknown and expensive. This was to provide a maximum of information. The spacers and straining rings for segments 2 and 3 were supplied by Sigri, the other two by the French company Carbone Lorraine. Data important for the design are compiled in Table 8. As can be seen, Carbone Lorraine used different materials for the two components. Depending on the manufacturing process, e.g. arrangement of the fibres, fibre content etc., the products of the two companies exhibited essentially different properties. For example, the thermal conductivity was clearly different. Furthermore, for most data there was also a dependence on the direction. Thus, the compressive strength of the French material differed by a factor of 2. The expansion coefficient was valid for the entire operating temperature range for both materials.

	Sigri	Carbone Lorraine	
designation	spacer and straining ring	spacer (Aerolor 412)	straining ring (Aerolor 22)
fibre content / vol. %	32		
density / (kg/m^3)	1250-1450	1650	1650
bending strength / (N/mm^2)	< 80	< 100	< 100
tensile strength / (N/mm^2)	< 55	< 55	< 55
compressive strength / (N/mm^2)	< 50		
radial		> 200	> 120
axial		> 100	> 60
shear strength / (N/mm^2)	< 15	< 20	< 200
Young's modulus / (N/mm^2)	$2\cdot10^4$-$4\cdot10^4$	$4.5\cdot10^4$	$2.5\cdot10^4$
expansion coefficient at 20 °C - 900 °C / K^{-1}			
radial	$0.4\cdot10^{-6}$-$0.6\cdot10^{-6}$	$1.6\cdot10^{-6}$-$1.8\cdot10^{-6}$	$1.4\cdot10^{-6}$-$1.6\cdot10^{-6}$
axial	$4\cdot10^{-6}$-$6\cdot10^{-6}$	$3.2\cdot10^{-6}$-$3.6\cdot10^{-6}$	$5\cdot10^{-6}$-$7\cdot10^{-6}$
thermal conductivity /(W/mK)			
radial	15	19	50
axial	12	7	15

Table 8: Data of CFC materials

The spaces between ducting shrouds and pressure wall originally were to be filled with carbon felt blankets. Since the thermal conductivity in helium atmosphere was unknown, it was to be measured in the Poensgen apparatus of Figure 2 for two grades made available by Sigri. But the electrical insulation already failed at a sample temperature of 250 °C because carbon from the blankets had deposited there. A second attempt failed, too. Investigations at INTERATOM showed that the cause for the observed weight loss of the samples was the outgassing of physically absorbed water. For this reason and due to the meanwhile more stringent requirements to be met by the materials, carbonaceous materials were ruled out for the intermediate loop of a reactor plant. Since the other components had already been delivered, however, no modifications could be made here any more.

The actual insulation consisted of fibre blankets wrapped upon the ducting shrouds.

The advantages of the wrapping method over stuffing were considered to be more homogeneous fibre density and less fibre breakage, see also the fibre blanket insulation with metallic cover plates. In view of the different stressing at the hot and cold gas sides, the experts had proposed a subdivision. The high-temperature fibres used were of Saffil with a content of more than 95 % Al_2O_3 from ICI in Frankfurt. According to the experts, these fibres were suitable for temperatures of up to 750 °C; they covered the diameter range from 725 mm to 825 mm. The closure was a wire mesh with a mesh width of 1 mm and a wire diameter of 0.63 mm. Together with straining straps of 1 mm thickness, this served to compress the blankets. For the region up to the pressure tube, fibres were selected that were suitable for lower temperatures. Cerablanket 800 from Gossler in Hamburg with almost equal contents of Al_2O_3 and SiO_2 was used here.

Mounting the blankets and the whole insulation was a novelty. There was no experience in wrapping the fibres and concerning the attainable densities. A special device had therefore been developed by INTERATOM. Initial wrapping tests had been performed with carbon felt blankets. The compression of the initially applied Saffil blankets was effected by means of the above-described wire mesh. The blankets wrapped upon were about 12 mm oversized to achieve a close contact between the outer blankets and the pressure tube. A subsequently placed sheet-metal jacket was then braced by a wedge so that the diameter was 10 mm undersized compared to the pressure tube. After sliding this arrangement into the pressure tube, the wedge was removed and the insulation sprang back, so that the blankets fitted closely. For the five segments, the mean fibre densities specified in Table 9 were achieved.

Density [kg/m^3]	Segment 1	Segment 2	Segment 3	Segment 4	Segment 5
Saffil blankets Cerablankets	127 125	127 126	127 131	138 131	129 130

Table 9: Mean fibre densities

The differences in density were very small. By re-inserting the wedge it was possible to remove the insulation again. In the next step, the spacers and straining rings were inserted and bolted to each other. The instrumentation on the outer side and the subdivision of the cooling systems follows earlier investigations. The experiments were carried out in the high-pressure channel with air and helium. Because graphite corrosion could not be ruled out, the temperature was limited to 300 °C in the experiments. In a second test series, a flow displacer carrying a disk that could be shifted in the axial direction was mounted, see Bröckerhoff and Stausebach [BRÖ83b]. Apart from the pressure measuring points, the insulation and instrumentation did not have to be changed.

Figure 99 shows the tube wall and cooling water temperatures of the top and bottom sectors for the tests with helium and the first test series. The gas data are specified. The pressure gradient measured in the direction of flow is related to the unit length. In contrast to the experiments with air, which are not being dealt with here, the tube wall temperatures were approximately the same throughout for both quadrants. Due to the lower gas density, the effects of forced and natural convection were smaller.

Gas and solid conductance was dominant. The wall temperatures increased in the flow direction of the cooling water, which was adjusted to equal values at the outlet. Because of the significantly higher thermal conductivity of the spacers fabricated by Carbone Lorraine, the highest tube wall temperatures of almost 90 °C were measured there. As can be furthermore seen from the diagram, the front measurement section, designated I, only contained one spacer, the rear section II had two. As expected, this also led to higher heat losses.

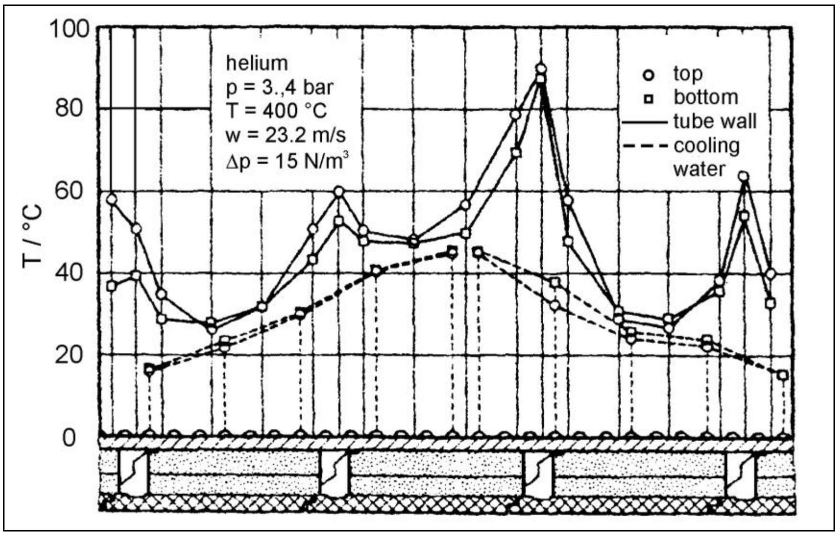

Figure 99: Wall and water temperatures

Figure 100 contains Nusselt numbers for measurement sections I and II as a function of pressure. It can be clearly seen that the Nu numbers are higher by a factor of 2 in section II. As already mentioned above, this is attributable to the two spacers and their higher thermal conductivity. The upper two quadrants exhibited the highest values of 4.6 and 7.5 at a pressure of 38 bars and were thus clearly below the air values. In comparison to stuffed fibre insulations, however, the Nusselt numbers could not yet be regarded as satisfactory in terms of either height or distribution. Improvements of the insulating behaviour would have been attainable by increasing the flow resistance of the insulation in the axial and radial directions and using spacer materials with lower thermal conductivity.

Concerning the investigations on this insulation carried out after the measurements in the HP channel in the ADI facility, reference is made to Henßen et al. [HEN84b], Henßen [HEN84a] and Mauersberger [MAU84a]. The experimental programme approximately corresponded to that of the HP channel tests, although hot gas temperatures of 950 °C could be adjusted. In addition, the insulation was exposed to axial pressure gradients of up to 50 N/m^2. At the end, cycling tests with 30 temperature cycles were run, increasing the temperature from 300 °C to 900 °C within a period of 3 h, maintaining it at this value for 1 h and then decreasing it to a level of 300 °C within 5 h.

In these investigations, too, whose results are not shown, the very high wall temperatures were striking to note. In the region of the spacers, far higher temperatures were measured in the rear section II than in measurement section I. The authors believe that this is attributable, on the one hand, to the higher thermal conductivity of the spacers used in section II. Moreover, the temperature peaks of the wall were explained by enhanced convection in the region of the spacers. In the front measurement section, pronounced temperature differences were measured between the top and bottom sectors in the region of the spacers. They suggested the influence of intense natural convection, which was superimposed by stronger forced convection in the region of the spacers in measurement section II, since only minor temperature differences between top and bottom quadrant were measured there. The authors expect possible improvements of the insulating behaviour both by the realization of the proposals already discussed and by higher fibre densities.

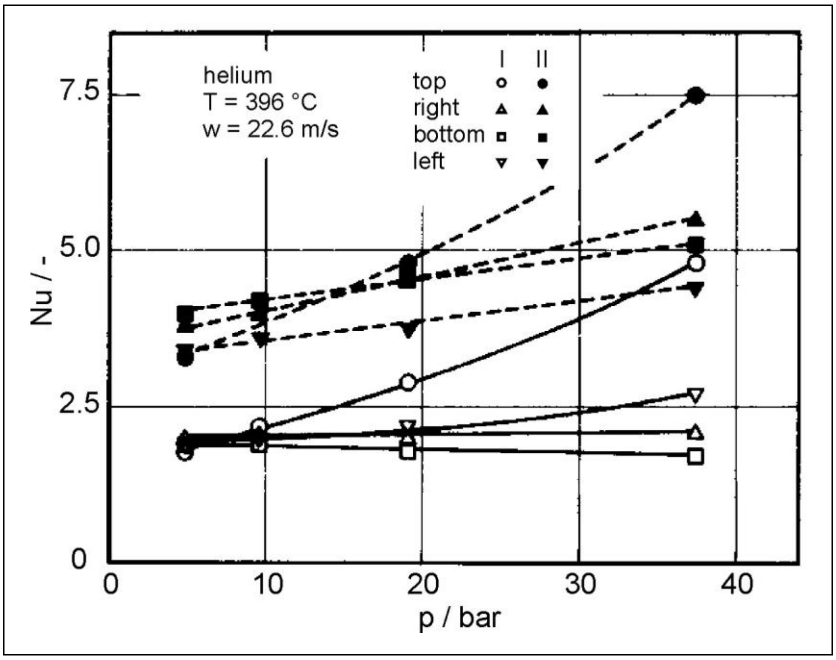

Figure 100: Nusselt numbers as a function of pressure

More promising seemed to be a modified design which, among other things, had spheres instead of the massive spacers of CFC. A brief description and initial results can be found in Klas and Bröckerhoff [KLA84a], a more extensive description in Bröckerhoff [BRÖ86a]. The pressure tube carrying the insulation was made available by INTERATOM. Concerning its dimensions, the cooling systems and their subdivision in the circumferential and longitudinal directions, it corresponded to the tube already used in earlier investigations. Figure 101 schematically shows a cutout of the test object. The insulation also consisted of graphitic ducting shrouds at the hot gas side, wrapped-on fibre blankets and spacers. The figure shows test segment 3 in full length and the two neighbouring zones 2 and 4. There were five sections in total. The first and fifth section served again as the inlet and outlet; the three central sections constituted the measurement segment. The length of the measurement segments had been increased to 984 mm, the 4 mm gap width between the ducting shrouds had been maintained. The outer and inner diameters of the shrouds were 780 mm and 630 mm, respectively. Due to the different temperature stressing on the hot and cold gas sides, two fibre materials were also used for the insulation with CFC spacers. Saffil fibres covered the diameter range from 780 mm to 825 mm. Cerablanket was used for the region up to the pressure tube. The fibre blankets were also wrapped upon the ducting shrouds using the method already described and successfully tested. Compression of the blankets took place in the same way, too. The main difference between this insulation and the one described before was the use of differently shaped spacers for radially and axially fixing the ducting shrouds. The adjustability of these shaped bodies permitted the ducting shrouds to be aligned irrespective of the tolerances of the pressure tube. In the region of the spacers, however, the fibres were stuffed by hand, since wrapping was only suitable for longer undisturbed regions.

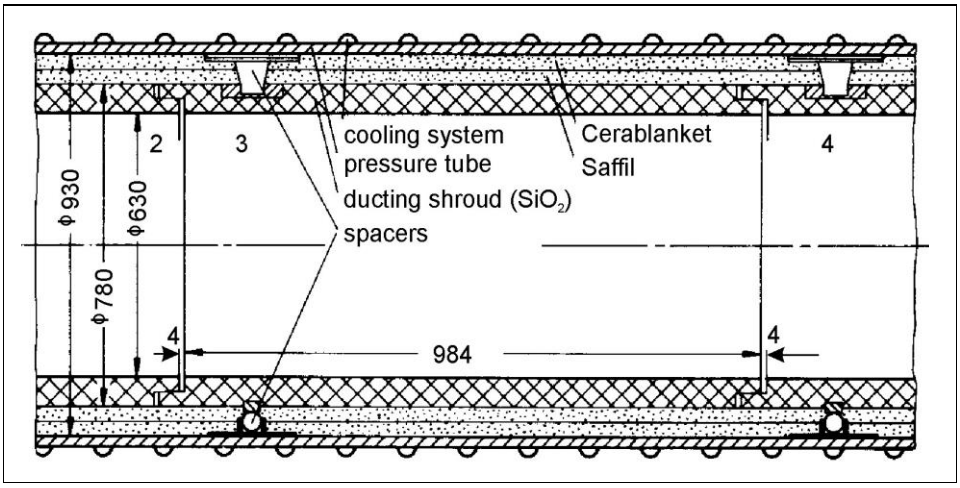

Figure 101: Ceramic fibre blanket insulation

The ducting shrouds from Sigri had been made of ASI-grade material. The spacers were dense shaped bodies of high-purity Al_2O_3 and Si_3Ni_4. Si_3Ni_4 was used for segments 2 and 4 and Al_2O_3 for segments 3 and 5. The spacers were bolted to the pressure tube by means of metallic elements. For the radial support of the shrouds opposite the support tube, four spheres of 50 mm diameter were uniformly distributed over the circumference, ensuring full contact and load application by point-type support. The spheres accommodated thermal relative motions between pressure wall and ducting shrouds due to rolling. In order to reduce the surface pressure on both sides, two cylindrical pressure plates of Al_2O_3 were inserted. The ceramic axial support bearings had the task of fixing the respective shrouds in the axial direction. This body was connected to the load-bearing wall by a conical tensioning fixture at the base. The spherical head end ensured full support on the pressure ring with the body in a slanted position. The pressure ring was also intended to reduce the surface pressure upon load application to the ducting shroud.

The thickness and density of the blankets as delivered – 95 % Al_2O_3 – from ICI were 45 mm and 37 kg/m^3, respectively, according to [BRÖ86a]. Three layers were needed for insulation. The mesh needed for bracing was made of 1.4571 stainless steel. The density of the Cerablanket fibres from Gossler – 52 % Al_2O_3 and 48 % SiO_2 – was 128 kg/m^3. The tensioning jacket also made of 1.4571 enabled a diameter reduction of the three layers to 910 mm in the tensioned condition, thus increasing the fibre density to 150 kg/m^3.

After completion of the first three test runs, the insulation was modified on account of the results which suggested strong convection movements in the fibres. Disassembly was therefore required. Foils of Sigraflex from Sigri were wrapped as convection barriers to suppress or reduce gas movements. Their thickness was 0.2 mm. A total of six foils were needed for each segment, three for the Saffil and three for the Cerablanket fibres. Upon re-installing the insulation, the mesh used for bracing the Saffil blankets was replaced by a split tensioning sheet of 1.4541, 0.5 mm in thickness, which overlapped at the sliding connections. The meshes had become distorted due to the temperatures. Straps of 1.4541 with a width of 15 mm were used for compression. On the outer side, in contrast to the CFC insulation, a tripartite sheet-metal jacket with three wedges that had to be removed after sliding in the arrangement was used. Tripartition enabled a more uniform bracing and thus also an approximately constant fibre density across the circumference.

Mounting took place with the pressure tube in the vertical position. First of all, the metallic outlet part for segment 5 was installed. It served to fix the ducting shroud of this segment. After mounting the support elements at the upper end, this segment was fixed. The other sections and the first short segment, for the fixation of which a metallic inlet part was needed, were mounted in the same way.

Prior to re-installation, wrapping tests had become necessary again with the aim of examining the combination of fibres and graphite foils for its suitability. The foils tended to tearing or breaking due to their low strength. This initially resulted in lower precompression. The tripartite tensioning sheet also used here finally led to mean fibre densities of 150 kg/m^3, with less effort than expected, since it slid easily onto the outer foil layer. About 80 % of the fibres used in the first measurements were used again in remounting.

Five test series were run in the HP channel, namely

- without metallic ducting shroud,
- with metallic ducting shroud (diameter D = 595 mm),
- without metallic ducting shroud and with displacer (D = 510 mm),
- without metallic ducting shroud and with displacer (D = 510 mm), after modification, and
- without metallic ducting shroud and with displacer (D = 510 mm), after modification, but without external water cooling.

The gaps between the graphite tubes had proved to be too large in this case, too, so that experiments with closed hot gas side were also necessary. The wrapped foils had led to a marked reduction of the temperatures on the pressure tube wall and to reduced heat losses. In the last series, in which for reason of time only one operating state could be adjusted, the heat losses due to heat radiation and free convection were dissipated to the outside air.

Figure 102 shows tube wall temperatures in the region of measurement sections 2, 3 and 4 of the top sector for three test runs after [BRÖ84a] and [BRÖ84c]. For simplification, the coolant temperatures and the temperatures in the bottom quadrant are not shown. The two bottom curves for the tests with water cooling permit a direct comparison. Their ascent in the region of the second and fourth segments is attributable to cooling water heating across the length. The influence of the axial support elements can be seen particularly clearly in the rear measurement section, where the wall temperatures amounted to 94 °C. After placing the foils and the associated increase in radial flow resistance, the temperatures decreased to about 65 °C. A minor increase was only observed at the rear support element. After switching off the water cooling, the wall temperatures increased to values between 120 °C and 150 °C. This increase by a factor of 2 appears high, but it must be borne in mind that the available insulation thickness of the fibres contributing to temperature reduction was only 75 mm.

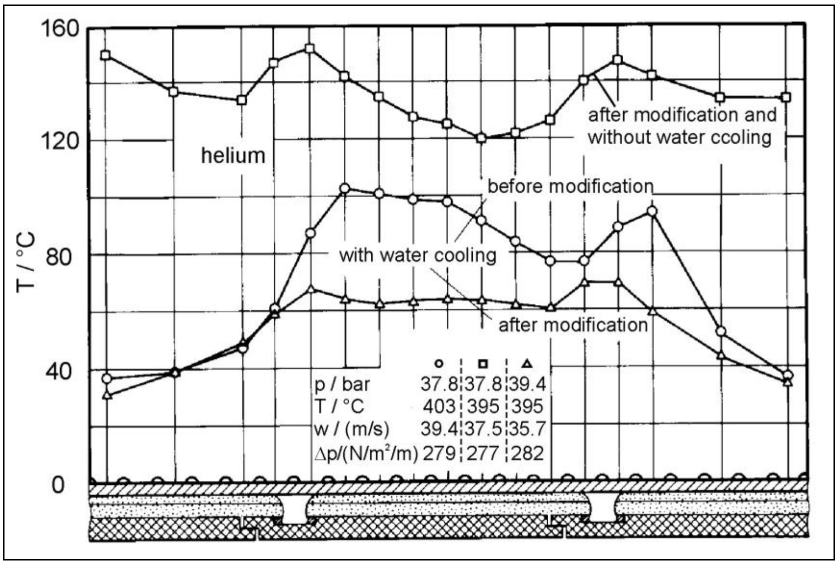

Figure 102: Wall temperatures

The heat losses in Figure 103 apply to the front measurement section, the first series and helium tests. The pressure dependence was approximately linear. The highest value of about 2000 W/m^2 was measured at a gas temperature of 397 °C. It was thus 55 % below that of the insulation with massive spacers of CFC. The improvement is basically attributable to the reduced solid conductance. The rear section shows almost equally high losses.

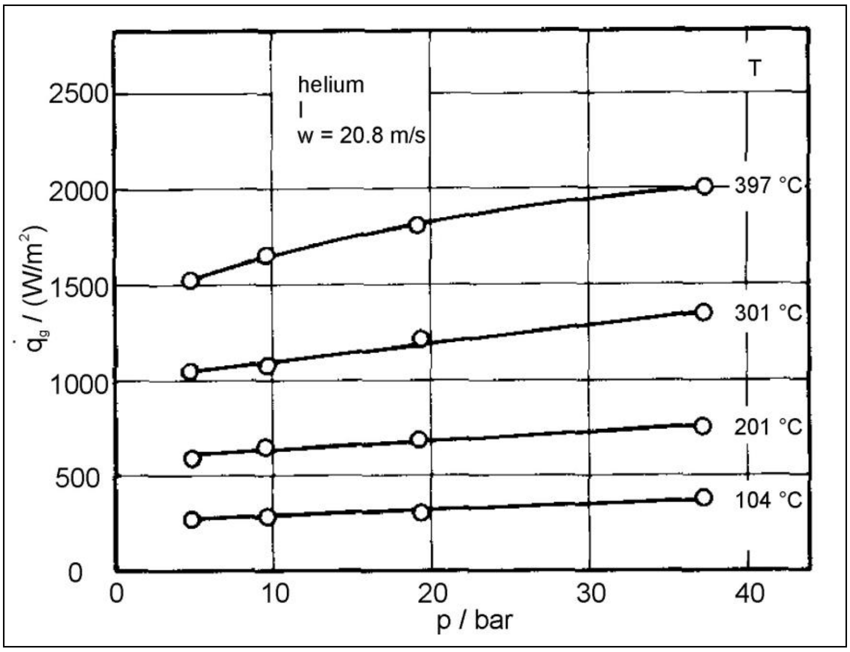

Figure 103: Heat losses as a function of pressure

A comparison of total losses for the tests prior to and after modification of the insulation is shown in Figure 104. The results apply to the front measurement region and to the tests with the highest gas velocity, i.e. with flow displacer. A comparison with the results of Figure 103 shows that the gas velocity has approximately doubled from 20.8 m/s to 38.8 m/s, see open symbols, at the highest pressure leading to an increase of the heat losses by 50 %. This approximately applies to all temperature levels. In the lower pressure range, however, the losses were almost the same for both measurement series. After modifying the insulation, in contrast, only a slight dependence on gas pressure was found. The decrease in permeability of the insulation in the radial direction thus led to a clear reduction of total heat losses and also reduced the dependence on the pressure differences.

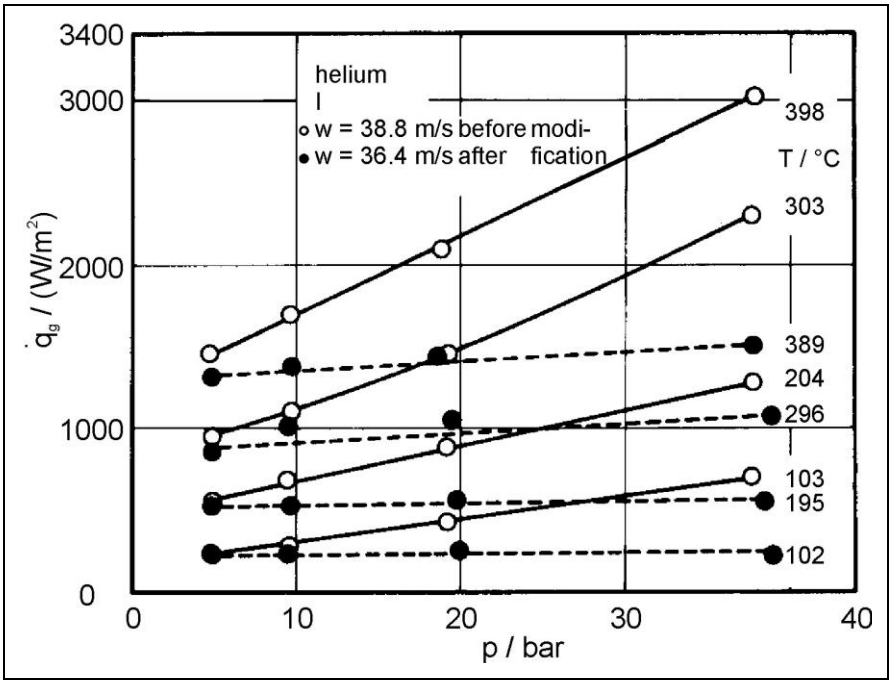

Figure 104: Heat losses as a function of pressure

The positive effect of the graphite foils on the insulating behaviour can be seen from Figure 105. The data apply to section I, the highest temperature and an averaged velocity of 37.4 m/s. In the first test run, the differences between the top and bottom sectors strongly increased with rising pressure. Whereas only a slight increase of the Nu numbers from 1.1 to 1.45 was observed in the bottom quadrant, they increased from 1.7 to 4.4 at the top. The modification of the insulation caused a clear reduction of the Nu numbers in all sectors and a homogenization. At the highest pressure, the corresponding values were 1.38 and 1.15. Since the influence of the axial pressure gradients was also only slight, the modified design was to be considered good from the point of view of thermal behaviour.

INTERATOM had therefore decided in favour of testing such an insulation in the KVK facility. The test components and the investigations have been described by Bröckerhoff and Zentis [BRÖ87]. For reasons of time, the insulation could neither be mounted nor investigated in Bensberg. Mounting took therefore place at the KFA together with staff from INTERATOM. The experiments were carried out in the HP channel.

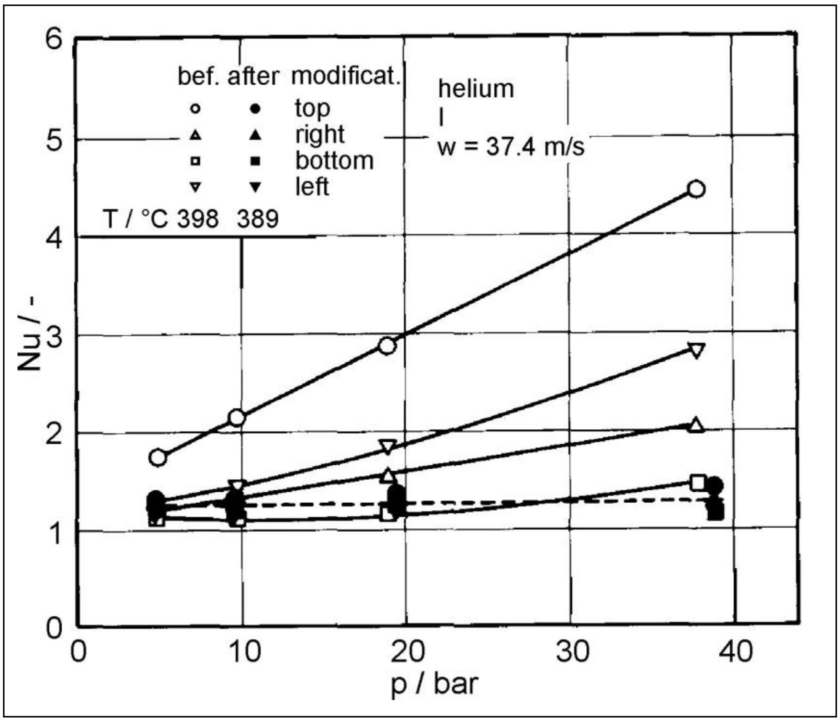

Figure 105: Nusselt numbers as a function of pressure

Figure 106 schematically shows a cutout from the mounted insulation. It consisted on the inner side of 60 mm thick Masrock ducting shrouds, whose inner diameter was 700 mm. Masrock, which consists of silicon oxide, only has a low thermal conductivity and above all a low expansion coefficient. The length of the individual tube segments was 1000 mm. First of all, Saffil fibre blankets were wrapped upon these segment by the method described before. In addition, metallic foils were mounted to reduce free convection in the radial direction. The first fibre layers were then pressed to a density of about 160 kg/m^3 by means of an intermediate sheet of 1.4541. On the colder outer side, Cerablankets and foils were compressed to a mean density of 180 kg/m^3 using a tensioning sheet also made of 1.4541. The tensioning device used corresponded to that already described. It enabled a close fitting of the outer blankets to the support tube and also later dismounting. Centring of the ducting shrouds opposite the support tube was effected by four spheres of Al_2O_3 evenly distributed over the circumference.

Two support elements each offset by 180 °, also made of Al_2O_3, ensured an axial fixation of the ducting shrouds opposite the support tube. The sphere shown in the drawing is offset by 45 .

Four segments of 1000 mm length each were available for measuring the heat losses. At both ends, shorter sections were mounted for adaptation to the pressure tube totalling 6000 mm in length. Two axial sections were provided with thermocouples for measuring the temperature profiles in the four sectors. Further thermocouples were attached to selected support elements. After having installed the insulation in the support tube, the entire assembly was slid into the pressure tube, whose inner diameter was 1160 mm, and fixed at both ends in the flange region. The large gap of 25 mm between pressure and support tubes permitted numerous thermocouples to be mounted on one panel of the support tube. A total of 28 thermocouples were installed in four radial positions over a length of 1140 mm for

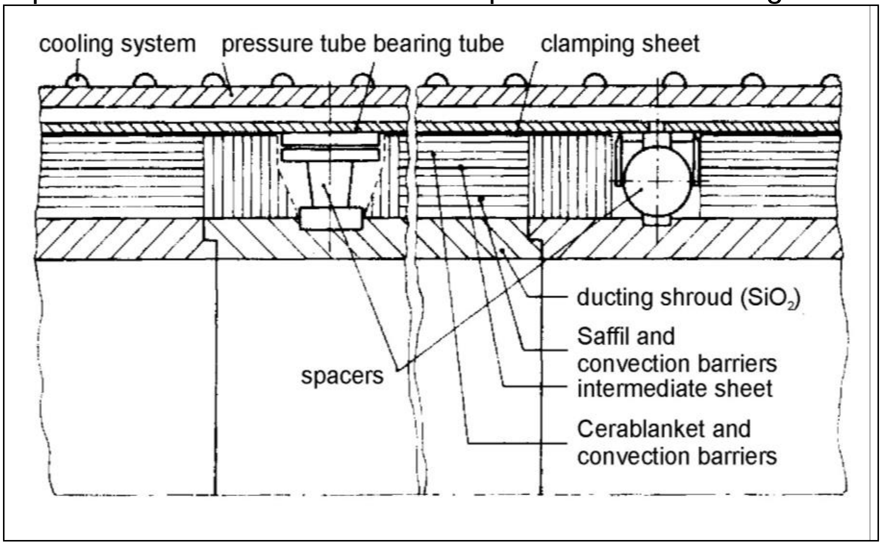

Figure 106: Ceramic insulation

measuring the temperatures in the region of the sliding connections of neighbouring shrouds and of the support elements as well as in the undisturbed region. Since the pressure tube did not have external cooling systems due to the initially planned measurements in the KVK facility, the first measurements in the HP channel were also to be performed without external forced cooling. For the determination of the tube wall temperatures 22 thermocouples were installed primarily at the top and bottom. After the first measurements with helium, however, it was found that unsealed holes in the support tubes had led to unexpectedly high heat losses and tube wall temperatures. The downtime necessary due to damage to the blower motor was used to upgrade the insulation, i.e. seal the untight locations. Moreover, cooling segments representing a new development were mounted, which enabled the heat losses to be determined in four sectors. Mounting of the segments specially manufactured for this tube made it necessary to dismount the thermocouples initially installed on the pressure tube and remount them on the cooling segments.

Figure 107 shows pressure tube and cooling water temperatures across the length of the insulation whose structure is schematically indicated. Due to free convection, which still existed in spite of wrapped foils, wall temperatures of up to 190 °C occurred in the rear region of the top sector. The bottom side only displayed temperatures between about 40 °C and 70 °C. Since only cooling water inlet and outlet temperatures were measured, only the corner points were determined, which are connected by dotted straight lines. A reduction of the gap between pressure and support tubes would have led to an improvement in insulating behaviour.

On the basis of these results, INTERATOM and Balcke-Dürr as manufactorer of the compoments developed the design shown in Figure 108 for the primary gas duct after Jansing [JAN84]. As a modification to Figure 107, ceramic spacers were provided in this version at both ends of the ducting shrouds to be made of graphite. This was to ensure adequate damping of the tubes in the event of earthquakes. The other materials corresponded to those of the insulation presented last. This insulation was to be examined in the KVK facility. A flow displacer was provided to increase the gas velocity. The hot gas then flowed through the gap between displacer and shroud, the cold gas through the gap between support and pressure tubes.

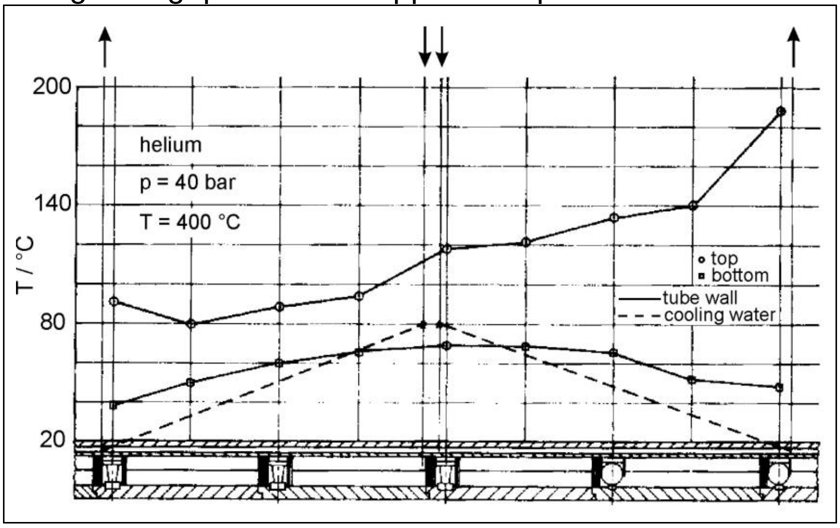

Figure 107: Wall and water temperatures

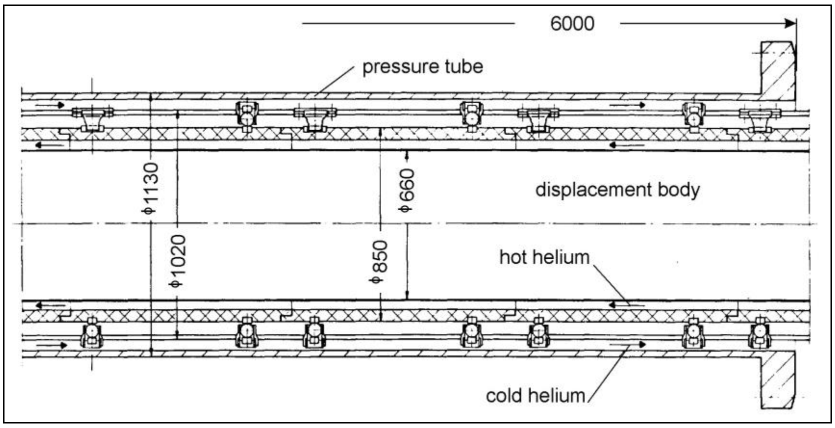

Figure 108: Primary gas duct (ceramic)

The cutout in Figure 109 after [BRÖ84b] shows part of this insulation with support tube; pressure tube and cold gas gap are lacking. The ceramic support elements were inserted from outside through holes in the wall of the metallic support tube. The fibre material for the entire region was to be Saffil. Graphite foils served as radial convection barriers.

For the secondary duct INTERATOM and Balcke-Dürr had returned to a design with metallic liner, as described by Jansing [JAN84] and Klas [KLA84b], see Figure 92. The test segment corresponded to PNP conditions in its radial dimensions with the outer diameter of the pressure tube (15Mo3) being 1220 mm and the inner liner diameter 700 mm. The insulation had been mounted onto a support tube. In accordance with earlier experience, Saffil fibres had been used for the inner side and Cerablanket fibres for the outer side. The corresponding fibre densities were 160 kg/m^3 and 130 kg/m^3, respectively. The two fibre layers were separated by a thin-walled intermediate sheet. The ducting shroud made of Incoloy 800 – another source refers to Inconel 617 – was fixed by v-shaped spacers opposite the support tube.These spacers sealed the insulation space gastight in the axial direction. As shown in the diagram, they were not fixed to the ends of the inner liner. The only opening was at the expansion joint of the inner liner. A perforated tube between liner and insulation ensured the necessary pressure compensation. The sliding connection of the ducting shroud was coated with yttrium-stabilized ZrO_2.

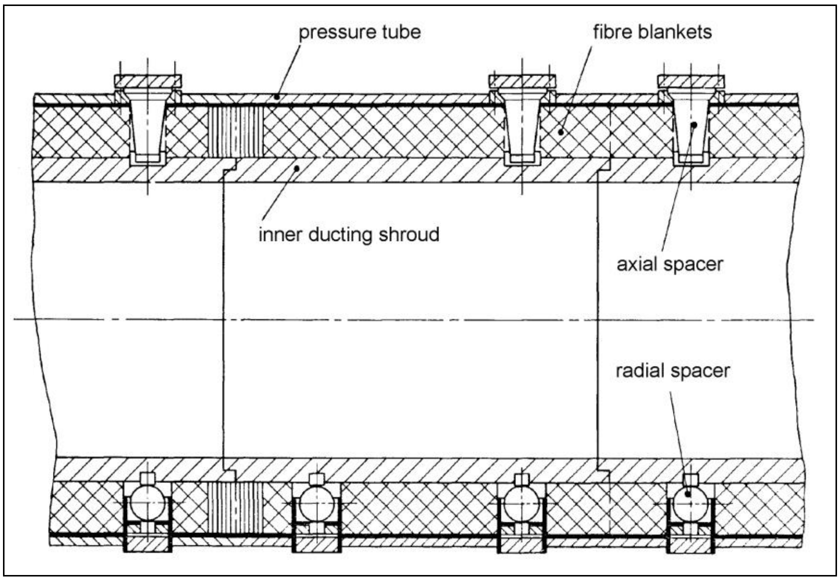

Figure 109: Primary gas duct (cutout)

For the secondary duct INTERATOM and Balcke-Dürr had returned to a design with metallic liner, as described by Jansing [JAN84] and Klas [KLA84b], see Figure 110. The test segment corresponded to PNP conditions in its radial dimensions with the outer diameter of the pressure tube (15Mo3) being 1220 mm and the inner liner diameter 700 mm. The insulation had been mounted onto a support tube. In accordance with earlier experience, Saffil fibres had been used for the inner side and Cerablanket fibres for the outer side. The corresponding fibre densities were 160 kg/m^3 and 130 kg/m^3, respectively. The two fibre layers were separated by a thin-walled intermediate sheet. The ducting shroud made of Incoloy 800 – another source refers to Inconel 617 – was fixed by v-shaped spacers opposite the support tube. These spacers sealed the insulation space gastight in the axial direction. As shown in the diagram, they were not fixed to the ends of the inner liner. The only

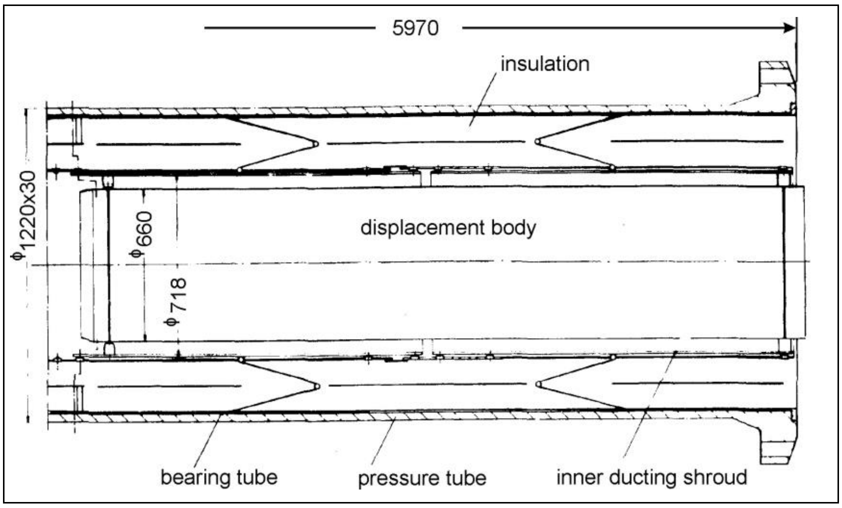

Figure 110: Secondary gas duct (metallic)

opening was at the expansion joint of the inner liner. A perforated tube between liner and insulation ensured the necessary pressure compensation. The sliding connection of the ducting shroud was coated with yttrium-stabilized ZrO_2.

Further details concerning the left-hand side of this test object are shown in Figure 111 after [BRÖ84b] et al. The end pieces were fixed to the ends of support tube and inner liner. The insert thus obtained was installed in the pressure tube by means of a screwed connection at the flanges. Friction disks of Al_2O_3 had been used as spacers because of the thermal expansions between ducting shroud and perforated cylinder. The spaces near the v-shaped end pieces in the flange region had to be stuffed by hand. This insulation was also planned for bends and expansion bellows. For the insulation of expansion bellows, however, ring-shaped fibre blankets were to be used to utilize their resilience. Thermal studies on a stuffed angular bellow expansion joint are described by Lang, Klas and Schumacher [LAN82].

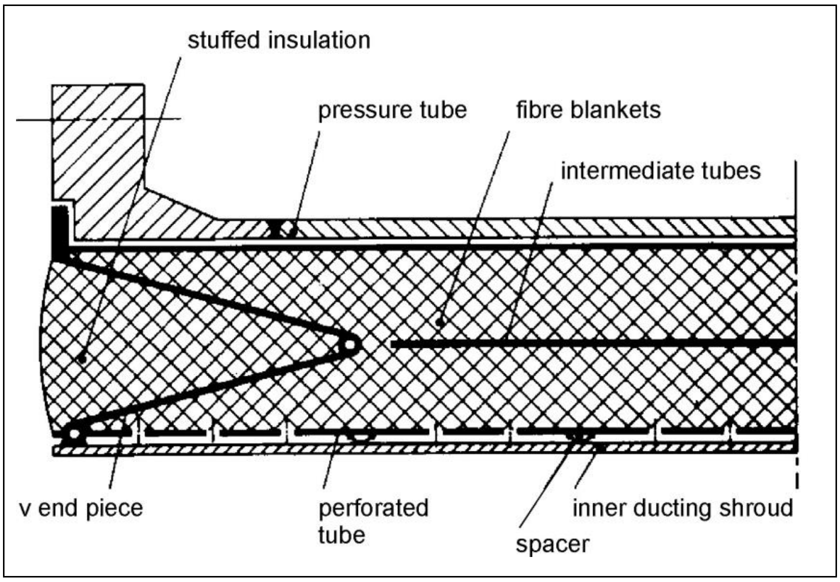

Figure 111: Secondary gas duct (cutout)

Klas [KLA84b] as well as Stehle and Klas [STE84] report on investigations in the KVK facility concerning this insulation. Actual values remained markedly below the defined thermal conductivity. The heat losses were 70 % below the design calculations. The suitability of the component was thus demonstrated.

Further work on large components lined with insulations and summarizing investigations on these components, primarily in the KVK facility, will be briefly mentioned in the following chapters.

An axial valve developed by Klinger in cooperation with KWU is shown in Figure 112 after Kruschik and Berdan [KRU84a] as well as Kruschik and Hiltgen [KRU84b]. The approximately 4200 kg valve was provided for a duct diameter of 800 mm, a pressure of 51 bars and a temperature of 900 °C. The maximum closing time was 15 s. It had been designed as a two-way valve with seal gas charging between the two closing cones. In the event of a rapid pressure reduction due to an accident, the valve closes automatically due to the occurring pressure differences. The leak rate should not exceed a value of 0.1 mbars/s. This low value was achieved by arranging all the gear elements inside the thermally insulated valve box. The insulation consisted of moulded vacuum parts with metallic liners at the inlet and outlet and of moulded parts without liner at the annular channel. Henßen, Mauersberger and Kruschik [HEN86]. report on tests in the ADI facility.

In the following, two designs based on cover plates from HRB will be described. The first version was provided as a thermal protection system for prestressed concrete vessels, the second for lining a hot gas duct.

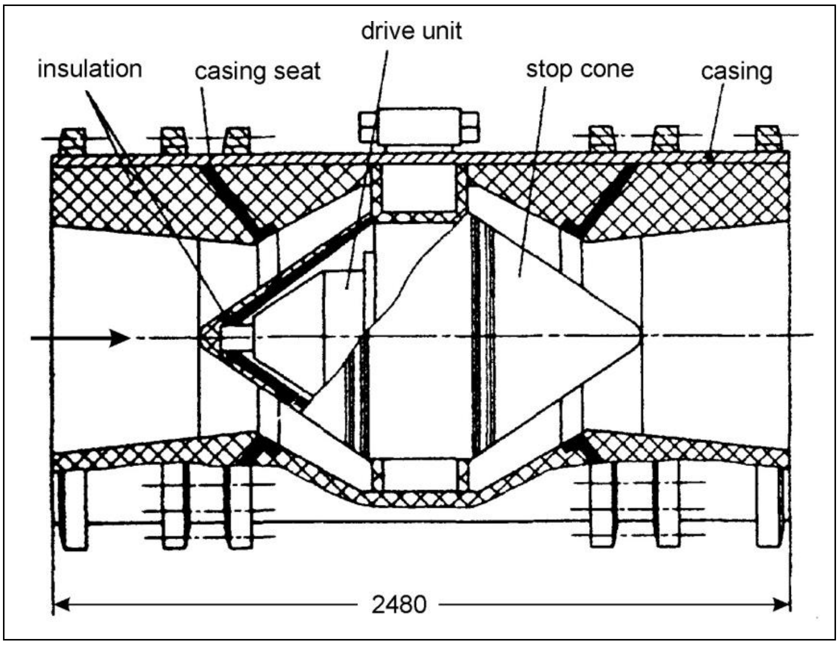

Figure 112: Axial valve

The studs and cover plates of the vessel insulation were made of St37 and 15Mo3, respectively. The pressure tube from the duct system of the HHV facility, which had to be prepared for the planned investigations, required a modification of the initially square cover plates 8 mm in thickness. The edge lengths were adapted with 600 mm and 400 mm to the dimensions of the tube. Eight studs were needed across the circumference of the tube. The insulation material was Cerablanket. A total of six fibre blankets were compressed to a mean density of 200 kg/m^3 and a thickness of 100 mm after bracing the cover plates via the studs. The sealing foils needed underneath the cover plates overlapped. They prevented dust discharge and, moreover, served as convection barriers. Following the insulation for the THTR, each cover plate was centrally bolted to a threaded stud welded to the vessel wall. The insulation was installed at KFA by fitters from the British Darchem supply company. The power of the electric heater for the test arrangement in the vertical position was 139 kW. Measurements had been carried out at the IRB. Temperatures of up to 600 °C were reached with helium. The maximum pressure was 55 bars. Since work at the IRB could not be continued, the measurement series were not evaluated, so that no published results are available.

Figure 113 shows a cutout of an insulation with cover plates further developed by HRB. This insulation featured fibre blankets with a high content of aluminium oxide.

Cover plates formed the closure on the inner side. Barriers between the blankets were to prevent axial and radial through-flow, see Bröckerhoff et al. [BRÖ84b]. The gap between cover plate and cover was required for the expected depressurization rate of 2 bars/s. The insulation was held by two studs in the centre of the cover plates, thus achieving redundancy. Each element was designed for fully accommodating the load. The elements were prestressed by springs to compensate the elongations occurring and cooled with gas. In the hypothetical case of a break of a holding element, it had to be expected that fragments were passed into the helium loop. The cover plates were secured against torsion. Each plate could expand and move without being forced. On account of the low weight of this insulation, only little stressing occurred inside the studs, above all in the vertical position. As in the insulation for the THTR, the support tube was made of 15Mo3. Corresponding to Knaul [KNA84] and Elter [ELT85] two versions were developed with the material for the fibre blankets being Al_2O_3 in each case. In the insulation described by Knaul, the cover plates and holding elements were made of fibre-reinforced carbon, MA754, the cup springs of Inconel X-750, the convection barriers of X10CrNiTi18/9 and the pressure sleeves of Al_2O_3; for the insulation after Elter X10CrNiTiAl32/20 had been chosen for the cover plates and studs, NiCr30/20 separation sheets, X10CrNiTi18/9 wire mesh, Hastelloy C-276 small parts and Cr_2C_3 and Ni/Ag coatings. Pre-run investigations on components for these hot gas insulations are described by Mauersberger [MAU84b].

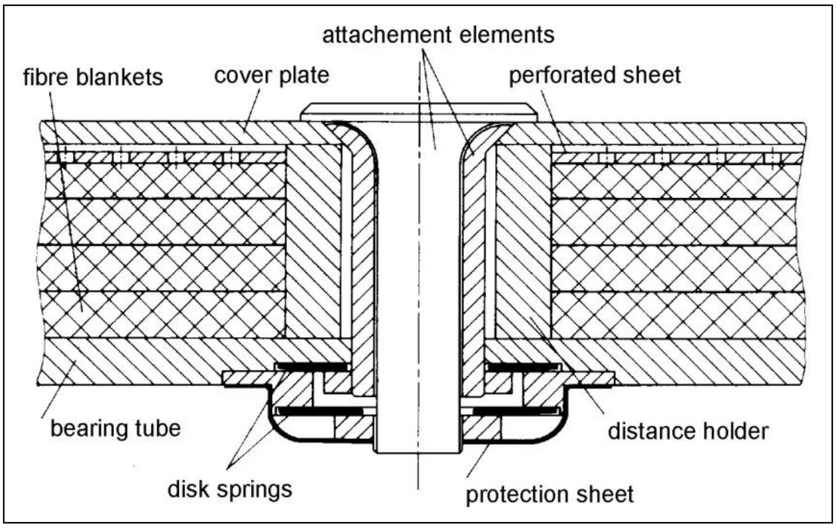

Figure 113: Cover plate insulation

A 90 ° elbow with blanket insulation and cover plates of fibre-reinforced carbon for the primary hot gas duct is shown in Figure 114. Compared to segmented bends, elbows offer the advantage of simpler in-service inspections due to fewer weld seams. The elbow with inside insulation shown in the figure was therefore ordered. The pressure housing with the cooling systems was supplied by Gessner in Untereschbach. The shroud material was carbon fibre composite (CFC), mentioned before when presenting the test pieces for straight pipes. Tripartitioning was made for reasons of mounting.

The inlet and outlet parts, designated 1 and 3 in the diagram, had short cylindrical pieces for adaptation to the metallic pressure housing. The shroud pieces opposite the pressure-bearing part were radially fixed by four ceramic spheres of Al_2O_3 each at the inlet and outlet, as also indicated. Three support elements of the same material, arranged in the 45 ° plane, represented the fixed point in the axial direction. The connection between two CFC parts was effected in each case by four pinned tags distributed over the circumference. For reasons of strength, thickenings of about 37 mm were required in the region of the spacers and tags. The wall thickness of the shrouds manufactured by Sigri was 10 mm in the other regions.

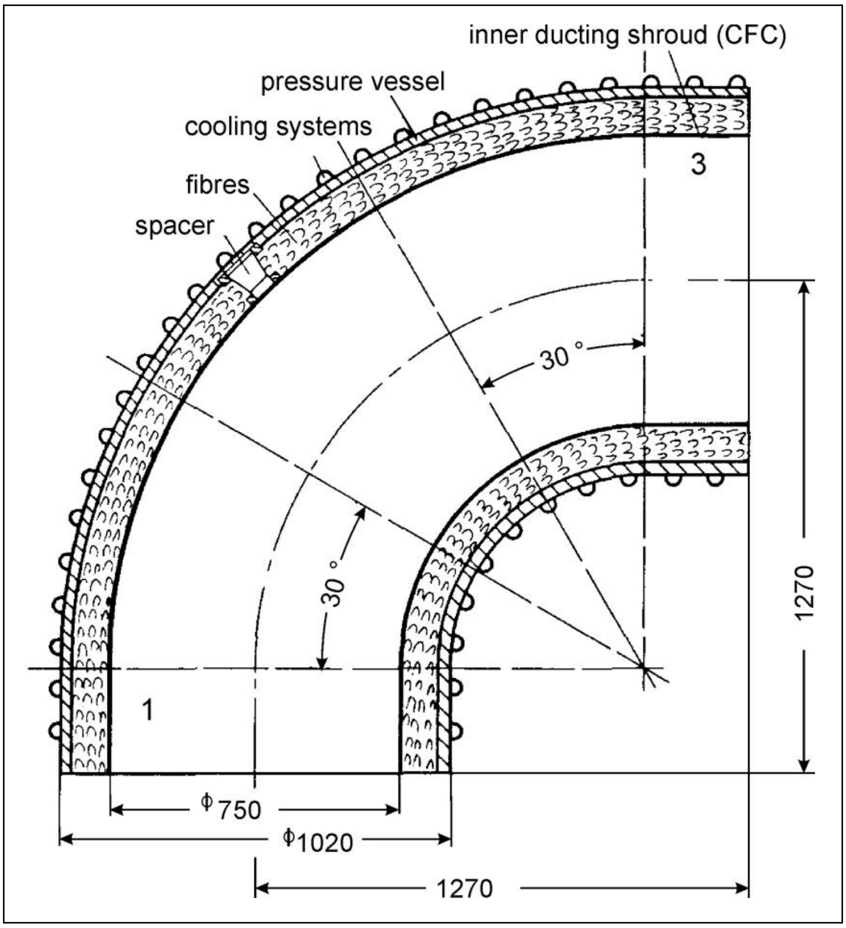

Figure 114: 90° elbow

Figure 115 shows the shroud of a segment as delivered. Mounting took place together with INTERATOM at the IRB of KFA. Saffil blankets of Al_2O_3 together with graphite foils were wrapped on the CFC parts. These foils had the task of reducing or even preventing free convection. The outer closure was a sheet-metal jacket with which the blankets had been compressed. The three segments completed in this way were then axially and radially fixed in the pressure housing provided by KFA.

The remaining gap between tensioning sheet and pressure housing with a width of about 25 mm was subsequently stuffed with a fibre cord so as to prevent through-flow. No further details will be given for reasons of simplification. All the parts used inside had been made available by INTERATOM. During mounting, thermocouples of Incoloy 800 – the insulation was to be tested later on in the KVK facility – had been installed on the inner and outer sides of the ducting shroud, in the region of the sliding connections, on some spacers, on the sheet-metal jacket and within the fibres.

In the region of the two flanges, wire meshes of stainless steel had been used to prevent the discharge of fibrous material from the test component.

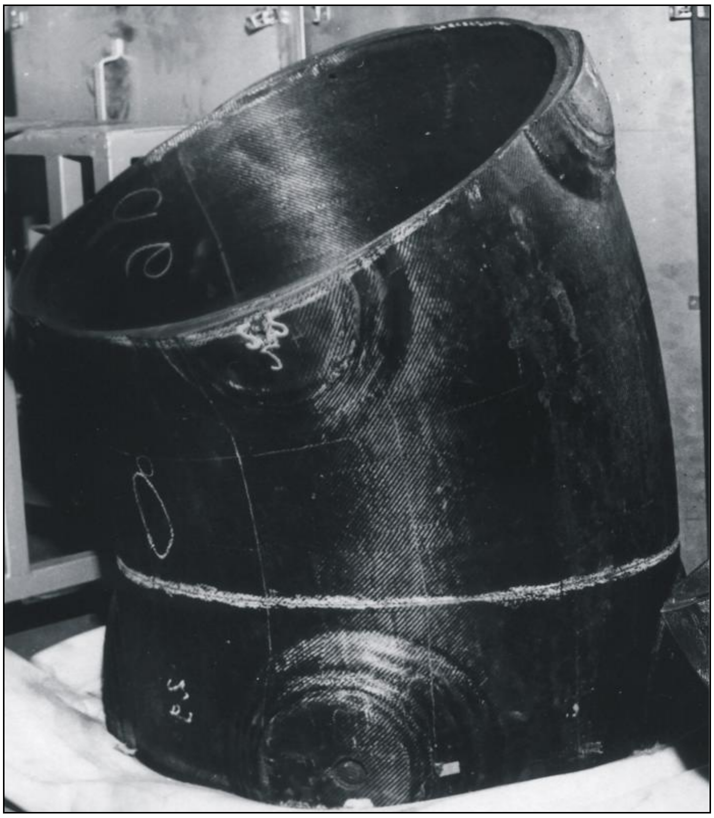

Figure 115: CFC shroud for 90 ° elbow

In conformity with earlier investigations in the HP channel, first of all, tests with air and then with helium were performed. Pressures of about 39 bars, 19 bars, 9 bars and 4 bars were adjusted at the temperature levels of 100 °C, 200 °C and 300 °C. No changes in insulating behaviour had become apparent during the experiments with these parameters. During the following test at a pressure of 39 bars and a temperature of 400 °C, the heating power of only 300 kW proved to be too high, since the gas temperatures were steadily rising. The pressure control of the channel had meanwhile been switched from automatic to manual. An attempt to completely run down the heating power was not successful, since the gas temperatures continued to rise and had meanwhile reached values of about 430 °C. Furthermore, the safety valve responded more and more frequently, i.e. the pressure in the channel also increased. The gas pressure had been lowered to 33 bars via the quick release to relieve the channel walls. The gas was then rapidly cooled to normal operating values with the aid of the bypass cooler. The strong increase of the gas temperatures had lasted for about 33 minutes. The impacts on the test component – temperatures of 430 °C were also reached at the ducting shroud – only became apparent after a time delay. Since evaporation temperature was reached in one cooling system on the outer side of the pressure housing, severe damage to the inner insulation had to be assumed. The failure of numerous thermocouples on the inner side of the insulation was also indicative of damage. In order not to jeopardize the safety of the operating crew and to bring the facility into a safe operating condition, the channel was immediately shut down.

The inspection of the components after dismounting the elbow and the feed and wake sections showed that about 55 % of the CFC parts were partially or completely burnt, see Figure 116. This corresponded to about 1.5 segments. The material was primarily burnt in the region of the thickenings and holes for fixing the thermocouples. The mesh of stainless steel was molten at the outlet. Parts of the Saffil blankets had baked on the outer and bottom sides of the insulation and were entrained with the gas flow. The remaining insulation of about 1.5 segments was intact. The surfaces of these parts still had the structure as delivered. Chalk marks were still discernible. Even the thermocouples and their mounts were still operational there.

Figure 116: Destroyed ducting shroud

Queries to the Sigri manufacturer with respect to limiting conditions of operation had not led to any express warning e.g. concerning the test temperatures. In a discussion with experts about the cause of damage and the necessary consequences, first of all, the manufacturing process had been explained. The nondestructive testing of the components and investigations of specimens from projecting lengths had not shown any defects. Acceptance certificates had been issued for each of the numerous manufacturing steps. No lubricants had been used in workshop machining. Ash analyses had revealed contamination of 800 ppm and 1200 ppm, respectively, for the tube parts and thickenings. On the whole, no distinct reason could be found for the ignition. The lower limit at which the material ignites could not be specified. Local overheating was ruled out, since no hot gas streaks had to be expected in the HP channel. Possible causes were

- variations of the material properties of the complex ceramic material with respect to its structure,
- contamination of the material,
- influences due to machining,
- catalytic effects due to contamination and contacts with metallic parts, e.g. thermocouples, screws and mounts, as well as
- contamination from the HP channel.

Despite agreement between those involved and although requested by the project partners, no new test components could be manufactured, so that reliable statements on the thermal behaviour of an elbow insulated in this way are not possible.

10.5 Rigid ceramic insulation

In the French EDF3, EDF4 and St. Laurent II reactors, the insulations after Tarbès and Menestrier [TAR67] were of pumice concrete, whose main constituents were pumice from the Lipari Islands and cement. The pumice rock was in part already processed, dried and cleaned in the quarry. During heating in the factory, attention had to be paid that the bricks did not excessively shrink. After quality control, the materials were mixed while adding some water, poured into hexagonal moulds and dried. The blocks thus obtained, which were very fragile at this stage, were then heated in water at a temperature of 90 °C. After drying, a special treatment took place for about three weeks at temperatures between 250 °C and 300 °C. This treatment required a lot of skill because of the vapour formation in the bulk and the associated stresses.

A great disadvantage of pumice concrete was that the required insulation thicknesses had to be 600 mm for reasons of strength, although the temperature differences to be reduced were only in the range of 120 K. The accommodation of the insulating layers in the reactor required an enlargement of the diameter by about 1 m. This led to an increase in costs. In comparison to the foil and fibre insulations described above, the pumice concrete had a further disadvantage. For reasons of nuclear cleanliness, as already mentioned, a tight skin had been provided in the EDF3 between insulating layer and reactor interior. However, this was not possible in EDF4 and St. Laurent II for economical reasons, and dust filters and thin wire screens were provided instead. In spite of the pretreatment, the pumice concrete contained excess water, which could not be completely expelled. A large portion of water was above all introduced into the reactor by the mortar required for sealing the joints. Since this water could not be removed prior to commissioning the plant to the extent necessary for achieving a sufficiently dry atmosphere, however, these pumice concrete insulations were and are no candidates for high-temperature reactors requiring a high degree of cleanliness.

The development work for the use of pumice concrete at elevated temperatures was continued with the aim of increasing its strength and thus achieving smaller layer thicknesses. One possibility was seen in the use of binders suitable for temperatures of up to 450 °C. These binders were based on aluminate and a granular clay material. The thermal conductivity of these materials was specified as 0.4 W/(mK) at a mean temperature of 250 °C. A disadvantage according to Dubois et al. [DUB69] was, however, shrinkage under irradiation.

Figure 117 schematically shows a liner insulation composed of an arrangement of blocks after [TAR67]. Since the associated data relate to tests in the Megabidon facility, these are pumice concrete blocks stacked on each other without any sealing, as seen on the left, and placed in front of the liner. The gaps between liner and blocks and between neighbouring blocks are drawn overdimensionally for the sake of clarity. According to the authors, the vessel height and vessel diameter were 6.1 m and 2.6 m, respectively. The test gas was carbon dioxide. At a pressure of 30 bars and a hot gas temperature of 400 °C, total losses of 30.8 kW or an effective thermal conductivity of 0.6 W/(mK) resulted for the arrangement on the left. The hot gas which had risen upwards and was cooled on the outer wall dropped downwards in the gap between liner and blocks and could enter the interior again between the blocks, as symbolized by the arrows. Heat transport was clearly reduced by the sealings shown schematically on the right. The heat losses across the gap were determined to be 26.7 kW, so that losses of 4.1 kW were obtained for the blocks due to pure heat conduction.

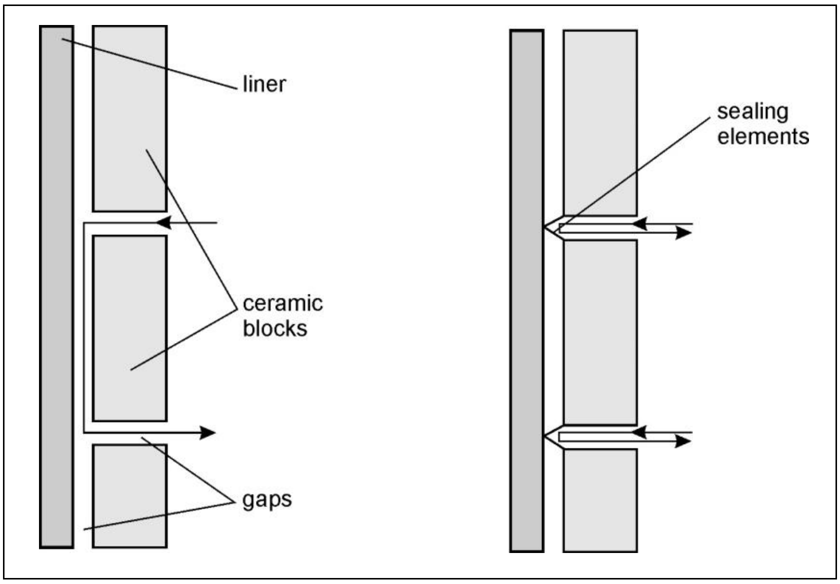

Figure 117: Arrangement of rigid ceramic blocks

A candidate material for high-temperature reactors is carbon brick, as was shown by the AVR pebble-bed reactor on the premises of Research Centre Jülich. Carbon brick is an intermediate product in the fabrication of graphite. The starting material is petrol coke, a residue from oil production. It is first roasted removing any volatile constituents left and then ground. Following this, a binder such as pitch-like hydrocarbon is added. The mass produced is then processed into so-called green compacts by extrusion pressing. The compacts are carbonized at temperatures between 1000 °C and 1500 °C. During this process all hydrocarbons escape. The product of this sinter-like process is called carbon brick. It is hard and brittle. Carbon is present in carbon brick in the amorphous form. Carbon brick contains about 3 % to 5 % ash. During the graphitization process at temperatures between 2500 °C and

2800 °C the C-atoms orient towards graphite crystals. The blocks packed in carbon powder are heated to crystallization temperature within three to five days and must then be slowly cooled. Due to its generally low thermal conductivity compared to metals, carbon brick is used for lining blast furnaces. It was also used in the EVA-II facility for the insulation of short connecting ducts.

One manufacturer was or is Sigri in Meitingen. Some data taken from the company's brochure [SIG] are compiled in Table 10. The densities differ by almost 20 %. This difference depends on the porosity, namely total porosity ε_g and apparent porosity ε_s. The differences here are more than 40 %. Like all the physical properties of the material, especially the thermal conductivity depends on the starting material used. All the values specified in the table were obtained at 20 °C ambient temperature according to the manufacturer. Information about the type of gas is lacking. It may be assumed, however, that the measurements were performed in air. The RUD-N material exhibits the lowest value. The very high ash content of 8 % could be markedly reduced, according to the manufacturer, depending on the pretreatment. Particular attention is drawn to the value of the bending strength, σ_B, whose half value had to be taken as a basis due to the lack of tensile strength in calculating thermal stresses in the outer fibres of rings, as described by Bröckerhoff and Lang [BRÖ77b].

Designation	RUD-N	5 RUG-S	RDN-RM
true density ρ_t / (kg/m^3)	1880	2170	2050
density ρ / (kg/m^3)	1530	1670	1440
porosity ε_g / %	18.6	23	30
porosity ε_s / %	16.7	15.5	29
bending strength σ_B / (N/mm^2)	6.9	9.8	5.9
Young's modulus / (N/mm^2)	9218	7747	?
expansion coefficient α /(10^{-6}/K)	3.4	3.1	3.9
thermal conductivity λ / (W/(mK))	2.9	34.8	8.12
ash content / %	8	0.3	0.6

Table 10: Data of some carbon brick varieties

In the search for a simple and low-cost solution for lining straight tubes, this material offered itself. The design used followed a proposal by Felten from CEA in Saclay [FEL73], who wanted to use rings of Masrock. The experimental setup including pressure tube and insulation is shown in Figure 118. The flow direction of the cooling water is indicated. The drawing shows the insulation made of RUD-N carbon brick. It consisted of a total of five rings that were undersized in comparison to the inner diameter of the pressure tube, see [BRÖ77b]. Their outer diameter was 927 mm, the inner diameter 627 mm. This gave an arithmetic gap of 1.5 mm between tube and rings, provided that the rings were exactly fixed. This gap was not sealed at the first ring. The two arrows point to this gap. The first and last rings served as feed and wake, respectively. They were bevelled to reduce the inlet and outlet losses. The three central rings 2, 3 and 4 were cylindrical. They represented the measurement region. For this reason, they were positioned exactly underneath the water cooling indicated. Apart from the metallic mounts, the design did not contain any metallic parts. The four mounts per segment were to protect the carbon brick rings against torsion and displacement. For this purpose, the rings were externally provided with milled recesses. The pegs of the mounts were inserted in the pressure tube wall. This solution had been considered necessary, since tests with the test section in the vertical position were also planned and the total weight of the insulation should not solely rest on the mount of a ring.

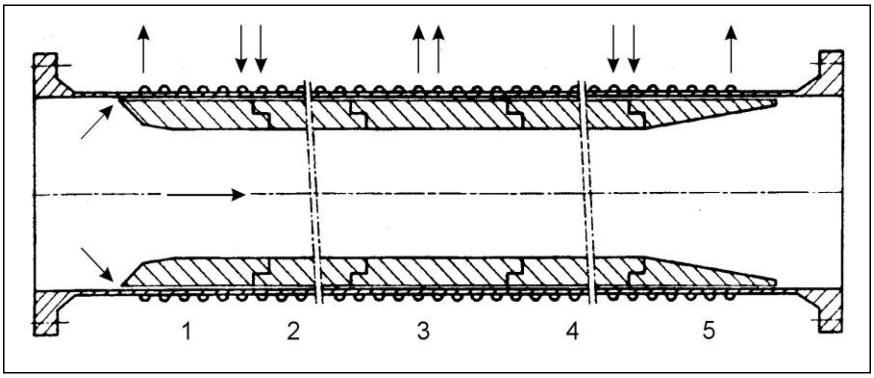

Figure 118: Carbon brick insulation

For more details see Figure 119. The length of a ring was 800 mm. In order to avoid a direct gas stream in the sliding connections of neighbouring rings from inside to the cooled pressure tube, the rings at the colder outer side should be very close to each other, whereas inside an expansion gap of 1.5 mm was necessary. Each carbon brick ring had an inside groove of 5 mm x 5 mm into which, if required, a seal could have been placed to prevent a bypass stream between tube wall and carbon brick rings. In the first test series, these seals were lacking in all rings. The central segment 3 was provided with thermocouples in the top, right, bottom and left sectors for the measurement of temperatures in the radial direction. These thermocouples were placed in plugs of carbon brick inside the ring. The holes for accommodating the plugs are indicated in the diagram. Thermocouples on the outer side of ring 3

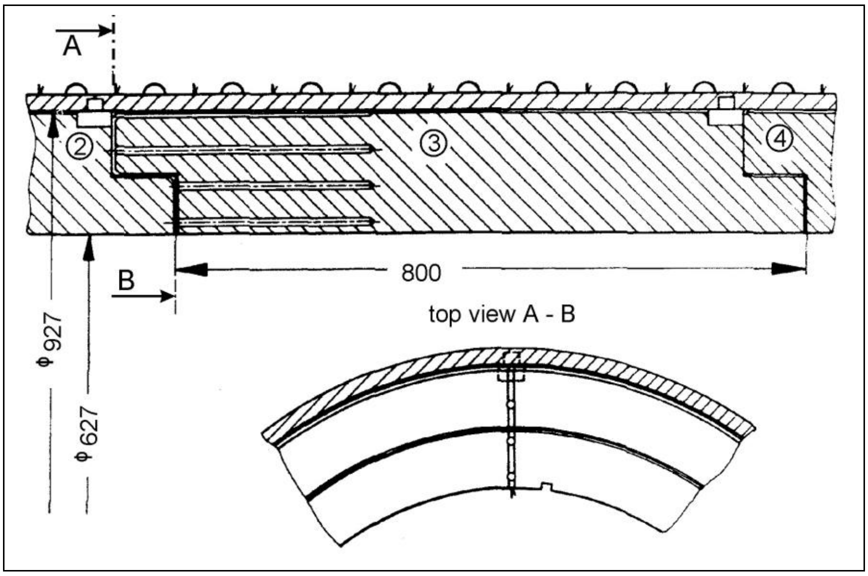

Figure 119: Details of the carbon brick insulation

were fixed with HS 40 adhesive. The measuring leads of all thermocouples were passed inside in 3 mm deep and 6 mm wide grooves, as can also be seen, from where they led in four 6 mm deep and 10 mm wide grooves to the measurement lead-throughs in the direction of flow. These grooves, which were arranged approximately 35 mm off-centre, and the position of the thermocouples in the insulation can also be seen in the top view A-B. The further instrumentation corresponded to that of insulations already presented before.

Due to the unexpectedly poor thermal behaviour of the insulation, the results are not presented in detail. The temperatures measured in ring 3 showed almost linear temperature profiles for all gas conditions. Pressure and temperature had no influence. In the sliding connections between the rings, however, increased heat transports to the cooled tube wall occurred due to radial through-flow. This was reflected in pronounced temperature peaks. The consequence was differently high heat losses and thermal conductivities in the different sectors. Since the gaps and expansion joints represented a major problem, further investigations were required to demonstrate the effectiveness of sealed gaps. In detail, the following measures were taken and measurements performed:

- The first two rings 1 and 2 were sealed with a Teflon cord against through-flow. The cord was placed in grooves provided for this purpose [BRÖ77c]. Due to thermal stresses four of the five rings broke, as described by Bröckerhoff and Lang [BRÖ77d], see Figure 120. The cracks were puttied to be able to continue the experiments.

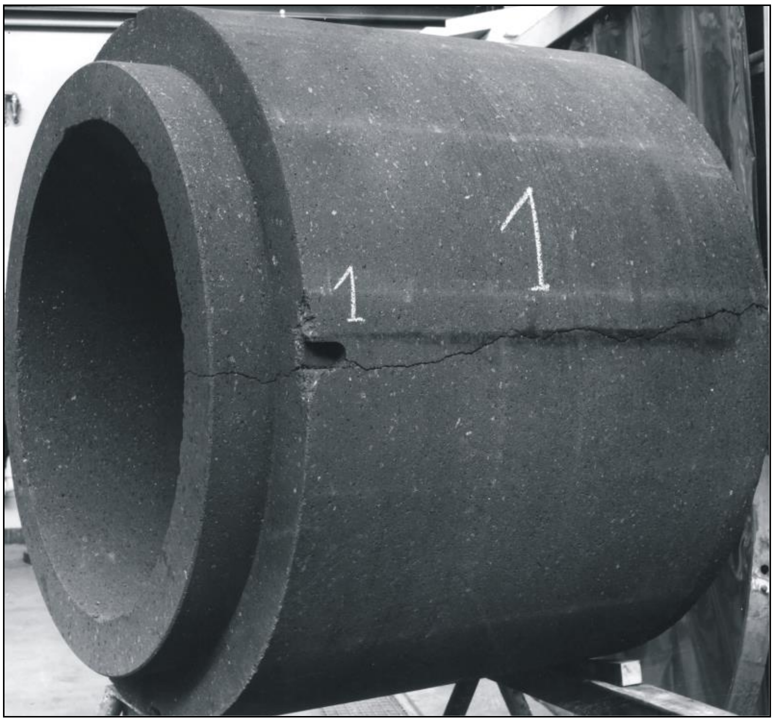

Figure 120: Carbon brick ring with crack

- All rings were sealed with a Teflon cord [BRÖ78b]. In this way, a clear homogenization of the heat losses and temperatures was achieved. The pressure and velocity dependence observed before could thus be largely eliminated.

- The insulation was subjected to high axial pressure gradients with the aim of checking the effectiveness of the seals, [BRÖ78c]. The diameter of the flow displacer was 510 mm. In the remaining gap, velocities of 45 m/s were achieved with air and 62 m/s with helium. This meant a maximum pressure drop of 0.005 bars across the length of a ring. Due to the corrosion risk, the hot gas temperature was limited to 300 °C for the use of air.

- The insulation was exposed to temperatures of up to 570 °C in the vertical arrangement in atmosphere almost at rest using an electric heater [BRÖ80b]. The pressure dependence of the heat losses, which amounted up to 12000 W/m^2, was slight.

Due to this experience – need for accuracy of fit in manufacturing, formation of gaps with the danger of forced through-flow and sensitivity to thermal stresses – fully ceramic insulations were not used. The effort for eliminating the problems would have been to high.

10.6 Combinations

Jones and Brislin [JON74] give a summarizing description of work on thermal insulations for the Fort St. Vrain reactor. In normal operation, the helium flowed downwards to the class C insulation at the bottom and then flowed radially outside into the twelve steam generator pipes. The mean temperature of the hot gas had been fixed at 776 °C. On the upper side of the insulation, however, local hot gas streaks of up to 1100 °C could occur. In order to protect the walls against the high temperatures, the class C insulation shown in Figure 121 on the left was therefore developed for this region. Three 75 mm thick blocks of Masrock were stacked on a layer of fibre blankets with cover plates. Masrock, which consists of silicon, offered itself as a thermal insulator. It is resistant to thermal shocks and has a very small expansion coefficient of $0.6 \cdot 10^{-6}$ K^{-1}, so that no expansion gaps were required between the individual blocks. Forced flows to the cold wall could thus be ruled out. Another advantage was the low thermal conductivity of about 0.7 W/(mK), see Hosegood and Jones [HOS74]. Further information cannot be found even in Hedgecock and Patriarca [HED74], who concerned themselves in detail with the materials used in the Fort St. Vrain reactor. This applies, in particular, to the two grades shown in the diagram. It may be assumed, however, that the top layer of dense material had been chosen for reasons of strength. Due to the greater solid content, the thermal conductivity was probably higher than that of the other two layers for which a porous material was to be used. A disadvantage in this case, too, is recrystallization with the consequence of a volume enlargement at temperatures above 1000 °C.

Nakase et al. [NAK84] describe an insulation of metallic foils and ceramic fibres for a coaxial duct and investigations within the framework of a Japanese programme. The experiments were carried out in the KH-200 helium loop of Kawasaki Heavy Industries (KHI) at pressures and temperatures up to 40 bars and 1000 C. The mass flows were varied between 0.1 kg/s and 0.2 kg/s. The metallic parts used on the inner side of the insulation were made of Inconel 600. 32 foils 0.05 mm in thickness were used. The thickness of the foil insulation, which corresponded to that of the Darchem insulation with Z-pieces etc. already presented, was 25.3 mm. Kaowool with a stuffing density of 300 kg/m^3 was chosen for the outer 44.5 mm thick fibre insulation with V-pieces. The temperatures and heat fluxes measured were in agreement with calculated values.

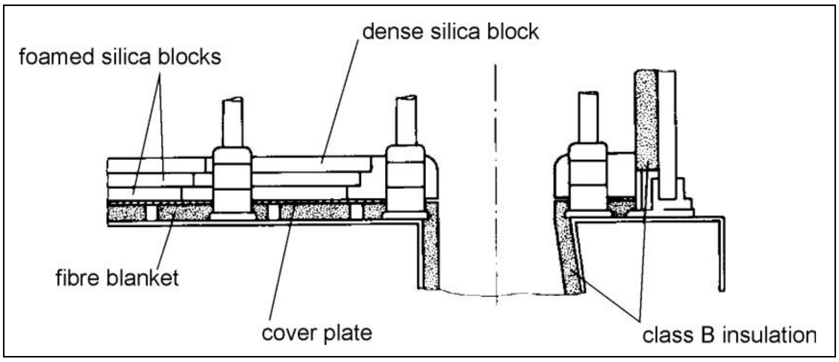

Figure 121: Insulations of the Fort St. Vrain reactor

11. Depressurization

The investigations concerning depressurization were by far not so comprehensive as those in the field of thermal behaviour. This may above all be due to the numerous studies on the development of vessel insulations, which were generally not subjected to very high depressurization rates on account of their size and numerous holes. Incidentally, this also applies to the development of hot gas ducts for PNP applications. However, much higher demands were made on the insulations for tubes in HHT plants. Therefore, the following descriptions primarily deal with investigations for direct-cyle plants, although not in conformity with the chronology of the investigations carried out.

12. Selections of Insulations

As far as was known, the first investigations had been carried out on metallic fibre insulations in France and Ispra/Italy. In the literature available, little is known about measurements performed elsewhere. There are only a few references to experimental investigations. Work at Ispra served as a basis for our own measurements, presented in the following, on selections of ceramic materials that could have been used e.g. as ducting shrouds.

Figure 122 schematically shows the test facility according to Bröckerhoff [BRÖ74b]. The main component was an earlier used autoclave 1 with the volume V_1, which was designed for a pressure of about 100 bars. The two volumes V_1 and V_2 were separated by a rupture disk 3. If ball cock 2 was opened after filling both gas volumes to the initial pressure p_0, the rupture disk broke due to the overpressure prevailing in volume V_1, and the gas could escape through the cross-section of orifice 4 at a defined escape rate. The two pressure curves in the vessel and in sample 5 arranged below were recorded by light-beam oscillograph 9 after amplification of the signals of pressure transducer 6 via measuring amplifier 7 and carrier-frequency amplifier 8. Because of the higher sound velocity, helium at ambient temperature served as the test gas in most cases. Five flow orifices each were used for four pressure stages. In this way, a wide parameter field could be covered. The gas pressure was adjusted by means of a pressure gauge. Because of the bang caused by the rupturing disk, the maximum initial pressure p_0 was fixed at 12 bars. The cylindrical samples – diameter D 75 mm , height H 80 mm – had been manufactured with due regard to the size of the pressure vessel. They had a hole on the bottom cylinder surface to accommodate a measuring probe tightly attached with adhesive on the sides, which served for measuring the static pressure in the centre-line. Samples of the 4 BDN and HP carbon brick varieties as well as the AS2-500 graphite grade from Sigri were available.

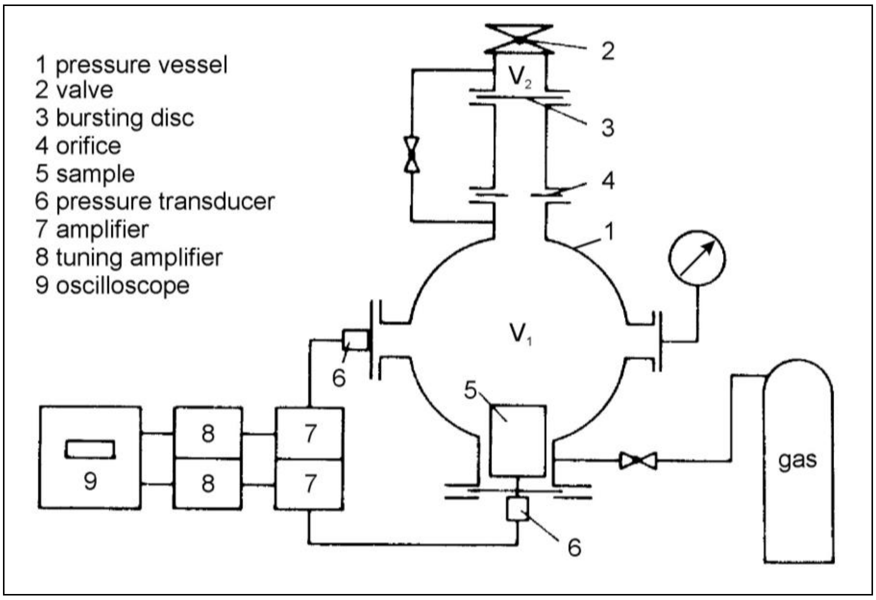

Figure 122: Depressurization test facility

Figure 123 shows two measured gas curves for the gas volume V_1 and the carbon brick sample HP (V_2) at an initial pressure of 3.92 bars. After opening the ball cock, the pressure decreased very rapidly to the ambient pressure p_a. The depressurization rate was determined graphically. For this purpose, a tangent was applied to the curve $p_{Pr}(t)$ of the sample so as to give a maximum slope. As can be seen from the figure, the transition of p_0 in the pressure curve of the sample only occurred gradually. The reason is to be seen in the flow resistance. The transition was sharp in the outer volume. The depressurization rate was determined from the paper feed v, the initial

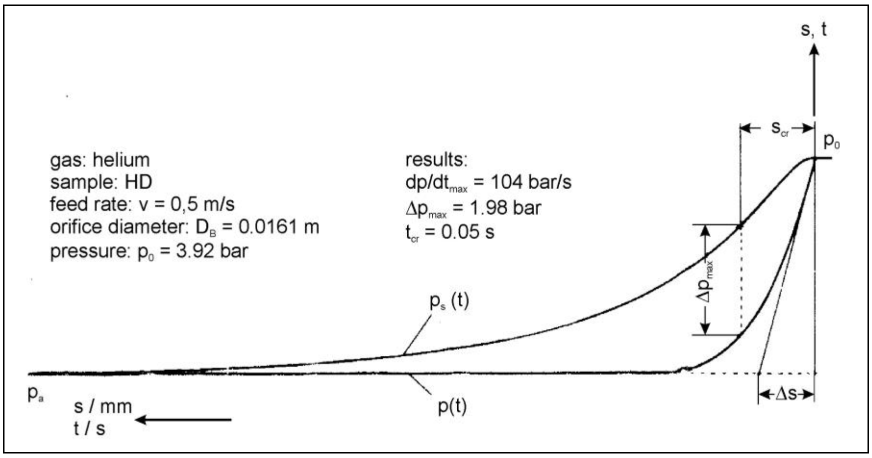

Figure 123: Pressure curves and test data

pressure p_0 and the tangent section Δs. The pressure difference in the sample increased from zero to the maximum value Δp_{max}. Upon pressure compensation it attained the value of zero.

The maximum pressure differences for tests on one of the three samples used (4 BDN) and using nitrogen and helium as the test gases are shown in Figure 124 as a function of the depressurization rate. Two straight lines were obtained for both gases. At the same initial pressure, the depressurization rates were higher by a factor of 3.4 and the loads by a factor of 1.4 using helium. The depressurization rates had been raised up to 330 bar/s, that is far above the value of about 20 bar/s fixed at that time as the upper limit for HHT plants. In comparison to the strength of the samples, low stressing values of 3.4 bars were obtained under helium.

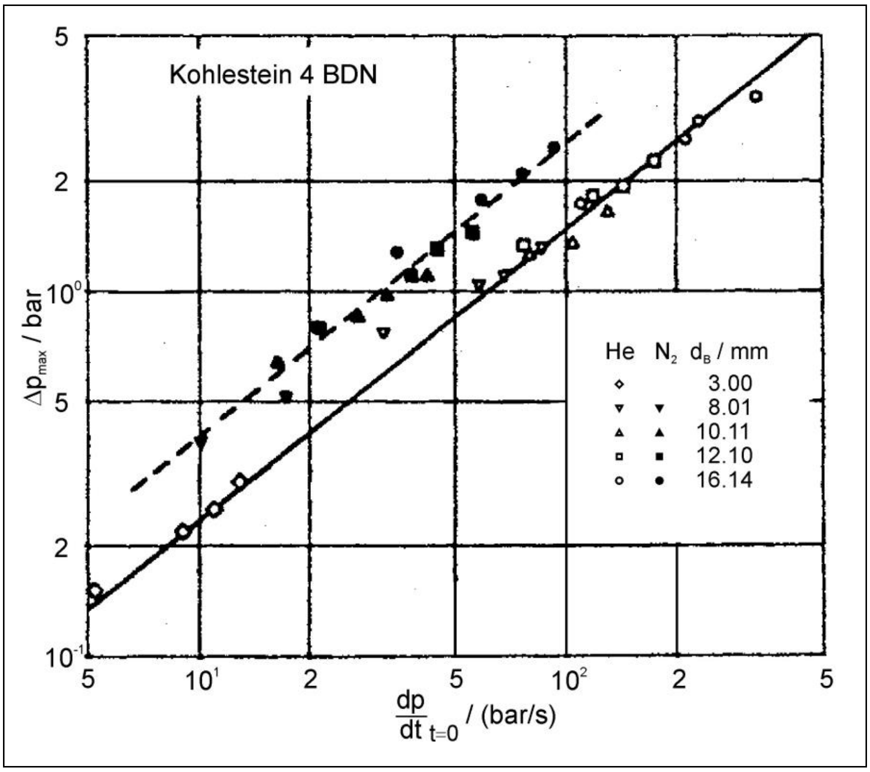

Figure 124: Pressure differences as a function of the depressurization rate

Measurement results in the non-dimensional form are shown in Figure 125. The maximum pressure differences are made non-dimensional with the expression $D^2 \cdot \rho/\eta^2$. The abscissa value $dp'/dt_{t=0}$ represents the product of the depressurization rates $dp/dt_{t=0}$ in the outer volume and the expression $D^3 \cdot \rho/(a \cdot \eta^2)$, where ρ denotes the density, η the viscosity and a the sound velocity. Three curves were obtained. The fitted lines through the points displayed a uniform slope of m = 0.79, if the results were represented in the form of $\Delta p'_{max} = A \cdot dp'^m/dt_{t=0}$. Factor A was calculated as 2.4, 1.9 and 1.3 for HP, 4 BDN and graphite. It is assumed that the porosity of the samples represents a further parameter, which had not been taken into account in the above considerations. Maximum tensile stresses in the materials were obtained from the data determined. The samples investigated did not exhibit any visible external damage such as cracks after termination of the experiments.

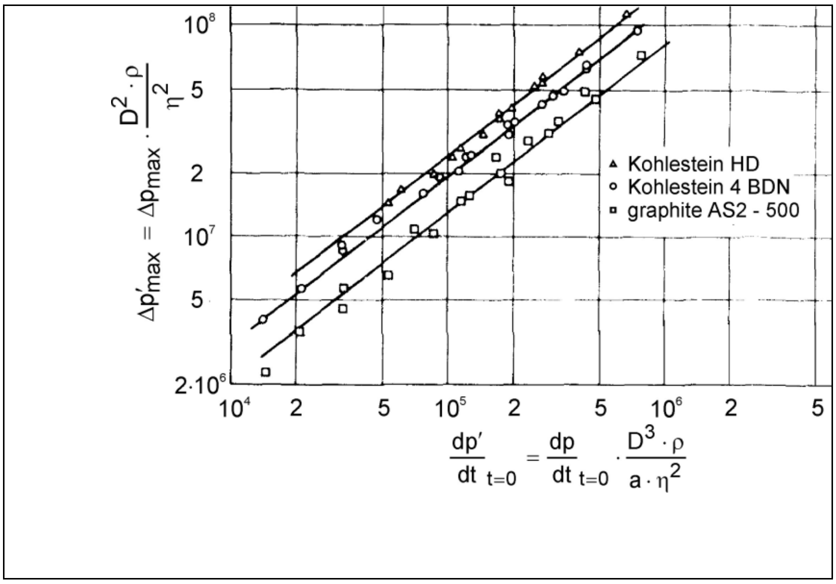

Figure 125: Pressure differences as a function of the depressurization rate (non-dimensional) for carbon brick and graphite

13. Complete insulating systems

As already mentioned before, the first extensive investigations had been carried out at Research Centre Ispra/Italy in the years 1970 and 1971 on behalf of Gutehoffnungshütte (GHH), Oberhausen, for Geesthacht II. Later on, the costs for carrying out the experiments were borne by KFA, and the tests were first supervised by staff from Ispra and then in part from Jülich. The work, test facilities and test pieces are described in the report [GHH71].

The following description refers to two reports by Aranovitch and colleagues [ARA71a] and [ARA71b] and Aranovitch and van Asselt [ARA72] and to a travel report on a visit to Ispra, see Bröckerhoff [BRÖ71]. Other publications on the investigations carried out there are not available or not known. Figure 126 schematically shows the experimental arrangement. The vessel is drawn in the horizontal position for reasons of space. During the experiments, the arrangement was not in the vertical position, but inclined, as shown and explained in the following. The insulation to be tested was installed in a tube, whose outer diameter and length were 560 mm and 1500 mm, respectively. The outer pressure vessel had a diameter of 610 mm. The length of the cylindrical part was 2000 mm. The outflow nozzle shown on the right in the drawing served to accommodate the orifice, with which the different escape cross-sections could be adjusted, and two rupture disks. The maximum possible outer diameter of the orifice was 193.4 mm. The tube with the insulation was inserted into the vessel after taking off the spherically dished vessel head. The bobbin design insulation was supplied by Darchem. The test pieces were two bobbins of 600 mm length each mounted behind each other and marked 2 and 3. Bobbin 3 had a system of slots at the rear open end for depressurization, bobbin 4 only two 4 mm holes offset by 180 °. The respective other end was closed.

The two shorter sections 1 and 4 served as feed and wake, but did not have any inserts, that is foils or wire mesh, and were only regarded as filling pieces. All bobbins were rigidly welded to the test tube on one end by continuous circular seams. The absolute pressure, p, and the pressure differences, Δp, were measured by pressure transducers and the stresses on the inner liner by strain gauges. The temperatures caused by rapid stress relief were to be measured by thermocouples.

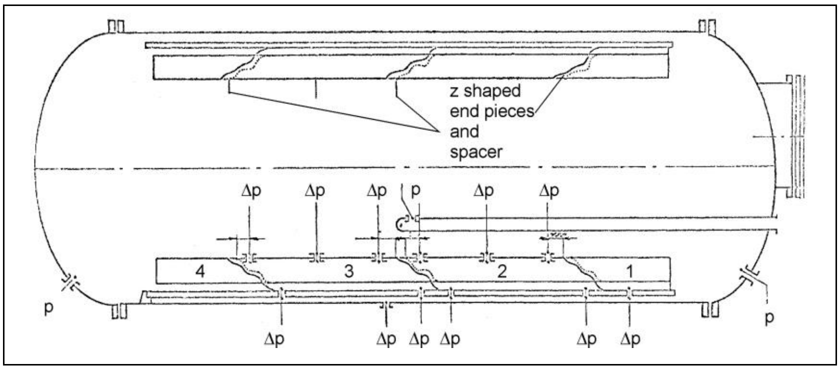

Figure 126: Vessel and insulation (measuring point scheme)

The tests were carried out with nitrogen and helium at ambient temperature. Planned were tests between 0.2 bar/s and 100 bar/s at a maximum initial pressure of 25 bars. After reaching the final vessel pressure, the 6 mm thick upper rupture disk in the outflow nozzle was caused to break due to a pressure of 68 bars. The internal pressure of the test vessel then destroyed the second rupture disk, whose thickness was 2 mm, and the gas could escape. For reasons of safety, the test facility, see Figure 127, was only operated with the roof opened. Moreover, the inclined position was intended to prevent parts falling onto the experimental hall after bursting of the disk. The outflow opening was covered by a wire cage for collecting the destroyed rupture disk. This cage was secured by a steel rope attached to the experimental arrangement. In spite of this measure, the cage with parts of the rupture disk was only found at a distance of about 400 m after a test with helium.

In initial experiments, depressurization rates of 3.85 bar/s were achieved for nitrogen and 7.8 bar/s for helium. As flow rate or permeability measurements had shown, the main resistance during rapid depressurization was to be expected on the overlaps. The internal flow resistance of the foils was negligible. It soon became evident that at higher depressurization rates the resistance on the overlaps would soon lead to a destruction of the bobbins, i.e. to a pressure difference higher than 1 bar, the value guaranteed by Darchem. It was therefore decided to provide four breather holes of 6 mm diameter on the overlaps of bobbin 3. No modifications were to be made to bobbin 4. Nearly all the experiments performed until then were repeated. Maximum depressurization rates of 5 bar/s were achieved with nitrogen. X-ray studies suggested that the inner structures had not changed. However, further modifications to the overlaps proved to be necessary. On bobbin 3, three of the previously provided holes were closed and three larger ones with diameters of 6.4 mm, 7.2 mm and 7.4 mm drilled; bobbin 4 was provided with the same holes as bobbin 3. After an experiment with helium and at a transient of 15 bar/s, the ducting shroud of bobbin 4 showed a buckling of the inner liner during an inspection. The records of the oscillograph had already indicated an anomaly. An evaluation of the measuring results revealed a pressure difference of less than 1 bar between insulation and vessel interior, which was below the critical value specified by Darchem. In order to avoid further buckling, bobbin 4 was provided with additional holes on the overlaps. Beside the existing four holes, ten further holes with a diameter of 7.2 mm and another fourteen holes with a diameter of 7.2 mm and offset by 180 ° were provided. The last test with helium and the highest depressurization of 22.4 bar/s resulted in two further buckles on bobbin 4. However, the reason for this damage was now clearly no longer the flow resistance of the overlaps, but the breather holes of the rear end piece which, as already mentioned, only had two holes.

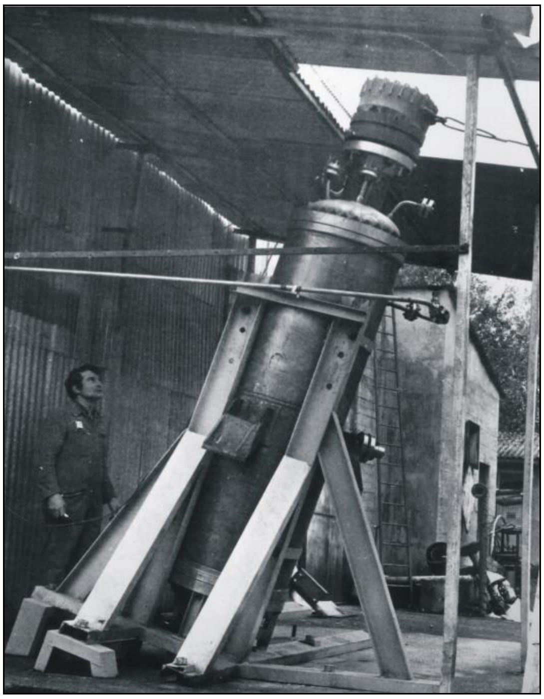

Figure 127: Depressurization test facility (Ispra)

The maximum pressure differences acting across the ducting shroud are shown in Figure 128 as a function of the depressurization rate for the two bobbins 3 and 4. The test gas was nitrogen. For bobbin 3 a linear course was obtained, whereas two curves could be drawn for bobbin 4. This is attributable to the change in flow

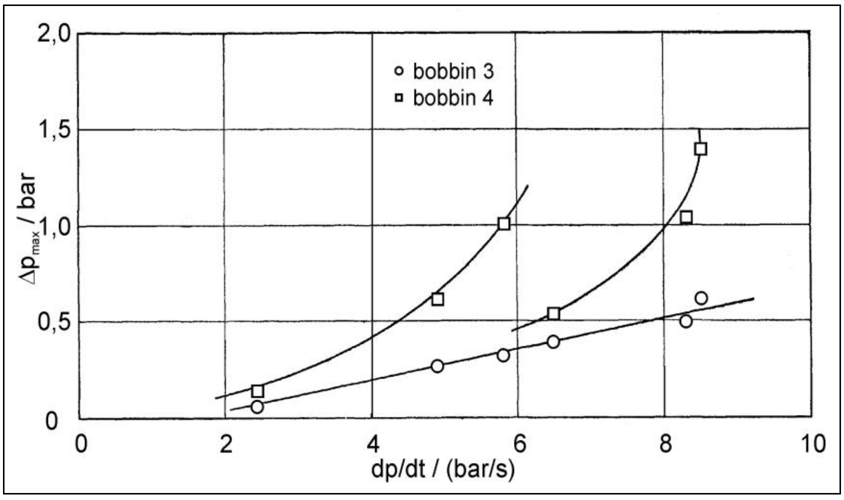

Figure 128: Pressure differences as a function of the depressurization rate

resistance on the overlap after the helium test, in which the transient was 7.8 bar/s. No modification had been made to bobbin 3. At a depressurization rate of about 8.5 bar/s a stress of 1.4 bar was observed for bobbin 4. This was above the value guaranteed.

Table 11 contains the few data valid for helium from the last experiments. Also specified are the times t_{kr}, at which the maximum pressure transients occurred, which were much higher than under nitrogen. Bobbin 3 was less stressed than bobbin 4, where the die maximum pressure difference across the ducting shroud was 1.62 bars.

	Bobbin 3		Bobbin 4	
$dp/dt_{t=0}$ / (bar/s)	t_{kr} / s	Δp_{max} / bar	t_{kr} / s	Δp_{max} / bar
9.20	0.700	0.170	0.450	0.406
17.7	0.230	0.690	0.690	1.395
22.4	0.225	0.780	0.385	1.620

Table 11: Depressurization data using helium

The buckling on the shroud of bobbin 4 are clearly visible in Figure 129. The damage had been observed after a test with helium, A after a test with a depressurization rate of 15 bar/s, B after a depressurization of 22.4 bar/s. It should be emphasized here once more that the experiments had been carried out with gases at ambient temperature. At temperatures as had to be expected in the reactor, the damage observed would certainly have occurred already at lower loads. However, these measurements did not allow any conclusion to be drawn concerning an impairment of the insulation power, which would definitely have had to occur after the depressurization tests. In the event of continuing or resuming the work for HHT applications, further development would be urgently required here.

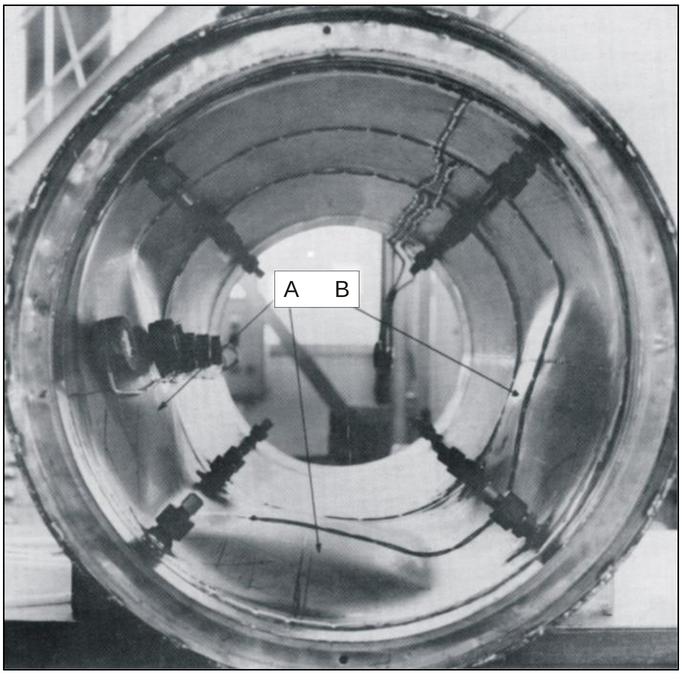

Figure 129: Buckled ducting shroud

Von der Weyden [WEY71] described measurements on two metallic insulations for the THTR, which had been performed at the Bertin company in France. The investigations served to obtain knowledge about the performance of the insulations, see Section 7.1.2.1.1, both from the aspect of thermal behaviour, as already described before, and concerning compressive load and depressurization. At the beginning of a test run, the permeability of each insulation was first determined by means of the experimental arrangement shown in Figure 1. These experiments were necessary in order to be able to compare the insulations mounted under difficult conditions with the normal design as produced by the manufacturer with respect to their internal resistances. For reasons of cost, only two compressive load and depressurization tests were carried out with helium as the medium. In the other experiments nitrogen was used. Since, however, the mechanical loads were to correspond to those under helium, the same pressure transients had to be produced in the insulations. The conversion of the transients required for the nitrogen tests was effected using the results from the permeability measurements. At temperatures of 100 °C on the hot face, depressurization rates of about 0.17 bar/s were obtained for nitrogen and of 0.37 bar/s for helium. Since these transients were a factor of 5 above the depressurization rates to be expected later in the reactor and since no damage had been observed in the insulations, von der Weyden assumed that the insulations were suited for use in the THTR.

The large depressurization test facility used at the former KFA is schematically shown in Figure 130. Pressure vessel 1 accommodating the insulation – here the fibre insulation tested before in the HP channel – was first evacuated by vacuum pump 8. Then the helium taken from high-pressure storage tank 7 was fed into the vessel. After opening valves 4, the gas flowed through orifice 3 into low-pressure storage tank 5. The orifice served as a flow limiter, with which desired pressure transients could be adjusted. The helium from the low-pressure storage tank was finally delivered back into the high-pressure storage tank via compressor 6. Except for the insulations to be examined, this experimental arrangement remained unchanged for all tests.

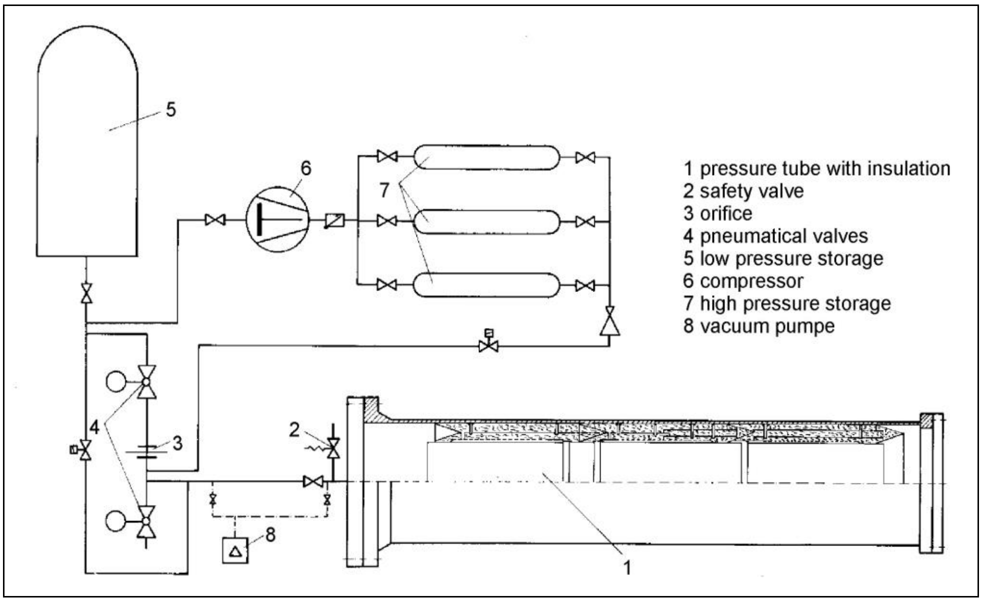

Figure 130: Depressurization test facility

The first insulation tested even before the thermal investigations in the ARGAS facility was a bobbin insulation from Darchem, see Henßen [HEN76]. The test run was started with helium at ambient temperature. Pressure transients of 17 bar/s were achieved. Following this, liner temperatures between 400 °C and 600 °C and pressure transients of up to 9 bar/s were adjusted. In a subsequent inspection of the insulation no damage or deformation of individual parts or of the overall system due to depressurization was identified, nor were any friction welds observed on sliding connections.

Following these investigations, the fibre insulation with one intermediate tube and two intermediate tubes already described was tested in the HP channel, see Lang and Weise [LAN77]. The absolute pressures were measured in two planes using pressure transducers from Hottinger. With a length of 340 mm, the pressure transmitting tubes had the same length for all measuring points. The diameter of these tubes was 4 mm. Figure 131 shows the position of these points. The pressure variation in the free cross-section was measured at measuring point E located on the inner wall of the pressure tube. The reference points were located, as can be seen in the drawing, in two cross-sections of the insulations, measuring points 2 and 3 on the inner wall of the pressure tube, measuring points 1 and 5 in the gap between ducting shrouds and perforated cylinders. The tests were carried out at ambient temperature and with helium as the test gas at pressures from 15 bars to 39 bars. The orifice diameter was 90 mm. Thus, pressure transients of up to 32.3 bar/s were attainable.

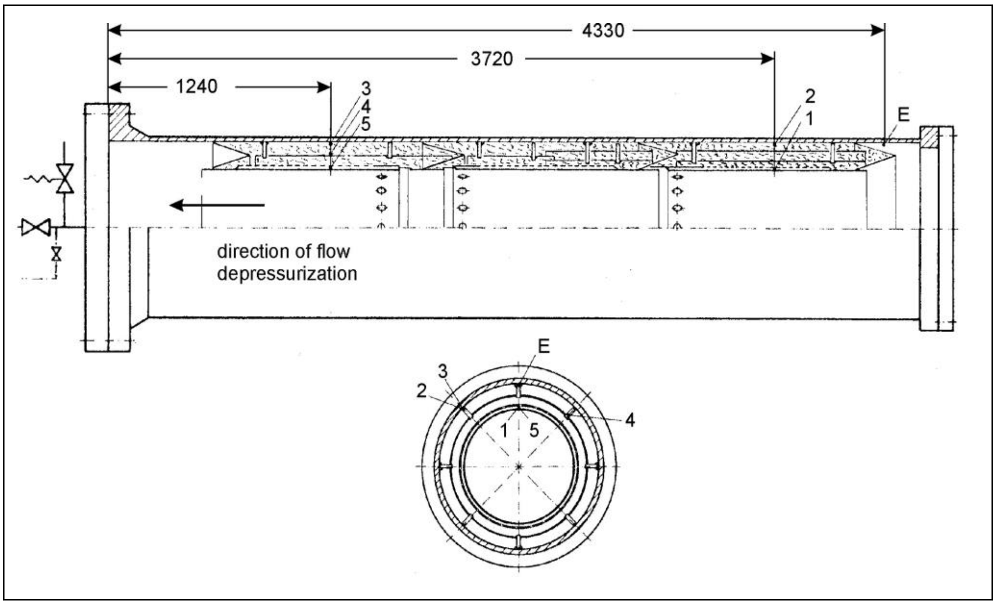

Figure 131: Arrangement of pressure measuring points

The following diagrams show the influence of the two designs, which were identical with respect to the number, diameter and position of the breather holes, but differed by their gap widths. In the cases depicted, the initial pressure was 39 bars, the depressurization rate 30 bar/s.

Figure 132 shows the maximum pressure differences as a function of time for the region with great gap width between ducting shroud and perforated cylinder. The ducting shroud was loaded with a pressure difference 0.4 bars. The corresponding value for the design with a gap width of only 4 mm was 1.2 bars, see Figure 133.

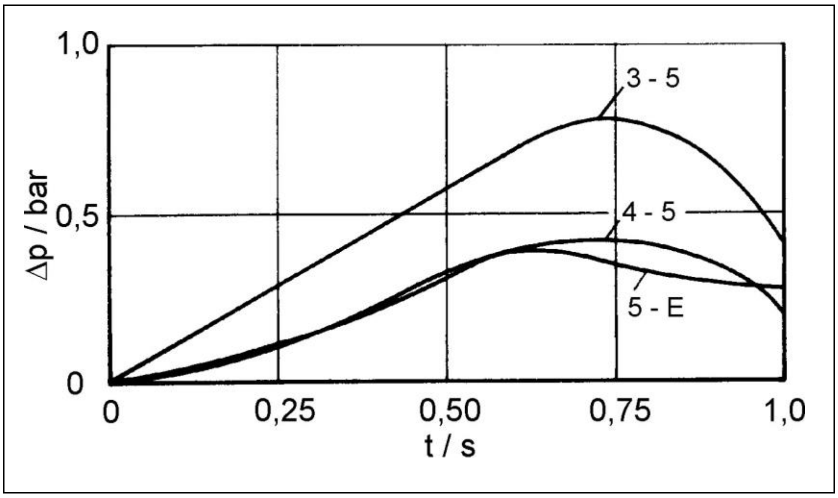

Figure 132: Pressure differences as a function of time

It was thus 0.2 bars above the design value for hot gas conditions. The higher load could be explained by the smaller escape cross-section, which represented a larger flow resistance.

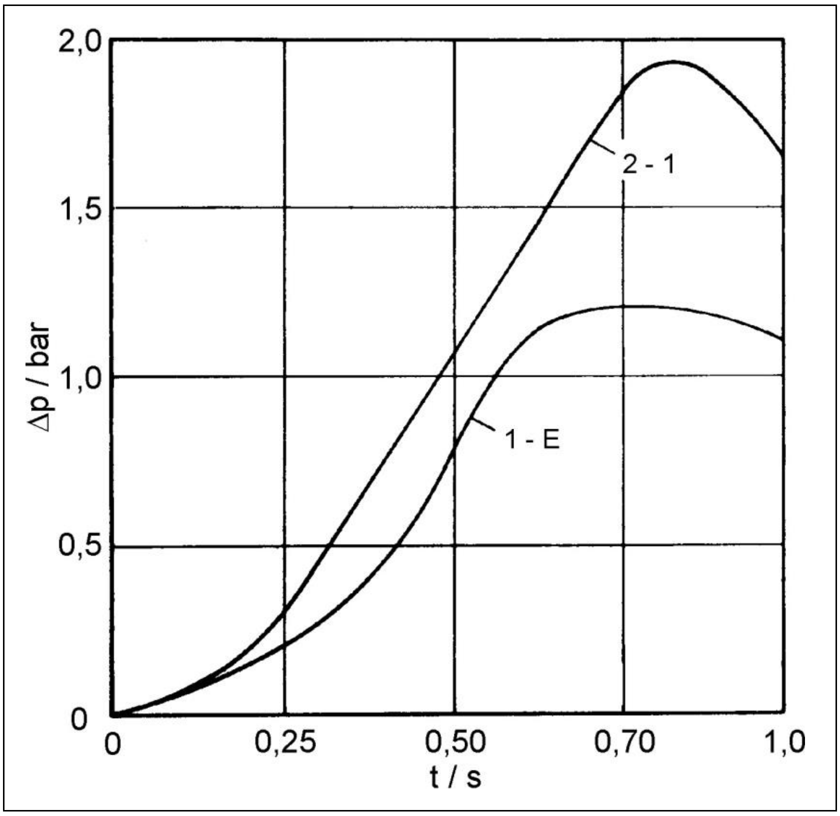

Figure 133: Pressure differences as a function of time

Moreover, the two intermediate tubes represented an additional resistance. One intermediate tube would have been sufficient. Since the tubes only had a few holes, the gas could primarily only escape from the fibre volumes in the axial direction. This eventually led to a load of 1.92 bars, see Figure 133. In spite of the pressure differences that were higher than expected, no buckling was observed in the two ducting shrouds and, indeed, had not been expected in view of the low temperatures. Only at temperatures of about 950 °C would any damage have to be expected. Fibrous material emerging from the sliding connections was regarded as a disadvantage. This deficiency could have been eliminated by inserting a fine-meshed wire mesh near the overlap.

In the same experimental facility, a further fibre insulation was tested in the vertical position, see Henßen et al. [HEN77]. The inner diameter and length of the pressure tube were 880 mm and 2950 mm. The supplier was Brown-Sulzer Turbomaschinen (BST). The design corresponded to versions already discussed featuring metallic components such as ducting shrouds, V-pieces and intermediate tubes. The insulating material was first of all Kaowool. In a remount, one half of the test section was stuffed with Refrasil on the hot gas side. The stuffing density was 180 kg/m^3, the thickness of the insulation 140 mm.

Thirty experiments were carried out in total, the helium temperature being about 850 °C on the hot face and the pressure being varied between 20 bars and 34 bars. The depressurization rates could be kept almost constant between 14 bar/s and 16 bar/s by means of different orifice cross-sections. The maximum measured loads of 0.15 bars did not lead to any damage of the ducting shrouds. These had been designed for a buckling pressure of 1 bar at an operating temperature of 850 °C according to the manufacturer. In addition to depressurization tests, experiments were also carried out concerning thermal behaviour in vacuum and at pressures of up to 38 bars.

The aim of further tests in the depressurization channel was the testing of a bellows expansion joint, see Lang, Klas and Schumacher [LAN82]. These investigations were intended to clarify details concerning the design of such a component for the operational hot gas duct of the KVK facility. This also included the influence of the deflection movements of the test section on the temperatures in the region of the expansion joint. The test object, see also Stehle and Klas [STE84], consisted of an internally insulated angular expansion joint with subsequent straight pipe. The inside flow diameter was 250 mm, the diameter of the pressure tube 680 mm. Its length was 3000 mm. The insulation selected was a stuffed fibre insulation with a gas duct of Incoloy 800. Its structure corresponded to the known designs. The gaps were stuffed with Saffil on the hot inner surface and with Kaowool on the outer surface. Since only pressure transients of 5 bar/s were expected for the tests in the KVK facility, no depressurization gap was provided between the ducting shroud and the insulation. Instead, a depressurization cavity was created by covering the shroud with two wire meshes, coarse- and fine-meshed. In this way, a gap with a width of 4 mm was produced. The bellows of the expansion joint was protected by sheets against the fibres. The cavities between the corrugations of the expansion joint were densely stuffed with fibres to increase the flow resistance. The expansion joint region was gastight sealed by means of two v-shaped end pieces at both ends. An internal expansion joint served to accommodate the thermal expansions of a ducting shroud. Comparable bellows expansion joints were used in the KVK facility for shaped pieces, e.g. bends or tees, for sealing the insulation space. The solution with sliding connections or overlaps selected before had been abandoned.

Pressure transients of about 13 bar/s and 6.2 bar/s led to buckling pressures of 1.94 bars and 0.8 bars on the shroud in experiments under helium at ambient temperature. The shroud had been designed for an overpressure of 3 bars. The stresses due to rapid pressure transients had not led to a change in thermal behaviour.

Further test objects according to Bröckerhoff and Stausebach [BRÖ86b] were the two insulations already presented featuring graphitic shrouds on the inner side, which were internally wrapped with Saffil blankets and on the colder outer surface with Cerablankets. The first-mentioned design was provided with carbon fibre composite bulk components (CFC) as radial spacers, the second with four spheres and one axial supporting element of ceramics to reduce heat losses. In both cases, bobbins 2 and 3 were selected for measuring the pressure variations. The positions of the pressure measuring points in testing the insulation with CFC spacers can be seen from Figure 134. The pressure variations were measured in the centre of the two bobbins and in the region of the spacers, namely on the inner surface of the pressure wall, on the separation surface between the different insulating materials and on the outer surface of the ducting shrouds. In addition, the pressure in the free cross-section was determined. This configuration was also selected for the second insulation. For pressure transmission, probe tubes of 6 mm outer and 4 mm inner diameter were used, which were passed from outside through the pressure tube wall. The pressure transducers from Hottinger, which work according to the inductive principle, were fed by carrier-frequency mains amplifiers. The maximum signal output was 10 V. The signals were passed to a multichannel amplifier, which transduced the input signals, adapted to the loops. The measured values were passed from the amplifier to a loop oscillograph. The signal course was finally recorded on photosensitive paper. The absolute pressures were determined in the free flow cross-section and on the face between the two fibre blankets. The absolute pressure transducers covered the measuring range between 1 bar und 50 bars. The other two pressure probes in each measurement plane – pressure tube inner surface and ducting shroud outer surface – were connected differentially to each other.

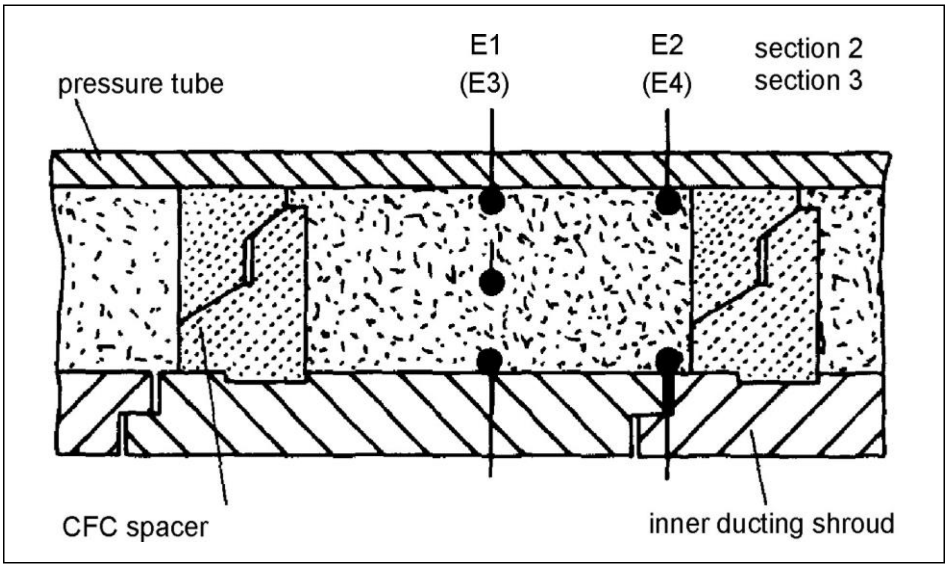

Figure 134: Arrangement of pressure measuring points

According to the experimental programme of INTERATOM, the tests were performed at absolute pressures of up to 40 bars. The range of the depressurization rate was defined up to about 10 bar/s. For a constant gas volume this value could be controlled either via the cross-section of the outflow orifice or via the absolute pressure. The output pressures required were adjusted with the aid of a precision pressure gauge. Figure 135 shows the measured pressure differences between pressure wall and graphite tube for the second bobbin of the insulation with CFC spacers as a function of the pressure change rates in the free cross-section. The values determined three times for each operating point are depicted by a straight line. As expected, higher values were measured in the centre of the bobbin, since the gas had to travel a longer distance to reach the expansion and mounting gaps between two ducting shrouds. In this location, the major mass of the gas contained in the insulation should have flown out. For bobbin 3', higher values were found in the region of the spacer, not shown here, where the gas was presumed to flow to the front spacer, since the rear gap represented the higher flow resistance. In terms of absolute values, the pressure differences were so low that they did not constitute a danger for the ducting shrouds. The pressure transients determined from the absolute pressures within the insulation showed more or less the same values as those in the free cross-section. Similar values were measured for the second insulation with spherical spacers, so that they are not specified here.

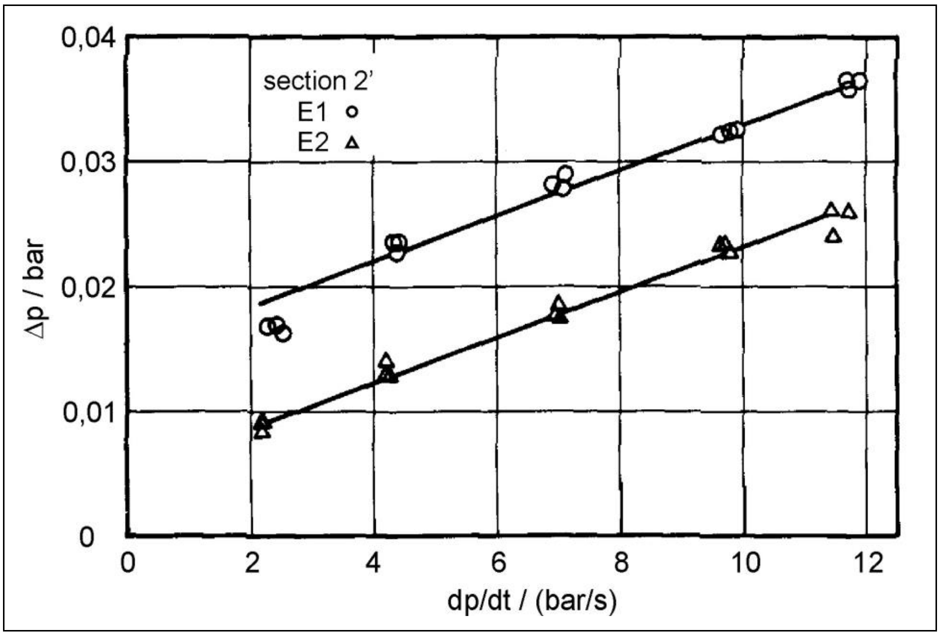

Figure 135: Pressure differences as a function of the depressurization rates

Lang and Weise [LAN78] report on depressurization tests on a carbon brick ring made of RUD-N. The test piece was also supplied by Sigri. The wall thickness of the ring was 150 mm, its length 800 mm, its outer diameter 580 mm. Five measuring tubes of stainless steel were used for measuring the pressures inside the body. The outer and inner diameters were 6 mm and 4 mm, respectively. They were centred within the holes by carbon brick tubes of 10 mm outer diameter. In contrast to earlier tests, a measuring sensor from Setra working according to the capacitive principle was used for determining the differential pressures. It permitted high measurement accuracies.

The test were carried out with helium at ambient temperature and gas pressures between 15 bars und 39 bars. Maximum pressure transients of 60 bar/s were achieved. The highest load in the carbon brick was 3.3 bars. It occurred in all experiments after about 0.6 s. No damage was observed in any of the tests, so that the suitability of the material had been demonstrated by this test, too, despite some inhomogeneities observed.

14 Development programme for shaped fibre structures at the manufacturer Balcke-Dürr AG and testing in the KVK test loop

Within the framework of the project "Development of metallic components for the loops of the Prototype Plant for Nuclear Process Heat" Balcke-Dürr AG was directly involved in early 1984 in the "Development programme for the insulation of the PNP components" under way since 1981 at Didier-Werke.

The aim of this programme was to demonstrate the applicability and functionability of the novel shaped fibre structure insulation for the He/He intermediate heat exchangers for all operating and accident conditions.

Up to then, an insulation concept with predensified insulating fibre modules had been envisaged which, however, needed a metallic liner. However, the development state of the metallic materials at that time did not yet permit the application of a metallic liner for the high temperatures of up to 1000 °C and the envisaged time of application in the primary loop. Moreover, further disadvantages were caused by heat bridges due to the necessary load diversion and by the danger of fretting at the required sliding connections.

The concept with a graphite shroud and wrapped-on and densified fibre insulation meanwhile developed for the horizontal primary hot gas duct and also already tested in the primary test section could not be taken into consideration either, since the requirement is not directly comparable to that in the He/He intermediate heat exchanger due to the temperature profile in this hot gas duct (Figure 136).

Thus, for example, the entire insulation in the upper region of the original central riser is at a temperature of approx. 950 °C. For these high temperatures and the envisaged lifetime, however, a sufficient resilience even of the highest-quality Saffil insulation blankets could not yet be ensured, so that the avoidance of possible backflows could not be demonstrated.

With the new shaped fibre structure insulation, however, a concept was found which enabled liner-free application and did not depend on the resilience of the fibre blankets.

The insulation here had first the task of separating the heat-exchanging spaces from each other so that the rated temperature profile and efficiency could be achieved. At the same time, however, the temperature losses were to be limited and the temperature load on the metallic components minimized.
The insulation materials developed by Didier-Werke were pressed fibre structures with different densities. The base material mainly consisted of Saffil fibres (95 %

A1203 and 5 % SiO_2), which were conditioned with system-compatible inorganic binders and mostly organic conditioning and shaping additives.

For the application of the insulating material developed, the "central riser of the URKO He/He intermediate heat exchanger" was selected as representative after having examined all possible locations of use. In this central riser, the requirements are the highest with respect to erosion resistance and the danger of backflow due to the direct flow load of approx. 30 m/s and the hot gas temperature of 950 °C up to 1,000 °C. This region continues to be representative also for HTR hot gas ducts.

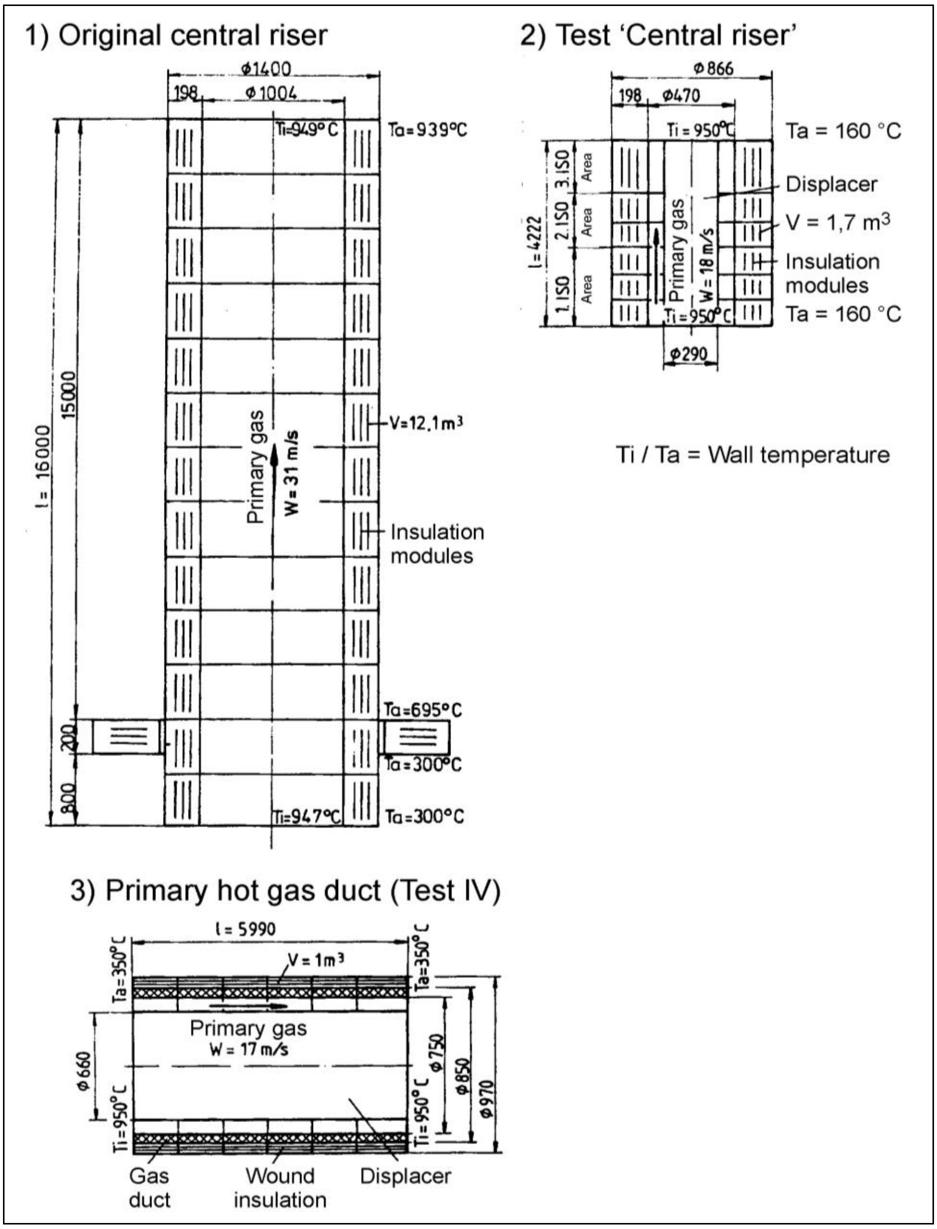

Figure 136: Test unit ‚Central riser'

Prior to application in the original component, however, a test component had to be manufactured in order to evaluate and confirm this concept with respect to the fabrication and mounting of the shaped fibre structures thermal behaviour (temperature gradients, temperature distribution) the applicability and strength behaviour in hot-gas-carrying components the gap flows induced by the joint parameters.

In 1985 the insulation programme was extended by the development and manufacture of a "central riser insulation test section".

The test section was completed by the end of 1986 and installed into the KVK facility in early 1987.

The subsequent tests were intended to experimentally determine the theoretically not sufficiently determinable component loads and impacts, as far as permitted by the experimental design (integral test). The test results furthermore serve to provide analytical support (reference data) and should also be used in the region of the steam reformer, the hot gas armature and the hot gas ducts.

14.1 Construction of the central riser test section and PNP Materialconcept

The test section (Figure 137) represents the configuration of the insulation system of the original central riser on a reduced scale. It was vertically installed into the primary KVK pipe system between primary test section IV and the hot gas collector test vessel (Figure 138). The hot gas thus flows from bottom to top as in the original component. The total length of the test section is 6 m, the total weight approx. 8.5 t.

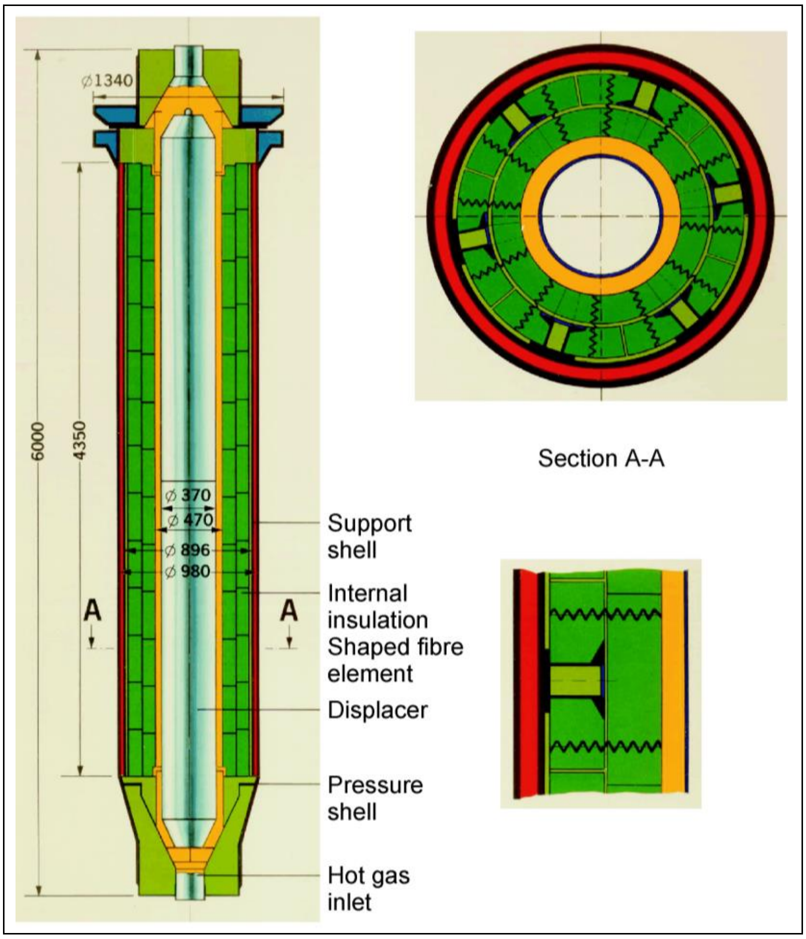

Figure 137: Test unit ‚Central riser'

The test section essentially consists of the pressure cell, the support shell, the inner shaped fibre structure insulation system, the insulation stuffing regions and the experimental internals for adaptation to the KVK line and simulation of original conditions.

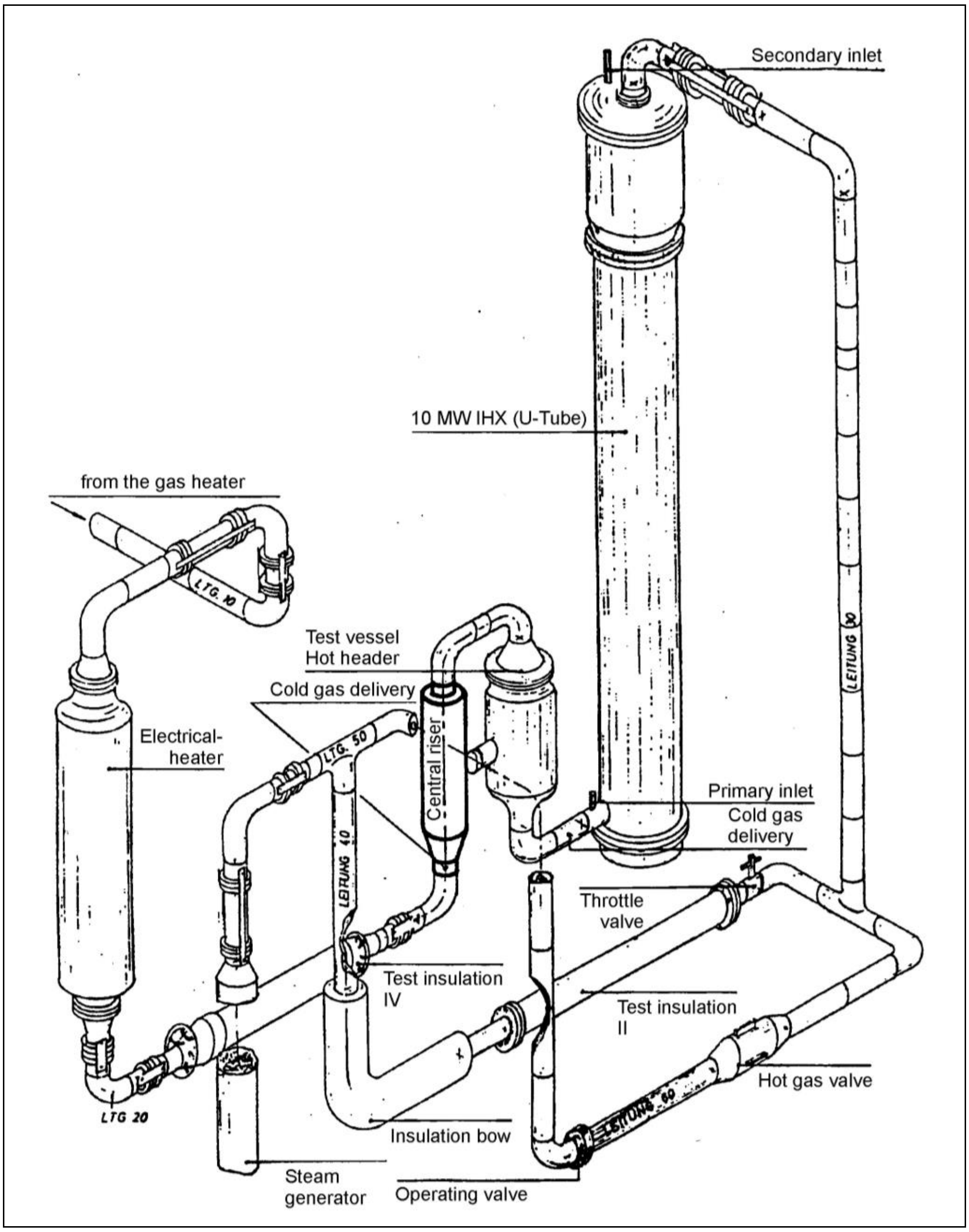

Figure 138: Test unit 'Central riser'
Test plant KVK

The construction of the metallic components does not show any major special features, so that only the actual test object, namely the shaped fibre structure insulation system will be described in more detail below.

The inner insulation consists of two segmented rings of shaped fibre structures of different density. These rings are axially divided into 12 layers (A–M) and provide a total insulation length of 4222 mm. Due to the radially two-layered configuration the temperature gradients in the endangered regions are reduced and thus are the stresses in the shaped fibre structures.

The outer ring connected to the support shell is composed of shaped fibre structure segments with a density of 250 kg/m^3, which are connected with the support shell wall via welded metallic retaining studs. In the case of thermal expansion they thus follow the metallic structures to be protected.

In the outer segments, the shaped fibre structure segments of the inner ring with a density of 550 kg/m^3 are then fixed by means of screwed-in spiral springs (Figure 139).

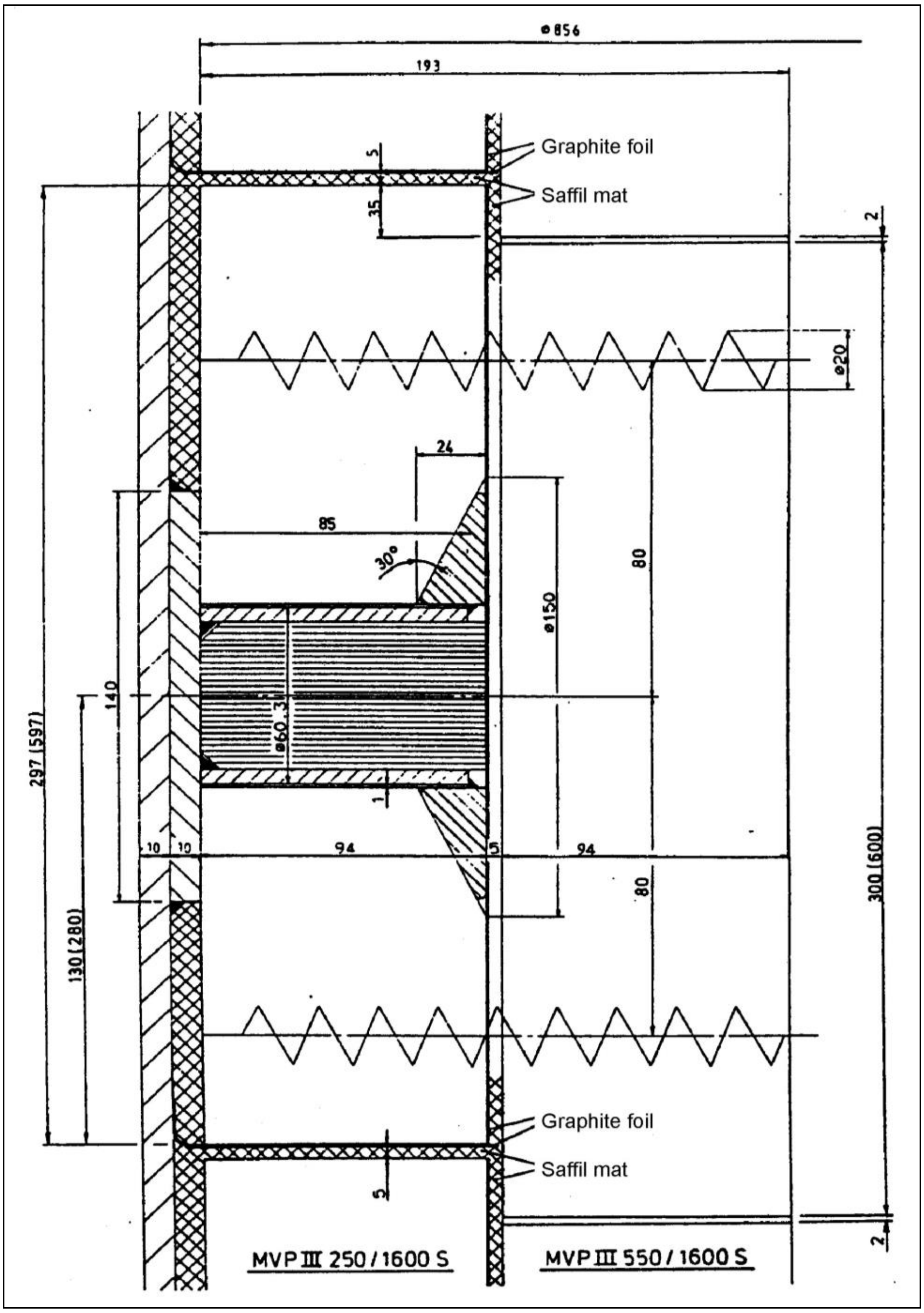

Figure 139: Test unit ‘Central riser’

This cover layer forms with its inner diameter the hot gas flow configuration. It is erosion-resistant due to its higher material density and has no surface coating and therefore does not require an additional liner.

In order to compensate for installation tolerances and voids, Saffil insulation blankets (stuffing density 120 kg/m^3) are inserted in the gap between support shell and outer ring (10 mm) and between outer and inner ring (5 mm). This has also been done in the axial and azimuthal gaps (5 mm) of the outer ring.

Moreover, graphite foils are placed as convection barriers between the outer and inner ring and in the axial gaps of the outer ring.

In this way, radial and axial creep flows between the individual shaped fibre structures are largely suppressed.

Furthermore, the outer and inner fibre structures of each layer are offset with respect to each other in the axial and azimuthal direction, so that direct continuous joints from inside to outside are avoided (Figure 140). However, offsetting was selected in such a way that only one inner shaped body segment is only fixed to one outer shaped body segment. This provides a favourable possibility of segment motion and a homogeneous loading of the fastening springs.

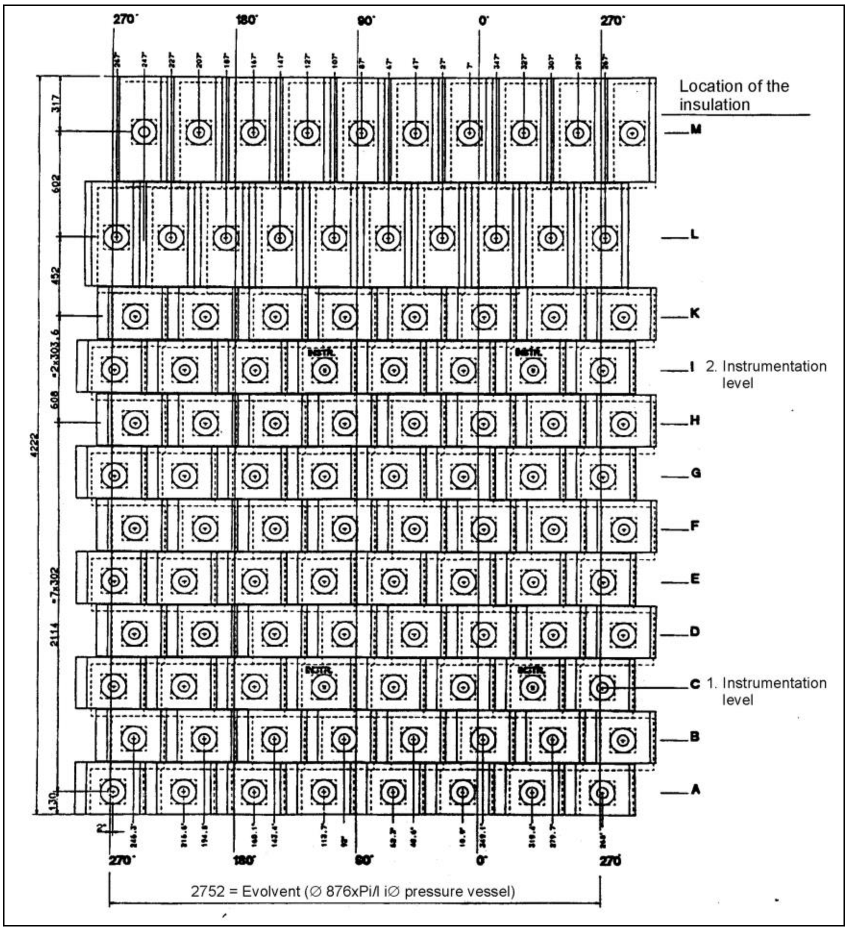

Figure 140: Test unit ‘Central riser’
Layout of pressure boundary (Wind up)

The individual layers are additionally alternately offset by 30° on the circumference.

In the mounting condition (original component) the ring of the inner shaped bodies is closed. Due to the hot gas temperature and the different strain behaviour of support shell and inner insulation in the operating state, however, it opens and forms gaps between the individual segments.

Since the geometries and temperature profiles of the test section are not exactly the same as for the original component, however, the gaps are formed differently. In the original component, the gaps open up to approx. 2 mm, whereas this is not the case in the test component.

In order to avoid **constraints in the shaped bodies,** and thus damage, predefined joints have therefore already been taken into consideration for the test component in the as-mounted state.

Since the joints formed or predefined are small and the graphite foils located behind them also act as a barrier here, no particularly adverse effects on the insulation system arise.

To cover the different joint parameters, determine the resulting influences on the insulating effect and the mechanical performance of the insulation configuration and make allowance for shaped body formats as large as possible, the total insulation system is axially divided into the following three regions :

- 1st insulation region = 7 layers (A - G) in the bottom part of the test section, with the formation of joints corresponding to the strain behaviour in the test component.

- 2nd insulation region = 3 layers (H - K) in the central part of the test section, with the formation of joints corresponding to the average strain behaviour in the original component.

- 3rd insulation region = 2 layers (L + M) in the upper part of the test section, with the formation of joints corresponding to the strain behaviour in the test component, but with larger shaped fibre structure formats.

Based on a shaped fibre structure geometry of 300 mm height and 7-segment division (51.4°) for the 1st and 2nd insulation region and of 600 mm height and 9-segment division (40°) for the 3rd insulation region, which had been defined on account of the results of the stress studies performed by Interatom and after matching to the maximum possible raw block dimensions, the following theoretically required gap sizes were calculated and determined:

insulation region gap	shaped fibre structure geometry	installation gap operation
1st insulation region	300 mm/51.4° 2.0 mm 1.5 mm	0 mm 0 mm
2nd insulation region	300 mm/51.4° 3.6 mm 4.9 mm	1.6 mm 3.4 mm
3rd insulation region	600 mm/40° 4.0 mm 1.5 mm	0 mm 0 mm

The gap dimensions can be further enlarged by applying an additional outer insulation on the pressure shell and thus changing the strain conditions. This provides the possibility of examining the impacts of extreme joint parameters on the insulation system.

In order to prevent any mutual influences of the individual regions due to bypasses or backflows that could influence the results and unambiguous evaluation, the three insulation regions are axially separated from each other by the installation of metal foils.

In order to prevent these foils from fluttering in the separation regions, a wire-reinforced ceramic cord was placed in a groove of the upper shaped fibre structure segments.

The connecting regions to the KVK pipe above and below were filled with stuffed fibre insulation (stuffing density 160 kg/m^3).

V-shaped barrier sheets were welded into this regions to restrict backflows.
The annular gap between support shell and pressure shell is also kept very small (17 mm) and limited by metallic gaskets to avoid backflows. At the same time, the support shell is welded to the pressure shell flange at the upper end and thus unilaterally sealed.

<u>Materials</u>

The following materials were used:

pressure shell	= 15 Mo 3
support shell, spacer rings	= 15 Mo 3/17 Mn 4
internals, holding tubes, holding disks	= Incoloy 800 H
insulation blankets and insulating wool	= Saffil LD 48/1600
shaped fibre structure insulation segments or	= MVP III 250/1600 S MVP III 550/1600 S
shaped fibre structure insulation studs	= MVP III 250/1600 S
convection barriers	= graphite or 1.4541
fastening springs	= Inconel 617 S
ceramic cord	= Al_2O_3/SiO_2
shaped fibre structure cementing compound	= Resitect 180 KV

Features of the insulation concept

The essential differences between the above-described shaped fibre structure insulation system and known wrapped, stuffed or module insulation systems are as follows:

A liner-free application as the ducting shroud is given due to the erosion resistance. The resilience properties of fibre blankets play a minor role with respect to the functionability of the insulation system, since the fibre blankets merely compensate for voids and installation tolerances and are thus intended to avoid any detrimental backflow.

Homogeneous insulation density permits good thermal behaviour.

The mounts hardly cause any heat bridges.

The type of fixing the individual segments to the holding shell defines the position of the components, so that damaging thermal stresses due to different strains are avoided.

Due to simple shaped body geometries there are no fracture-prone areas e.g. due to graduations; moreover, the fabrication of the shaped fibre structures becomes less expensive.

The graphite foils inserted between the shaped fibre structures serve as a convection barrier and reduce the danger of bypasses.

Application in large-area insulation regions such as the outer flow shell or holding shell is possible.

Manufacturing tolerances of the metallic shells can be compensated.

The prerequisite for a positive effect of these differences is, however, that the components are manufactured properly and the insulation system is accurately assembled.

14.2 Manufacturer experience in mounting a fibre insulation system

Mounting of the shaped fibre structures into the support shell took place in the horizontal position. The support shell had already been installed in the pressure shell which rested in rollers. In this way, this unit could always be rotated into the favourable gravity position for mounting the segments.

The working steps were documented by photographs and records. For possible post-operation studies, the mounting position of each individual shaped fibre structure is recorded in the support shell development drawing by entering the shaped-body number.

Mounting was constantly supervised by the quality office and the workshop management.

According to the Operation Management working rule and the associated drawings, mounting of the shaped fibre structure insulation system took place as follows:

- Inserting the Saffil blanket (approx. 30 mm bulk thickness and approx. 300 mm height) into the support shell in the region of shaped fibre structure position A (1st insulation region). Cutting out this Saffil blanket in the region of the support sheets (140 x 140 mm).

- Placing on the 1st outer shaped fibre structure segment MVP III 250/1600 S (position A).

- Inserting the holding tube, positioning it in a form-fitting manner and internally welding it to the support sheet.

- Pressing the shaped fibre structure on with the aid of the mounting device until the Saffil blanket behind is densified to 10 mm.

- Inserting the holding disk and welding it to the holding tube.

- Inserting a shaped fibre structure stud MVP III 250/1600 S into the holding tube.

- Circumferential insertion and fixing of the remaining outer shaped fibre structure segments (position A) as described above. However, the respective last shaped fibre structure on the circumference must be inserted axially. Between the segments one Saffil blanket (15 mm bulk thickness) must always be inserted azimuthally and compressed to 5 mm thickness.

- Cutting off the Saffil blankets along the edges of the outer shaped fibre structure.

- Placing the Saffil blanket (15 mm bulk thickness) onto the outer shaped bodies.

- Placing the graphite foil on the Saffil blanket with the graphite foil ends overlapping.

- Placing the 1st inner shaped fibre structure segment MVP III 550/1600 S at the envisaged location of the outer shaped fibre structure.

- Pressing the shaped fibre structure on with the aid of the mounting device until the Saffil blanket behind is densified to 5 mm.

- Screwing the inner and outer shaped fibre structures by means of 4 helical springs at the marked locations (for easier mounting the spring travel had already been provided in the inner shaped fibre structure outside the support tube prior to its installation).

- Separating the spring projection of approx. 20 mm while protecting the shaped fibre structure with a thin sheet against damage.

- The spallations produced on the shaped body in the region of the spring screw-in points were cleaned removing loose insulating material and subsequently surface-treated with Resitect 180 kV insulating compound. The Resitect 180 kV had been diluted with monoaluminium phosphate solution so as to obtain a brushable mixture.

A thermal post-treatment was not required.

- Row A was completed as described before.

The radial gap of 1.5 mm had to be adjusted between the segments using sheet metal spacers. However, the respective last shaped fibre structure on the circumference had to inserted axially.

- Cutting off the Saffil blanket and graphite foil at the upper edge of the outer shaped fibre structure.

Covering the outer shaped fibre structures with Saffil blanket (20 mm bulk thickness) on the upper front side.

- Graphite foil segments were placed on the Saffil blanket in an overlapping manner.

- Placing the outer metal sealing of segment parts and spot welds on the holding shell.

- Inserting the outer and inner layers B, while pressing the front-side Saffil blanket of layer A to 5 mm.

According the associated drawing, layer B is offset by approx. 30° on the circumference with respect to layer A.

In order to achieve the axial gap of 2.0 mm between the inner shaped fibre structures during mounting, sheet metal spacers of the corresponding thickness were placed between layers A and B and later removed again.

- Installation of the thermocouples for the 1st measurement plane in the shaped body segments of layer C by Interatom.

- Inserting the remaining layers C - G for the 1st insulation region.

- Placing a cord in the groove of the upper shaped fibre structures for pressing on the metal foil still to be placed on.

- The 1st insulation region was separated from the 2nd insulation region by metal foil segments up to the inner diameter and the segments were spot-welded to the support shell.

- Inserting layers H - I for the 2nd insulation region

- Installation of the thermocouples for the 2nd measurement plane in the shaped body segments of layer I by Interatom.

- Inserting layer K for the 2nd insulation region

- Placing a cord in the groove of the upper shaped fibre structure for pressing on the metal foil still to be placed on.

The 2nd insulation region was separated from the 3rd insulation region by metal foil segments up to the inner diameter and the segments were spot-welded to the support shell.

- Inserting layers L and M for the 3rd insulation region

- The remaining region up to the convection barrier was stuffed with Saffil and the V-sheet welded in.

14.3 Manufacturing quality assurance for fibre structure insulation systems in HTR plants

For the purpose of ensuring proper manufacture and acceptance, working rules and material rules were established within the framework of developing ceramic materials, which contain the quality-assuring flow description of the essential working and testing steps and the material requirements from ordering the material up to the finally accepted component.

These comprise:

- reception control and storage of the semi-finished products at the processor
- identification of the semi-finished products
- instructions for repairing defects on the fibre structures
- pressure and acceptance tests
- working sample location plan, bills of material, drawings
- deviations
- cleaning
- packaging
- transport
- documentation

14.3.1 Construction supervision and acceptance

Inspection and dimensional check of the shaped fibre structures

The shaped fibre structures were dimensionally measured using an aluminium template.

The template is manufactured so that it exceeds by 0.25 mm the permissible maximum dimension of outer radius-RA inner radius-Ri.

Actual size template Ra - Ri = 94.25
Target size drawing Ra - Ri = 93.5 to 94.0

Inspection results

All the shaped fibre structures correspond to the dimensional requirements and are free of inadmissible visual damage. Individual deviations (edge damage, press marks, spalling) were tolerated.

14.3.2. Experience from the test office perspective

In mounting the shaped fibre structures care must be taken that the holding spirals can be screwed into the inner shaped fibre structures without spalling using suitable devices.

Material spallations in the region of the connecting/holding elements (helical spring screw-in points) are to be avoided, since otherwise the spallations can be enlarged under flow load. It was defined in an instruction for repairs that spallations should be treated with a cementing compound. The shaped bodies can thus be repaired. For the holding spirals, a high accuracy to size must be observed with respect to diameter and slope. The same strict dimensional requirement must also be fulfilled by the mounting device.

14.3.3 Manufacturer experience in mounting the fibre insulation structure

The reference concept jointly developed by Interatom, Didier-Werke and Balcke-Dürr for the shaped fibre structure insulation system was installed for the first time in this form in the "central riser test section".

As was to be expected for a first-of-its-kind construction, minor optimization measures had to be carried out during mounting the shaped fibre structures to come as close as possible to the theoretical approaches for the interplay of the individual components and to improve mountability. As already mentioned, mounting was constantly supervised by the workshop management and the quality office. Especially at the beginning of work, in addition, in-depth assistance was provided by the special departments of the companies involved.

Interim checks were constantly performed, so that problems could be recognized at an early stage and jointly eliminated rapidly.

In this connection, for example, it was possible to improve the mounting device and thus mounting operations **during mounting of the first** shaped fibre structure segments in layer A and to optimize the insulation blanket density by accompanying component tests.

In the further course of mounting, the spalling problem in the region of the spring screwing-in points was also recognized and eliminated.

Taking the optimization measures into consideration, the entire insulation system was mounted without any problem. Finally, an inspection and a dimensional check were made and it was found that the axial and azimuthal gaps between the shaped fibre structure segments envisaged due to the strain behaviour were achieved on average. Due to the flexible connection of one outer with one inner segment, however, the gaps are formed slightly irregularly after removing the sheet metal spacers. But this has no influence on total strain behaviour.

Instrumentation concept

The test section contained two measurement planes, one arranged in layer C of the 1st insulation region and the other in layer I of the 2nd insulation region.

Both measurement planes were identically equipped with thermocouples. For statistical support of the measured data and for accommodating possible failures of individual thermocouples, each measurement plane is divided into two opposite measuring locations.

15. Experimental data, description of experiments and results with PNP hot gas insulations

15.1 Based on the previously described material developments and insulation concepts, a concept for the insulation of the ‘high-temperature reactor with heat exchanging component’ connecting line (Figure 143) was developed within the framework of the PNP project.

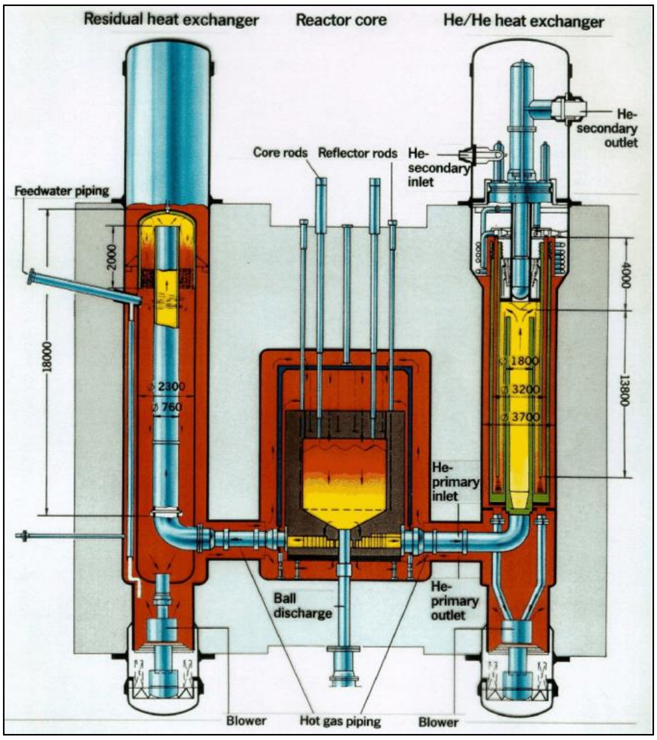

Figure 141: Reactor PNP-500

Six detailed goals were pursued in the investigations:

15.2.A Performance of the insulation under normal operating conditions

In these measurement series, results were expected with respect to the radial and axial temperature profiles as a function of pressure, temperature and axial pressure gradients. These steady-state operating conditions were needed as input parameters of a finite-element calculation for the thermal and strength design. In addition, these results have been included in an overall evaluation of the insulation concept.

15.2.B Performance of the total structure in the case of different azimuthal cold gas distribution and temperature distribution

The azimuthally and axially locally different heat flux induced by the configuration of the insulation concept causes stresses and loads due to different strains on the support tube in connection with the external heat transfer and temperature conditions. The associated temperature differences have been determined for the design and dimensioning of compensation elements for different cold gas distributions. The results additionally served to optimize the thermodynamic computer model for the hot gas duct and also as designers' requirements for the maximum permissible cold gas mass flow distribution in the cold gas duct.

15.2.C Performance of the insulation during normal startup and shutdown

In addition to the performance of the insulation under operating conditions, the performance during startup and shutdown at 10 K/min (hot gas region) in non-steady-state operation was of interest for optimizing the computer models.

15.2.D Performance of the insulation during normal startup and shutdown with the most unfavourable azimuthal cold gas distribution and temperature distribution

The performance of the insulation during startup and shutdown with the most unfavourable azimuthal cold gas distribution was to be seen as the final most stringent requirement of the two preceding investigations.

15.2.E Performance of the insulation in afterheat removal operation

The hot gas duct to the afterheat removal systems must meet very high requirements, since the components here are exposed to very high temperature transients (hot gas side) of +196 K/min. The associated temperature profiles are important for dimensioning the single components as well as the total line and have been incorporated in the model calculations.

15.2.F Performance of the insulation in case of a ‘restart of plant within 1.5 h’ accident

This accident may also be a factor determining the design of the primary hot gas duct. The conditions mentioned occur when the reactor is shut down by an error message and the fault is corrected within 1.5 h. If the fault is corrected, the reactor would be restarted (hot start). If the fault cannot be corrected within 1.5 h, the reactor would be shut down in a controlled manner. For this reason, the temperature profile inside the insulation after reaching the normal condition of "hot standstill" up to 1.5 h must be determined. This involves loads on the metallic support structures and the compensation elements that must be included in the design and dimensioning. Furthermore, test section restart provides operating data for the subsequent components after such an accident.

15.3 Planning constraints, experimental constraints, test results

For the above experimental goals, the following planning and experimental constraints are proposed:

15.3.A Performance of the insulation under normal operating conditions

In these test series, the insulation was tested under normal operating conditions. This means:

hot gas temperature 400 - 971 °C (400 - 950 °C)
cold gas temperature 300 °C (279 °C)
system pressure 40 bar
axial pressure gradient 46 Pa/m

cold gas flow velocity 10 m/s (corresp. to)*
cold gas distributionazimuthally identical

The cold gas temperature of 279 °C results from the maximum operating temperature of 950 °C in the KVK and the temperature difference between hot gas and cold gas decisive for the heat losses (see Table). In these measurements, the temperature profile inside the insulation and the support tube temperature in the azimuthal and axial direction have been determined. The total heat losses of the test arrangement and selected local heat fluxes have been determined.

15.3.B Performance of the insulation in the case of different azimuthal cold gas distribution

In these test series, the parameters of test series 15.3.A) had been adopted, varying the azimuthal cold gas distribution and temperature at the hot gas temperature of 950 °C and the cold gas temperature of 279 °C as follows:

e.g. 6 injections at 0°, 60°, 120°, 180°, 240°, 300°

The distribution of the cold gas mass flows to the six injections was defined after defining the mixing device and its cold gas outflow.

As in 15.3.A), the test goal was to determine all temperature profiles and the heat losses.

15.3.C Performance of the insulation during normal startup and shutdown

In this case, the arrangement had been started up and shut down with the accident transient of + 10 K, the hot gas temperature being 950 °C and the cold gas temperature 279 °C and the cold gas mass flow being homogeneously distributed on the circumference. Startup and shutdown always proceeded from steady-state conditions. The transient behaviour was to be recorded three times in total. The test result is considered to be the transient temperature profiles in the azimuthal and axial direction.

15.3.D Performance of the insulation during normal startup and shutdown with the most unfavourable cold gas distribution (see 15.3b) and temperature distribution

These tests had been carried out as a complement to 15.3.C) with the cold gas distribution defined in 15.3.B).

15.3.E Performance of the insulation in afterheat removal operation

In these tests, the transient behaviour of the component was determined in afterheat removal operation. For this purpose, the test arrangement was run at 279 °C (steady-state) on the hot and cold gas side. The hot gas side was then run up to 950 °C at +196 K/min. After completion of the transient, steady-state conditions were to be awaited again. The cold gas distribution corresponds to that determined in 15.3.B). The test result is again the determination of the transient temperature profiles in the axial and radial direction.

15.3.F Performance of the insulation in case of a 'restart of plant within 1.5 h' accident

It was envisaged for this test series to first bring the test arrangement under normal conditions to steady-state conditions. This gives:

hot gas temperature 971 °C (950 °C)1)
cold gas temperature 300 °C (279 °C)1)
system pressure 40 bar
axial pressure gradient 46 Pa/m
cold gas flow velocity 10 m/s (corresp. to 1)
cold gas distributionafter 3b)

After reaching steady-state conditions, the mass flow of the hot and thus also of the cold gas was interrupted (for approx. 1 minute). The support tube temperature was slowly raised by the heat stored in the ducting shrouds and the surrounding pressure tube was actively cooled to simulate the conditions in original application (liner cooling). After 1.5 h the mass flow of the hot and cold gas was raised again relatively rapidly to full throughput (approx. 3 - 5 minutes). The test result was the determination of the temperatures in the axial and radial direction from the steady state through "hot standstill" up to renewed steady state.

15.4 Envisaged test arrangement

The currently envisaged test arrangement is shown in principle in Figure 142. The configuration is divided into four parts:

- pressure shell
- support tube
- inner insulation
- displacer

The inner insulation consists of graphite ducting shrouds, which are fixed via spherical spacers in the radial and via shaped bodies in the axial direction to the support tube. The wrapped fibre blanket insulation of A1203 fibres and radial convection barriers of graphite foils are provided between the shroud and the support tube. In the axial direction, the ducting shrouds are subdivided into six subsections. The dimensions can be seen from Figure 142, the arrangement of a displacer on the hot gas side being determined by the mass flow of the test facility and the axial pressure gradient.

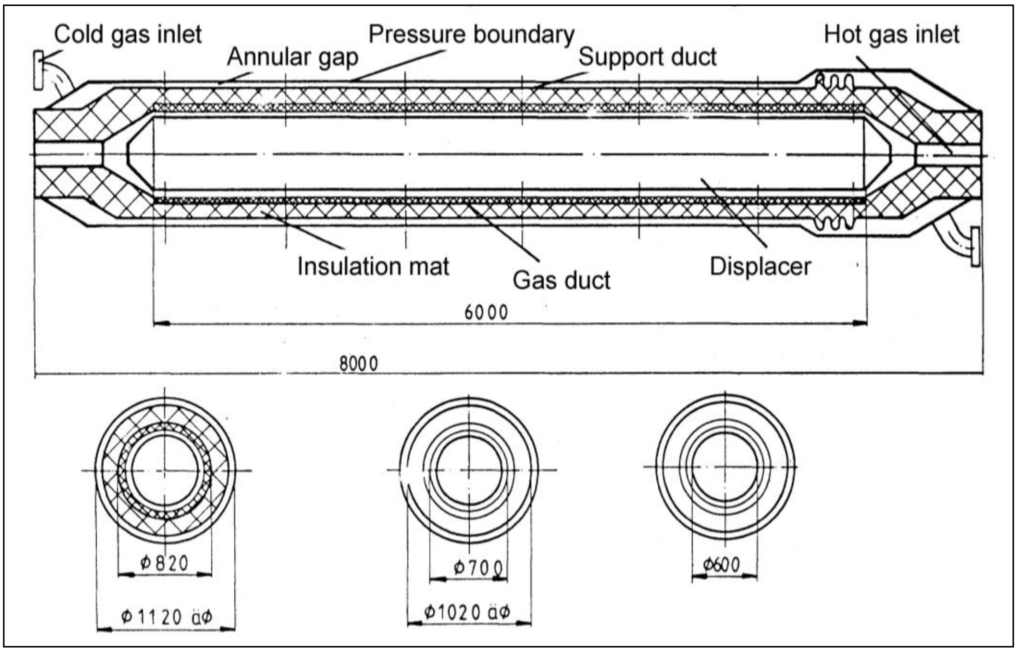

Figure 142: Test subcomponent IV-Primary

15.5 Test loop

The selected test arrangement had been installed in parallel to the heat exchanger studies in the KVK and experimentally tested. (Figure143)

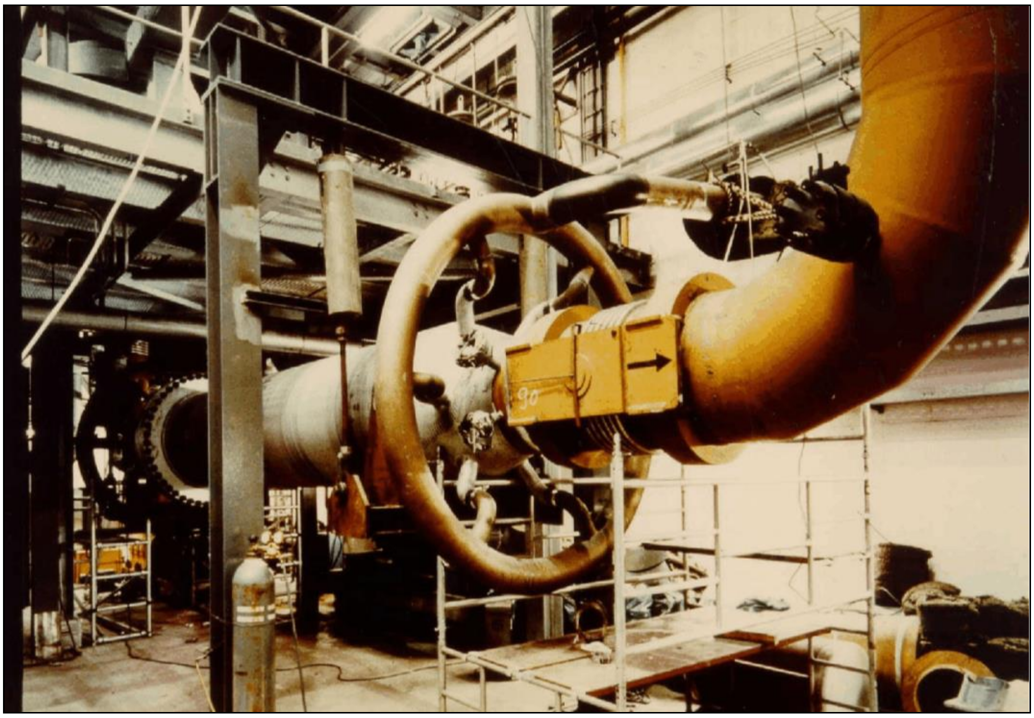

Figure 143: Hot gas pipe for primary circuit

	PNP 500	KVK	test section IV
operating temperature with control band	971°C	953°C (maximum duration)	950°C
normal temperature transient	± 2 - 5 K/min	± 2 - 5 K/min	± 5 K/min
accident transient	± 10 K/min	± 10 K/min	± 10 K/min
cold gas temperature	300°C	250°C	279°C (t PNP500 is to be retained)
operating pressure	40 bar	40 bar	40 bar
cold gas/hot gas	0.39 bar	can be varied	0.4 bar
temp. transient afterheat removal	+ 196 K/min	v 200 K/min	+ 196 K/min

16. Proposal for the data sheet of a Hot Gas Insulations

HTR-E	Data sheet	Project: PNP Sheet: 1
	Piping	
01	Corresponding system	Primary hot gas pipe
02	Corresponding piping list	/
03	Classification grade	Test unit
	Design data	
04	Max. operating pressure	Pressure pipe 46 bar
05	Max. operating temperature	Pressure pipe 400 bar
06	Test pressure	Pressure pipe / bar
07	Test temperature	Pressure pipe 20 bar
08	Test medium	Water 59.8 bar
09	Leak rate	He-leak test 10^{-6} mbar • l/s
10	Vacuum	Yes/no temp. yes 20 °C
11	Operating time	ca. 10.000 h
	Construction details	
12	Insulation	Test 60 mm
13	Shielding	/ mm
14	Surface/paint	Zinc-powder / Al lacquer
15	Corrosion allowance	1 mm
16	Operating data	Normal operation
17	Medium hot gas temperature	953 °C 10.000 h
18	Max. hot gas temperature	1000 °C max. 50 h
19	Medium cold gas temperature	280 °C (full capacity)
20	Max. cold gas temperature	350 °C (full capacity)
21	System pressure	40 bar
22	Δp cold gas / hot gas	0.4 bar
23	-	-
24	Max. pressure transient	-3 bar/s
25	Δp hot gas	46 Pa/m
26	Hot gas velocity	17 m/s
27	Cold gas velocity	7.2 m/s
28	He-flow rate	2.5 kg/s
29	Max. temperature transients	±2 K/min
30	Accident data	Accident operation max. 500 h
31	a) Hot gas temperature	280 °C
32	Cold gas temperature	280 °C
33	Helium mass flow	2.5 kg/s
34	System pressure	40 bar
35	-	-

HTR-E	Data sheet		Project: PNP Sheet: 2
36		Temperature transient from 280 °C to 953 °C (hot gas)	+196 K/min
37	b)	Hot gas temperature	953 °C
38		Cold gas temperature	280 °C
39		Helium mass flow	2.5 kg/s
40		System pressure	40 bar
41		There after mass flow = 0	
42		Duration of accident = 1.5 h	
43		Effect: Increase of the cold gas temperature	
44		Design data	
45	a)	Pressure vessel	
46		Pressure	46 bar/-1 bar
47		Release of pressure	10 bar/s
48		Temperature (max.)	400 °C
49		Temperature distribution azimutal axial	-100 °C -100 °C
50		Consideration of the parameters from the thermodynamic calculations	
51	b)	Support pipe	
52		Pressure (overpressure)	1 bar
53		Release of pressure	10 bar/s
54		Temperature (max.)	500 °C
55		Temperature distribution azimutal axial	-100 °C -100 °C
56		Consideration of the parameters from the thermodynamic calculations	46 Pa/m
57		Internal fixtures	
58		Pressure	No pressure impact, but external overpressure caused by transients -10 bar/s
59		Temperature	953/1000 °C
60		Temperature transients	±5 K/min 1000 cycles ±196 K/min 5 cycles

HTR-E	Data sheet	Project: PNP Sheet: 3

61	Materials		
62	Pressure pipe	1.5415	DIN 17115, Sheet 2
63	or	1.7335	DIN 17155, Sheet 2
64	Support pipe	1.7415	DIN 17155, Sheet 2
65	Internals		
66	Hot gas-side	1.4876	VdTÜV 412 and SEW 470
67	-	ASR-1RG	WVS 423.05
68	-	1.4828	VdTÜV 412 and SEW 470
69	-	Al203 Wool	WVS 422.05
70	-	Al203 Wool	WVS 421.05
71	-	Graphite foil	WVS 423.05
72	Cold areas	1.4541	VdTÜV 411
73	-	Al203/Si02 Wool	WVS 421.05
74	Expansion joint	1.5415	DIN 17155, Sheet 2 or similar Material
75	Ceramic coating	ZrO_2	WVS-424-05

17. Résumé

In the preceding report, work on hot gas ducts and insulations for high-temperature reactors performed under numerous projects for a period of almost 15 years is summarized.

In the introduction, the necessity of insulations and their significance for the vessels and pipes of gas-cooled reactors is pointed out. Especially because of the high gas pressures involved, these systems must be mounted on the inner surfaces of the structures to be insulated. After a description of the requirements to be fulfilled, insulation systems classified according to the materials used or their structures are listed. This is followed by sections on heat transport in porous media and general issues concerning the behaviour during rapid depressurization.

Heat transport in insulations is composed of several portions. Of particular significance is the pressure of the medium with which the systems are filled. It may contribute to markedly increasing the thermal conductivity due to free convection, if the insulations do not provide sufficient gas flow resistance, i.e. if they are porous or permeable. Moreover, pressure gradients on the hot gas side of the insulations may enhance the transport of hot gas to the cold wall due to high velocity or in bends – forced convection – and thus lead to higher heat losses. However, flow through the insulation systems should be ruled out as far as possible. This requires suitable convection barriers reducing permeability. Besides convection, in general, thermal radiation furnishes a significant contribution, above all in fibre insulations due to the large pore volume. Equations from the literature for the calculation of the effective thermal conductivities and radiation conductivities in fibrous materials are given.

In the case of rapid depressurization within the reactor, the inner ducting shrouds are subjected to pressure loads. This loading depends on the size of the outflow cross-sections and the absolute pressure. Large cross-sections lead to low loads. In this case, however, there is the danger of forced through-flow resulting in elevated heat losses. The position and size of the outflow cross-sections must therefore be optimized.

In the presentation experimentally and computationally determined results, first of all, the test facilities used are described. These include small as well as large devices available at the former KFA, at German project partners and also abroad. The focus of work at the Institute for Reactor Components (IRB) of KFA was above all on the investigation of insulations for hot gas ducts. These investigations are therefore described at great length, although not comprehensively. For comparison, investigations on insulations for pressure vessels performed essentially in Great Britain, but also in France during the development of carbon-dioxide-cooled reactors are also referred to.

Two test facilities were used to investigate the thermal conductivity of different insulating materials according to the guarded hot plate procedure. Testing comprised fibrous materials and rigid ceramics The parameters were gas pressure and gas temperature, fibre density and nature of gas. Due to the high radiation portion, the thermal conductivities of the fibrous materials increase with rising temperatures of the samples examined, whereas they decrease with temperature in rigid ceramics.

For investigations concerning the thermal behaviour of large components, the HP channel, the ARGAS facility, and later on the HHV facility specifically constructed for development work under the HHT project were available. The facility for the long-term testing of insulations, ADI, was built by the HRB company. INTERATOM in Bensberg followed with the construction of the large KVK facility. The smaller HVK facility set up by GHH for HHT applications on the KFA campus was later put into operation again in São Paulo and used for testing an insulation with KFA support. Like KVK facility, the HENDEL facility in Tokai mura, Japan, enabled the testing of full-scale components.

The metallic foil insulations of cover plate design for pipes corresponded in their structure, apart from the inner ducting shrouds, to those of the vessels of British gas-cooled reactors. However, the first measurements in the HP channel revealed structurally induced gaps that were too large, so that increased heat transport to the cooled tube wall due to free convection was observed above all for measurements in air. This led to different heat losses across the circumference of the horizontally positioned tube and also to high outside temperatures of the pressure-bearing wall. A reduction in size of the circumferential gaps caused a homogenization of the losses and temperatures in the insulation. Measurements in the HHV facility on a modified foil insulation, however, still showed structural weaknesses that were attributable, among other things, to the large dimensions of this insulation.

The so-called bobbin design, completely prefabricated at the manufacturer's, was not suited for the envisaged applications, since it was only intended for straight pipes and the heat losses were too high. Moreover, there were restrictions with respect to the diameters of the tubes to be insulated.

The insulation for the hot gas ducts of the THTR in Schmehausen, also made of metal, had already been developed and tested in France at a very early stage. It was also used in French pressure vessels. It consisted of fine wire meshes and foils. This so-called METALISOL insulation was subjected to thermal cycling in helium atmosphere at HRB. The aim of these tests was primarily to study the behaviour of individual components with respect to friction welding.

Numerous experiments were carried out on fibre insulations – stuffed and in blanket form. The stuffed insulations with metallic closed gas duct showed satisfactory thermal behaviour. These systems were superior to the metallic foil insulations both in terms of measured values and their distribution. But mounting was very difficult. Moreover, due to the stuffing procedure, no constant stuffing density across the length and circumference could be guaranteed. Furthermore, fibre breakage and consequently dust discharge had to be expected. For this reason, fibre blankets were used, whose low density was increased by means of tightening devices. Since compressing took place on large areas, only minor destruction of fibres was expected. On the hot inner surface, metallic cover plates were first used as in the case of liner insulations. In the course of development, ceramic ducting shrouds of graphite or Masrock were also used, above all, because of the high temperatures in process heat plants. However, the open systems were susceptible to local and axial pressure gradients, so that graphite foils or thin metallic sheets were wrapped in to reduce the permeability. The latest state of the art was finally cover plates and other components of the insulation of carbon fibre composite.

A segmented stuffed bend with at first closed and then open metallic hot gas duct proved suitable in all cases. During the investigation of a 90 ° elbow with fibre blankets and ducting shrouds of carbon fibre composite, an ignition of the carbonaceous parts occurred for unclarified reasons destroying half of the insulation.

Tubes of carbon brick were investigated as all-ceramic insulations. The disadvantage of this relatively simple design was the through-flow of the gaps between the individual rings and between pressure wall and rings. Moreover, minor temperature differences already caused cracks due to excessively high tangential stresses, so that this concept was not further pursued.

Depressurization tests on samples of carbon brick and graphite did not lead to destruction even at high transients. Experiments in Ispra on a metallic insulation had already led to buckling of the gas duct at ambient temperature of the test media. The flow resistance at the outflow point was too high. Larger outflow cross-sections adopted later in all insulations eliminated this drawback. Investigations on some complete systems at the KFA demonstrated their suitability.

A large portion of this report comprises the experience from the development of metallic components within the framework of the PNP project. The manufacturing companies such as Didier or Balcke-Dürr have tried together with Interatom and others involved in the project to realize pragmatic solutions from the aspect of economic feasibility, high-temperature reactor requirements and helium atmosphere. Designs were described in the report for the insulation of metallic HTR components as well as for the primary and secondary connecting lines to the reactor.
Calculation approaches and the verification of the calculations with the experimental results were described. The conceptual design of the test components, the experimental setup and the description of the largest test facility – KVK – for such components were illustrated.

Another equally important chapter of the report is devoted to the description of the manufacturers' experience from the fabrication and mounting point of view. Production operations, manufacturing procedures, working devices, welding processes and testing methods were described. The insight into the quality assurance requirements valid at that time and the data sheet for future generations will provide manufacturers with approaches to a safe and also economical fabrication of high-temperature components.

18. Recommendations for the HTR-E Programme

The present report provides a comprehensive picture of the previous developments in connection with insulations in helium-cooled high-temperature reactor plants. Some of the information given could be needed in future in the further development of such plants.
Although the activities were very extensive, the following fields have not yet been completely covered and should be further developed within the framework of the HTR programme:

- depressurization at high temperatures and pressure (direct-cycle plants)
- connections and transitions, e.g. hot gas ducts with pressure vessels or lines with large components
- bends
- insulated sliding connections
- insulated bellows expansion joints

The concept of the (primary) hot gas duct or of the internal insulation on metallic components has proved feasible. Whereas the material costs already stabilized into a competitive purchasing price in the course of the projects due to the rapid development, the internals (e.g. insulation mounts, intermediate foils) represented an essential cost factor. The painfully slow assembly due to the high precision required led to long delivery times and correspondingly high costs.
One of the greatest challenges for work in the HTR-E project is therefore to optimize the economic efficiency of the solutions already tested e.g. by:

- developing standard designs as a basis for series production
- optimizing the working devices
- shortening the production operations
- simplifying the testing methods

Only by achieving economic efficiency for individual components and systems of the high-temperature reactor plant while maintaining its safety will it be possible to secure the predicted role of the high-temperature reactor in the nuclear field.

19. References

ACH73 Achenbach, E.: Strömung durch Krümmer kreisförmigen Querschnitts; Jül – 1000 – RB, 43 p. (1973)

ACH88 Achenbach, E.: Berechnung der effektiven Wärmeleitfähigkeit für die Isolierung einer HTR-Heißgasleitung unter Berücksichtigung von freier Konvektion und Temperaturstrahlung; Conference Proceedings Jahrestagung Kerntechnik, pp. 89/92 (1988)

ACH91 Achenbach, E.: Computation of Heat Transfer Through a Horizontally Arranged HTR Fibre Insulation; Nuclear Engineering and Design, No. 126, pp. 379/386 (1991)

ARA71a Aranovitch, E., Dufresne, J., Farfalatti-Casali, F., van Asselt, D.: Depressurization Tests on a Darchem Insulation System for High Temperature Gas Reactors; Contract of Collaboration No. 014-70-PiSGD GHH/KFA Jülich, EUR/C-IS/200/71.e, 49 p. (1971)

ARA71b Aranovitch, E., Crutzen, S., Dufresne, J., Farfalatti-Casali, F.: Thermal Insulation Systems for Prestressed Concrete Vessels of High Temperature Gas Reactors; Conference Proceedings Jahrestagung Kerntechnik, pp. 315/318 (1971)

ARA72 Aranovitch, E., van Asselt, D.: Rapid Depressurization of a Multilayer Insulation System for High Temperature Gas Reactors; Conference Proceedings Jahrestagung Kerntechnik, (1972)

AST78 N. N.: Standard Test Method for Steady-State Thermal Transmission Properties by Means of the Guarded Hot Plate; ANSI/ASTM C 177-76, 53 p. (1978)

BAR85 Barnert, H., Bröckerhoff, P., Elter, C., Singh, J.: AVR-Umbau: Konzept der Primärgasleitungen und -anschlüsse; Conference Proceedings of Jahrestagung Kerntechnik, pp. 563/566 (1985)

BEC31 Beckmann, W.: Die Wärmeübertragung in zylindrischen Gasschichten bei natürlicher Konvektion; Forschung im Ingenieurwesen, Volume 2, No. 5, pp. 165/178 (1931)

BOB70 Bobleter, A., Chiron, M., Grossin, R., Naudin, P.: THTR 300 MW_{el} Darchem Insulation Tests; Société Bertin & Cie., Final Report, 164 p. (1970)

BÖD84 Böder, H., Gruber, U., Popp, G.: Bauteile aus kohlenstoffaserverstärktem Kohlenstoff für Heißgasleitungen; series "Energiepolitik in Nordrhein-Westfalen", ISSN 0175-2553, Volume 16-II, pp. 641/652 (1984)

BRÖ71 Bröckerhoff, P.: Druckentlastungsversuche und Besprechung weiterer Fragen; Travel Report, 18 p. (1971)

BRÖ73 Bröckerhoff, P.: Wärmeleitfähigkeit von Faserstoffen, Möglichkeiten der Berechnung; Jül – 992 – RB, 49 p. (1973)

BRÖ74a Bröckerhoff, P., Scholz, F.: Untersuchungen an einer Folienisolierung in einem horizontalen Druckrohr; Jül – 1109 – RB, 126 p. (1974)

BRÖ74b Bröckerhoff, P.: Druckentlastungsversuche an porösen Probekörpern; Conference Proceedings Reaktortagung des Deutschen Atomforums, pp. 579/582 (1974)

BRÖ75a Bröckerhoff, P.: Wärmeleitfähigkeit einer Faserisolierung für Hochtemperaturisolierungen; Chemieingenieurtechnik, Annual Volume 47, No. 18, p. 767 (1975) or MS 277/75

BRÖ75b Bröckerhoff, P., Scholz, F.: Untersuchungen an zwei gestopften Faserisolierungen in einem horizontalen Druckrohr; Jül – 1241, 102 p. (1975)

BRÖ76 Bröckerhoff, P.: Testisolierungen für die Heißgasleitung der HHV-Anlage; Jül – 1334, 36 p. (1976)

BRÖ77a Bröckerhoff, P., Scholz, F.: Wärmedämmverhalten von dicht gestopften Faserisolierungen bei hohen Temperaturen und Drücken; Verfahrenstechnik, Annual Volume 11, No. 4, pp. 237/240 (1977)

BRÖ77b Bröckerhoff, P.: Erste Messungen an einer Kohlesteinisolierung; Jül – 1430, 109 p. (1977)

BRÖ77c Bröckerhoff, P.: Weitere Messungen an der konstruktiv verbesserten Kohlesteinisolierung; No. 1, Jül – 1458, 134 p. (1977)

BRÖ77d Bröckerhoff, P., Lang, H.: Stresses in Thermal Insulations of Hot Gas Ducts Caused by Temperature Gradients and Pressure Transients; Preprints of the Fourth International Conference on Structural Mechanics in Reactor Technology, Vol H: Structural Engineering of Prestressed Reactor Pressure Vessels, Paper H6/2, San Francisco (1977)

BRÖ78a Bröckerhoff, P.: Insulation Systems for the Hot Gas Ducts of High Temperature Reactors and Their Behaviour at High Pressures and Temperatures; Journal of Non-Equilibrium Thermodynamics, Vol. 3, pp. 231/243 (1978)

BRÖ78b Bröckerhoff, P.: Weitere Untersuchungen an der konstruktiv verbesserten Kohlesteinisolierung; No. 2, Jül – 1481, 51 p. (1978)

BRÖ78c Bröckerhoff, P.: Verhalten der Kohlesteinisolierung unter dem Einfluß hoher axialer Druckgradienten; Jül – 1529, 49 p. (1978)

BRÖ80a Böckerhoff, P.: Messungen an einer Fasermattenisolierung; Conference Proceedings of Jahrestagung Kerntechnik, pp. 713/716 (1980)

BRÖ80b Bröckerhoff, P.: Verhalten der Kohlesteinisolierung bei vertikaler Versuchsanordnung; Jül – 1659, 49 p. (1980)

BRÖ81a Bröckerhoff, P.: Thermal Conductivity of Reactor Insulations; High Temperatures – High Pressures, Vol. 13, pp. 701/709 (1981)

BRÖ81b Bröckerhoff, P.: Einfluß von Druckgradienten auf die Wirksamkeit einer Fasermattenisolierung; Conference Proceedings of Jahrestagung Kerntechnik, pp. 447/450 (1981)

BRÖ82a Bröckerhoff, P.: Investigations on Thermal Insulation; Proceedings of the Conference "Gas-Cooled Reactors Today", Vol. 1, British Nuclear Energy Society (BNES), pp. 145/150 (1982)

BRÖ82b Bröckerhoff, P.: Experimentelle Untersuchungen an einem innen isolierten Heißgaskrümmer; Conference Proceedings Jahrestagung Kerntechnik, pp. 113/116 (1982)

BRÖ83a Bröckerhoff, P.: On the Thermal Conductivity of Ceramic Fibrous and Rigid Insulations; Plenum Press, Ed. J. G. Hust, Plenum Publishing Corporation, pp. 369/379 (1983)

BRÖ83b Bröckerhoff, P., Stausebach, D.: Erste Untersuchungen an einer gewickelten Fasermattenisolierung mit massiven Abstandhaltern aus faserverstärktem Kohlenstoff; Jül – 1840, 62 p. (1983)

BRÖ83c Bröckerhoff, P., Stausebach, D.: Weitere Untersuchungen an einer Fasermattenisolierung mit massiven Abstandhaltern unter dem Einfluß axialer Druckgradienten; Jül – Spez – 221, 39 p. (1983)

BRÖ84a Bröckerhoff P.: Wärmetechnische Untersuchungen an Isolationssystemen für Heißgasleitungen; series "Energiepolitik in Nordrhein-Westfalen", ISSN 0175-2553, Vol.16-II, pp. 604/612 (1984)

BRÖ84b Bröckerhoff, P., Singh, J., Schmitt, H., Knaul, J., Hiltgen, H., Stausebach, D.: Status of Design and Testing of Hot Gas Ducts; Nuclear Engineering and Design, No. 78, pp. 215/221 (1984)

BRÖ84c Bröckerhoff P.: Research on Thermal Insulation for Hot Gas Ducts; Specialists' Meeting on Heat Exchanging Components of Gas-Cooled Reactors, International Atomic Energy Agency IWGGCR-9, Paper No. 27 (1984)

BRÖ84d Bröckerhoff, P.: Abschlußbericht über die Untersuchungen am ISOBOX-System; Internal Report KFA-IRB-IB-2/84, 79 p. (1984)

BRÖ86a Bröckerhoff, P.: Untersuchungen an einer Faserisolierung mit keramischen Abstandhaltern; Jül – Spez – 350, 56 p. (1986)

BRÖ86b Bröckerhoff, P., Stausebach, D.: Druckentlastungsversuche an zwei Fasermattenisolierungen; Conference Proceedings of Jahrestagung Kerntechnik, pp. 351/354 (1986)

BRÖ87 Bröckerhoff, P., Zentis, A.: Wärmetechnische Untersuchungen an einer keramischen Isolierung; Conference Proceedings of Jahrestagung Kerntechnik, pp. 565/568 (1987)

BRU75 Bruners, R., Lang, H., Noack, G.: Untersuchungen an einer Faserisolierung in der ARGAS-Anlage; Jül – 1227, 19 p. (1975)

BUR84 Burger, R.: Entwicklung eines neuartigen Hochtemperatur-Isolierwerkstoffes und Anwendung im PNP-Projekt; series "Energiepolitik in Nordrhein-Westfalen", ISSN 0175-2553, Vol.16-I, pp. 344/363 (1984)

BÜT84 Büttner, D., Fricke, J., Reiss, H.: Wärmeleitfähigkeit von evakuierten Hochtemperatur-Superisolationen unter variabler Druckbelastung – Einsatz der großen Zweiplattenapparatur LOLA I mit Schutzringen;

Vakuum-Technik, Annual Volume 34 , No. 1, pp. 3/9 (1984)

CHA74 Chaboseau, J., Cornille, Y., Chapelot, A., Patarin, L.: HTGR Component Testing; ANS Topical Meeting on Gas-Cooled Reactors: HTGR and GCFBR, CONF-740501, pp. 162/175 (1974)

CHE71 Chekhovskoi, V. Y., Petrov, V. A., Petrova, I. I., Lyukshin, E. N.: Thermal Conductivity of Pyrographite at High Temperatures; High Temperature, Vol. 9, No. 1, pp. 80/84 (1971)

COL75 Colquhoun, J., Davidson, J., Bolton, A. D.: The Design, Commissioning and Operation of Hinkley Point B AGR Power Station Pressure Vessel Insulation; Conference on Experience in the Design, Construction and Operation of Prestressed Concrete Pressure Vessels and Containments for Nuclear Reactors, The Institution of Mechanical Engineers, pp. 101/109 (1975)

COW67 Cowap, P. G., Furber, B. N.: The Performance of Stainless Steel Foil Insulation in a Helium Atmosphere; Dragon Project Report 462, 19 p. (1967)

CZE52 Czerny, M., Genzel, L.: Energiefluß und Temperaturverlauf im Glasbad von Schmelzwannen als Folge von Wärmeleitung und Wärmestrahlung; Glastechnische Berichte 25, pp. 387/392 (1952)

DAV67 Davidson J.: The Heat Transfer Behaviour of Metallic Foil Insulation in High Pressure Gas; The Institution of Mechanical Engineers, Vol. 181, Part 31, pp. 48/56 (1967)

DEL69 Delort, Lecour, Soulier: Isolation Thermique par Toile et Tôle Metallique; Deuxieme Réunion d'Information sur les Travaux Relatifs aux Cuves de Réacteur en Béton Precontraint et à leur Isolation, EURATOM, Brussels, 14 p. (1969)

DIN79 N. N.: Bestimmung der Wärmeleitfähigkeit mit dem Plattengerät, Durchführung und Auswertung; Deutsches Institut für Normung e. V., DIN 52612 Part1 (1979)

DUB69 Dubois, F., Mauny, P., Bernard, A., Elleuch, M. F.: Nouveaux Types des Bétons Calorifuges pour Réacteurs Nucléaires; Contract Euratom No. 047-66-7 TEGF, C. E. A. No. 8454/r, 23 p. (1969)

DUM85 Dumm, K., Klas, E., Stausebach, D.: Entwicklung von Heißgasleitungen für Hochtemperaturreaktoren im Temperaturbereich bis 950 °C; 3R International, Annual Volume 24, No. 9, pp. 507/512 (1985)

ELT85 Elter, C.: Die Heißgasleitungen des THTR-300 und ihre Weiterentwicklung; 3R International, Annual Volume 24, No. 9, pp. 504/507 (1985)

EUC32 Eucken, A.: Die Wärmeleitfähigkeit keramischer feuerfester Stoffe; Beilage zu „Forschung auf dem Gebiet des Ingenieurwesens“, Edition B Vol. 3, VDI-Verlag GmbH, pp. 1/16 (1932)

EXN84 Exner, R.: Entwicklungsschritte zur Realisierung des He/He-Zwischenwärmetauschers (URKO) und Funktionsbeschreibung des Apparates; series "Energiepolitik in Nordrhein-Westfalen", ISSN 0175-2553, Vol. 16-I, pp. 194/208 (1984)

FEL73 Felten, P.: Assemblage et Fixation des Structures Isolantes de Céramique dans les Caissons de Béton des Réacteurs à Haute Température; Preprints of the Second International Conference on Structural Mechanics in Reactor Technology, Paper H5/5, Berlin (1973)

FUR69 Furber, B. N., Davidson, J.: The Thermal Performance of Porous Insulants in a High Pressure Gas Environment; Second Conference on Prestressed Concrete Reactor Vessels and Their Thermal Insulation, Paper No. 28, Brussels (1969)

FUR75 Furber, B. N., Hopkins, I. H. G., Stuart, R. A.: The Development of Criteria for the Design of Insulation for Nuclear Reactors; Conference on Experience in the Design, Construction and Operation of Prestressed Concrete Pressure Vessels and Containments for Nuclear Reactors, The Institution of Mechanical Engineers, pp. 93/100 (1975)

FUR82 Furber, B. N., Sheppard, M. A.: Liner Insulation for Gas-Cooled Reactors – 21 Years of Development; Proceedings of the Conference "Gas-Cooled Reactors Today", Vol. 1, British Nuclear Energy Society (BNES), pp. 139/144 (1982)

GAR75 Garrard, R. S., Salmons, B. H.: The Quality Assurance Function with Respect to the Design and Construction of Steel Structures for Pre-Stressed Nuclear Vessels; Conference on Experience in the Design, Construction and Operation of Prestressed Concrete Pressure Vessels and Containments for Nuclear Reactors, The Institution of Mechanical Engineers, pp. 169/177 (1975)

GHH70 N. N.: Heliumversuchskreislauf HVK, Anlagenbeschreibung; Gutehoffnungshütte Sterkrade AG, Abteilung Kerntechnik, 46 p. (1970)

GHH71 N. N.: Rahmenprogramm für Versuche an Heißgasisolierungen im Entwicklungsprogramm Hochtemperaturreaktoren mit Heliumturbine großer Leistung (HHT); Gutehoffnungshütte Sterkrade AG, Abteilung Kerntechnik, 40 p. (1971)

GHT72 N. N.: Metallic Metalisol Insulations, Test Synthesis; Groupement Industriel Français Pour les Réacteurs à Haute Température (GHTR), 49 p. (1972)

GRÖ63 Gröber, H., Erk, S., Grigull, U.: Die Grundgesetze der Wärmeübertragung; 3rd edition, Springer-Verlag Berlin/Göttingen/Heidelberg (1963)

GRO65 Grosse, H., Scholz, F.: Der Hochdruck-Gaskanal; Thiemig, Kerntechnik, Annual Volume 7, No. 4, pp. 150/158 (1965)

HAG67 Hager, N. E., Steere, R. C.: Radiant Heat Transfer in Fibrous Thermal Insulation; Journal of Applied Physics, Vol. 38, No. 12, pp. 4663/4668 (1967)

HAM66 Hammeke, K., Pietralla, G., Presser, K. H.: Thermodynamische Stoffwerte von Luft, Kohlendioxid und Stickstoff bei hohen Temperaturen und Drücken; Jül – 383 – RB, 48 p. (1966)

HAR70 Harth, R., Hammeke, K.: Thermodynamische Stoffwerte von Helium im

Bereich von 0 – 3000 °C und 0,2 – 200 bar; Jül – 666 – RB, 99 p. (1970)

HAR84 Harth, R., Nießen, H. F., Vau, V., Merken, R.: Vorstellung der Versuchsanlage EVA II und ihrer Aufgabenstellung; series "Energiepolitik in Nordrhein-Westfalen", ISSN 0175-2553, Vol.16-I, pp. 92/98 (1984)

HED74 Hedgecock, P. D., Patriarca, P.: Materials Selection for Gas-Cooled Reactor Components; ANS Topical Meeting on Gas-Cooled Reactors: HTGR and GCFBR, CONF-740501, pp. 525/559 (1974)

HEL53 van der Held, E. F. M.: Der Strahlungsbeitrag an der Wärmeleitung; Allgemeine Wärmetechnik, Annual Volume 4, No. 11/12, pp. 236/240 (1953)

HEN76 Henßen, J., Lang, H., Lonzen, G., Noack, G.: Untersuchungen an einer Metallfolienisolierung in der ARGAS-Anlage und im Druckentlastungsversuchsstand; Jül – 1318, 50 p. (1976)

HEN77 Henßen, J., Lang, H., Lonzen, G., Weise, H.-J.: Untersuchungen an einer Faserisolierung im Druckentlastungsversuchsstand; Jül – 1405, 34 p. (1977)

HEN84a Henßen, J.: Anlage zum Dauertest von Isolierungen (ADI); series "Energiepolitik in Nordrhein-Westfalen", ISSN 0175-2553, Vol.16-II, pp. 613/620 (1984)

HEN84b Henßen, J., Lonzen, G., Bauer, R., Klas, E.: Test einer Heißgasleitung unter repräsentativen Bedingungen; Conference Proceedings of Jahrestagung Kerntechnik, pp. 101/104 (1984)

HEN86 Henßen, J., Mauersberger, R., Kruschik, J.: Strömung und Wärmeübergang in Helium-Armaturen großer Nennweite; Conference Proceedings of Jahrestagung Kerntechnik, pp. 121/124 (1986)

HIS84 Hishida, M., Tanaka, T., Shimomura, H., Sanokawa, K.: Construction and Performance Tests of Helium Engineering Demonstration Loop (HENDEL) for VHTR; Specialists' Meeting on Heat Exchanging Components of Gas-Cooled Reactors, International Atomic Energy Agency IWGGCR-9, Paper No. 29 (1984)

HOS74 Hosegood, S. B., Jones, H.: The Design and Development of Thermal Insulation for High Temperature Gas Cooled Reactors; ANS Topical Meeting on Gas-Cooled Reactors: HTGR and GCFBR, CONF-740501, pp. 487/524 (1974)

INE94 N. N.: Main Parameters of the HTR-10, Preliminary Design; INET, 38 p. (1994)

IVE74 Mc. Iver, R. F., Sage, R. J., Simon, R., Harper, C.: Installation and Initial Performance of Experimental Duct Liners; Dragon Project Report 889, 46 p. (1974)

JAN84 Jansing, W.: Vorstellung der KVK-Anlage und ihrer Aufgabenstellung; series "Energiepolitik in Nordrhein-Westfalen", ISSN 0175-2553, Vol.16-I, pp. 76/91 (1984)

JAN84a Janßen, K., Persicke, H.: Graphitwerkstoffe für heißgasführende Komponenten; series "Energiepolitik in Nordrhein-Westfalen", ISSN 0175-2553, Vol. 16-II, S. 633/640 (1984)

JON69 Jones, G.: Mechanical Properties of Fibrous Insulation Materials Considered for the Thermal Barrier for a Prestressed Concrete Reactor Vessel; Gulf General Atomic, U. S. Atomic Energy Commission, Contract AT (04-3)-633 Project 901, 42 p. (1969)

JON74 Jones, G., Brislin, R. J.: Development Program for the Fort St. Vrain Thermal Barrier; The American Society of Mechanical Engineers, Annual Winter Meeting, Paper 74 – WA/HT – 1, New York, 8 p. (1974)

JON75 Jones, H., Hedgecock, P. D.: Thermal Protection System for the Concrete Support Floor at Fort St. Vrain; Conference on Experience in the Design, Construction and Operation of Prestressed Concrete Pressure Vessels and Containments for Nuclear Reactors, The Institution of Mechanical Engineers, pp. 111/118 (1975)

KIN69 Kinkead, A. N., Pitchfort, B. E.: Performance of Thermal Insulation Immersed in Helium; Dragon Project Report 666, p. 26 (1969)

KIR85 Kirchhoff, R., van Heek, H.: Betriebserfahrungen mit Hochtemperatur-Rohrleitungen in einer Versuchsanlage zur Kohlevergasung; 3R International, Annual Volume 24, No. 9, pp. 513/518 (1985)

KLA84a Klas, E., Bröckerhoff P.: Experimentelle Untersuchungen an einer Fasermattenisolierung für die Primärleitung einer HTR-Anlage; Conference Proceedings Jahrestagung Kerntechnik, pp. 97/100 (1984)

KLA84b Klas, E.: Testergebnisse der sekundären Heißgasleitung (KVK); series "Energiepolitik in Nordrhein-Westfalen", ISSN 0175-2553, Vol. 16-II, pp. 621/632 (1984)

KLA84c Klas, E.: Bauteilversuche für die primäre Heißgasleitung (HGL); series "Energiepolitik in Nordrhein-Westfalen", ISSN 0175-2553, Vol. 16-II, pp. 582/591 (1984)

KNA84 Knaul, J.: Das Isolationskonzept mit Deckplatten und Halteelementen; series "Energiepolitik in Nordrhein-Westfalen", ISSN 0175-2553, Vol. 16-II, pp. 566/581 (1984)

KNI67 Knirsch, H., Schmiedel, F.: Behälterisolierungen für Hochtemperatur-Reaktoren mit Heliumkühlung; Euratom Information Meeting on Prestressed Concrete Reactor Vessels and Their Thermal Insulation; Brussels (1967)

KOG67 Koglin, B.: Der Wärmetransport in Schaumstoffen; PhD thesis Berlin D 83, 87 p. (1967)

KON78a Konuk, A.: Natural, Forced and Mixed Convection in Fibrous Insulation; Instituto de Energia Atômica, São Paulo, Publ. IEA 503, CEN – AFR 056, 98 p. (1978)

KON78b Konuk, A., Rodriguez, F. A.: Temperature Distribution in a Coaxial Ring Duct for HTR Applications; Instituto de Energia Atômica, São Paulo, Publ. IEA 509, CEN – AFTR 57, 80 p. (1978)

KON84 Kondo, J., Tadokoro, Y., Hishida, M., Okamoto, M., Tanaka, T., Sanokawa, K.: The Computer Programs for Analysing Two-Dimensional

Permeation Flow Within Horizontal Thermal Insulation; Japan Atomic Energy Research Institute, JAERI – M 84 – 179, 54 p. (1984)

KRA34 Kraußold, H.: Wärmeabgabe von zylindrischen Flüssigkeitsschichten bei natürlicher Konvektion; Forschung im Ingenieurwesen, 5th volume, No. 4, pp. 186/191 (1934)

KRÄ73 Krämer, H., Noack, G.: Hochtemperatur-Helium-Versuchsanlage HHV; offprint from the Annual Report of Kernforschungsanlage Jülich GmbH, 5 p. (1973)

KRU84a Kruschik, J., Berdan, F.: Auslegung und konstruktive Entwicklung des Klinger Heißgas-Axial-Ventils; series "Energiepolitik in Nordrhein-Westfalen", ISSN 0175-2553, Vol. 16-II, pp. 499/516 (1984)

KRU84b Kruschik, J., Hiltgen, H.: The Klinger Hot Gas Double Axial Valve; Specialists' Meeting on Heat Exchanging Components of Gas-Cooled Reactors, International Atomic Energy Agency IWGGCR-9, Paper No. 23 (1984)

LAK71 Lakin, R. W.: Internal Insulation of Reinforced Concrete Pressure Vessels; Nuclear Engineering International, pp. 337/343 (1971)

LAN77 Lang, H., Weise, H.-J.: Druckentlastungsversuche an einer gestopften Faserisolierung in einem horizontalen Druckrohr; Jül – 1451, 25 p. (1977)

LAN78 Lang, H., Weise, H.-J.: Druckentlastungsversuche an einem zylindrischen Kohlesteinrohr; Jül – 1535, 28 p. (1978)

LAN82 Lang, H., Klas, E., Schumacher, G.: Thermische und Druckentlastungsversuche an einem innenisolierten Angular-Kompensator mit zyklischer Auslenkung unter Helium bis 1000 °C und 35 bar; Jül – Spez – 181, 39 p. (1982)

LAR59 Larkin, B. K., Churchill, S. W.: Heat Transfer by Radiation Through Porous Insulations; A. I. Ch. E. Journal, Vol. 5, No. 4, pp. 467/474 (1959)

MAU84 Mausbeck, H., Baust, E.: Situation des FE-Programms auf dem Gebiet der wärmeführenden und wärmeaustauschenden Komponenten im Rahmen des PNP-Projektes; series "Energiepolitik in Nordrhein-Westfalen", ISSN 0175-2553, Vol. 16-I, pp. 4a/30 (1984)

MAU84a Mauersberger, R.: Facility for Endurance Tests of Thermal Insulations; Specialists' Meeting on Heat Exchanging Components of Gas-Cooled Reactors, International Atomic Energy Agency IWGGCR-9, Paper No. 28 (1984)

MAU84b Mauersberger, R.: Vorlaufende Bauteiltests für die Heißgasleitungskonzepte; series "Energiepolitik in Nordrhein-Westfalen", ISSN 0175-2553, Vol. 16-II, S. 592/603 (1984)

MEN84 Mendte, K., Maus, W.: Planungsanforderungen und Entwicklungsziele des He/He-Zwischenwärmetauschers; series "Energiepolitik in Nordrhein-Westfalen", ISSN 0175-2553, Vol. 16-I, pp. 178/193 (1984)

MIT79 N. N.: Progress Report, National Research & Development Program on Direct Steelmaking Using High Temperature Reducing Gas; Agency of

Industrial Science and Technology (MITI), 131 p. (1979)

MUL30 Mull, W., Reiher, H.: Der Wärmeschutz von Luftschichten, seine experimentelle Bestimmung und graphische Berechnung; Oldenbourg, Beihefte zum Gesundheits-Ingenieur, No. 28, Series 1, 26 p. (1930)

NAK84 Nakase, T., Midoriyama, S., Roko, K., Yoshizaki, A.: Two Layers Thermal Insulations Tests for Designing of Hot Gas Ducts; Specialists' Meeting on Heat Exchanging Components of Gas-Cooled Reactors, International Atomic Energy Agency IWGGCR-9, Paper No. 24 (1984)

NAR69 Narinski, D. A., Sheinin, B. I.: Effective Thermal Conductivity of Steel Foil Insulation; High Temperature, Vol. 7, No. 3, pp. 394/397 (1969)

NAU72 Naudin, P., N. N.: Etat d'Advancement des Techniques Françaises en Matière de Protection Thermique Pour Réacteurs Nucleaires; Scéance Technique 3/10 International Nuclear Industries Fair, Basel (1972)

NFE85 N. N.: Nukleare Fernenergie, Zusammenfassender Bericht zum Projekt Nukleare Fernenergie (NFE); Jül – Spez – 303, 294 p. (1985)

NOA77 Noack, G., Weiskopf, H.: Die Hochtemperatur-Helium-Versuchsanlage (HHV), Aufbau und Beschreibung der Anlage; Jül – 1403, 69 p. (1977)

NUS13 Nusselt, W.: Die Übertragung der Wärme bei der Bone-Schnabel-Feuerung; Zeitschrift des Bayerischen Revisions-Vereins, No. 13 and 14, Annual Volume 17, pp. 125/127 and pp. 137/139 (1913)

POE12 Poensgen, R.: Ein technisches Verfahren zur Ermittlung der Wärmeleitfähigkeit plattenförmiger Stoffe; Zeitschrift des Vereins deutscher Ingenieure, No. 56, p. 1643 (1912)

POL62 Poltz, H.: Einfluß der Wärmestrahlung auf die Isolierwirkung poröser Dämmschichten; Allgemeine Wärmetechnik, Vol. 11, No. 4, pp. 64/71 (1962)

SAI94 Saito, S., N. N.: Design of High Temperature Engineering Test Reactor (HTTR); Japan Atomic Energy Research Institute 1332, 247 p. (1994)

SCH27 Schmidt, E.: Wärmeschutz durch Aluminiumfolie; VDI Journal, Vol. 71, No. 40, pp. 1395/1400 (1927)

SCH61 Schmidt, Th. E.: Über die Wärmeleitzahl von Isolierstoffen; Forschung auf dem Gebiet des Ingenieur-Wesens, Vol. 27, pp. 10/14 (1961)

SCH65 Schmidt, E.: Ausströmen von Gasen aus Behältern hohen Innendrucks; Chemie-Ingenieur-Technik, Annual Volume 37, No. 11, pp. 1091/1094 (1965)

SCH81 Schumacher, G.: PNP-spezifische Versuchseinrichtungen; Technical Report, 82 p. (1981)

SIG N. N.: Collection of data from Sigri

STA84 Stausebach, D.: Planungsanforderungen und Ziele der Entwicklungsaufgaben an Heißgasleitungen; series "Energiepolitik in Nordrhein-Westfalen", ISSN 0175-2553, Vol. 16-II, pp. 550/565 (1984)

STE84 Stehle, H., Klas, E.: Status of the Development of Hot Gas Ducts for

HTRs; Specialists' Meeting on Heat Exchanging Components of Gas-Cooled Reactors, International Atomic Energy Agency IWGGCR-9, Paper No. 25 (1984)

STR60 Strong, H. M., Bundy, F. P., Bovenkerk, H. P.: Flat Panel Vacuum Thermal Insulation; Journal of Applied Physics, Vol. 31, No. 1, pp. 39/50 (1960)

TAR67 Tarbès, B., Menestrier, S.: Pumice Concrete, Thermal Insulator in a Gas Under Pressure; The Institution of Mechanical Engineers, Vol. 181, Part 31, pp. 41/47 (1967)

TEB92 Tebroke, Th., Achenbach, E.: Berechnung des Wärmetransportes durch einen waagerechten porösen Ringspalt infolge Leitung, Strahlung und Konvektion bei variablen Stoffwerten; Jül – 2586, 123 p. (1992)

THI59 Thipgen, J. J., Short, B. E.: The Apparent Thermal Conductivity of Fibrous Materials; Transactions of the ASME, Paper A – 293, pp. 1/8 (1959)

TYE83 Tye, R. P., Desjarlais, A. O.: Factors Influencing the Thermal Performance of Thermal Insulations for Industrial Applications; ASTM STP 789, F. A. Govan, D. M. Greason and J. D. McAllister, Eds., American Society for Testing and Materials, pp. 733/748 (1983)

VER51 Verschoor, J. D., Greebler, P., Manville, N. J.: Heat Transfer by Gas Conduction and Radiation in Fibrous Insulations; Transactions of the ASME, Paper 51 – A – 54, pp. 961/968 (1951)

WEY71 von der Weyden, H. D.: Eine Versuchsreihe zum Studium des Verhaltens von metallischen Isolierungen in Helium; Preprints of the First International Conference on Structural Mechanics in Reactor Technology, Part H: Prestressed Concrete Pressure Vessels, Paper H6/6, Berlin (1971)

WIL71 Williams, A. J.: Investigation into Structural Behaviour of Insulation of the Prestressed Concrete Pressure Vessels of Wylfa Nuclear Power Station; Preprints of the First International Conference on Structural Mechanics in Reactor Technology, Part H: Prestressed Concrete Pressure Vessels, Paper H6/5, Berlin (1971)

YAS82 Yasuno, T., Okamoto, Y., Aochi, T.: Design and Component Test Programme for the Experimental VHTR; Proceedings of the Conference "Gas-Cooled Reactors Today", Vol. 1, British Nuclear Energy Society (BNES), pp. 125/132 (1982)

ZEH64 Zehender, H.: Einfluß der freien Konvektion auf die Wärmeleitfähigkeit einer leichten Mineralfasermatte bei tiefen Temperaturen; Kältetechnik, Vol. 16, No. 10, pp. 308/311 (1964)

20. Nomenclature

Latin Symbols

A	m^2	area
a	-	prefactor, ratio, polynomial coefficient
a	m/s	sound velocity
Al_2O_3	-	alumina
B	m^2	permeability
C	m^{-1}	pressure drop coefficient
c	Ws/(kgK)	specific heat capacity
CO_2	-	carbon dioxide
d	m, mm	thickness
D	m, mm	diameter
F	-	factor for geometry and absorption
F	N	force
f	-	outflow factor
f	s^{-1}	**frequency**
g	m/s^2	gravity
H	-	quantity for determining the orientation
H	m	height
He	-	helium
k	m	extinction number
L	m	free path
L	m	length
M	kg/kmol	**molecular weight**
m	-	quantity for determining the adsorption
$\dot{m}$	kg/s	mass flow
n	m^2	refractive index
N_2	-	nitrogen
p	bar	pressure
$\dot{Q}$	kW, W	heat flux
$\dot{q}$	W/m^2	heat flux density, heat loss
R	J/(kgK)	gas constant
r	m, mm	radius
s	mm	feed
Si_3N_4	-	silicon nitrite
SiO_2	-	silica
T	°C, K	temperature
t	h, min, s	time
V	m^3	volume
v	m/s	velocity

x	m	coordinate, length of insulation, gap width
x	mV	pressure indication
y	m	coordinate
ZrO_2	-	zirconia

Greek Symbols

α	K^{-1}	expansion coefficient
β	K^{-1}	**expansion coefficient**
Δ	-	difference
δ	µm	fibre diameter
ε	-	emission number, ratio (radiation)
ε	%	porosity
η	kg/(ms)	dynamic viscosity
Θ	-	cylindrical angle coordinate
κ	-	adiabatic exponent
λ	W/(mK)	thermal conductivity
π	-	pressure ratio, pi
ρ	kg/m^3	**density**
σ	$W/(m^{-2}h^{-4})$	radiation coefficient
σ	N/mm^2	**stress**
Ψ	-	stream function

Indices

A	geometry
a	absolute
B	bend, orifice
CO_2	**carbon dioxide**
eff	effective
F	solid
G	gas
g	total
h	hot
He	helium
I	insulation
i	number
k	cold
K_1, K_2	**convection**
kr	critical
L	air
max	maximum
N_2	**nitrogen**
0	initial state
p	at constant pressure
Pr	sample, test specimen
s	apparent
S	sound, radiation
t	actual
U	environment, subsonic
W	water

Characteristic numbers

Da	-	Darcy number
Fo	-	Fourier number
Gr	-	Grashof number
Nu	-	Nusselt number
Pe	-	Peclet number
Pr	-	Prandtl number
Ra	-	Rayleigh number

Abbreviations

ADI	Anlage zum Dauertest von Isolierungen (facility for the long-term testing of insulations)
AGR	advanced gas (cooled) reactor
ARG	Allgemeine Rohrleitungsbau GmbH
ARGAS	ARGON GAS
AVR	Arbeitsgemeinschaft Versuchsreaktor (Experimental Nuclear Power Plant Jülich)
BBC	Brown Boveri & Cie
BBK	Brown Boveri Krupp
BST	Brown Boveri-Sulzer Turbomaschinen
CAFL	Compagnie des Ateliers et Forges de la Loire
CEA	Commissariat à l'Energie Atomique
CFC	carbon fibre composite
CL	Creusot Loire
EDF	Electricité de France
ERANS	Engineering Research Association of Nuclear Steelmaking
EVA	Einzelrohr-Versuchsanlage (test unit with single reformer tube)
FZJ	Forschungszentrum Jülich (Research Centre Jülich)
GA	General Atomic
GAST	Gasgekühltes Sonnenturm-Kraftwerk (gas-cooled solar tower power plant)
GHH	Gutehoffnungshütte
GHT	Gesellschaft für Hochtemperaturreaktor-Technik
HD	high pressure (circuit)
HENDEL	Helium Engineering Demonstration Loop
HHT	high-temperature reactor with helium turbine
HHV	Hochtemperatur Helium Versuchsanlage (high-temperature helium test facility)
HRB	Hochtemperatur-Reaktorbau GmbH
HTR	high-temperature reactor
HTTR	high-temperature test reactor
HVK	Heliumversuchskreislauf (helium test facility)
ICI	Imperial Chemical Industries
IEA	Instituto de Energia Atômica
IGV	Institut für Grenzflächenforschung und Vakuumtechnik (Institute of Surface Research and Vacuum Physics)
INET	Institute of Nuclear Energy Technology
INTERATOM	Internationale Reaktorbau GmbH
IRB	Institut für Reaktorbauelemente (Institute for Reactor Components)

ISOBOX	insulation boxes
ITP	Institute of Technical Physics
JAERI	Japan Atomic Energy Research Institute
KFA	Nuclear Research Centre (Jülich)
KHI	Kawasaki Heavy Industry
KVK	Komponenten-Versuchs-Kreislauf (component test loop)
KWU	Kraftwerkunion
MAN	Maschinenfabrik Augsburg Nürnberg
MHD	magnetohydrodynamics
MITI	Ministry of International Trade and Industry
NFE	Nukleare Fernenergie (long-distance nuclear energy transport)
NPG	Nuclear Power Group
NPW	nuclear process heat
PBMR	pebble-bed modular reactor
PNP	Prototyp-Anlage Nukleare Prozeßwärme (Prototype Plant for Nuclear Process Heat)
RWTH	Rheinisch-Westfälische Technische Hochschule (Aachen University of Technology)
THTR	thorium high-temperature reactor